

# **Origin and evolution of ureilite vein metal – Fe, Ni, Co and Ni-isotope systematics of ureilite vein metal and ureilite silicates**

Dissertation

zur Erlangung des Doktorgrades

der Mathematisch-Naturwissenschaftlichen Fakultäten

der Georg-August-Universität zu Göttingen

vorgelegt von

Dipl.-Min.

Aron D. Gabriel

aus Berlin

Göttingen 2009

D 7

Referentin/Referent: Prof. Dr. Andreas Pack

Korreferentin/Korreferent: Prof Dr. Addi Bischoff

Tag der mündlichen Prüfung:

## Table of Contents

1	Introduction.....	8
1.1	What are meteorites?.....	8
1.2	Weathering and shock.....	8
1.3	Meteorite classification .....	10
1.3.1	Chondrites .....	10
1.3.2	Achondrites .....	16
1.3.3	Primitive Achondrites.....	19
2	The ureilite group.....	20
2.1	Introduction .....	20
2.2	Mineralogy.....	20
2.2.1	Silicates.....	20
2.2.2	Vein material .....	22
2.2.3	Spherule inclusions in olivine .....	23
2.3	Ureilite bulk rock chemistry.....	24
2.3.1	Lithophile elements.....	24
2.3.2	Siderophile elements.....	25
2.3.3	Rare Earth Elements (REE) .....	25
2.3.4	Noble gases .....	27
2.3.5	Oxygen isotopes .....	27
2.3.6	Carbon isotopes.....	28
2.3.7	Ureilite formation age and cosmic ray exposure age .....	29
2.3.8	The $^{60}\text{Fe}$ - $^{60}\text{Ni}$ short-lived isotope chronometer .....	30
2.4	Ureilite genesis .....	32

2.4.1	Parent body composition .....	32
2.4.2	Thermal history of ureilites .....	33
2.4.3	Igneous processes on the ureilite parent body.....	34
2.4.4	Reduction on the ureilite parent body.....	35
3	Goals of this study .....	38
4	Thermodynamics.....	39
4.1	Theoretical background.....	39
4.2	Gibbs free energy of reaction .....	41
4.3	Activity coefficients of Fe, Co and Ni in Fe-Co-Ni metal.....	42
4.4	Activity coefficients of $\text{Fe}_2\text{SiO}_4$ in olivine.....	45
4.5	Activity coefficients of $\text{Ni}_2\text{SiO}_4$ and $\text{Co}_2\text{SiO}_4$ in olivine.....	47
4.6	Comparison of the regular solution model with Hirschmann's model.....	49
5	Mass balance calculations.....	52
5.1	Mass balance calculations of the UPB's core .....	52
5.2	Model of the UPB core formation process.....	53
6	Sampling .....	60
6.1	Allan Hills 84136 (ALH84136) .....	60
6.2	Allan Hills 77257 (ALHA77257) .....	61
6.3	Dar al Gani 340 (DaG340) .....	61
6.4	Elephant Moraine 87517 (EET87517).....	62
6.5	Elephant Moraine 96042 (EET96042).....	62
6.6	Elephant Moraine 96331 (EET96331).....	63
6.7	Kenna .....	63
6.8	Graves Nunataks 95205 (GRA95205) .....	64
6.9	Lewis Cliff 85440 (LEW85440) .....	64
7	Sample preparation and analytical procedures .....	65

7.1	Sample preparation .....	65
7.2	Electron microprobe measurements.....	65
7.2.1	Measurements at the Institute of mineralogy in Cologne.....	65
7.2.2	Measurements at the University of Göttingen .....	66
7.2.3	The Co-problem.....	67
7.3	Laser-ablation-ICP-MS measurements of silicates .....	69
7.4	Ni-Isotope analyses.....	74
8	Results .....	76
8.1	Data of individual ureilites.....	76
8.1.1	ALH84136 .....	76
8.1.2	ALHA77257 .....	80
8.1.3	DaG340 .....	84
8.1.4	EET87517 .....	87
8.1.5	EET96042.....	91
8.1.6	EET96331.....	95
8.1.7	GRA95205.....	99
8.1.8	Kenna.....	103
8.1.9	LEW85440.....	106
8.2	Ni and Co in ureilite silicates .....	110
8.3	Ni and Co in vein metal.....	114
8.4	Ni-isotope data .....	116
9	Discussion .....	118
9.1	Thermodynamic equilibrium between vein metal and ureilite olivine.....	118
9.1.1	Calculation of Fe-Ni and Fe-Co-exchange equilibrium temperatures.....	118
9.1.2	Equilibration temperatures for ALH84136.....	120
9.1.3	Equilibration temperatures for EET96331 .....	121

9.1.4	Is ureilite olivine and vein metal in equilibrium?.....	121
9.2	Relation between primary metal component of the ureilite parent body and the ureilite vein metal .....	123
9.2.1	Initial bulk composition of the ureilite parent body .....	123
9.2.2	Calculation of the composition of the undepleted mantle.....	123
9.2.3	Calculation of the composition of the primary metal component in the ureilite parent body .....	125
9.2.4	Comparison of vein metal and the modeled primary metal component .....	127
9.2.5	Equilibration between the primary metal component and ureilite olivine.....	129
9.2.6	Metal depletion in ureilites .....	131
9.2.7	Scenarios for vein metal generation .....	133
9.3	Ureilite vein metal as a primary component.....	134
9.3.1	Constraints for metal fractionation processes on the ureilite parent body ....	134
9.3.2	Modeling of fractional melting on the ureilite parent body.....	141
9.3.3	Modeling of batch melting on the ureilite parent body .....	150
9.4	Ureilite vein metal as a secondary component.....	157
9.4.1	The complete removal of the initial chondritic metal portion .....	157
9.4.2	Secondary addition of metal from silicate reduction .....	157
9.4.3	Secondary addition of metal from an metal-rich impactor .....	158
9.5	Ureilite vein metal as mixture of primary and secondary components.....	162
9.5.1	Batch and fractional melting and addition of Ni-poor metal from silicate reduction .....	162
9.5.2	Batch and fractional melting and addition of metal from an impactor.....	163
9.6	Ni-Isotope systematics .....	165
10	Conclusions.....	171
11	References.....	174
12	Appendix.....	183

12.1	Ureilite data .....	183
12.1.1	ALHA84136 .....	183
12.1.2	ALHA77257 .....	186
12.1.3	DaG340 .....	190
12.1.4	EET87517 .....	193
12.1.5	EET96042 .....	197
12.1.6	EET96331 .....	200
12.1.7	GRA95205 .....	203
12.1.8	Kenna .....	207
12.1.9	LEW85440 .....	209
12.2	Bulk chondrite compositions .....	212

# 1 Introduction

## 1.1 What are meteorites?

Meteorites are fragments of extraterrestrial bodies that can provide unique insights into the history and evolution of our solar system and our planet. Today, more than 31000 different meteorites are known (GRADY and WRIGHT 2006). Many of these meteorites are considered to represent fragments of bodies from the asteroid belt, a region in space between 2 and 4 AU from the sun. Others are fragments of Mars (e.g. BOGARD and JOHNSON 1983) and the Moon (e. g. WARREN et al. 1989).

Meteorites are grouped into primitive meteorite and differentiated meteorites. Primitive meteorites are meteorites whose parent bodies have not experienced a planetary differentiation process. Many primitive meteorites contain small silicate spherules, so called chondrules, and are hence termed chondrites. Differentiated meteorites are meteorites that represent products of igneous processes – fragments of metal cores, igneous residues, cumulates or breccias of residues or cumulates. As primitive structures such as chondrules are destroyed during this process, this group is termed achondrites. Primitive achondrites have experienced high degrees of thermal metamorphism but only small degrees of igneous differentiation.

## 1.2 Weathering and shock

Meteorites show different degrees of terrestrial weathering. The degree of weathering depends on the climate of the locality and the terrestrial age. Several weathering scales are used to classify meteorites. The NASA meteorite workgroup distinguishes 3 degrees of weathering (A, B and C) for Antarctic meteorite finds (Table 1).

**Table 1 Weathering scale applied by the NASA meteorite group for Antarctic meteorites. Table taken from NORTON (2002)**

A	Minor rustiness; rust haloes on metal particles and rust stains along fractures are minor
B	Moderate rustiness; large rust haloes occur on metal particles and rust stains on internal fractures are extensive
C	Severe rustiness; metal particles have been mostly, if not totally, converted to rust and specimen is stained by rust throughout

A more sophisticated weathering scale has been developed in WLOTZKA (1993) for ordinary chondrites. Based on weathering effects observed in polished thin sections, 7 degrees of weathering (W0 – W6) are distinguished (Table 2).

**Table 2 Weathering scale developed in WLOTZKA (1993) for ordinary chondrites. Table taken from NORTON (2002)**

W0	No visible oxidation of metal or sulfide. A limonitic staining may already be noticeable in transmitted light.
W1	Minor oxidation of metal and troilite; minor oxide veins
W2	Moderate oxidation of metal and troilite, about 20 – 60% being affected
W3	Heavy oxidation of metal and troilite, 60 – 95% being replaced
W4	Complete (>95%) oxidation of metal and troilite, but no alteration of silicates
W5	Beginning alteration of mafic minerals, mainly along cracks
W6	Massive replacement of silicates by clay minerals

Depending on their impact history, meteorites show different degrees of shock. A common shock classification system is the Stöffler-Keil-Scott classification in STÖFFLER et al. (1991) and RUBIN and SCOTT (1997), based on the effects of shock in olivine, orthopyroxene and plagioclase. The Stöffler-Keil-Scott shock classification distinguishes 6 progressive degrees (S1 – S6) of shock (Table 3).

**Table 3 Meteorite shock classification based on STÖFFLER et al. (1991) and RUBIN and SCOTT (1997). Table taken and modified from NORTON (2002).**

S1	<i>Unshocked</i> - olivine and plagioclase show sharp optical extinction; P <5 GPa
S2	<i>Very weakly shocked</i> - olivine and plagioclase show undulose extinction and common irregular fractures; P 5 – 10 GPa
S3	<i>Weakly shocked</i> - Olivine shows planar fractures (shock lamellae). Feldspar does not show planar fractures. Opaque melt veins and pockets of melted material appear; P 15 – 20 GPa
S4	<i>Moderately shocked</i> – olivine shows planar fractures and a weak mosaic pattern. Plagioclase shows undulose extinction and planar fractures. Opaque melts and melt pocket become more abundant; P 30 – 35 GPa
S5	<i>Strongly shocked</i> – olivine shows strong mosaic patterns. Plagioclase is completely transformed into maskelynite glass. Opaque shock veins consist of crystalline silicate material, troilite and metal; P 45 – 55 GPa
S6	<i>Very strongly shocked</i> – olivine and pyroxene show solid state recrystallization and melting along crystal edges next to melt pockets. Some olivine changes to ringwoodite; P 75 – 90 GPa

## 1.3 Meteorite classification

### 1.3.1 Chondrites

Chondrites are aggregates of primitive components, such as chondrules, Ca-Al-rich inclusions (CAIs), amoeboid olivine aggregates (AOAs), FeNi-metal and fine grained matrix (WEISBERG et al. 2006). It is assumed that these primitive components have formed by condensation and evaporation processes in the protoplanetary disk (e.g. EBEL 2006, FEDKIN and GROSSMAN 2006) and thus represent one of the most primitive materials known in our solar system.

Several groups of chondrites are distinguished based on their chemical composition, oxidation state, isotopic composition and occurrence of primitive components (BREARLEY and JONES 1998). The three largest groups of chondrites are enstatite chondrites (E) with 483 known specimen, ordinary chondrites (O) with over 32000 known specimen and carbonaceous chondrites (C) with 1102 known specimen (GROSSMAN 2009). The enstatite chondrite group is subdivided into a low-iron (EL) and high-iron (EH) group. The ordinary chondrite group is subdivided into a group with high total iron (H), one with low total iron (L) and one with low total iron as well as low metallic iron (LL). Carbonaceous chondrites are subdivided into 8 groups of distinct compositional and isotopic composition: CI, CM, CR, CV, CO, CK, CB and CH (BREARLEY and JONES 1998, WEISBERG et al. 2006). The designating letter to the group is determined by typical chondrite of that group (e.g. I for Ivuna, M for Mighei, R for Renazzo). Two smaller groups of chondrites are Rumuruti chondrites (R) with 102 known specimen and the Kakangari chondrites grouplet (K) with 3 known specimen (GROSSMAN 2009).

Chondrites are assigned numbers (1-7) to reflect their petrographic type (Table 4). This classification is based on the work of VAN SCHMUS and WOOD (1967). The types 1 and 2 represent aqueous alteration of the chondrite. The degree of alteration decreases with increasing number. Type 3 chondrites are texturally primitive chondrites. Type 3.1 to 6 chondrites have experienced increasing degrees of thermal alteration.

**Table 4 Criteria for the chondrity classification after petrographic type after VAN SCHMUS and WOOD (1967). Table taken from WEISBERG et al. (2006).**

Criteria	Petrographic type					
	1	2	3	4	5	6
(1) Homogeneity of olivine and pyroxene	-/-	Mean deviation of pyroxene $\geq$ 5%, olivine 5%	<5% deviation to uniform	Uniform ferromagnesian minerals		
(2) Structural state of low-Ca pyroxene	-/-	Predominantly monoclinic	>20% monoclinic	$\leq$ 20% monoclinic	orthorhombic	
(3) Degree of development of secondary feldspar	-/-	Minor primary grains	Secondary <2- $\mu$ m grains	Secondary 2 – 50 $\mu$ m grains	Secondary >50- $\mu$ m grains	
(4) Igneous glass in chondrules	Absent or altered	Mostly altered some preserved	Clear, isotropic	Devitrified	absent	
(5) Metallic minerals (maximum wt% Ni)	-/-	<20 taenite minor or absent	>20 kamacite and taenite in exsolution relationship			
(6) Sulfide minerals (average Ni content)	-/-	>0.5	<0.5			
(7) Chondrules texture	No chondrules	Sharp chondrule boundaries	Some chondrules can be discerned, fewer sharp edges	Chondrules poorly delineated		
(8) Matrix texture	Fine grained opaque	Mostly fine-grained opaque	Opaque to transparent	Transparent, recrystallized		
(9) Bulk carbon (wt%)	3 - 5	0.8 – 2.6	0.2 - 1	<0.2		
(10) Water (wt%)	18 – 22	2 – 16	0.3 – 3	<1.5		

The chondrite groups can be resolved by bulk lithophile element ratios, such as Al/Si, Mg/Si and Ca/Si-ratios (BREARLEY and JONES 1998). E-chondrites give the lowest (Al, Mg, Ca)/Si-ratio, while C-chondrites give the highest ratios. Ordinary chondrites are clustered in between. Fig. 1 shows the Ca/Si-ratios of different chondrite groups.

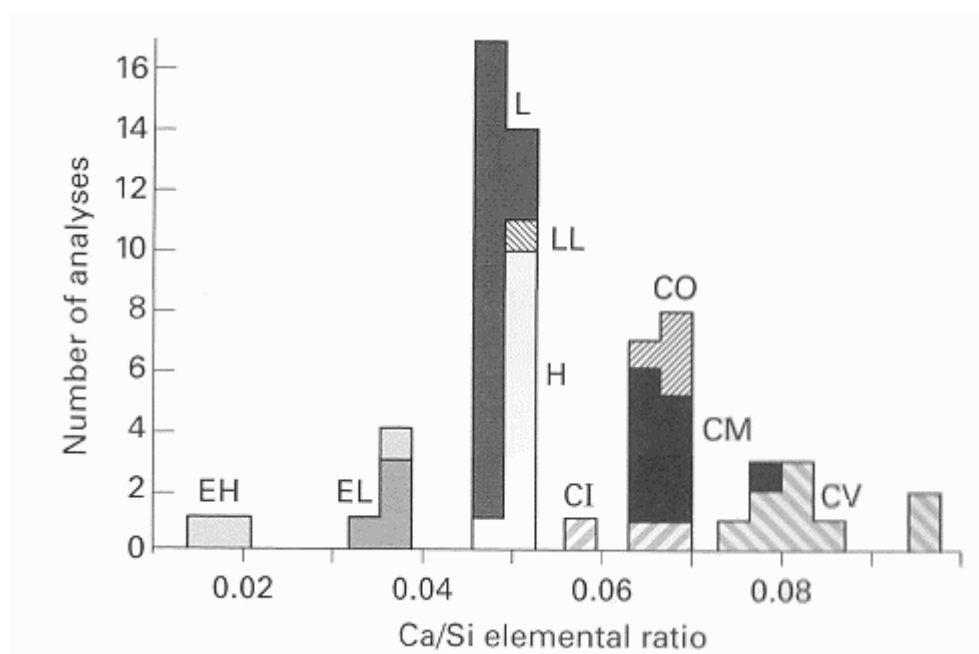


**Fig. 1** A histogram showing the bulk Ca/Si-ratio of different chondrites. E-chondrites giving Ca/Si-ratios of < 0.04, O-chondrites giving Ca/Si-ratios of 0.045-0.054 and carbonaceous chondrites giving Ca/Si-ratios of > 0.055. Diagram taken from NORTON (2002).

The chondrite groups can also be resolved by their bulk oxygen isotopic composition. Oxygen possesses three stable isotopes: The most abundant is  $^{16}\text{O}$  (99.76 %), less abundant are  $^{17}\text{O}$  (0.04 %) and  $^{18}\text{O}$  (0.20 %) (LODDERS and FEGLEY 1998).  $\delta^{18}\text{O}$  refers to the  $^{18}\text{O}/^{16}\text{O}$ -ratio of a sample relative to the  $^{18}\text{O}/^{16}\text{O}$ -ratio of a standard material. A standard material commonly used in geosciences is terrestrial ocean water, “standard mean ocean water” (SMOW).  $\delta^{18}\text{O}$  is given as deviation from SMOW in ‰.  $\delta^{17}\text{O}$  is calculated in a similar way.

In mass dependent isotope fractionation processes, fractionation in  $\delta^{18}\text{O}$  is approximately twice as large as  $\delta^{17}\text{O}$ , due to the mass differences between  $^{16}\text{O}$ ,  $^{17}\text{O}$  and  $^{18}\text{O}$ . In a three-isotope oxygen plot,  $\delta^{17}\text{O}$  is plotted against  $\delta^{18}\text{O}$ . Samples that have formed by mass dependent fractionation of a common reservoir will therefore plot on a line with a slope of  $\sim 0.5$ . All terrestrial samples plot on such a line in the three-isotope oxygen diagram. This line is known as terrestrial fractionation line (TFL).

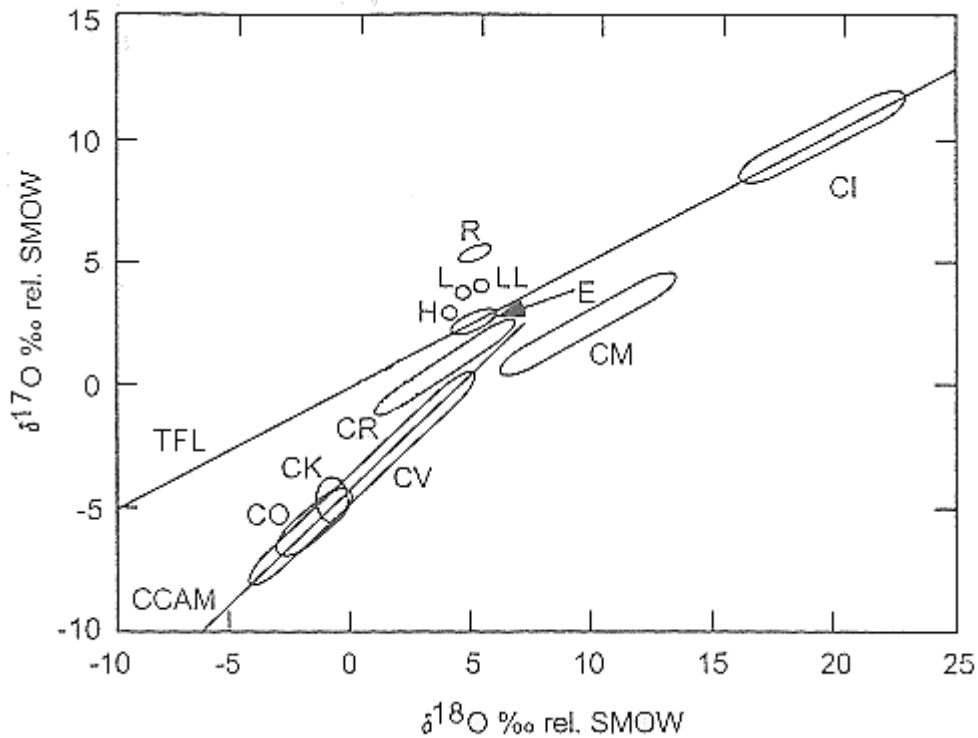


Fig. 2 Three oxygen isotope plot of bulk chondrites. R-, L-, LL, and H-chondrites plot above the TFL. E-, CI-, CM- and CR-chondrites plot on slope  $\sim 0.5$ -lines and CO- and CV-chondrites plot on the slope  $\sim 1$  CCAM-line. Diagram taken and modified from BREARLEY and JONES (1998).

In a three-isotope oxygen plot, most chondrite groups plot at a distinctive position (Fig. 2). R, H, L and LL-chondrites form distinct clusters above the TFL. Enstatite chondrites and CI-carbonaceous chondrites plot on the TFL. CM-chondrites plot on lines with a slope of  $\sim 0.5$  below the TFL, while CR-chondrites define a line with a slope of  $\sim 0.7$ . The lines defined by CI-, CM- and CR-chondrites are considered to be a result of isotope fractionation during aqueous alteration on their parent bodies (BREARLEY and JONES 1998). Anhydrous minerals in CO-, CV- and CK-chondrites plot along a line with a slope of  $\sim 1$ , below the TFL. This line is called carbonaceous chondrite anhydrous mineral line (CCAM-line). This has been interpreted as the result of a mixing process between  $^{16}\text{O}$ -enriched solids and a nebular gas component at the  $^{16}\text{O}$ -poor end of the line (BREARLEY and JONES 1998).

*Carbonaceous chondrites (C)* are characterized by lithophile element concentrations (normalized to Mg and Cl1)  $\geq$  Cl1 (BREARLEY and JONES 1998) and oxygen isotopic compositions that plot on or below the TFL (WEISBERG et al. 2006).

CI-chondrites are, except for very volatile elements, a close match to the composition of the solar photosphere (BREARLEY and JONES 1998). CI-chondrites are therefore considered to represent the average solar system composition and are thus used as reference material.

Nine CI-chondrites are known (GROSSMAN 2009), each belonging to the petrographic type 1. CI1-chondrites do not contain chondrules or CAIs. It is not clear whether they were destroyed during aqueous alteration or were never present (BREARLEY and JONES 1998). CV-chondrites are characterized by high abundance of large CAIs and AOAs (WEISBERG et al. 2006). Of the 153 known CV-chondrites all are of type 3, except for Mundrabilla 012, which is of type 2 (GROSSMAN 2009). CV-chondrites are subdivided into oxidized (CV<sub>ox</sub>) and reduced (CV<sub>red</sub>) subgroups, based on their metal/magnetite ratios and Ni concentrations in sulfides and metal (BREARLEY and JONES 1998, WEISBERG et al. 2006). CM-chondrites are the most abundant group of C-chondrites with 360 known specimen (GROSSMAN 2009). CM-chondrites are of petrographic type 2, except for 24 meteorites, which are type 1 (GROSSMAN 2009). 176 CO-chondrites are known (GROSSMAN 2009). The petrologic type ranges from 3.0 to 3.8 (GROSSMAN 2009). CK-chondrites are of petrographic type 3 – 6 and represent the only group of carbonaceous chondrites that experienced extensive (> type 4) thermal alteration. 182 CK-chondrites are known, of which 19 meteorites are of type 3 (GROSSMAN 2009). CK- and CV-chondrites show similar mineralogical and chemical properties, such as oxygen isotopic compositions (Fig. 2), which supports a close relationship between both groups (WEISBERG et al. 2006). Unlike other carbonaceous chondrites, CK-chondrites do not plot on a line but form a distinct cluster (Fig. 2) in the three isotope oxygen plot, as thermal alteration does not influence the oxygen isotopic composition. The 118 CR-chondrites are of type 2, except for 6 meteorites, which are unclassified or type 1. CR-chondrites are metal-rich, containing ~7 vol% metal (BREARLEY and JONES 1998). CH-chondrites are characterized by high FeNi-metal abundances of ~20 vol% (WEISBERG et al. 2006). The 21 known specimen are of type 3 (GROSSMAN 2009). CB-chondrites contain the highest abundance of FeNi-metal in carbonaceous chondrites with 60-80 vol% metal (WEISBERG et al. 2006). Based on the metal abundance, CB-chondrites are divided into CB<sub>a</sub>- (metal ~60 vol%) and CB<sub>b</sub>-chondrites (metal >70 vol%). Of 13 known CB-chondrites, 5 are CB<sub>a</sub>, 6 are CB<sub>b</sub> and 2 are unclassified (GROSSMAN 2009).

*Ordinary chondrites (O)* are characterized by refractory lithophile element concentrations (normalized to Mg and CI1) lower than CI1. Ordinary chondrites are of petrographic type 3 – 6. As thermal metamorphism does not influence the oxygen isotopic composition, the three ordinary chondrite groups form distinct clusters above the TFL in the three isotope oxygen diagram (Fig. 2). O-chondrites show different oxidation states which can be distinguished in

the Urey-Craig-diagram (Fig. 3). The Urey-Craig-diagram plots the molar (Fe-metal + FeS)/Si-ratio against the molar FeO/Si-ratio (BREARLEY and JONES 1998).

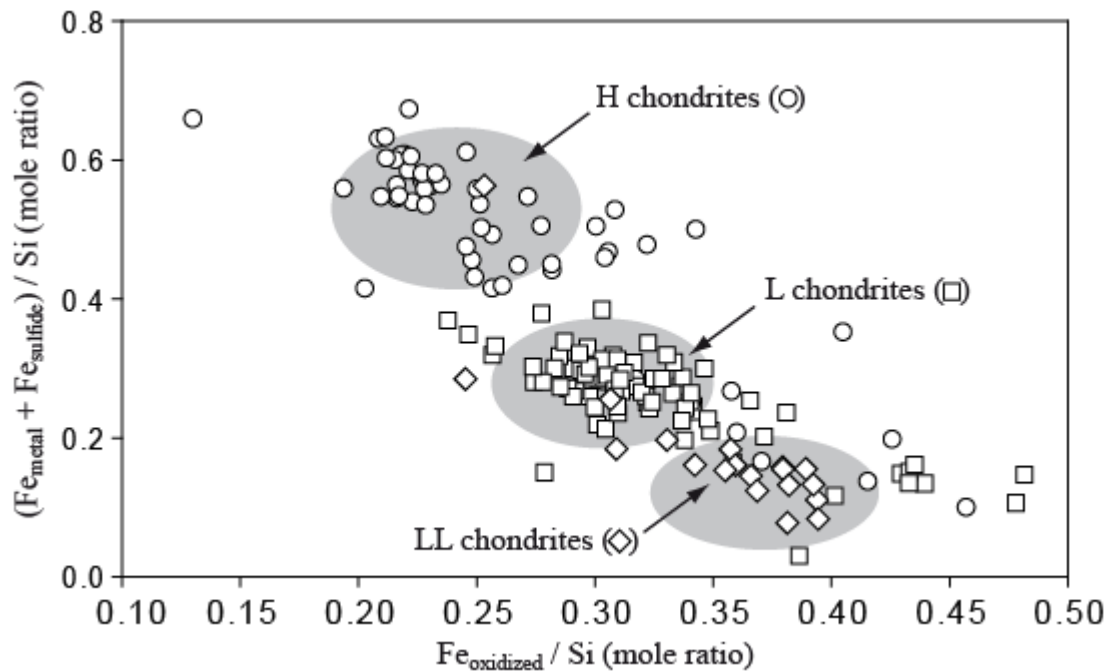


Fig. 3 A Urey-Craig diagram of bulk O-chondrites. H-, L and LL-chondrites can be distinguished. Meteorite data taken from JAROSEWICH (1990).

Ordinary chondrites can also be distinguished by their total iron content and the amount of fayalite in their olivine. H-chondrites contain 16-20 mole% *fa* and 15-19 wt% total Fe, L-chondrites contain 21-25 mole% *fa* and 1-10 wt% total Fe, while LL-chondrites contain 26-32 molt% *fa* and 1-3 wt% total Fe (NORTON 2002).

*Enstatite chondrites (E)* are characterized by enstatite being the primary mineral phase in their chondrules (WEISBERG et al. 2006). They have formed under extremely reducing conditions, probably in a region close to the sun, inside the mercury orbit (NORTON 2002). E-chondrites contain a wide variety of unusual sulfide, metal and nitride phases, such as oldhamite (CaS), niningerite [(Mg, Fe, Mn)S] or sinoite (Si<sub>2</sub>N<sub>2</sub>O) (WEISBERG et al. 2006). They are subdivided into EL (low-iron) and EH (high-iron) chondrites. EL-chondrites contain ~25 wt% total iron with ~3.5 wt% sulfide, while EH-chondrites contain ~30 wt% total iron with ~5 wt% sulfide (NORTON 2002). E-chondrites are of the petrographic type 3 – 6 (GROSSMAN 2009).

*Rumuruti-like chondrites (R)* are meteorites that are similar to ordinary chondrites with respect to their refractory lithophile elements. In the three isotope oxygen plot, they form a

well-defined cluster above the ordinary chondrites (Fig. 2)( BREARLEY and JONES 1998). In contrast to ordinary chondrites, Rumuruti-like chondrites are very oxidized. FeNi-metal is absent and their olivine is very FeO-rich ( $f_{a_{37-40}}$ ). Most of the R-chondrites have been subject to thermal metamorphism and are of petrographic type  $> 3.1$  (WEISBERG et al. 2006).

### 1.3.2 Achondrites

Heating of a primitive asteroidal body, by decay of short lived isotopes such as  $^{26}\text{Al}$  or  $^{60}\text{Fe}$ , can lead to melting processes within the asteroid. Shortly after the beginning of melting basaltic crust can be formed and, if the melting persists, FeNi-metal and sulfides can migrate to form a metal core (McCoy et al. 2006). Meteorites that are derived from such a differentiated parent body are called achondrites.

*Lunar meteorites* have been associated with the moon as their Fe/Mn-ratios, oxygen isotopic composition and mineralogy are similar to lunar rock samples obtained from Apollo- and Luna-missions (WEISBERG et al. 2006). Lunar meteorites span a wide range of rock types including brecciated and unbrecciated mare basalts, highland regolith breccias, intermixed mare/highland breccias and highland impact melt breccias (WEISBERG et al. 2006).

*The SNC-meteorites* (shergottites, nakhlites and chassignites) have been associated with Mars. Their oxygen isotopic composition differs from those of other meteorites and they plot on a similar line with a slope of  $\sim 0.52$  above the TFL (CLAYTON and MAYEDA 1996). This suggests a similar parent body for the SNC-meteorites (WEISBERG et al. 2006). Ages of SNC-meteorites range from  $\sim 4.5$  Ga to at least 330 Ma, suggesting a large parent body (MCSWEEN and TREIMAN 1998). The isotopic composition and abundance of Ar and other noble gases trapped within impact-melted glass in the shergottites EETA79001 is similar to the martian atmosphere as determined by the Viking Spacecraft (MCSWEEN and TREIMAN 1998). SNC-meteorites represent volcanic rocks (basaltic shergottites and nakhlites) and plutonic rocks (Iherzolitic and olivine phyrlic shergottites, Chassigny, ALH84001) (WEISBERG et al. 2006).

*The HED-clan* consists of eucrites, howardites and diogenites. Eucrites and diogenites are basalts and orthopyroxene cumulates, while howardites are polymict breccias of eucritic and diogenitic composition (WEISBERG et al. 2006). Similar Fe/Mn-ratios in pyroxenes and oxygen isotopic composition suggest a genetic connection between the HED-meteorites (WEISBERG et al. 2006). The Vesta asteroid and eucrites show similar visible and infrared reflectance

spectra, which led to the suggestion that Vesta is the HED parent body (MITTLEFEHLDT et al. 1998).

*Angrites* are extremely alkali depleted basalts. They consist of Ca-Al-Ti-rich pyroxenes, Ca-rich olivine and anorthitic plagioclase (WEISBERG et al. 2006). It has been suggested, that angrites formed from CAI-enriched melts (WEISBERG et al. 2006).

*Aubrites* represent highly reduced achondrites with a close relation to enstatite chondrites and are also termed enstatite achondrites (NORTON 2002). They consist of ~75-90 vol% of FeO-free enstatite and minor plagioclase, FeO-free diopside and forsterite. They are considered to have formed by partial melting at high temperatures (WEISBERG et al. 2006).

*Mesosiderites* are breccias composed of equal portions of Fe-Ni-metal plus troilite and silicate material. The FeNi-metal is found in fine grained matrix of millimeter to submillimeter sized grains, intimately mixed with equally fine grained silicate grains. The silicate material occurs as clasts of basalts, gabbros, and pyroxenites with minor dunite and rare anorthosite (WEISBERG et al. 2006).

*Pallasites* are olivine-metal assemblages, with olivine representing 35 – 85 vol% of the material (WEISBERG et al. 2006). Four different kinds of pallasites can be distinguished based on differences in their silicate mineralogy and composition, their metal composition and their oxygen isotopic composition. The four groups are the main group pallasites, the Eagle Station grouplet, the pyroxene-pallasite grouplet and the Milton ungrouped pallasite. These differences suggest that the pallasites do not stem from a single parent body. (WEISBERG et al. 2006)

*Iron meteorites* consists mostly of metallic iron with 5 – 20 wt% Ni, although individual exceptions with up to 60 wt% Ni are known (MITTLEFEHLDT et al. 1998). Many iron meteorites show a typical texture of intergrown high-Ni taenite and low-Ni kamacite lamellae when etched. This texture is called Widmanstätten texture. A miscibility gap between high-Ni and low-Ni phases below 800°C leads to the precipitation of low-Ni kamacite along the octahedron planes of the host material during slow cooling (MITTLEFEHLDT et al. 1998). Iron meteorites with a Widmanstätten texture are therefore termed octaedrites. Octaedrites are distinguished into several subgroups based on the width of the kamacite lamellae. Iron meteorites with Ni contents below 6 wt% Ni that consist almost entirely of kamacite show

no Widmanstätten textures and are called hexaedrites (MITTFEHLDT et al. 1998). Iron meteorites that show no Widmanstätten texture and consist entirely of taenite are called ataxites (NORTON 2002).

A classification that provides more genetic insights into the iron meteorites is based on their trace element content of the metal phase. Ga, Ge and Ir are commonly used to classify iron meteorites. Ga and Ge are the most volatile siderophile elements and, analogous to chondrites, more volatile elements tend to be more strongly fractionated (MITTFEHLDT et al. 1998). Iridium is strongly fractionated between liquid metal and solid metal (MITTFEHLDT et al. 1998). The trace elements are plotted on a logarithmic scale against the bulk Ni-concentration in the iron meteorite. Early works distinguished four groups and termed them I – IV in order of decreasing Ga and Ge content (MITTFEHLDT et al. 1998). When more advanced techniques allowed higher resolution of trace element concentrations letters were added to further subdivide the 4 original groups (NORTON 2002). Three groups (IAB, IIAB, IIIAB and III CD) have been recombined when transitional iron meteorites were found (NORTON 2002).

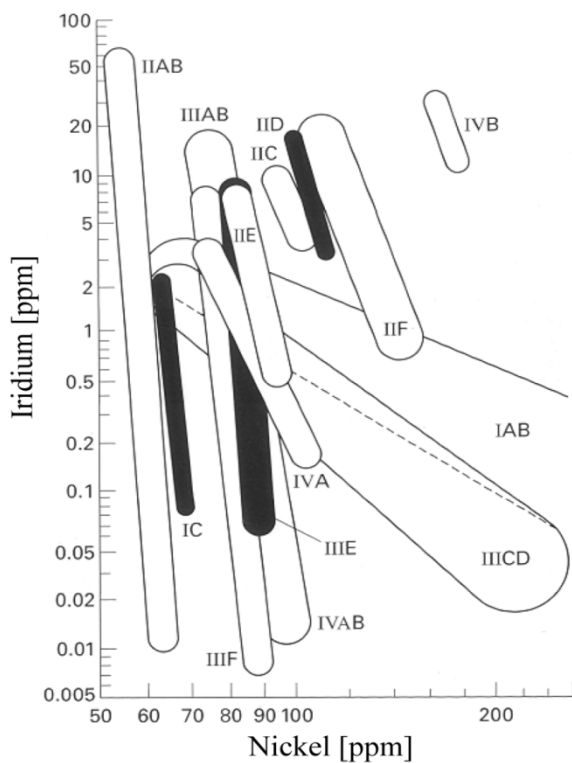


**Fig. 4** Plot of Iridium abundance against Nickel abundance in iron meteorites. Several groups can be distinguished. Diagram taken from NORTON (2002).

Today, 13 groups of iron meteorites are distinguished (MITTLEFEHLDT et al. 1998). On a plot of Ir against Ni (Fig. 4), some groups (for example IIAB, IIC, IID) plot in steeply dipping fields of similar shapes. This has been interpreted as the result of fractional crystallization from a metallic melt and the meteorites of these groups are hence termed magmatic iron meteorites (MITTLEFEHLDT et al. 1998). The IAB and IIICD group plot in differently shaped fields, which suggests a different origin and are hence called non-magmatic iron meteorites. The formation of non-magmatic iron meteorites remains yet unclear (MITTLEFEHLDT et al. 1998).

### **1.3.3 Primitive Achondrites**

Primitive achondrites are meteorites of approximately chondritic composition but with igneous or metamorphic textures (MITTLEFEHLDT et al. 1998). Brachinites (primitive dunitic wherlites), acapulcoites, lodranites, silicates from IAB and IIICD irons are considered to be primitive achondrites (MITTLEFEHLDT et al. 1998). Ureilites are also considered to be primitive achondrites (e. g. WEISBERG et al. 2006, MITTLEFEHLDT et al. 1998). Since ureilites are the central meteorite group of this work, they will be reviewed in detail in the next chapter.

## 2 The ureilite group

### 2.1 Introduction

Ureilites are well equilibrated carbon-rich ultramafic rocks. They represent the second most abundant group of achondrites with 251 known specimens (GROSSMAN 2009). The first ureilite fell in 1886 near Novo-Urei in Russia (NORTON 2002). Although clearly achondritic in terms of their texture and mineralogy, ureilites show features of primitive meteorites, such as high abundances of noble gases, high siderophile trace element abundances and CV- and CM-chondrite-like bulk oxygen isotopic composition (MITTFELDLT et al. 1998).

Ureilites are divided into two subgroups: monomict and polymict ureilites: Polymict ureilites are complex breccias containing clasts of typical monomict ureilites (which are discussed later in this chapter) and a variety of other components, including carbon, suessite, sulfides and minor apatite (GOODRICH et al. 2004). Some of the lithic clasts in polymict ureilites resemble material from a variety of other meteorites, such as enstatite chondrites, Angrites, aubrites and feldspathic melt rocks (MITTFELDLT et al. 1998). The composition of olivine and pyroxene in polymict ureilites is consistent with a derivation from monomict ureilites (GOODRICH et al. 2004). Plagioclase is common in polymict ureilites, but very rare in monomict ureilites (MITTFELDLT et al. 1998). Twenty polymict ureilites are currently known (GROSSMAN 2009). Monomict ureilites will be reviewed in greater detail in the remainder of this chapter.

### 2.2 Mineralogy

#### 2.2.1 Silicates

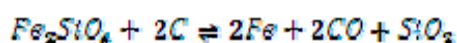
Ureilites typically consists of olivine and pyroxene and about 10 wt% of an interstitial carbonaceous material referred to as vein material (MITTFELDLT et al. 1998). Three types of ureilites are distinguished as based on their mineralogy. In the majority of all ureilites (~80 %), pigeonite ( $Wo_{\sim 7-13}$ ) is the sole pyroxene (MITTFELDLT et al. 1998). Augite-bearing ureilites are rare (~10 %) and contain augite in addition to orthopyroxene or pigeonite. The third type of ureilites are olivine-orthopyroxene-ureilites and show orthopyroxene ( $Wo_{4.5-5}$ ) instead of or in addition to pigeonite.

Modal pyroxene/(pyroxene+olivine) ratios range from 0 to ~0.9, averaging at ~0.3 (MITTLEFEHLDT et al. 1998). Typical ureilite textures show coarse grained, anhedral olivines and pyroxenes that meet in triple junctions. Olivines may contain small, rounded inclusions of pyroxenes (MITTLEFEHLDT et al. 1998).

A pronounced elongation in olivines and pyroxenes has been described in several ureilites, such as Kenna, Novo-Urei, Dingo pup Donga, RC027 and Dyalpur (BERKLEY et al. 1976, BERKLEY et al. 1980, GOODRICH et al. 1987b). Fabric analyses (BERKLEY et al. 1976, BERKLEY et al. 1980) show that this elongation reflects a foliation of the {100} crystal face of the olivine and a lineation defined by the crystallographic [001] axis of the olivine and pyroxene. Some ureilites show a mosaiced texture and much smaller grain sizes, which has been interpreted as a result of shock (MITTLEFEHLDT et al. 1998).

The olivine geochemistry is similar for all ureilites except for the amount of fayalite (*fa*), which ranges from *fa*<sub>2</sub> (ALH84136) to *fa*<sub>23</sub> (e.g. CMC04044, GROSSMAN 2009), with a maximum in *fa* distribution at ~*fa*<sub>20</sub> (MITTLEFEHLDT et al. 1998). Within each ureilite *fa* is constant in olivine cores. Coexisting pyroxenes span a similar range with respect to FeO concentrations, which indicates olivine/pyroxene equilibrium (MITTLEFEHLDT et al. 1998). Ureilite olivines are characterized by high CaO (0.3 - 0.45 wt%) and Cr<sub>2</sub>O<sub>3</sub> (~0.56-0.85 wt%) concentrations (MITTLEFEHLDT et al. 1998).

A characteristic feature of ureilite olivines and pyroxenes are reduction rims usually associated with carbonaceous material (e.g. BERKLEY et al. 1976, BERKLEY et al. 1980, GOODRICH et al. 1987b). These rims are almost FeO-free (*fa*<sub>0</sub>-*fa*<sub>2</sub>) and riddled with tiny inclusions of low-Ni metal. Most of these rims are narrow (10-100µm), although some ureilites (ALH82130, HaH126) show very large reduction rims with almost completely reduced olivine grains (MITTLEFEHLDT et al. 1998). Reduction rims are smaller and less frequently found in pyroxene grains. These reduced rims have been attributed to a solid state reaction, where the fayalite-component of the olivine has reacted with intergranular carbon (Eq. 1) to form high mg# residual olivine and Ni-poor metal (e.g. WASSON et al. 1976, SINGLETARY and GROVE 2003).



Eq. 1

### 2.2.2 Vein material

The vein material occurs along silicate grain boundaries but can also intrude the silicates along cracks and cleavage planes (MITTLEFEHLDT et al. 1998). It contains carbon phases, FeNi-metal and interstitial silicates. The carbon phases are mainly graphite, but other minerals such as chaoite,  $\mu\text{m}$ -sized grains of lonsdaleite and diamond have also been identified in several ureilites (VDOVYKIN 1972, VDOVYKIN 1975, BERKLEY et al. 1976, MARVIN and WOOD 1972).

Carbon concentrations in ureilites range from 0.2 wt% (e.g. Goalpara) to up to  $\sim 6$  wt% (e.g. North Haig) (GRADY et al. 1985, WIIK 1972, JAROSEWICH 1990, MCGALL and CLEVERLY 1968, TAKEDA 1987) with an average carbon content of  $\sim 3$  wt%. The ureilite carbon content does not correlate with  $f_a$ . The graphite is usually fine grained, although large mm-sized euhedral graphite crystals have also been found within several ureilites (BERKLEY and JONES 1982, TREIMAN and BERKLEY 1994).

The origin of the carbon has been subject to discussion. WLOTZKA (1972) pointed out, that ureilite olivines were not in equilibrium with carbon in the vein material, which led to the assumption that carbon was introduced into the system by a "late event". Subsequent work on silicate reduction in the presence of carbon (e.g. BERKLEY and JONES 1982, WALKER and GROVE 1993) has shown that the reduction (Eq. 1) is strongly pressure dependent, as large volumes of CO-gas are formed. Reduction therefore may be stabilized by the depth in which the ureilite material is positioned on the ureilite parent body. WASSON et al. (1976), HIGUCHI et al. (1976) and WILKENING and MARTI (1976) proposed a carbon-rich impactor to account for the high noble gas and carbon concentrations in ureilites. The presence of large graphite crystals in relatively unshocked ureilites would contradict the impact-hypothesis (BERKLEY and JONES 1982, WACKER 1986). WEBER et al. (1976) pointed out that carbon in carbonaceous chondrites occurs mostly in form of hydrocarbons. It would therefore be unlikely that large amounts of noble gases, which are typical for ureilites, could be retained during graphitization of the hydrocarbons. Instead, a model with graphite as nebular condensate was invoked to account for carbon in ureilites (WEBER et al. 1976). A similar model had been proposed by JANSSENS et al. (1987). RAI et al. (2003) argues, that if ureilite noble gases were implanted into the carbon phases from a plasma, the  $(^{132}\text{Xe}/^{36}\text{Ar})_0$ -ratio is a function of the temperature of the plasma. KALLEMEYN et al. (1996) argues that  $\Delta^{17}\text{O}$  (the deviation of  $\delta^{17}\text{O}$  from the TFL) of any meteorite is a function of nebular temperature and therefore of

formation location. The lack of correlation of  $(^{132}\text{Xe}/^{36}\text{Ar})_0$  and  $\Delta^{17}\text{O}$  in ureilites led RAI et al. (2003) to suggest that carbon in ureilites is not related to ureilite silicates. A strong argument for a primary origin of the carbon are cohenite-bearing metal-sulfide spherule inclusions in ALHA77257, ALHA78262 and ALHA78019 described in GOODRICH and BERKLEY (1986). These spherule inclusions were interpreted as droplets of a primary metal liquid that has been entrapped during olivine crystallization (GOODRICH and BERKLEY 1986). The presence of cohenite within these droplets suggests that at least some of the carbon in ureilites is primary in origin.

Published Ni-concentrations in vein metal range from <1 to ~9 wt%. Cobalt concentrations range from 0.1 to 0.6 wt% and P abundances range from 0.1 to 0.4 wt%. Silicon ranges from 0 to ~4 wt% (BERKLEY et al. 1980, BERKLEY 1986). Several authors proposed that ureilite vein metal represents residual metal formed by the removal of a S-rich melt (e.g. TAKEDA 1987, JONES and GOODRICH 1989, HUMAYUN et al. 2005, WARREN et al. 2006, RANKENBURG et al. 2008). However, as VAN ORMAN et al. (2009) pointed out, the removal of only S-rich melt is not a perfect explanation of siderophile element abundances in ureilite vein metal.

Other minor phases that have been identified in the vein metal include schreibersite (MITTLEFEHLDT et al. 1998), suessite (KEIL et al. 1982) and interstitial silicate. These interstitial silicates are fine grained and common in ureilites. They usually consist of Low-Ca pyroxene ( $\text{Wo}_{1-14}$ ) and augite ( $\text{Wo}_{26-43}$ ) (MITTLEFEHLDT et al. 1998). Interstitial silicates show much higher mg# than the core of the main pyroxene grains and lower Mn/Mg, Cr/Mg, Na/Mg, Ti/Mg and Al/Mg-ratios (GOODRICH et al. 1987a).

### **2.2.3 Spherule inclusions in olivine**

Spherule inclusions have been reviewed in great detail in GOODRICH and BERKLEY (1986). They have been found in ALHA78262, ALHA77257, ALHA82130, ALHA78019 and PCA82506. Minerals found in spherule inclusions are cohenite, Fe-Ni-metal, sulfides and rare phosphorus-bearing minerals (GOODRICH and BERKLEY 1986). GOODRICH and BERKLEY (1986) report Ni concentrations of bulk spherule inclusions ranging from 2.7 wt% in ALH82130 ( $fa_6$ ) to 6.6 wt% in ALHA78262 ( $fa_{21}$ ), Co-concentrations range from 0.37 wt% in ALH82130 ( $fa_6$ ) to 0.62 wt% in ALHA78262 ( $fa_{21}$ ). Reported Ni concentrations in spherule Fe-Ni-metal range from 5.8 wt% in ALH82130 ( $fa_6$ ) to 12.2 wt% in ALHA78262 ( $fa_{21}$ ), while Co-concentrations in Fe-Ni-metal range from 0.56 wt% in ALH82130 ( $fa_6$ ) to 0.88 wt% in ALH82130 ( $fa_6$ ). From the

distribution of C and Ni, as well as the present mineral phases, GOODRICH and BERKLEY (1986) concluded that spherule inclusions represent a Fe-Ni-S-C-liquid. The presence of cohenite and sulfide within the same spherule indicates that the liquid has been entrapped prior to the separation of an S-rich and a C-rich liquid melt.

## 2.3 Ureilite bulk rock chemistry

### 2.3.1 Lithophile elements

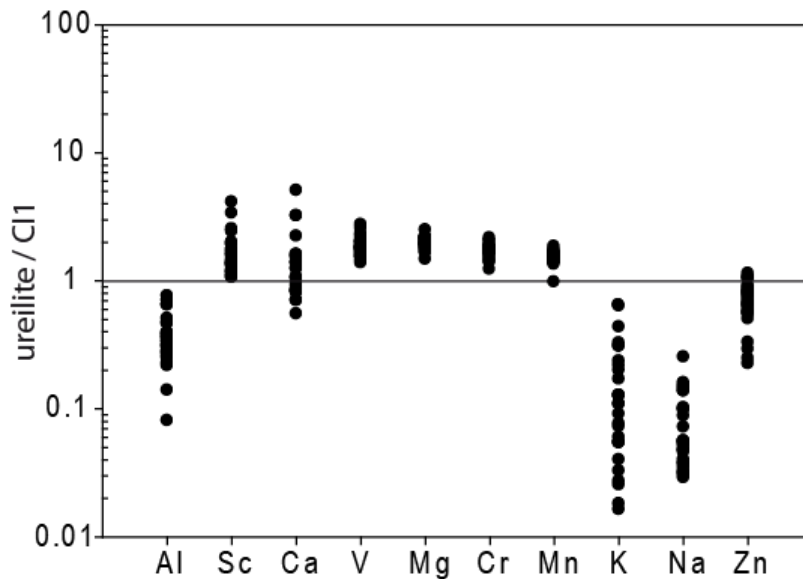


Fig. 5: CI1-normalized lithophile element concentrations of 27 bulk monomict ureilites. Bulk ureilite data from compiled data in WARREN et al. (2006), CI1-data taken from LODDERS and FEGLEY (1998). Sc, V, Mg, Cr and Mn are enriched while Al, K and Na are slightly depleted. Ca and Zn occur in near-CI1-chondritic concentrations.

Ureilites are enriched in Sc, V, Mg, Cr and Mn ( $\sim 2 \cdot \text{CI1}$ ) relative to CI1 (Fig. 5). The lithophile element Ca is usually present in near-chondritic abundances, depending on pyroxene content and species. Very Ca-poor ( $0.09 \cdot \text{CI1}$  – Haverö (WIIK 1972, WÄNKE et al. 1972) and very Ca-rich ( $3.7 \cdot \text{CI1}$  – LEW88774, WARREN et al. 2006) ureilites have also been reported. Zn is present in nearly chondritic abundances. Elements that are typical constituents of feldspar such as Al, K and Na (and Sr, Rb) are slightly depleted in bulk ureilites, which has been interpreted as loss of a basaltic component (MITTFEHLDT et al. 1998). Ureilite Ca/Al-ratios are superchondritic, ranging from  $\sim 2$  to  $14 \cdot \text{CI1}$  (MITTFEHLDT et al. 1998). Bulk ureilites show a negative FeO/MnO-correlation similar to olivine and pyroxene and Mn/Mg-ratios are nearly constant at  $0.61 \pm 0.07 \cdot \text{CI1}$  (MITTFEHLDT et al. 1998).

### 2.3.2 Siderophile elements

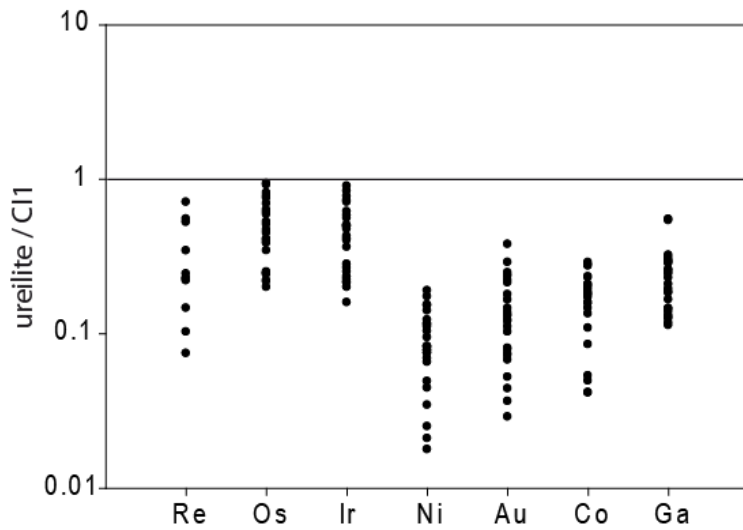
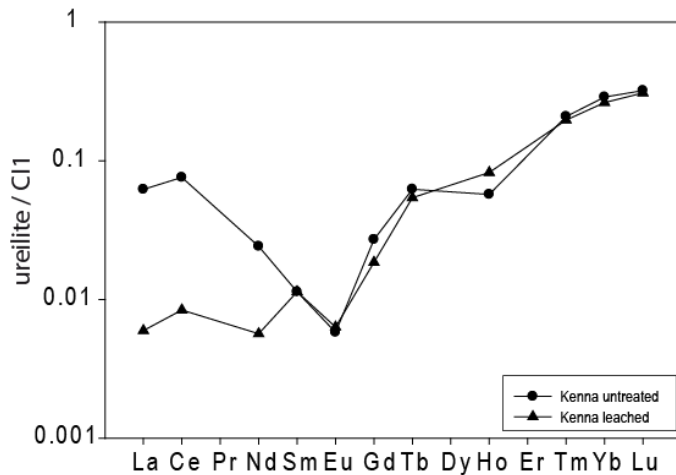


Fig. 6: CI1-normalized bulk siderophile element concentrations of several monomict ureilites. Data taken from compiled ureilite data in WARREN et al. (2006), CI1-data taken from LODDERS and FEGLEY (1998).

The refractory siderophile elements, Re, Os and Ir (and W, MITTLEFEHLDT et al. 1998) are depleted ranging from  $\sim 0.1$  to  $1 \cdot CI1$ . More volatile siderophile elements such as Ni, Au, Co, Ga and Ge are more depleted than the refractory siderophile elements (e.g. MITTLEFEHLDT et al. 1998, WARREN et al. 2006) with Ni ranging from  $0.02$  to  $0.24 \cdot CI1$ , Au ranging from  $0.05$  to  $0.38 \cdot CI1$ , Co ranging from  $0.05$  to  $0.44 \cdot CI1$  and Ga ranging from  $0.11$  to  $0.55 \cdot CI1$ . Siderophile element concentrations (relative to CI1) generally increase in the order:  $Ni < Au < Co < Ga < Ge$  (MITTLEFEHLDT et al. 1998). No correlation between siderophile element concentrations and olivine  $fa$  is observed (MITTLEFEHLDT et al. 1998).

### 2.3.3 Rare Earth Elements (REE)

In general, all ureilites are depleted in rare earth elements, relative to CI1. The first rare earth element patterns that were determined showed a distinctive V-shape (Fig. 7), with a severe middle-REE depletion (MITTLEFEHLDT et al. 1998). Eu values can be as low as  $\sim 0.006 \cdot CI1$  (Kenna - BOYNTON et al. 1976).



**Fig. 7:** Cl1 normalized Rare Earth Element composition of bulk ureilites. The ureilites show a typical V-shaped pattern and subchondritic values. Data taken from BOYNTON et al. (1976), WÄNKE et al. (1972) and GOODRICH et al. (1987b).

Ureilite REE-patterns published in EBIHARA et al. (1990) do not show V-shaped patterns but are depleted in the LREE as well (Fig. 8). Still, their data show a distinctive depletion in Eu. LREE-depleted and HREE-enriched patterns are typical for REE partitioning between melt and olivine and pyroxene (KENNEDY et al. 1993).

In some ureilites, for example RC027 (GOODRICH et al. 1987b), one subsample shows a typical V-shaped pattern, while another subsample shows a LREE-depleted pattern. In GOODRICH et al. (1987b) and GOODRICH et al. (1991) an inhomogeneously distributed LREE-rich component was proposed. The LREE-enriched component in ureilites can be removed by leaching with mild acids (BOYNTON et al. 1976, GOODRICH et al. 1991, GOODRICH et al. 1995). U-Pb, Th-Pb and Sm-Nd isotopic systematics in the Goalpara ureilite led TORIGOYE-KITA et al. (1995a) to the conclusion that the LREE-rich component might have been introduced into the ureilites as terrestrial contamination. GOODRICH et al. (1995) suggested that the LREE-rich component represents a metasomatic fluid.

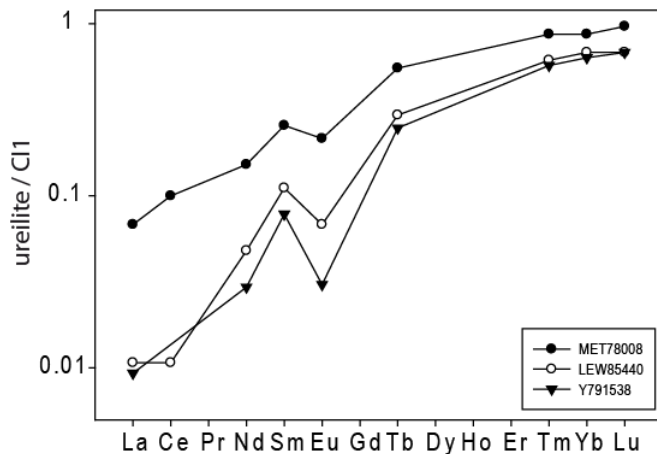


Fig. 8: CI1 normalized Rare Earth Element composition of bulk ureilites. The ureilites are severely depleted in the LREE but show a distinctive depletion in Eu as well. Data taken from EBIHARA et al. (1990).

### 2.3.4 Noble gases

Ureilites contain noble gases in chondritic abundances. The relative abundance pattern of noble gases is similar to a “strongly fractionated” or “planetary” type as it is in carbonaceous chondrites (WEBER et al. 1971, WEBER et al. 1976, WILKENING and MARTI 1976, RAI et al. 2003), as opposed to the solar or cosmogenic type. Analysis of carbonaceous vein material showed that noble gases are enriched at least 600-fold relative to the silicates of the same ureilite (WEBER et al. 1971, WEBER et al. 1976). Graphite in the vein material is the principal gas carrier, except for diamond-bearing ureilites, where the gas is hosted in the diamonds, while the graphite is virtually gas-free (RAI et al. 2003). The majority of the Ne and He in bulk ureilites is cosmogenic in origin and RAI et al. (2003) assume that the radiogenic contribution is negligible. Ureilites show very low  $^{40}\text{Ar}/^{36}\text{Ar}$ -ratios which is consistent with an early K-fractionation on the ureilite parent body (MITTFELDELT et al. 1998).

### 2.3.5 Oxygen isotopes

Unlike any other achondrite, ureilites plot on a slope  $\sim 1$ -line in an oxygen three-isotope plot (Fig. 9) at the CCAM-line, with  $\delta^{18}\text{O}$  ranging from  $\sim 5$  to  $\sim 9$  and  $\delta^{17}\text{O}$  ranging from  $\sim 0$  to 4 (CLAYTON and MAYEDA 1988, CLAYTON and MAYEDA 1996, YAMAGUCHI et al. 2005). This variability in oxygen isotopic composition led CLAYTON and MAYEDA (1988) to suggest that the ureilite parent body could not have undergone extensive melting, homogenization and differentiation. CLAYTON and MAYEDA (1988) further propose that ureilites must be products of isotopically heterogeneous material. No discrete grouping is observed that would indicate the presence of several parent bodies (CLAYTON and MAYEDA 1996). Different clasts from polymict ureilites Nilpena, DaG319 and EET83309 span much of the range of isotopic

compositions which suggests that they originated from a single heterogeneous parent body (CLAYTON and MAYEDA 1988, GUAN and LESHIN 2001, KITA et al. 2004). In contrast, FRANCHI et al. (1997) found 4 distinctive ureilite groups ( $\Delta^{17}\text{O} = -0.37 \pm 0.055$  (A),  $-0.63 \pm 0.031$  (B),  $-0.85 \pm 0.036$  (C) and  $-0.99 \pm 0.030$  (D)), containing 6 ureilites each. The groups C and D are poorly resolved and may represent a single group. Due to similarities in ureilite composition and textures, FRANCHI et al. (2001) interprets the groups as isolated regions within the ureilite parent body.

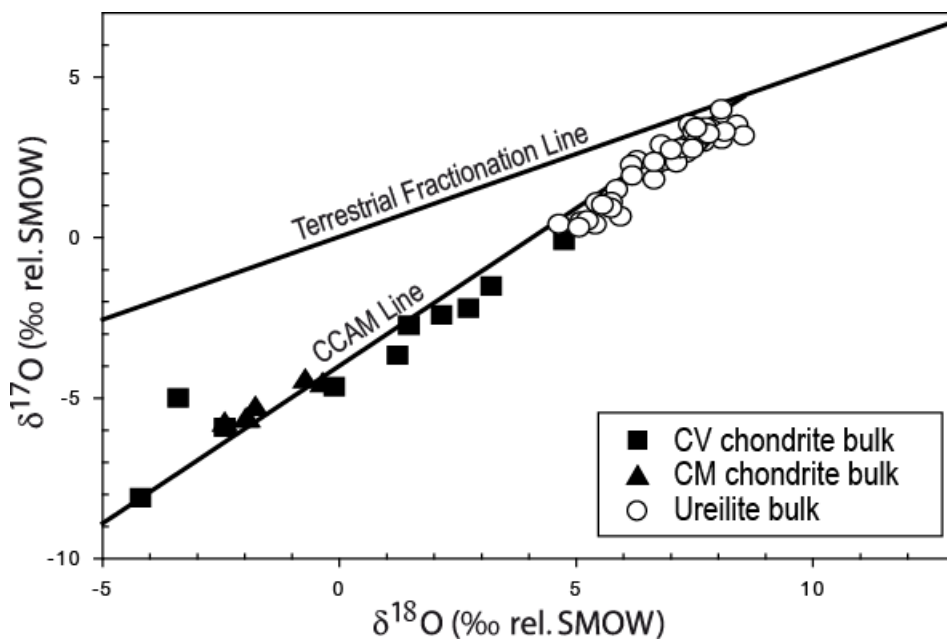


Fig. 9: Relationship between oxygen isotopic composition of bulk ureilites and oxygen isotopic composition of bulk CV- and CM-chondrites. Data taken from CLAYTON and MAYEDA (1996). Unlike any other achondrite, ureilites plot on a line, very similar to those defined by primitive CV- and CM-chondrites.

The line defined by ureilites in the three-isotope oxygen plot is very similar to the line defined by CV, CO and CM-chondrites. CLAYTON and MAYEDA (1996) therefore suggest that the ureilite parent body might have an origin similar to CV3- or CO3-chondrites, although the fit is not perfect. Ureilites show a good negative correlation between  $\Delta^{17}\text{O}$  and mg# (CLAYTON and MAYEDA (1988), CLAYTON and MAYEDA (1996), MITTFELDLT et al. 1998). WALKER and GROVE (1993) suggested that either both the variation in  $\Delta^{17}\text{O}$  and mg# are the result of a nebular process, or the variation in  $\Delta^{17}\text{O}$  represents an isotopically stratified parent body.

### 2.3.6 Carbon isotopes

While CV3-chondrites represent a possible parent body material for ureilites with respect to oxygen isotopes, this is not the case for carbon isotopes. Reported  $\delta^{13}\text{C}$  values of ureilites range from 1 to -12 (GRADY et al. 1985, GRADY and WRIGHT 2003, HUDON et al. 2004). The  $\delta^{13}\text{C}$

values of CO-, CV- and CK-chondrites range from -8 to -25 and  $\delta^{13}\text{C}$  values of CI, CM and CR-chondrites range from -5 to -12 (GRADY and WRIGHT 2003). Thus, CI or CM-chondrites are more suitable candidates for a ureilite parent body composition (RANKENBURG et al. 2007).  $\delta^{13}\text{C}$  correlates with ureilite olivine *fa* (HUDON et al. 2004). HUDON et al. (2004) suggested that this is a result of a change in  $\delta^{13}\text{C}$  during reduction processes on the ureilite parent body which shifted the residual carbon to heavier values.

### **2.3.7 Ureilite formation age and cosmic ray exposure age**

TAKAHASHI and MASUDA (1990) performed Rb-Sr and Sm-Nd dating in the MET 78008 ureilite. They found an internal Rb-Sr-isochrone at  $4.01 \pm 0.06$  Ga that they interpreted as a late igneous event or shock metamorphism. The calculated formation age of the whole rock based on Sm-Nd data is 4.5-4.6 Ga (TAKAHASHI and MASUDA 1990). GOODRICH et al. (1991) also reported Sm-Nd and Rb-Sr isotopic data of seven different ureilites. META78008, ALH82130 and PCA82506 give Sm-Nd model ages of  $\sim 4.55$  Ga (no error data given in GOODRICH et al. 1991), consistent with the data published in TAKAHASHI and MASUDA (1990). Model ages for META78008, ALH82130 and PCA82506 from Rb-Sr data range from 4.92 Ga to 3.42 Ga. GOODRICH et al. (1991) suggest the range in Rb-Sr data may be a result of terrestrial contamination, as Rb-concentrations in ureilites are extremely low. Kenna, Novo Urei and ALH77257 give a Sm-Nd model age of  $3.74 \pm 0.02$  Ga. LEW85440 gives a model Sm-Nd age of  $4.85 \pm 0.02$  Ga (GOODRICH et al. 1991).

META78008, ALH82130 and PCA82506 were devoid of a LREE-component (GOODRICH et al. 1991). GOODRICH et al. (1991) suggests that the LREE-rich component was a younger addition. According to GOODRICH et al. (1991), the 3.74 Ga-isochrone dates an event that substantially changed the chemical composition of the bulk meteorite.

Model ages obtained from U-Th-Pb isotopic systematics for Goalpara and META78008 in TORIGOYE-KITA et al. (1995a) and TORIGOYE-KITA et al. (1995c) give  $\sim 4.55$  Ga. The LREE-rich component leached from Goalpara shows a terrestrial signature for Th/U and Sm/Nd ratios, leading TORIGOYE-KITA et al. (1995a) to suggest that the LREE-rich component in ureilites might be the result of terrestrial contamination. GOODRICH et al. (1995) argues that it is unlikely that the samples have been contaminated by the same contaminant that time was not sufficient to allow introduction and equilibration of a contaminant and that LREE-

component free subsamples also plot on the 3.74 Ga-line. TORIGOEY-KITA et al. (1995b) replied that all meteorites fell on soils of similar phanerozoic ages and similar Sm-Nd composition. Rb-Sr systematics of ureilites appear to be dominated by terrestrial contamination and it is doubtful that a completely LREE-component free subsample had been separated (TORIGOEY-KITA et al. 1995b).

Cosmic ray exposure ages have been published in RAI et al. (2003) and references therein. The calculated cosmic ray exposure ages are based on the cosmogenic  $^3\text{He}$  and  $^{21}\text{Ne}$  contents of bulk samples and have been calculated for 28 ureilites. The ages range from 0.1 Ma to 47 Ma. Nearly 60% of the calculated cosmic ray exposure ages are less than 10 Ma. This indicates that the ureilites were not ejected by a single impact event (RAI et al. 2003).

### **2.3.8 The $^{60}\text{Fe}$ - $^{60}\text{Ni}$ short-lived isotope chronometer**

Short-lived isotopes are isotopes with half lives that are so short (up to  $10^8$  years) that they are extinct today (i.e.,  $^{41}\text{Ca}$ ,  $^{26}\text{Al}$ ,  $^{10}\text{Be}$ ,  $^{60}\text{Fe}$ ,  $^{53}\text{Mn}$ ,  $^{107}\text{Pd}$ ,  $^{182}\text{Hf}$ ,  $^{129}\text{I}$ ,  $^{244}\text{Pu}$ ,  $^{146}\text{Sm}$  MEYER and ZINNER 2006). Their presence can still be detected by mass-independent excesses of their daughter isotopes. Short lived isotopes can be produced either by stellar nucleosynthesis or by energetic particle irradiation (TACHIBANA et al. 2006).  $^{60}\text{Fe}$  is a short lived isotope with a half-life of  $\sim 1.49$  Ma (TACHIBANA et al. 2006) that is exclusively produced by stellar nucleosynthesis (MEYER and ZINNER 2006, BIZZARRO et al. 2007b, TACHIBANA et al. 2006). The former presence of  $^{60}\text{Fe}$  can be detected by its daughter isotope  $^{60}\text{Ni}$ .  $^{60}\text{Ni}$  is not only produced by the decay of  $^{60}\text{Fe}$ , but also by other nucleosynthetic processes (e.g. s-processes HEGER et al. 2000). The influence of  $^{60}\text{Fe}$  is therefore expressed as the deviation from the terrestrial  $^{60}\text{Ni}/^{58}\text{Ni}$ -ratio, normalized on the terrestrial  $^{61}\text{Ni}/^{58}\text{Ni}$ -ratio or  $^{62}\text{Ni}/^{58}\text{Ni}$ -ratio,  $\epsilon^{60}\text{Ni}^*$ . Due to the higher abundance of  $^{62}\text{Ni}$  (as opposed to  $^{61}\text{Ni}$ ), normalization on  $^{62}\text{Ni}/^{58}\text{Ni}$  can produce higher precision and accuracy. The possibility of nucleosynthetic anomalies in  $^{62}\text{Ni}$  could, however, leads to biased results (BIZZARRO et al. 2007a).  $^{61}\text{Ni}$  on the other hand is considered to be free of nucleosynthetic anomalies, but is more sensitive to isobaric interferences (problems arising in mass spectrometry from measuring ions and argides of similar mass/charge-ratio) due to its lower abundance (BIZZARRO et al. 2007a).

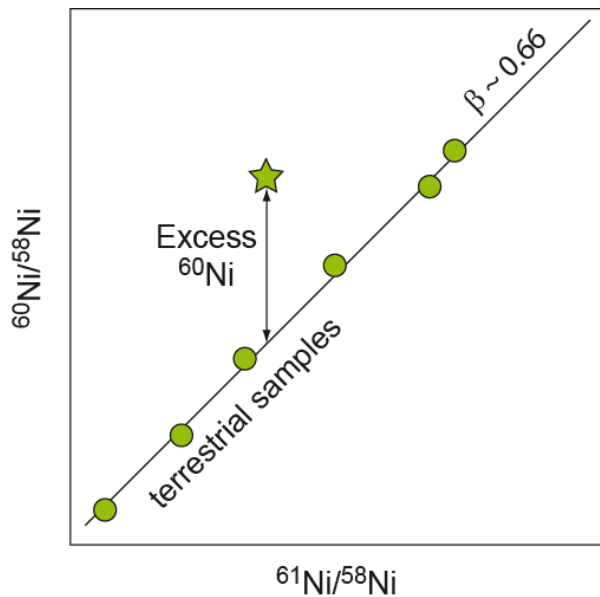


**Fig. 10** Illustration of a three-isotope Ni-diagram. The terrestrial fractionation line has a slope of  $\sim 0.66$ . Excess in  $^{60}\text{Ni}$  is the deviation from the terrestrial fractionation line.

Knowledge of the  $^{60}\text{Fe}/^{56}\text{Fe}$ -ratio at a given time (e.g. Pb-Pb-ages) is necessary to obtain chronological information from the  $^{60}\text{Fe}$ - $^{60}\text{Ni}$ -system. Based on their work on Bishunpur and Krymka troilite, TACHIBANA and HUSS (2003) suggested an initial  $^{60}\text{Fe}/^{56}\text{Fe}$  of  $(2.8 - 4.5) \cdot 10^{-7}$  assuming the chondrules formed 1-2 Ma after CAIs. MOSTEFAOUI et al. (2005) suggested an initial of  $^{60}\text{Fe}/^{56}\text{Fe}$  of  $9.2 \cdot 10^{-7}$  from studies of Semarkona troilite, while GOSWAMI et al. (2007) obtained an initial  $^{60}\text{Fe}/^{56}\text{Fe}$  of  $(2.31 \pm 1.8) \cdot 10^{-6}$  from their studies of pyroxene-rich chondrules of Semarkona.

Several sources have been proposed for  $^{60}\text{Fe}$ , including non-exploding Wolf-Rayet-stars, supernovae and AGB-stars (MEYER and ZINNER 2006). The high initials are inconsistent with a  $^{60}\text{Fe}$  production from a Wolf-Rayet-star (TACHIBANA et al. 2006, MEYER and ZINNER 2006). AGB-stars have been considered to be an unlikely source due to the rarity of encounters of molecular clouds and AGB-stars (TACHIBANA et al. 2006). Low-mass AGB-stars can be excluded due to insufficient neutron density for  $^{60}\text{Fe}$  production (MEYER and ZINNER 2006). Model calculations of Type II supernovae explosions predict initial  $^{60}\text{Fe}/^{56}\text{Fe}$ -ratios of  $3 \cdot 10^{-7}$  to  $>10^{-5}$  and can also account for other short-lived isotopes in the early solar system (TACHIBANA et al. 2006). Supernovae are therefore considered to have been a likely  $^{60}\text{Fe}$ -source (TACHIBANA et al. 2006, MEYER and ZINNER 2006).

For ureilites published  $\epsilon^{60}\text{Ni}^*$  is inconclusive. SHUKOLYUKOV and LUGMAIR (1993) gave  $\epsilon^{60}\text{Ni}^*$  of  $0.0 \pm 0.2$  for bulk PCA82506. KITA et al. (1998) conducted in-situ ion microprobe studies on

MET78008. Their data did not show resolvable excesses in  $^{60}\text{Ni}$  ( $-1 \pm 16 \text{ } \epsilon$  for olivine ( $^{56}\text{Fe}/^{58}\text{Ni} = 3145$ ),  $9 \pm 22 \text{ } \epsilon$  for vein material ( $^{56}\text{Fe}/^{58}\text{Ni} = 100$ ) and  $-43 \pm 49 \text{ } \epsilon$  for pyroxene ( $^{56}\text{Fe}/^{58}\text{Ni} = 5063$ ). From this data, KITA et al. (1998) concluded that ureilites might have formed 4-9 Ma after CAIs.

In BIZZARRO et al. (2007b), a uniform deficit of  $-0.243 \pm 0.02 \text{ } \epsilon$  was reported for a number of iron meteorites, main group pallasites and bulk ureilites (NWA2376, El Gouanem, SAH98055). From the deficits of  $\epsilon^{60}\text{Ni}^*$  in early accreted planetesimals, BIZZARRO et al. (2007b) concluded a late injection of  $^{60}\text{Fe}$  into the protoplanetary disc. A decoupling of  $^{26}\text{Al}$  and  $^{60}\text{Fe}$  injection into the early solar system excludes AGB-stars and type II supernova explosions as  $^{60}\text{Fe}$  source, as those would co-inject large amounts of  $^{26}\text{Al}$  (BIZZARRO et al. 2007b). Instead, an exploding Wolf-Rayet-star is suggested as  $^{60}\text{Fe}$ -source.

In contrast to the data presented in BIZZARRO et al. (2007b), other authors (QUITTÉ et al. 2006, CHEN et al. 2007, COOK et al. 2008, DAUPHAS and COOK 2008) have not found resolvable deficits in iron meteorites.

## 2.4 Ureilite genesis

### 2.4.1 Parent body composition

Due to the high C-content of ureilites ( $\sim 3 \text{ wt}\%$ ), many authors proposed that the ureilite parent body was of carbonaceous chondritic composition (e.g. WASSON et al. 1976, TAKEDA 1987). HIGUCHI et al. 1976 proposed a CV3-chondritic parent body based similar depletion of Bi, Tl, In and Cd relative to Rb. HIGUCHI et al. (1976) also noted that the oxidation state of ureilite olivine ( $\text{fa}_{12-20}$ ) is similar to the oxidation state expected from a fully equilibrated CV3-chondrite. Similarities between ureilites and the oxygen isotopic composition of CV3- and CO3-chondrites led CLAYTON and MAYEDA (1996) to suggest that the ureilite parent body might have a similar origin. Studies of the carbon isotope-system published in GRADY et al. (1985) revealed that carbon in CV3-chondrites is isotopically different from carbon in ureilites. GRADY et al. (1985) suggested that ureilites may be linked to enstatite meteorites and IAB-iron meteorites. Humayun et al. (2005) concluded that siderophile element depletion patterns are consistent with ureilites being residues of a carbonaceous chondritic parent body. Based on the oxygen isotope studies of CLAYTON and MAYEDA (1996), they suggest a CV3-chondritic parent body. However, reported carbon concentrations of  $\sim 3 \text{ wt}\%$

in ureilites are not consistent with a CV3-chondritic parent body, which is relatively low in carbon (~0.5 wt%, LODDERS and FEGLEY 1998), unless at least part of the carbon was injected into the UPB via impact. At present, no known chondritic composition constitutes a perfect match for the ureilite genesis. Despite the contradictions in carbon isotopic composition and abundance, many authors prefer a CV- or CM-like composition (e.g. KITA et al. 2004, GOODRICH et al. 2007).

#### **2.4.2 Thermal history of ureilites**

Impact heating has been proposed as heat source for ureilites (RUBIN 1988, RUBIN 2006). In contrast, KEIL et al. (1997) stated that impact heating cannot effectively raise the temperature by more than a few degrees and that even multiple impacts are ineffective on small asteroid. Furthermore only small amounts of melt can be generated by impact and most of it would be ejected from the impact craters (KEIL et al. 1997). In SONETT et al. (1970) electrical conduction heating by T Tauri solar winds from the pre-main-sequence sun has been suggested as heat source. Another heat source is the decay of short-lived radioactive isotopes, including  $^{26}\text{Al}$  and  $^{60}\text{Fe}$  (MOSTEFAOUI et al. 2005, YOSHINO et al. 2003).

Calculations of px-px- and px-ol-equilibration temperatures (based on the thermometers published in SACK and GHIORSO 1994, LINDSLEY and ANDERSEN 1983 and SINGLETARY and GROVE 2003) gave values ranging from 1150 to 1300°C for 32 monomict ureilites (TAKEDA 1987, SINHA et al. 1997, SINGLETARY and GROVE 2003) including ALH84136, LEW85440, EET87517, GRA95205 and Kenna. Microtextural features in ureilite minerals, such as spinoidal decomposition of augites and orthopyroxene lamellae in orthopyroxene in HH064 and Janalash (WEBER et al. 2003) and intracrystalline  $\text{Fe}^{2+}$ -Mg partitioning of orthopyroxene in Hughes 009 (GOODRICH et al. 2001) indicate a phase of rapid cooling between 1200 °C and 650°C during which the characteristic reduction rims were established. This phase of rapid cooling has been interpreted as the result of a single, major impact that might have caused the catastrophic breakup of the ureilite parent body and introduced the shock features (e.g. undulatory extinction and kink bands in silicates, “cloudy” pyroxene grains, diamonds and mosaicked textures; MITTFELDLT et al. 1998) into the ureilites. In contrast, WEBER et al. (2003) and RUBIN (2006) suggest that shock features were introduced into the ureilites by an earlier impact event. WEBER et al. (2003) also suggested that after a first excavation event which started the phase of rapid cooling from 1200°C – 650°C, a second excavation event led

to a even more rapid cooling, halting spinoidal decomposition and reduction at the silicate rims.

SINGLETARY and GROVE (2006) on the other hand proposed that the disruption of the ureilite parent body might not be the result of an impact. In their model large volumes of CO gas are produced from reduction and the subsequent build up of pressure leads to the disruption of the parent body.

Cosmic ray exposure ages of ureilites of <47 Ma (RAI et al. 2003) in contrast to ureilite formation ages of ~4.55 Ga (TORIGOYE-KITA et al. 1995a, TORIGOYE-KITA et al. 1995c) indicate that the disrupted material reaccreted, either on the surface of the original asteroid or into a secondary asteroidal body (GOODRICH et al. 2004). The similarities in the thermal history of the ureilites indicate that ureilites originated from the same parent body.

### **2.4.3 Igneous processes on the ureilite parent body**

Assuming that the original ureilite material was of a chondritic composition of some kind, the depletion in incompatible, lithophile elements, the absence of plagioclase and the superchondritic Ca/Al-ratios indicate a high degree of igneous processing on the ureilite parent body (GOODRICH 1992, MITTFELDLT et al. 1998).

Because of the pronounced orientation of silicate grains within the ureilites and observed depletions, early studies suggested that ureilites represent igneous cumulates (BERKLEY et al. 1980, GOODRICH et al. 1987a). The discovery of the heterogeneities in oxygen isotopes indicated that isotopic equilibrium on the ureilite parent body had not been attained. CLAYTON and MAYEDA (1988) therefore concluded that melting on a large scale on the ureilite parent body was unlikely. The presence of noble gases in near-chondritic abundances also argues against large scaled igneous processes (MITTFELDLT et al. 1998). Another problem of the cumulate model is that ureilites would represent only 10 to 30 wt% of the initial parent body material. No meteorite that would represent the complementary material has been described yet (RUBIN 1988, SCOTT et al. 1993, MITTFELDLT et al. 1998). Some authors therefore concluded that ureilites represent the sole rock type of a major fraction of the ureilite parent body (e.g. SCOTT et al. 1993). Because of these inconsistencies most recent studies assume that ureilites formed as a type of mantle restite (e.g. WARREN and KALLEMEYN 1992, SCOTT et al. 1993, WALKER and GROVE 1993, KITA et al. 2004).

The depletion in lithophile elements has been interpreted as loss of a basaltic component (WARREN and KALLEMEYN 1992, SCOTT et al. 1993), although no complementary basaltic rock has yet been identified. While feldspathic clasts are commonly found in polymict ureilites, they usually contain <3 vol% plagioclase (PRINZ et al. 1986, GOODRICH et al. 2004), which is not sufficient to account for the missing basaltic component (MITTFELDLT et al. 1998). It has therefore been suggested that the majority of the basaltic component was lost. WILSON and KEIL (1991) showed that small amounts of volatiles in melts close to the surface of a small asteroidal body can lead to an explosive eruption that can accelerate melt droplets above the escape velocity. Although this mechanism has been developed for the missing basaltic component in aubrites, WARREN and KALLEMEYN (1992) and SCOTT et al. (1993) suggested a similar process to be responsible for the missing basalt component in ureilites too. Another mechanism that has been suggested is the stripping of the outer basaltic crust by impacts (MITTFELDLT et al. 1998).

Partial melt modeling, using the MAGPOX-software, has been conducted to link the ureilite mineral assemblage to their presumed chondritic precursor materials in GOODRICH et al. (2004) and GOODRICH et al. (2007). Their results suggest that ureilites are the result of a rapid fractional melting process of a parent body of CV-like composition with superchondritic Ca/Al-ratio. KITA et al. (2004) conducted similar calculations with MELTS (GHIORSO and SACK 1995, ASIMOW and GHIORSO 1998) and suggest that ureilites are the product of a fractional melting process of a CM- or CI-like parent body. WARREN et al. (2006) performed calculations to determine percolation velocities of basaltic melts within the asteroid. Their calculations show that implausibly long time spans of several tens of Ma are necessary to remove the basaltic melt as a series of fractional melt steps. WARREN et al. (2006) therefore proposed that the basaltic melt was not removed until at least 20 % of the silicate component was molten.

#### **2.4.4 Reduction on the ureilite parent body**

Most ureilites show a pronounced positive and linear correlation between Fe/X (where X can be Mn, Cr, Ca, Al or Ti) and Fe/Mg in olivine cores (e.g. GOODRICH et al. 1987a). This has been interpreted as a FeO-reduction trend (GOODRICH et al. 1987a). Several authors (e.g. BERKLEY and JONES 1982, SINHA et al. 1997, SINGLETARY and GROVE 2003) therefore suggested that the heterogeneous FeO in ureilite olivine is a result of smelting (i.e. the reduction of fayalite in

the presence of carbon). Following the suggestion in WARREN et al. (2006), this model will be referred to as “smelted-core model” in this work.

The smelting reaction is strongly pressure dependent and it has been suggested that different olivine FeO concentrations might represent a layering with depth (WALKER and GROVE 1993, SINHA et al. 1997, GOODRICH et al. 2007). In this scenario, deeper samples are more ferroan and shallower samples are more magnesium-rich. From the necessary pressure to stabilize the more ferroan ureilite assemblages ( $\sim fa_{24}$ ), minimum parent body sizes can be inferred (WALKER and GROVE 1993). The pressure at which ureilites formed has been estimated to be between  $\sim 2$  MPa for the more magnesian ureilites and  $\sim 10$  MPa for the most ferroan ureilites (WARREN and KALLEMEYN 1992, WALKER and GROVE 1993, MITTFELDLT et al. 1998). The minimum size of the ureilite parent body (UPB) inferred from these calculations is  $\sim 100$  km, although the real UPB might have been considerably larger (WALKER and GROVE 1993, SINHA et al. 1997). The results in SINGLETARY and GROVE (2003) suggest that depth and temperature are inversely related. They have found that pyroxene-pyroxene-equilibration temperatures are positively correlated with mg# (SINGLETARY and GROVE 2003). To explain this inverse relation, SINGLETARY and GROVE (2006) have developed a model of a heterogeneous parent body that is composed of randomly mixed packages of isotopically distinct material. Assuming that  $^{26}\text{Al}$  is the primary heat source of the parent body, heterogeneously distributed CAI's will cause a heterogeneous temperature distribution (SINGLETARY and GROVE 2006).

The smelted-core model invokes several problems, which are reviewed in detail in WARREN and HUBER (2006). For every gram of FeO in olivine, 0.39 grams of CO-gas would form. The shift from 21 wt% FeO in more ferroan olivines to  $\sim 4$  wt% in more magnesian olivines would produce about 5.5 wt% of CO-gas. At 10 MPa pressure this would correspond to 88 vol% gas vs. 12 vol% solid. At lower pressures the relative volume of gas is even higher (97 vol% at  $P = 2$  MPa) (WARREN and HUBER 2006). GOODRICH et al. (2007), however, pointed out that the objections in WARREN et al. (2006) do not consider the progress of gas production during the smelting process. In their model, the onset of smelting results in a burst of gas production and high gas/melt-ratios ( $\sim 2.5$ ), which declines to  $< 0.05$  after a few % of smelting/melting (GOODRICH et al. 2007).

Another problem of the smelted-core model is the missing correlation of carbon with olivine FeO (WARREN and HUBER 2006). Assuming a more or less homogeneous starting material, different degrees of smelting would consume different amounts of carbon. For every mol% increase in olivine mg#, 0.1 wt% of carbon is consumed (Eq. 1). As a result, olivine  $f_a$  should be correlated with carbon content. No evidence for this predicted anticorrelation is observed in the data (WARREN and HUBER 2006). Similar to carbon, the smelting process would also produce different amounts of Fe-metal. For every gram of FeO in olivine reduced, 0.78 g of Fe-metal is formed (WARREN and HUBER 2006). As result, mg# and metal content in ureilites should show a positive correlation. Actual metal abundances appear to be anticorrelated with mg# (WARREN and HUBER 2006).

### **3 Goals of this study**

The first goal is to shed light on the relation between ureilite silicates and vein metal.

Understanding the origin of the vein metal will enhance our understanding of ureilite genesis and evolution. In this study, the elements Fe, Ni and Co are used to determine thermodynamic equilibrium between ureilite olivine and vein metal and to characterize the vein metal of different ureilite samples. Mass balance calculations are used to model the composition of metal components of parent bodies of chondritic-starting compositions. Batch melting and fractional melting models are applied to determine whether the vein metal represents a residual metal, a melt fraction or something entirely different.

The second goal is to determine whether the  $^{60}\text{Fe}$ - $^{60}\text{Ni}$  short-lived isotope chronometer can be applied to ureilites. Ni-isotopic studies of components with different Fe/Ni-ratios could provide insights in the chronology of  $^{60}\text{Fe}$ -addition in the early solar system as well as relative dating of igneous events on the ureilite parent body.

## 4 Thermodynamics

### 4.1 Theoretical background

In order to investigate if the vein metal is in equilibrium with the ureilite olivine, equilibration temperatures have been calculated for every ureilite sample. The thermodynamic calculations of metal-olivine equilibria are based on the exchange of Ni for Fe and Co for Fe:



The reactions Eq. 2 and Eq. 3 are independent of oxygen fugacity. The oxygen fugacity however does influence the amount of FeO in olivine. An increase in oxygen fugacity will increase the amount of FeO in the olivine, thus decreasing the mole fraction of Fe in the metal phase (SEIFERT et al. 1988). At equilibrium and 1 bar pressure, the Gibbs energies of both reactions (Eq. 2, Eq. 3) is linked to the equilibrium constant K by Eq. 4.

$$0 = \Delta G_{(1 \text{ bar}, T)}^0 + RT \ln K \quad \text{Eq. 4}$$

In Eq. 4,  $\Delta G^0$  is the Gibbs energy [J], R is the gas constant ( $8.3144 \frac{\text{J}}{\text{K} \cdot \text{mol}}$ ), T is the temperature [K] and K is the equilibrium constant. The equilibrium constant K for the reactions Eq. 2 and Eq. 3 is:

$$K^{\text{ol-metal}} = \frac{a_{\text{Fe}_2\text{SiO}_4}^{\text{ol}} \cdot (a_{\text{Ni}}^{\text{metal}})^2}{a_{\text{Ni}_2\text{SiO}_4}^{\text{ol}} \cdot (a_{\text{Fe}}^{\text{metal}})^2} \quad \text{Eq. 5}$$

The variable  $a_i^p$  refers to the activity of the component i in phase p. To relate the activities to mole fractions of the metal oxides, the activity coefficient  $\gamma_i^p$  is introduced. The activity coefficient describes the deviation from ideal behaviour of a component in a multi-component system. A component showing ideal behaviour has an  $\gamma_i^p = 1$ . The activities in Eq. 5 can be expressed as:

$$a_{M_2SiO_4}^{ol} = \left( X_{MSt_{0.5}O_2}^{ol} \cdot Y_{MSt_{0.5}O_2}^{ol} \right)^2 \quad \text{Eq. 6}$$

$$a_{Fe_2SiO_4}^{ol} = \left( X_{FeSt_{0.5}O_2}^{ol} \cdot Y_{FeSt_{0.5}O_2}^{ol} \right)^2 \quad \text{Eq. 7}$$

$$a_M^{met} = X_M^{met} \cdot \gamma_M^{met} \quad \text{Eq. 8}$$

$$a_{Fe}^{met} = X_{Fe}^{met} \cdot \gamma_{Fe}^{met} \quad \text{Eq. 9}$$

M can either be Co or Ni. For olivine, the mole fractions and activity coefficients were squared because of mixing of cation species on two sites (SEIFERT et al. 1988). Replacing the activities in Eq. 5 with the activity coefficients and mole fractions in Eq. 6 to Eq. 9 gives:

$$K^{ol-met} = \frac{\left( X_{FeSt_{0.5}O_2}^{ol} \cdot Y_{FeSt_{0.5}O_2}^{ol} \right)^2 \cdot \left( X_M^{met} \cdot \gamma_M^{met} \right)^2}{\left( X_{MSt_{0.5}O_2}^{ol} \cdot Y_{MSt_{0.5}O_2}^{ol} \right)^2 \cdot \left( X_{Fe}^{met} \cdot \gamma_{Fe}^{met} \right)^2} \quad \text{Eq. 10}$$

The distribution coefficient  $K_D$  for Eq. 2 and Eq. 3 is defined as:

$$K_D^{ol-met} = \left( \frac{X_{FeSt_{0.5}O_2}^{ol} \cdot X_M^{met}}{X_{MSt_{0.5}O_2}^{ol} \cdot X_{Fe}^{met}} \right) \quad \text{Eq. 11}$$

In Eq. 10 the mole fractions can be replaced by  $K_D^{ol-met}$  (Eq. 11):

$$K^{ol-met} = \left( K_D^{ol-met} \right)^2 \cdot \left( \frac{Y_{FeSt_{0.5}O_2}^{ol} \cdot \gamma_M^{met}}{Y_{MSt_{0.5}O_2}^{ol} \cdot \gamma_{Fe}^{met}} \right)^2 \quad \text{Eq. 12}$$

Eq. 12 can be rearranged and equated with Eq. 4, which gives:

$$\ln K^{ol-met} = 2 \ln K_D^{ol-met} + 2 \ln \left( \frac{Y_{FeSt_{0.5}O_2}^{ol} \cdot \gamma_M^{met}}{Y_{MSt_{0.5}O_2}^{ol} \cdot \gamma_{Fe}^{met}} \right) = - \frac{\Delta G_{(Fe,T)}^0}{RT} \quad \text{Eq. 13}$$

Rearranging of Eq. 13 gives:

$$\ln K_D^{ol-met} = - \frac{\Delta G_{(Fe,T)}^0}{2RT} - \ln \left( \frac{Y_{FeSt_{0.5}O_2}^{ol} \cdot \gamma_M^{met}}{Y_{MSt_{0.5}O_2}^{ol} \cdot \gamma_{Fe}^{met}} \right) \quad \text{Eq. 14}$$

Eq. 14 can be used to calculate the distribution coefficient of a Ni, Co and Fe between metal and olivine. The temperature T, the Gibbs energy of the exchange reaction,  $\Delta G_{(Fe,T)}^0$  and the activity coefficients  $\gamma_i^{ol}$  of the involved phases must be known. Unfortunately, it is not possible to rearrange Eq. 14 for T, as the involved activity coefficients and the Gibbs energy

are functions of temperature. In order to establish the equilibration temperature,  $\ln K_D^{qt-met}$  is calculated from the measured data. This  $\ln K_D^{qt-met}$  is now compared to a modeled  $\ln K_D^{qt-met}$  at a given temperature. The equilibration temperature is the temperature at which the modeled  $\ln K_D^{qt-met}$  equals the  $\ln K_D^{qt-met}$  calculated from the measured data. In this work, the goal search-plugin of Microsoft Office Excel 2007 was used to vary the temperature until the equilibrium condition was met.

## 4.2 Gibbs free energy of reaction

The Gibbs free energy of reaction is defined as the difference of the Gibbs free energy of formation of products and reactants (Eq. 15).

$$\Delta G_{Ni}^0 = 2\Delta_f G_{Ni}^0 + \Delta_f G_{Fe_2SiO_4}^0 - 2\Delta_f G_{Fe}^0 - \Delta_f G_{Ni_2SiO_4}^0 \quad \text{Eq. 15}$$

$$\Delta G_{Co}^0 = 2\Delta_f G_{Co}^0 + \Delta_f G_{Fe_2SiO_4}^0 - 2\Delta_f G_{Fe}^0 - \Delta_f G_{Co_2SiO_4}^0 \quad \text{Eq. 16}$$

As the Gibbs free energy of formation of elements in their reference state is defined to be zero, the equations simplify to:

$$\Delta G_{Ni}^{\#} = \Delta_f G_{Fe_2SiO_4}^0 - \Delta_f G_{Ni_2SiO_4}^0 \quad \text{Eq. 17}$$

$$\Delta G_{Co}^{\#} = \Delta_f G_{Fe_2SiO_4}^0 - \Delta_f G_{Co_2SiO_4}^0 \quad \text{Eq. 18}$$

Absolute values for the Gibbs free energies of formation can be found in the literature (e.g. ROBIE and HEMINGWAY 1995). The Gibbs free energy of reaction and the Gibbs free energy of formation is also often given in form of equations. These equations are based on regressions of experimental data. In this study, we use the equations published in SEIFERT et al. (1988), which are based on experiments published in O'NEILL (1987a) and O'NEILL (1987b). The form of the equation is given in Eq. 19 and the parameters are listed in (Table 5).  $\Delta G_{(p,T)}^{\#}$  is given in  $J \cdot mol^{-1}$  at 1 bar pressure and as function of the temperature.

$$\Delta G_{(p,T)}^{\#} = a + b \cdot T + c \cdot T \ln T \quad \text{Eq. 19}$$

Table 5 Parameters for the calculation of  $\Delta G_{(p,T)}^{\#}$  from SEIFERT et al. (1988)

Parameter	Eq. 2 (solid metal)	Eq. 2 (liquid metal)	Eq. 3 (solid metal)	Eq. 3 (liquid metal)
-----------	---------------------	----------------------	---------------------	----------------------

a	-86049	-69079	-111598	-79801
b	6.734	-53.444	246.885	102.183
c	-5.047	1.616	-30.901	-13.544

### 4.3 Activity coefficients of Fe, Co and Ni in Fe-Co-Ni metal

The metal alloys considered in this work are usually Fe-Ni-Co-alloys with  $X_{Ni} < 0.1$  and  $X_{Co} < 0.005$ . The activity coefficients were thus determined particularly for these compositions.

The activity coefficient of Fe in FeNi-metal is unity in solid and liquid binary alloys with  $X_{Ni} < 0.2$  (RAMMENSEE and FRASER 1981, TOMISKA and NECKEL 1985). RAMMENSEE and FRASER (1981) and TOMISKA and NECKEL (1985) give  $\gamma_{Ni}$  in binary FeNi-alloys  $< 1$ . The effect of temperature on  $\gamma_{Ni}$  in solid binary FeNi-alloys is small. At  $X_{Ni} = 0.1$ ,  $\gamma_{Ni}$  shifts from 0.671 at 1473 K to 0.659 at 1600 K. In this work, the activity coefficient of Ni in solid Fe-Ni alloys is assumed to be 0.665 at all temperatures. In liquid alloys, the  $\gamma_{Ni}$  was assumed to be 0.61 for all calculations.

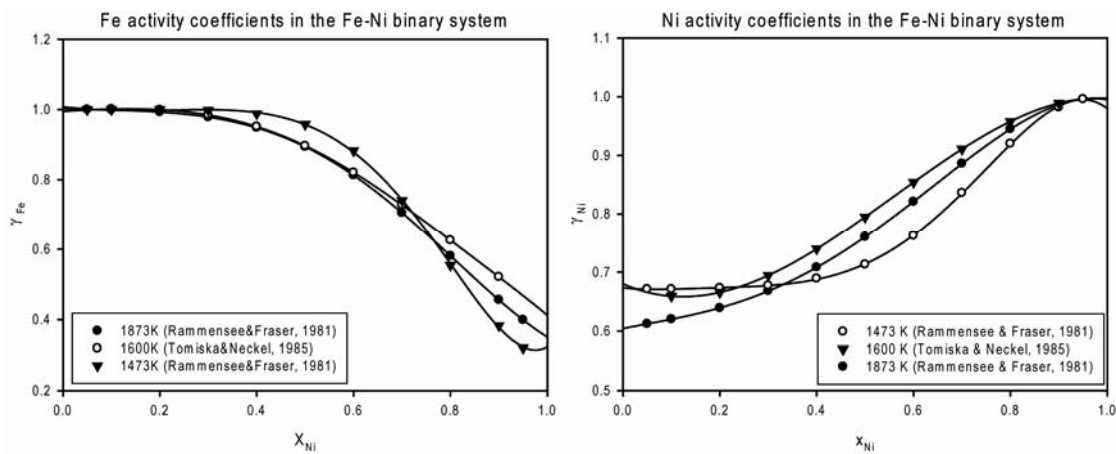


Fig. 11 Activity coefficients for Fe and Ni in Fe-Ni alloys as a function of  $X_{Ni}$ .

The activity coefficient of Co in FeNi-metal for  $X_{Co} < 0.01$  is only little investigated. SEIFERT et al. (1988) extrapolated data from FRASER and RAMMENSEE (1982) and TOMISKA et al. (1979) and suggested an increase of  $\gamma_{Co}$  with increasing  $X_{Ni}$  ( $X_{Ni} < 0.4$ ). In this study we use their method. The activity coefficient of Co in the Co-Ni-system published by TOMISKA et al. (1979) for solid (1600 K) and liquid (1800 K) metal are extrapolated for  $X_{Co} \approx 0$  (Fig. 12, left side). The form of the equation is given in Eq. 20 and the corresponding parameters in Table 6.

$$\gamma_{Co}^{Co-Ni} = aX_{Ni}^5 + bX_{Ni}^4 + cX_{Ni} + d \quad \text{Eq. 20}$$

Table 6 Parameters for calculating  $\gamma_{Co}^{Co-Ni}$  extrapolation of data from TOMISKA et al. (1979)

Parameter	$\gamma_{Co}^{Co-Ni}$ (solid)	$\gamma_{Co}^{Co-Ni}$ (liquid)
a	0.0744	0.0006
b	-0.2202	0.1505
c	0.0044	-0.0083
d	0.9998	1.0001

$\gamma_{Co}$  for  $X_{Ni} \sim 1$  in the Co-Ni binary system is 0.858 at 1600 K (solid) and 0.842 for the liquid alloy at 1800 K. For the Fe-Co system, RAMMENSEE and FRASER (1981) reported a  $\gamma_{Co}$  ( $X_{Fe} \sim 1$ ) of 1.15 for the solid alloy at 1473 K and 1.1 for the liquid alloy at 1873 K. FRASER and RAMMENSEE (1982) have published activity coefficients for the Fe-Co-Ni system at a fixed Fe/Ni = 9 and varying  $X_{Co}$ . We extrapolate these data to  $X_{Co} \approx 0$  (Fig. 12, right side). The regression is calculated as polynomial of the fifth order (Eq. 21), with the parameters listed in Table 7.

$$\gamma_{Co}^{Fe-Co-Ni} = aX_{Co}^5 + bX_{Co}^4 + cX_{Co}^3 + dX_{Co}^2 + eX_{Co} + f \quad \text{Eq. 21}$$

Table 7 Parameters for the calculation of  $\gamma_{Co}^{Fe-Co-Ni}$ . Regression calculated from data from FRASER and RAMMENSEE (1982)

Parameter	$\gamma_{Co}^{Fe-Co-Ni}$ (solid)	$\gamma_{Co}^{Fe-Co-Ni}$ (liquid)
a	-7.6325	-9.9828
b	23.437	30.603
c	-27.589	-35.549
d	15.383	19.129
e	3.8209	-4.4059

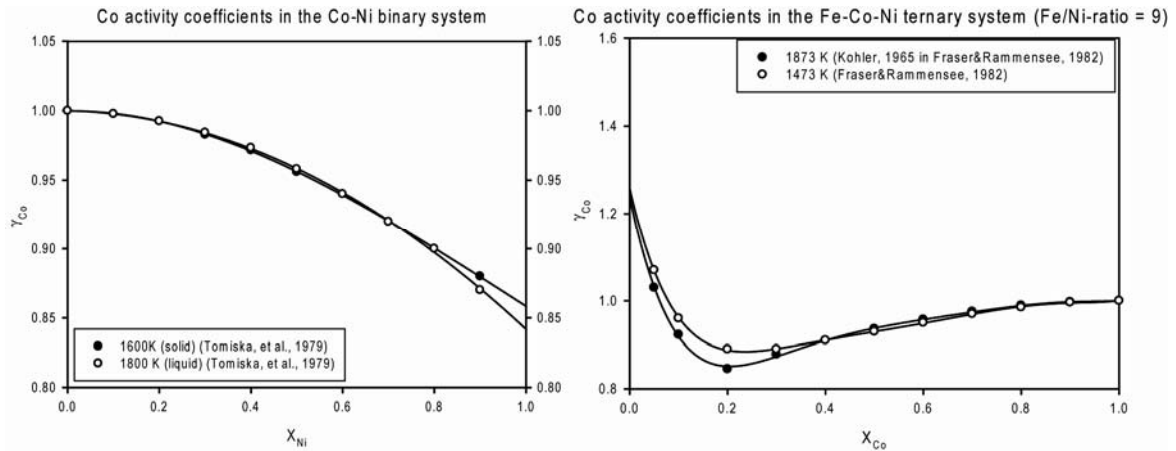


Fig. 12 (left) Activity coefficient of Co as a function of  $X_{Ni}$  in Co-Ni alloys (TOMISKA et al. 1979). Regression calculated as 3<sup>rd</sup> order polynomial to extrapolate  $\gamma_{Co}$  for  $X_{Co} \rightarrow 0$ . (right) Activity coefficient of Co as a function of  $X_{Co}$  in Fe-Co-Ni ternary alloys with a fixed Fe/Ni-ratios of 9 FRASER and RAMMENSEE (1982). Regression was calculated as 5<sup>th</sup> order polynomial to extrapolate  $\gamma_{Co}$  for  $X_{Co} \rightarrow 0$ .

Data from FRASER and RAMMENSEE (1982) give a  $\gamma_{Co} = 1.22$  for  $X_{Co} \approx 0$  at  $X_{Ni} = 0.1$  and 1473 K (solid metal) and  $\gamma_{Co} = 1.21$  for  $X_{Co} \approx 0$  at  $X_{Ni} = 0.1$  and 1873 K (liquid metal). The data from RAMMENSEE and FRASER (1981) give  $\gamma_{Co}$  for  $X_{Co} \approx 0$  at  $X_{Ni} = 1$  and the data of TOMISKA et al. (1979) give  $\gamma_{Co}$  for  $X_{Co} \approx 0$  at  $X_{Ni} = 0$ . From these 3 points of data, a  $X_{Ni}$ -dependent  $\gamma_{Co}$  is calculated (Fig. 13). The regression is calculated as a quadratic equation (Eq. 22), with the parameters listed in Table 8.

$$\gamma_{Co}^{Fe-Co-Ni} = aX_{Ni}^2 + bX_{Ni} + c$$

Eq. 22

Table 8 Parameters for the calculation of  $\gamma_{Co}^{Fe-Co-Ni}$  as a function of  $X_{Ni}$

Parameter	$\gamma_{Co}^{Fe-Co-Ni}$ (solid)	$\gamma_{Co}^{Fe-Co-Ni}$ (liquid)
a	-1.1196	-1.4591
b	0.828	1.2009
c	1.15	1.1

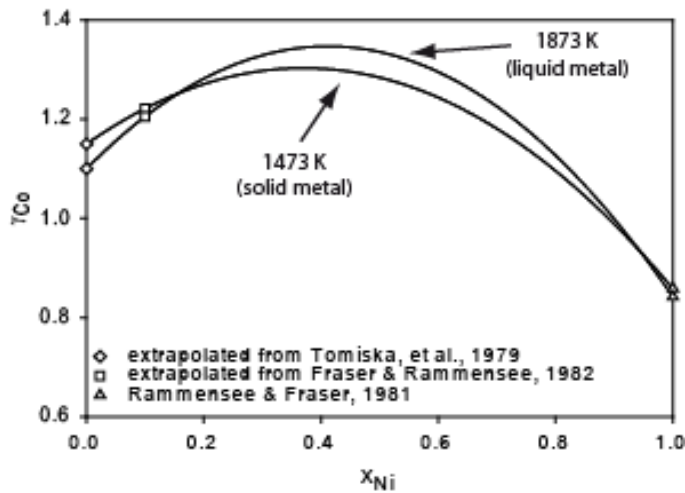


Fig. 13:  $\gamma_{Co}$  as a function of  $X_{Ni}$  for  $X_{Co} \sim 0$  in ternary Fe-Co-Ni alloys for solid and liquid metal extrapolated from data in TOMISKA et al. (1979), FRASER and RAMMENSEE (1982) and RAMMENSEE and FRASER (1981).

#### 4.4 Activity coefficients of $Fe_2SiO_4$ in olivine

The thermodynamic equations and explanations given in this chapter have been taken from WILL (1998). The simplest physical model to describe enthalpic changes in a crystal resulting from cation substitution is the nearest neighbour model. In a binary system (e.g. NaCl), three types of nearest neighbour atoms exist: AA, BB, AB. The energy of these pairs is termed  $\epsilon_{AA}$ ,  $\epsilon_{BB}$  and  $\epsilon_{AB}$  and the number of pairs is  $\frac{1}{2} N \cdot z$ , where N is the sum of A and B atoms and z is the coordination number. The total enthalpy of a solid solution can be expressed as:

$$H^{total} = \frac{1}{2} Nz (X_A \epsilon_{AA} + X_B \epsilon_{BB} + X_A X_B (2\epsilon_{AB} - \epsilon_{AA} - \epsilon_{BB})) \quad \text{Eq. 23}$$

$X_A$  and  $X_B$  are the mole fractions of component A and component B. The two terms  $\frac{1}{2} Nz X_A \epsilon_{AA}$  and  $\frac{1}{2} Nz X_B \epsilon_{BB}$  are enthalpies arising solely from the energetic interactions of nearest neighbours in the pure mineral end-members. Their sum gives the enthalpy of a pure mechanical mixture ( $H^{mech.mix}$ ). The term  $\frac{1}{2} Nz X_A X_B (2\epsilon_{AB} - \epsilon_{AA} - \epsilon_{BB})$  gives the energy necessary to form a chemically homogeneous solid solution, the enthalpy of mixing ( $\Delta H^{mix}$ ). The term  $2\epsilon_{AB} - \epsilon_{AA} - \epsilon_{BB}$  is commonly written as  $\Delta\epsilon$  and termed the characteristic potential. The enthalpy of mixing can therefore be expressed as:

$$\Delta H^{mix} = W_{AB} X_A X_B \quad \text{Eq. 24}$$

The parameter  $W_{AB}$  is the interaction parameter, which is commonly used to describe the mixing behaviour of different components in solid solution. For thermodynamic calculations,

interaction parameters are determined experimentally (WOOD and KLEPPA 1981, KAWASAKI and MATSUI 1983, SEIFERT and O'NEILL 1987).

Site occupancy data for olivine suggest a weak affinity of Fe to the M1-position, which would result in small differences between the interaction parameters  $W_{FeMg}^{M1}$  and  $W_{FeMg}^{M2}$  for the two sites in olivine (HIRSCHMANN 1991). SACK and GHIORSO (1989), however, assume the effect to be negligible. In this work, it is assumed that  $W_{FeMg}^{M1} = W_{FeMg}^{M2}$ . The equation for the regular solution model (Eq. 25) has been taken from WILL (1998).

$$\ln \gamma_{FeSi_{0.5}O_2}^{ol} = \frac{X_{Mg}Q - X_{Fe}JW_{FeMg}}{RT} \quad \text{Eq. 25}$$

The interaction parameter  $W_{FeMg}$  of  $6.28 \pm 0.33 \text{ kJmol}^{-1}$  has been taken from KAWASAKI and MATSUI (1983)(Fig. 14). This interaction parameter has been determined for olivine and co-existing garnet and orthopyroxene phases and may be subject to a larger uncertainty than quoted (SEIFERT et al. 1988). It is, however, consistent with calorimetric measurements published in WOOD and KLEPPA (1981). The interaction parameter has been determined from experiments in the range of 900-1400°C (KAWASAKI and MATSUI 1983). Calculations beyond this temperature may be subject to greater uncertainties.

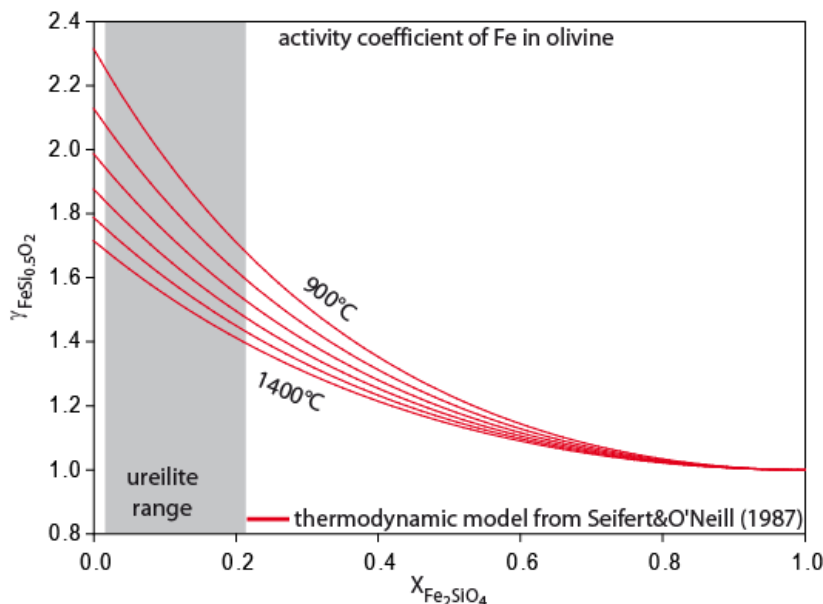


Fig. 14  $\gamma_{FeSi_{0.5}O_2}^{ol}$  as function of  $X_{Fe}$  at 100 °C intervals (900-1500°C). Calculations are based on the thermodynamic model published in SEIFERT et al. (1988).

#### 4.5 Activity coefficients of Ni<sub>2</sub>SiO<sub>4</sub> and Co<sub>2</sub>SiO<sub>4</sub> in olivine

Several activity models for the activity of Ni<sub>2</sub>SiO<sub>4</sub> and Co<sub>2</sub>SiO<sub>4</sub> have been published (SEIFERT and O'NEILL 1987, SEIFERT et al. 1988, HIRSCHMANN 1991). A simple model is the regular solution model that has been used by SEIFERT et al. (1988). The regular solution model ignores the effects of the temperature dependent intracrystalline cation ordering. In the regular solution model, activity coefficients  $\gamma_{Ni}^{ol}$  and  $\gamma_{Co}^{ol}$  are calculated as follows:

$$\ln \gamma_{Ni}^{ol} = \frac{W_{MgNi}^{ol} (X_{Mg}^{ol} + X_{Fe}^{ol})^2 - W_{MgFe}^{ol} (X_{Mg}^{ol} X_{Fe}^{ol})}{RT} \quad \text{Eq. 26}$$

$$\ln \gamma_{Co}^{ol} = \frac{W_{MgCo}^{ol} (X_{Mg}^{ol} + X_{Fe}^{ol})^2 - W_{MgFe}^{ol} (X_{Mg}^{ol} X_{Fe}^{ol})}{RT} \quad \text{Eq. 27}$$

The interaction parameter  $W_{MgCo}^{ol}$  has been experimentally determined to be  $1.37 \pm 0.9$  KJmol<sup>-1</sup> (SEIFERT and O'NEILL 1987) while  $W_{MgNi}^{ol}$  is  $0.35 \pm 0.9$  KJmol<sup>-1</sup>. Both parameters have been determined for the Mg-Ni- and the Mg-Co-System only. Due to the lack of data, it is assumed that  $W_{MgM}^{ol} = W_{FeM}^{ol}$ . Both interaction parameters have been obtained from experiments performed in the range of 927-1400°C. Within this temperature range, the interaction parameters are, within experimental uncertainty apparently independent of temperature. Extrapolation to higher temperatures will, however, introduce further uncertainties (SEIFERT et al. 1988).

To account for non-ideal interactions between divalent cations and long range ordering of cations between the M1 and M2 site, HIRSCHMANN (1991) introduced a more general thermodynamic model for minor elements in olivine based on cation ordering and symmetrical mixing enthalpies assuming  $\Delta S^{EX} = 0$  and therefore  $\Delta G^{EX} = \Delta H^{EX}$ . The activity coefficients for Ni<sub>2</sub>SiO<sub>4</sub> and Co<sub>2</sub>SiO<sub>4</sub> based on that model and published in HIRSCHMANN and GHIORSO (1994) were taken and fitted into functions of temperature and  $X_{fa}$ . The fitted activities (Eq. 28, Eq. 29) are shown in Fig. 15 and Fig. 16 along with the activity coefficients calculated from the model of SEIFERT et al. (1988).

$$\ln \gamma_{Ni}^{ol} = 0.02 - 0.62X_{fa} + 0.87X_{fa}^2 + (253 + 242X_{fa}) \frac{1}{T} + \frac{(-829316 + 625911X_{fa})1}{T^2} \quad \text{Eq. 28}$$

$$\ln \gamma_{Ni}^{ol} = 0.16 - 0.04X_{fa} + \left(0.04 + 1165.4 \frac{1}{T}\right)X_{fa}^2 + \frac{(-170 - 1162.5X_{fa})1}{T}$$

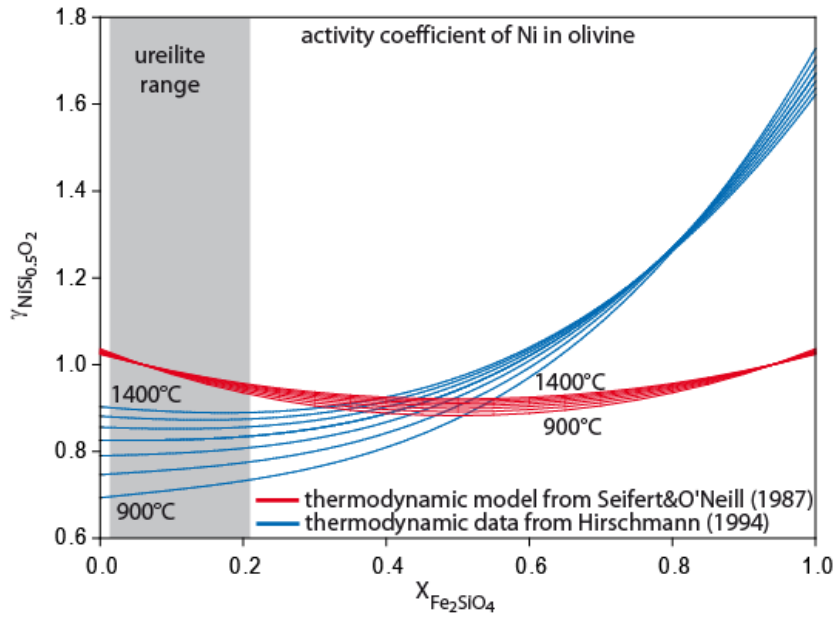


Fig. 15  $\gamma_{Ni_{0.5}O_2}^{ol}$  as function of  $X_{fa}$  at 100 °C intervals (900-1500°C). Calculations are based on data published in HIRSCHMANN and GHIORSO (1994) for 0.5 mol% of Ni<sub>2</sub>SiO<sub>4</sub> in otherwise pure (Mg, Fe)<sub>2</sub>SiO<sub>2</sub> and the thermodynamic models published in SEIFERT et al. (1988).

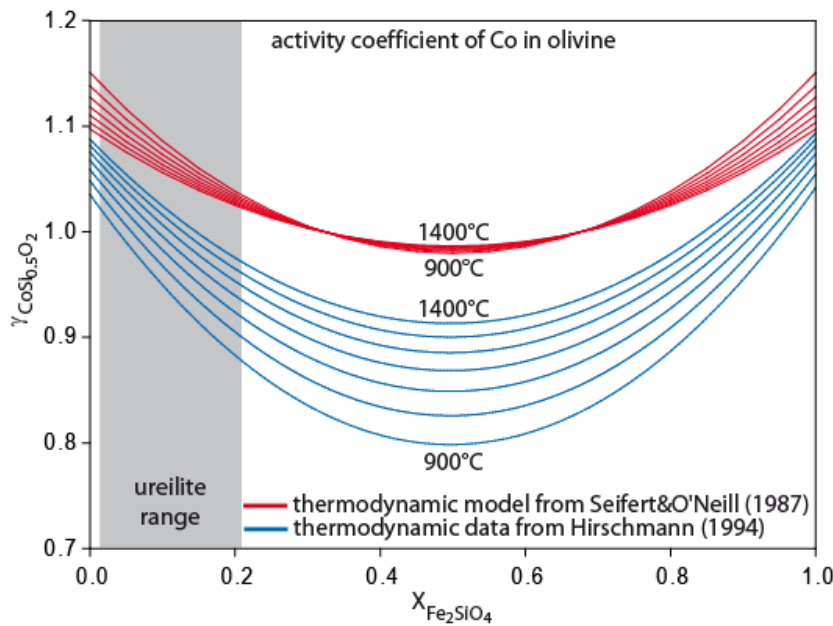


Fig. 16  $\gamma_{Co_{0.5}O_2}^{ol}$  as function of  $X_{fa}$  at 100 °C intervals (900-1500°C). Calculations are based on data published in HIRSCHMANN and GHIORSO (1994) for 0.5 mol% of Co<sub>2</sub>SiO<sub>4</sub> in otherwise pure (Mg, Fe)<sub>2</sub>SiO<sub>2</sub> and the thermodynamic models published in SEIFERT et al. (1988).

The activity coefficients calculated from the thermodynamic model of SEIFERT et al. (1988) are higher and less temperature dependent than those calculated by HIRSCHMANN and GHIORSO (1994) for  $fa < 20$ , which is the typical composition of ureilite olivine.

#### 4.6 Comparison of the regular solution model with Hirschmann's model

We calculated  $\ln K_{D(Fe-Ni)}^{ol-met}$ , with M either being Ni or Co, for experimental compositions published in SEIFERT et al. (1988) and compared them observed  $\ln K_{D(Fe-Ni)}^{ol-met}$  in those experiments (Fig. 17, Fig. 18). The experiments were performed at different temperatures in the range of 1260-1760°C and at different pressures (0.5 GPa and 3.5 GPa). To account for pressure differences, pressure correction terms given in SEIFERT et al. (1988) have been applied to the experimentally determined  $\ln K_{D(Fe-Ni)}^{ol-met}$ .

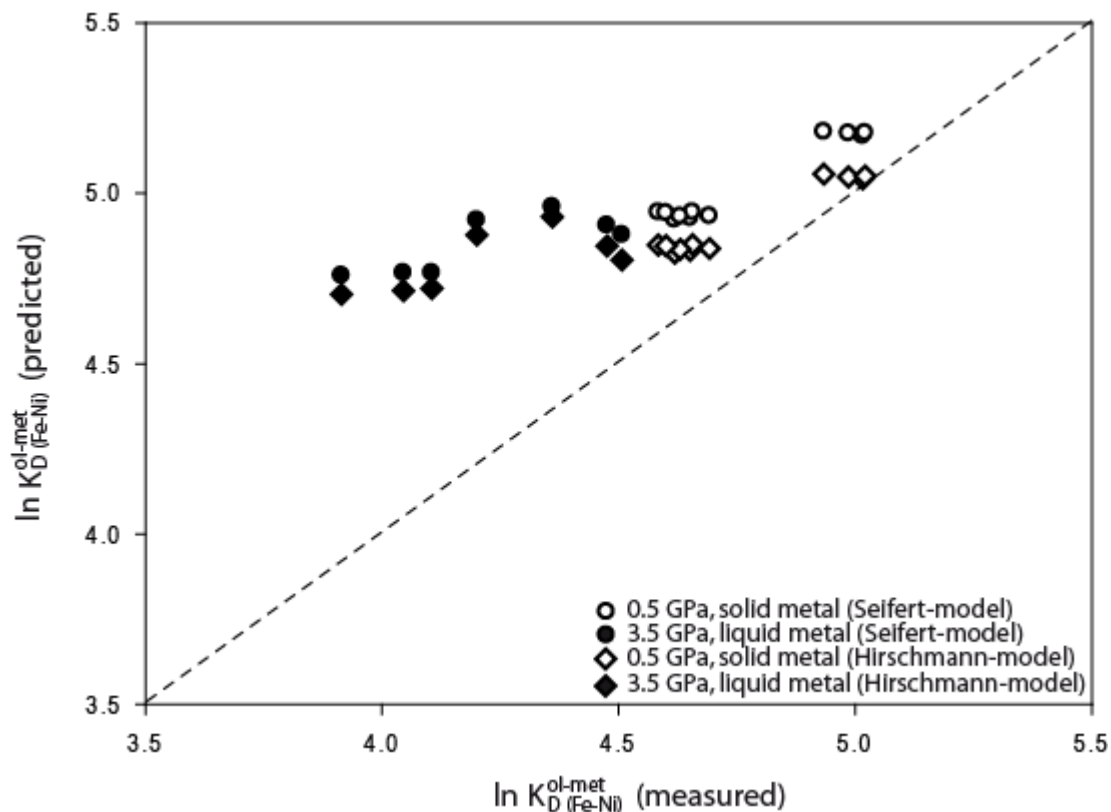


Fig. 17  $\ln K_{D(Fe-Ni)}^{ol-met}$  calculated with the regular solution model used by SEIFERT et al. (1988) (circles) and the activity model developed by HIRSCHMANN (1991) (diamonds) against  $\ln K_{D(Fe-Ni)}^{ol-met}$  calculated from experimental data in SEIFERT et al. (1988). Solid symbols represent experiments at 3.5 GPa and temperatures >1600°C and open symbols represent experiments at 0.5 GPa and temperatures <1420°C.

The calculated  $\ln K_{D(Fe-Ni)}^{ol-met}$  is higher than the experimentally determined in both models (Fig. 17). The  $\ln K_{D(Fe-Ni)}^{ol-met}$  calculated from the thermodynamic data in HIRSCHMANN (1991) generally show a lower offset of ~0.15 for experiments at 0.5 GPa and ~0.56 for experiments at 3.5 GPa than the  $\ln K_{D(Fe-Ni)}^{ol-met}$  calculated from the thermodynamic model in SEIFERT et al. (1988) (offset of ~0.26 for experiments at 0.5 GPa and ~0.61 for experiments at 3.5 GPa, respectively). The offset is the average difference between predicted and experimentally

determined  $\ln K_{D(Fe-Co)}^{ol-met}$ . The offset is smaller for experiments conducted at 0.5 GPa than for those conducted at 3.5 GPa. Since the  $\ln K_{D(Fe-Co)}^{ol-met}$  calculated with the thermodynamic model of HIRSCHMANN (1991) fits better with experimental data, it is chosen for the calculations in this work. The calculations show substantial differences between experimental data and predicted values. Some possible explanations have been discussed in SEIFERT et al. (1988). The data which show the largest discrepancies are the experiments performed at 3.5 GPa. It has been suggested that the assumptions applied when calculating the effect of pressure has been too simple (SEIFERT et al. 1988). The calculations in this work are done for a low-pressure environment. It might therefore be sufficient to assume a  $2\sigma$  error of  $\pm 0.15$  for the calculation of  $\ln K_{D(Fe-Co)}^{ol-met}$ .

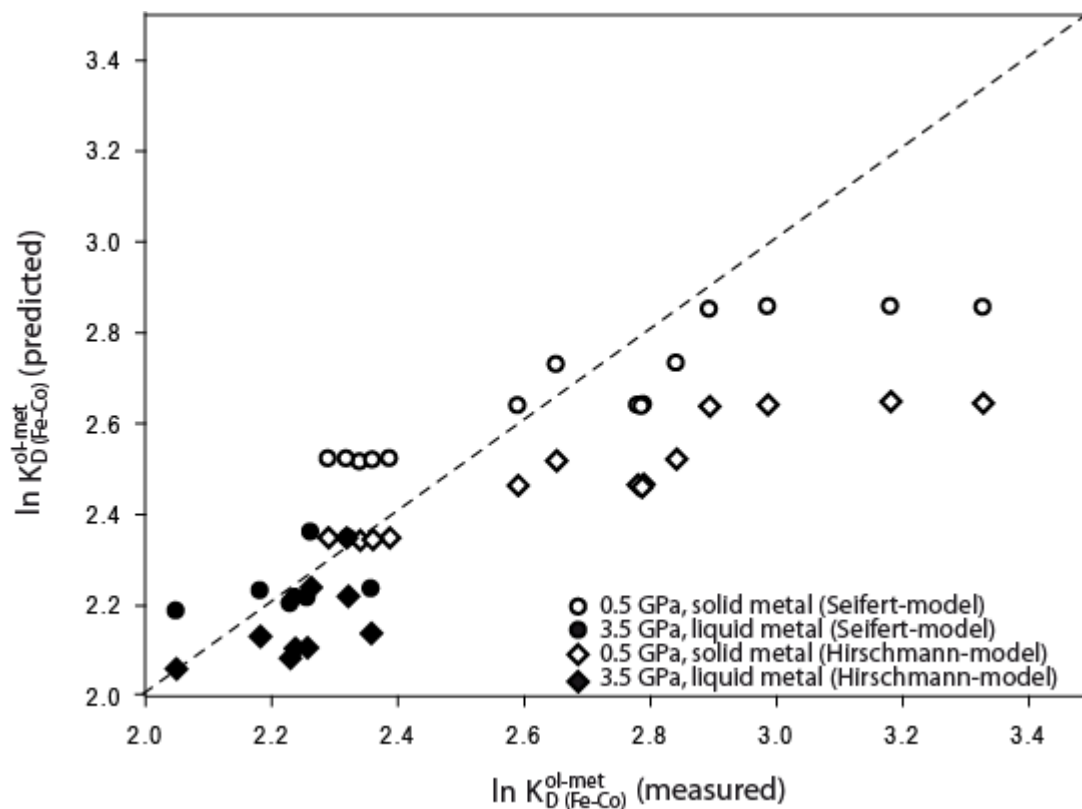


Fig. 18  $\ln K_{D(Fe-Co)}^{ol-met}$  calculated with the regular solution model used by SEIFERT et al. (1988) (circles) and the activity model developed by HIRSCHMANN (1991) (diamonds) against  $\ln K_{D(Fe-Co)}^{ol-met}$  calculated from experimental data in SEIFERT et al. (1988). Filled symbols represent experiments at 3.5 GPa and temperatures  $>1600^{\circ}\text{C}$  and open symbols represent experiments at 0.5 GPa and temperatures  $<1420^{\circ}\text{C}$ .

For the  $\ln K_{D(Fe-Co)}^{ol-met}$  the comparison between experimentally determined and model values turned out to be reverse (Fig. 18) to the data for  $\ln K_{D(Fe-Co)}^{ol-met}$ . The difference is  $\sim 0.11$  for experiments at 3.5 GPa and  $\sim 0.23$  at 0.5 GPa for calculations with the thermodynamic model

in HIRSCHMANN (1991) and  $\sim 0.07$  for experiments at 3.5 GPa and  $\sim 0.17$  at 0.5 GPa for calculations with the thermodynamic model in SEIFERT et al. (1988). For  $\text{Fe-Cr-Co}$  the Seifert-model fits better with experimental data and is therefore chosen for calculations in this work. A  $2\sigma$  error of  $\pm 0.15$  is assumed.

## 5 Mass balance calculations

### 5.1 Mass balance calculations of the UPB's core

The goal of this calculation is to determine the composition of the UPB's metallic core based on a chondritic starting composition and the composition of the undepleted mantle (ureilite + basaltic component) of the UPB.

First, all chondritic element concentrations must be converted to masses by multiplication with the UPB's mass (Eq. 30). In this work, only SiO<sub>2</sub>, MgO, Al<sub>2</sub>O<sub>3</sub>, Na<sub>2</sub>O, CaO, TiO<sub>2</sub>, Cr<sub>2</sub>O<sub>3</sub>, MnO (lithophile elements) and Fe, Ni and Co are considered in the mass balance calculation. For mass balance calculations the mass of the UPB is arbitrary as long as the same mass is used for all calculations.

$$m_{\text{element}}^{\text{UPB}} = c_{\text{element}}^{\text{chondrite}} \cdot m_{\text{total}}^{\text{UPB}} \quad \text{Eq. 30}$$

To calculate the composition of the UPB's mantle, lithophile elements are considered to be

incorporated into the mantle ( $\sum m_{\text{lithophile}}^{\text{UPB}} = \sum m_{\text{lithophile}}^{\text{mantle}}$ ) along with a fraction of FeO, NiO and CoO. The masses of FeO, NiO and CoO can be calculated from their mass fraction

( $X_{\text{metal}}^{\text{mantle}} = \frac{c_{\text{metal}}^{\text{mantle}}}{100}$ ) in the undepleted mantle and the masses of the lithophile elements:

$$m_{\text{FeO}}^{\text{mantle}} = \left( \sum m_{\text{lithophile}}^{\text{mantle}} + m_{\text{NiO}}^{\text{mantle}} + m_{\text{CoO}}^{\text{mantle}} \right) \cdot \frac{X_{\text{FeO}}^{\text{mantle}}}{(1 - X_{\text{FeO}}^{\text{mantle}})} \quad \text{Eq. 31}$$

$$m_{\text{NiO}}^{\text{mantle}} = \left( \sum m_{\text{lithophile}}^{\text{mantle}} + m_{\text{FeO}}^{\text{mantle}} + m_{\text{CoO}}^{\text{mantle}} \right) \cdot \frac{X_{\text{NiO}}^{\text{mantle}}}{(1 - X_{\text{NiO}}^{\text{mantle}})} \quad \text{Eq. 32}$$

$$m_{\text{CoO}}^{\text{mantle}} = \left( \sum m_{\text{lithophite}}^{\text{mantle}} + m_{\text{FeO}}^{\text{mantle}} + m_{\text{NiO}}^{\text{mantle}} \right) \cdot \frac{X_{\text{CoO}}^{\text{mantle}}}{(1 - X_{\text{CoO}}^{\text{mantle}})} \quad \text{Eq. 33}$$

To keep the equations simple, we define:  $A = \frac{X_{\text{FeO}}^{\text{mantle}}}{(1 - X_{\text{FeO}}^{\text{mantle}})}$ ,  $B = \frac{X_{\text{NiO}}^{\text{mantle}}}{(1 - X_{\text{NiO}}^{\text{mantle}})}$  and

$C = \frac{X_{\text{CoO}}^{\text{mantle}}}{(1 - X_{\text{CoO}}^{\text{mantle}})}$ . Inserting Eq. 32 and Eq. 33 into Eq. 31 gives:

$$m_{\text{FeO}}^{\text{mantle}} = m_{\text{lithophite}}^{\text{mantle}} \cdot \frac{(A + AB + AC + ABC)}{(1 - AB - BC - AC - 2ABC)} \quad \text{Eq. 34}$$

And:

$$m_{\text{NiO}}^{\text{mantle}} = C \cdot \frac{(m_{\text{lithophite}}^{\text{mantle}} + m_{\text{lithophite}}^{\text{mantle}} B + m_{\text{FeO}}^{\text{mantle}} B + m_{\text{FeO}}^{\text{mantle}})}{(1 - CB)} \quad \text{Eq. 35}$$

$$m_{\text{CoO}}^{\text{mantle}} = B \cdot (m_{\text{lithophite}}^{\text{mantle}} + m_{\text{FeO}}^{\text{mantle}} + m_{\text{NiO}}^{\text{mantle}}) \quad \text{Eq. 36}$$

To calculate the core composition, the masses of FeO, CoO and NiO in the mantle must be subtracted from their respective chondritic masses and normalized.

$$m_{\text{metal}}^{\text{core}} = m_{\text{metal}}^{\text{UPB}} - m_{\text{metal}}^{\text{mantle}} \quad \text{Eq. 37}$$

As neither C nor S will be incorporated into the silicate phase in relevant amounts, both elements have not been modeled along with Ni and Co, but added to the metal portion.

## 5.2 Model of the UPB core formation process

The goal of this calculation is to determine the concentrations of Fe, Ni and Co in melt and residual when melting the metal component of the undifferentiated UPB during the core formation process.

Two different types of metal melting are modeled in this work – batch melting and fractional melting. In fractional melting, the liquid metal is removed as it forms. In batch melting, the liquid metal stays in equilibrium with the solid metal until it is removed at a given degree of melting. The calculation of both processes is essentially identical. The calculations are based on a simple mass balance calculation (Eq. 38).

$$C_{\text{element}}^{\text{bulk}} = C_{\text{element}}^{\text{solid}} \cdot X_{\text{solid}} + C_{\text{element}}^{\text{liquid}} \cdot X_{\text{liquid}}$$

Eq. 38

C refers to the concentration of a given element in a respective component, while X refers to the weight fraction of the respective component. Information on the elemental concentrations of a respective element within each component is given by the distribution

coefficient  $D_{\text{element}}^{\text{metal/liquid}}$ . The distribution coefficient is defined as:

$$D_{\text{element}}^{\text{metal/liquid}} = \frac{C_{\text{element}}^{\text{solid}}}{C_{\text{element}}^{\text{liquid}}}$$

Eq. 39

Calculations of the behavior of Ni and Co in sulfur-rich systems in this work are based on the distribution coefficients published in CHABOT et al. (2003). Calculations on the behavior of Ni and Co in carbon-rich systems are based on the distribution coefficients published in CHABOT et al. (2006). From the data in both works regression curves were calculated (Fig. 19) to obtain distribution coefficients, depending on the sulfur or the carbon content of the melt.

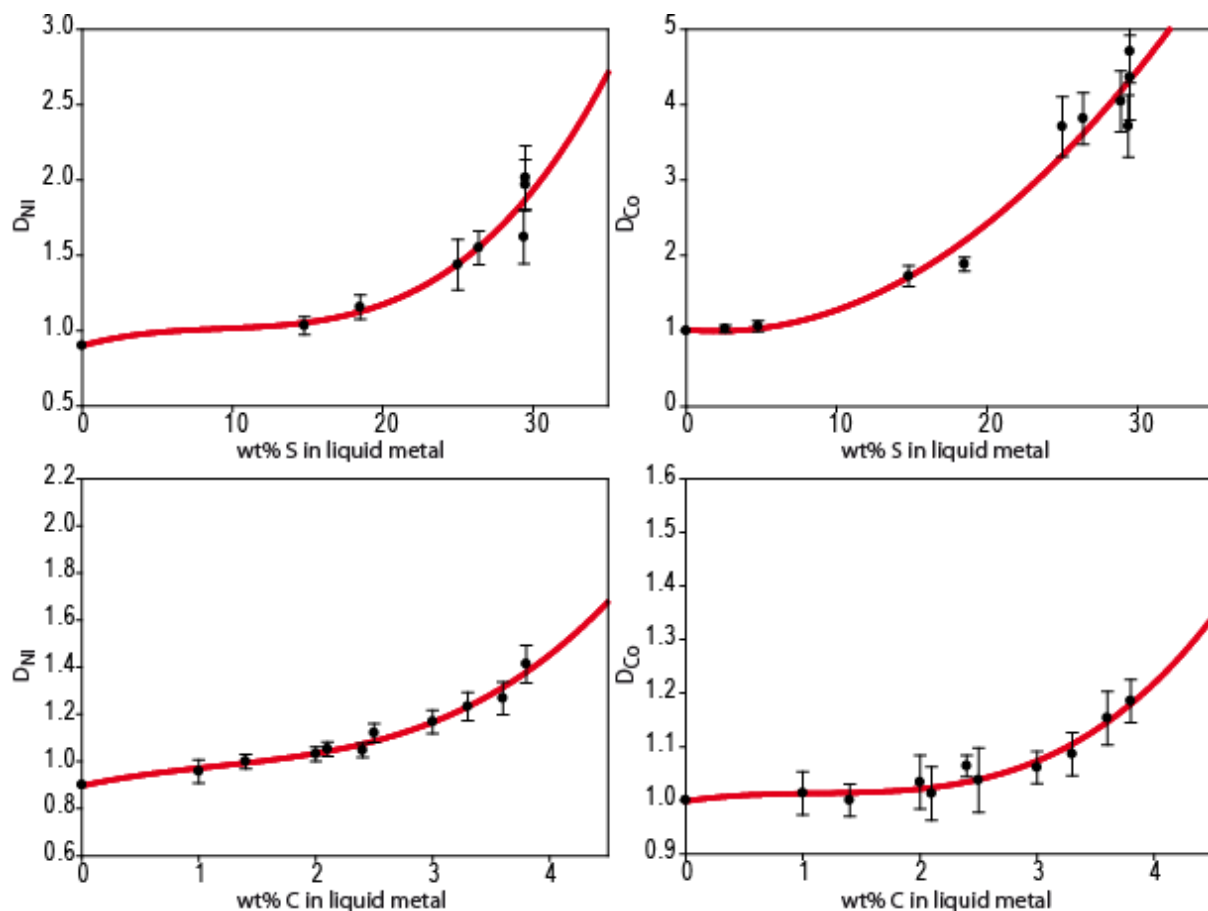


Fig. 19 Distribution coefficients of Ni and Co between solid metal and liquid metal. Data taken from CHABOT et al. (2003) and CHABOT et al. (2006). Red lines represent calculated regressions used in this work.

Regression curves have been calculated as cubic equations (Eq. 40) with the parameters given in Table 9.

$$D_{\frac{S}{T}}^{\text{element}} = a \cdot x^3 + b \cdot x^2 + c \cdot x + d \quad \text{Eq. 40}$$

X represents the concentration of either sulfur or carbon in liquid metal.

Table 9 Parameter for the calculation of  $D_{\frac{S}{T}}^{\text{Ni}}$  and  $D_{\frac{S}{T}}^{\text{Co}}$  for different amounts of sulfur and carbon in liquid metal

Parameter	$D_{\frac{S}{T}}^{\text{Ni}}$ (sulfur)	$D_{\frac{S}{T}}^{\text{Co}}$ (sulfur)	$D_{\frac{S}{T}}^{\text{Ni}}$ (carbon)	$D_{\frac{S}{T}}^{\text{Co}}$ (carbon)
a	0.00825	0.01380	0	0.00009
b	-0.02770	-0.04790	0.00443	-0.00260
c	0.03390	0.10910	-0.01830	0.02830
d	0.99830	0.89670	1.01590	0.89910

In a fractional metal melting process it is assumed that only two phases exist at any given time – liquid melt and a solid residual (containing FeNi-metal, troilite and cohenite):

$$X_{\text{solid}} = 1 - X_{\text{liquid}} \quad \text{Eq. 41}$$

Eq. 38 can therefore be rearranged to allow the calculation of concentrations of Ni and Co in solid residual (Eq. 42) and liquid metal (Eq. 43).

$$C_{\text{solid}}^{\text{element}} = \frac{C_{\text{bulk}}^{\text{element}}}{\frac{X_{\text{liquid}}}{D_{\frac{S}{T}}^{\text{metal}}} + (1 - X_{\text{liquid}})} \quad \text{Eq. 42}$$

$$C_{\text{liquid}}^{\text{element}} = \frac{C_{\text{bulk}}^{\text{element}}}{D_{\frac{S}{T}}^{\text{metal}}(1 - X_{\text{liquid}}) + X_{\text{liquid}}} \quad \text{Eq. 43}$$

In this work, the melting of a sulfur- and carbon-bearing metal-rich component is modeled. In fractional melting, any melt formed is immediately removed. The first melts that form in a System (either Fe-S or Fe-C), form at the eutectic point and are hence termed eutectic melts. The eutectic compositions for the Fe-S-System used in this work are 30.8 wt% S (Fig. 20, RANKENBURG et al. (2008) and references therein) and 4.4 wt% C for the Fe-C-System (Fig. 21, RAGHAVAN 1988).

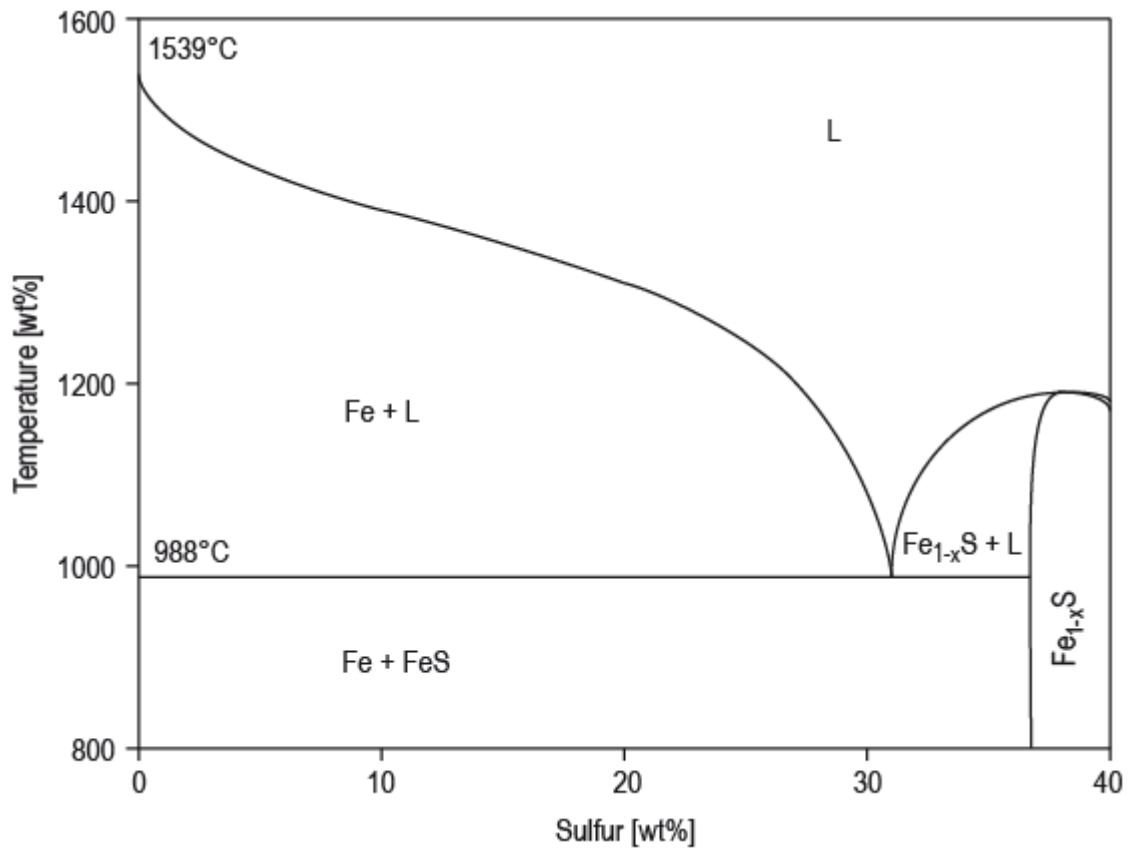


Fig. 20 Fe-rich side of the Fe-S phase diagram. Diagram taken and simplified from RANKENBURG et al. (2008)

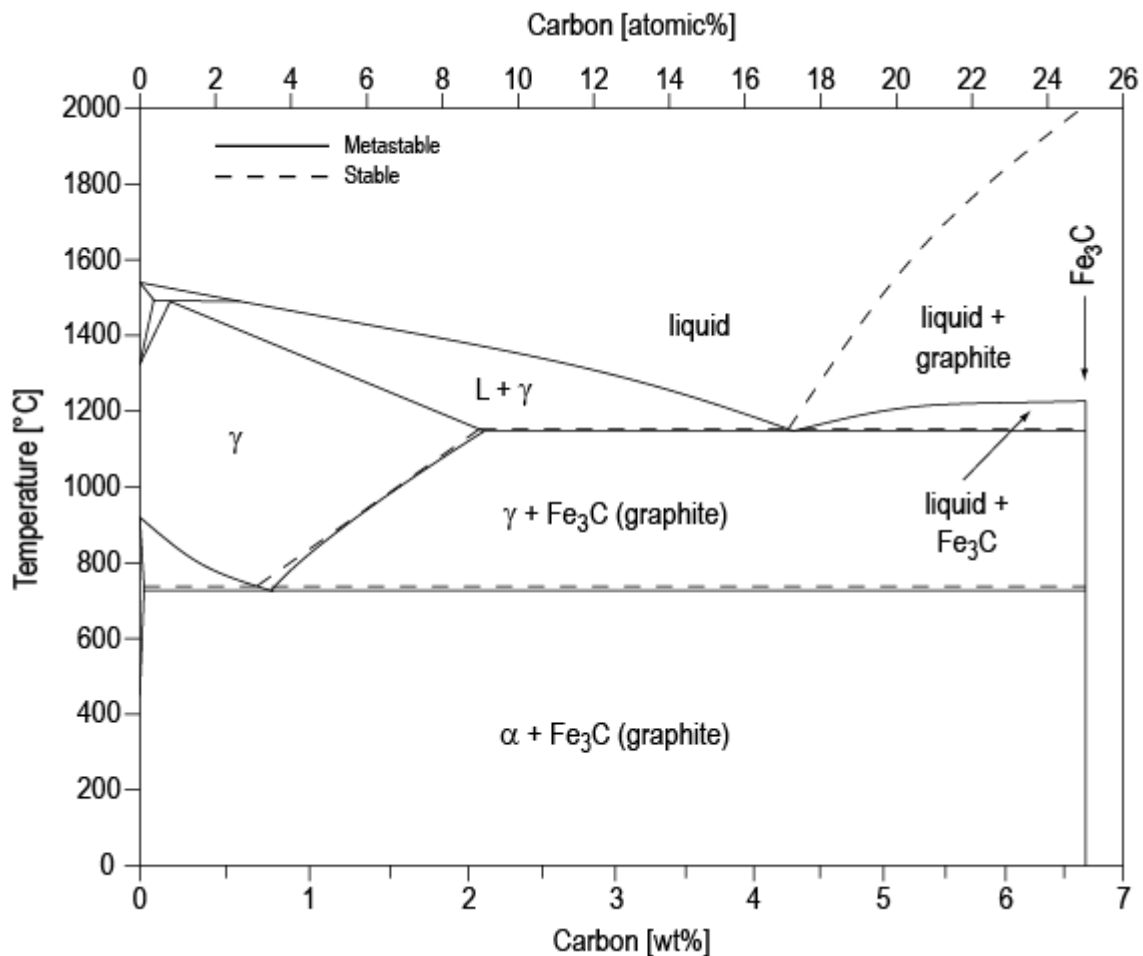


Fig. 21 Fe-rich side of the Fe-C phase diagram. Diagram taken and simplified from RAGHAVAN (1988).

First, sulfur-rich melt is formed (at  $\sim 990^\circ\text{C}$ ) and removed until sulfur is entirely removed from the mantle, then carbon-rich melt is formed (at  $\sim 1150^\circ\text{C}$ ) and removed until either carbon or iron are entirely removed from the mantle. Depending on the composition of the system, the final product is either a carbon-rich residual or a carbon- and sulfur-free melt. The distribution coefficients are constant during all stages of melting, as the carbon- and sulfur-concentration in the melt remain constant until either C or S are removed entirely. The calculations are done incrementally, with a stepwise (step size = 1 wt%) increasing  $X_{\text{liquid}}$ . In fractional melting,  $C_{\text{element}}^{\text{bulk}}$  always refers to the concentration of the preceding calculation step, while in batch melting,  $C_{\text{element}}^{\text{bulk}}$  refers to the concentrations of the starting composition.

The modeling of the batch melting process is more complicated. The calculations in this work are based on the ternary diagram published in GOODRICH and BERKLEY (1986) after VOGEL and RITZAU (1931) (Fig. 22). Until the temperature reaches  $\sim 1100^\circ\text{C}$ , only S-rich melt is formed. At

1100°C, S-rich melt and C-rich melt coexist. Therefore, Eq. 42 needs to be extended with an additional term for the second melt (Eq. 44).

$$C_{\text{residual}}^{\text{metal}} = \frac{C_{\text{bulk}}^{\text{metal}}}{\frac{X_{\text{S-rich liquid}}}{D(S)_F^{\text{metal}}} + \frac{X_{\text{C-rich liquid}}}{D(C)_F^{\text{metal}}} + (1 - X_{\text{S-rich liquid}} - X_{\text{C-rich liquid}})} \quad \text{Eq. 44}$$

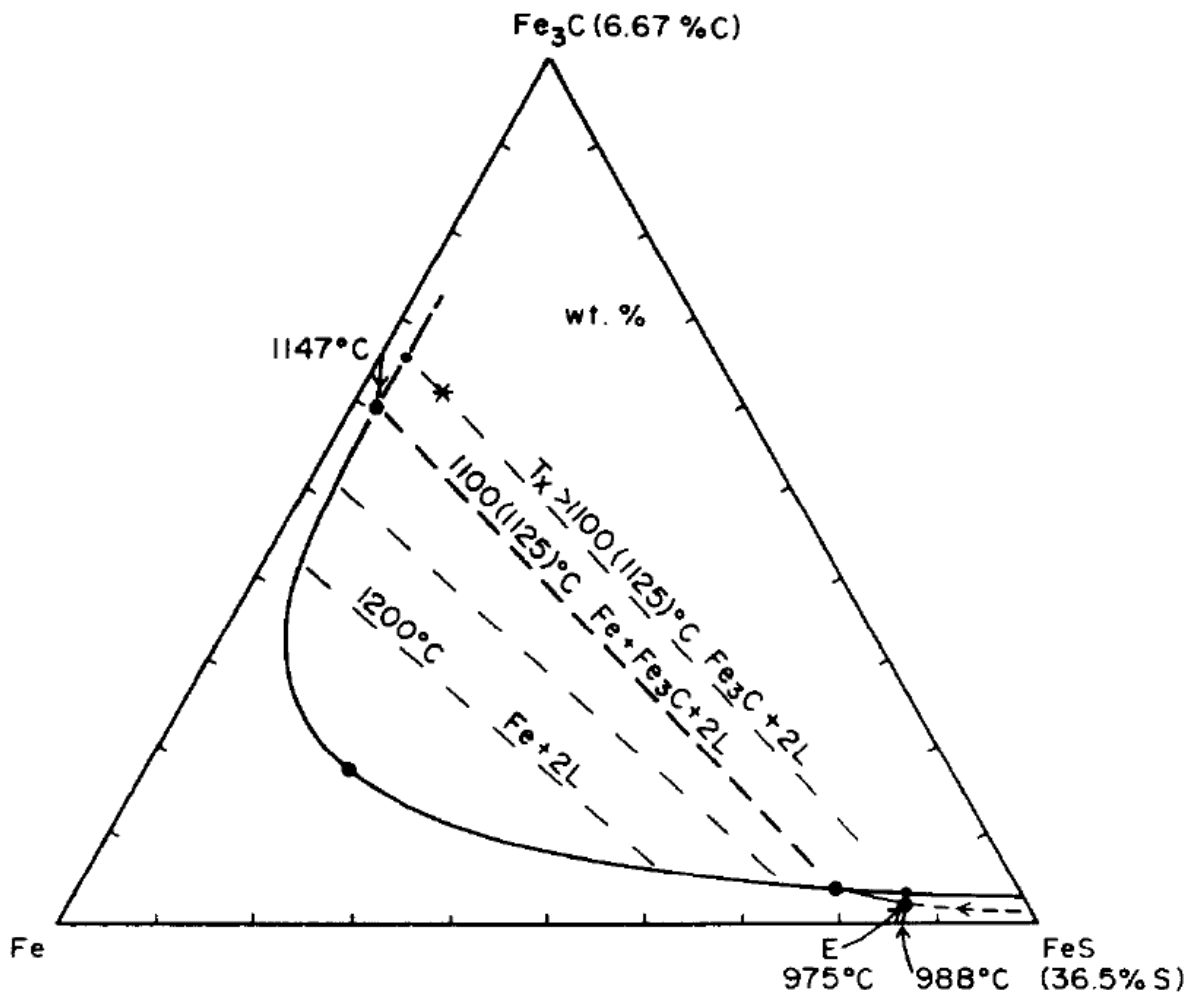


Fig. 22 Ternary diagram of the Fe-FeS-FeC-system taken from GOODRICH and BERKLEY (1986) after VOGEL and RITZAU (1931).

In contrast to fractional melting, the carbon- and sulfur-concentrations in the melt vary during the melting process, thus changing the distribution coefficients  $D(S)_F^{\text{metal}}$  and  $D(C)_F^{\text{metal}}$ . The concentrations of sulfur and carbon in the liquids remain unchanged until either sulfur or carbon is exhausted in the residual metal. At that point, the concentrations

in the respective liquids depend on the total mass of carbon and sulfur as well as the weight fractions of each liquid (Eq. 45).

$$C_{S\text{-rich liquid}}^{\text{sulfur}} = \frac{C_{\text{bulk}}^{\text{sulfur}} - X_{C\text{-rich liquid}} \cdot C_{C\text{-rich liquid}}^{\text{sulfur}}}{X_{S\text{-rich liquid}}} \quad \text{Eq. 45}$$

$$C_{C\text{-rich liquid}}^{\text{carbon}} = \frac{C_{\text{bulk}}^{\text{carbon}} - X_{S\text{-rich liquid}} \cdot C_{S\text{-rich liquid}}^{\text{carbon}}}{X_{C\text{-rich liquid}}} \quad \text{Eq. 46}$$

Although the diagram (Fig. 22) indicates minor changes, fixed values of 0.3 wt% carbon in the S-rich melt and 1.0 wt% sulfur in the C-rich melt are assumed for modeling (Fig. 22). This assumption has only little influence on the modeling results, but greatly simplifies the calculation process.

## 6 Sampling

Nine monomict ureilites with different fayalite ( $fa$ ) contents are used in this work: ALH84136 ( $fa_3$ ), EET87517 ( $fa_{8.0}$ ), LEW85440 ( $fa_{8.6}$ ), EET96331 ( $fa_{11.9}$ ), ALHA77257 ( $fa_{13.3}$ ), EET96042 ( $fa_{17.3}$ ), DaG340 ( $fa_{19.2}$ ), GRA95205 ( $fa_{19.9}$ ), and Kenna ( $fa_{20.4}$ ). Approximately 1g of each Antarctic ureilite was obtained from the NASA sample request program. 1g of Kenna and DaG340 was provided by Dr. Jutta Zipfel (Forschungsinstitut und Naturkundemuseum Senckenberg, Frankfurt).

The meteorites were chosen to cover a wide range of different  $fa$ -compositions.

### 6.1 Allan Hills 84136 (ALH84136)

Allan Hills 84136 was collected by the US Antarctic Search for Meteorite program (ANSMET) in 1984 (GROSSMAN 2009). The weight of the meteorite was 83.5 g. ALH84136 is an augite-bearing ureilite and moderately weathered (B) (GROSSMAN 1994). ALH84136 is probably paired with ALH82130 and ALH82106 (GOODRICH 1992, GROSSMAN 1994, MASON and MARTINEZ 1986).

The sample was described to contain anhedral to subhedral olivine and pyroxene grains, approximately 0.6 – 2.4 mm in diameter (MASON and MARTINEZ 1986). ALH84136 contains about 10% vein material (MASON and MARTINEZ 1986).

Olivine composition ranges from  $fa_0$  to  $fa_5$  with an average of  $fa_3$  (MASON and MARTINEZ 1986). GOODRICH (1992) reports  $fa_{4.5}$  for paired ALH82106 and  $fa_{5.1}$  for paired ALH82139. Reduction rims are extensive ( $> 100 \mu\text{m}$ , SINHA et al. 1997). Although paired, reduction rims are less extensive in ALH82130/106 ( $10 - 100 \mu\text{m}$ , SINHA et al. 1997).

Pigeonite composition is  $Wo_{10-12}$  and  $En_{83-85}$  (SINHA et al. 1997). Orthopyroxene is  $Wo_{5-7}$  and  $En_{83-85}$  (SINHA et al. 1997). Augite is  $Wo_{37-40}$  and  $En_{55-58}$  in ALH82130 and  $Wo_{36-40}$  and  $En_{54-57}$  in ALH81106 (SINHA et al. 1997). Pyroxene grains are clear and extremely fractured (MASON and MARTINEZ 1986).

GOODRICH and BERKLEY (1986) found eight spherule inclusions in ALH82130. The average composition of the spherules is 89.7 wt% Fe, 2.7 wt% Ni, 0.44 wt% Co, 0.96 wt% Cr, 0.56 wt% Si and 5.2 wt% C.

The  $\Delta^{17}\text{O}$  of bulk ALH84136 is -2.42 ‰ (CLAYTON and MAYEDA 1988). Equilibration temperature obtained from pyroxene-pyroxene-thermometer is 1215°C (SINHA et al. 1997).

## **6.2 Allan Hills 77257 (ALHA77257)**

ALHA77257 (also called ALH77257 in older publications) was collected by a joint operation of ANSMET and the Japanese National Institute of Polar Research (NIPR) in 1977 or 1978 (GROSSMAN 2009). The meteorite weighed 1995.7 g (GROSSMAN 1994). The meteorite shows only minor weathering (Grade Ae) (GROSSMAN 1994) and low shock (RANKENBURG et al. 2008). ALHA77257 consists of ~80% olivine and ~15% pigeonite and orthopyroxene (MASON 1981, BERKLEY et al. 1980, RANKENBURG et al. 2008, TAKEDA 1987).

Olivine grains are anhedral to subhedral and up to 4 mm in diameter (MASON 1981). Their composition is  $fa_{9-23}$  with an average of  $fa_{13}$  and high CaO (0.32 - 0.34 wt%) and high  $\text{Cr}_2\text{O}_3$  (0.65 - 0.74 wt%) (MASON 1981, BERKLEY et al. 1980, RANKENBURG et al. 2008, TAKEDA 1987, GOODRICH et al. 1987b). Olivine grains show undulose extinction (MASON 1981).

Pyroxene grains are anhedral to subhedral and up to 3 mm in diameter (MASON 1981). Pigeonite contains 3.4 - 3.47 wt% CaO and 8.17 - 8.8 wt% FeO and orthopyroxene contains 2.14 wt% CaO and 7.75 wt% FeO (TAKEDA 1987, GOODRICH et al. 1987b, BERKLEY et al. 1980). Orthopyroxene has only been reported by TAKEDA (1987). Pyroxene grains show coarse polysynthetic twinning (MASON 1981).

GOODRICH and BERKLEY (1986) observed more than 50 spherule inclusions in ALHA77257. Their composition ranges from 3.7 to 4.3 wt% Ni, 0.46 to 0.55 wt% Co, 0.1 to 0.16 wt% Cr, 0.03 to 0.06 wt% Si and 4.8 to 5.1 wt% C. Spherule inclusions from ALHA77257 represent more than 70 % of all spherule inclusions reported in GOODRICH and BERKLEY (1986).

The  $\Delta^{17}\text{O}$  of bulk ALH77257 is -1.08 ‰ (CLAYTON and MAYEDA 1988).

## **6.3 Dar al Gani 340 (DaG340)**

DaG340 was found in Libya in 1994. The mass of the meteorite was 591 g (GROSSMAN 2009). DaG340 shows complete oxidation of metal grains and troilite, with no alteration of silicates

(weathering grade W4) and low shock (GROSSMAN 1998). The meteorite is composed of ~79 % olivine and ~19 % pigeonite (SINGLETARY and GROVE 2003). The olivine-pyroxene-thermometer gives an equilibration temperature of 1224°C (SINGLETARY and GROVE 2003).

Olivine composition is  $fa_{20.3}$  with 0.4 wt% CaO and 0.81 Cr<sub>2</sub>O<sub>3</sub> (SINGLETARY and GROVE 2003). Mg x-ray mapping shows that 33.6% of total olivine is in reduced rims (SINGLETARY and GROVE 2003).

Pigeonite composition is  $Wo_{9.8}$  with 11.0 wt% FeO (SINGLETARY and GROVE 2003).

#### **6.4 Elephant Moraine 87517 (EET87517)**

EET87517 has been collected in 1987 by ANSMET and weighted 273 g (GROSSMAN 2009). The sample is severely weathered (Grade B/C) (GROSSMAN 1994) and the shock-level is low (RANKENBURG et al. 2008). The meteorite is composed of approximately equal amounts olivine (~45%) and pigeonite (~55%) (MASON and SCORE 1988, SINGLETARY and GROVE 2003). The olivine-pyroxene equilibration temperature of EET87517 is 1301°C (SINGLETARY and GROVE 2003).

Olivine grains are subhedral to anhedral with (0.3 to 1.8 mm in diameter) (MASON and SCORE 1988). Olivine composition is  $fa_{7.7-8}$  with 0.35 CaO and 0.38 Cr<sub>2</sub>O<sub>3</sub> (SINGLETARY and GROVE 2003, GROSSMAN 1994). No reduction rims have been found with Mg x-ray mapping (SINGLETARY and GROVE 2003).

Pigeonite grains are subhedral to anhedral with (0.3 to 1.8 mm in diameter) (MASON and SCORE 1988). Some grains show exsolution lamellae, which have been interpreted as augite (MASON and SCORE 1988). Pigeonite composition is  $Wo_{4.7}$  and  $Fs_8$  (GROSSMAN 1994, SINGLETARY and GROVE 2003).

#### **6.5 Elephant Moraine 96042 (EET96042)**

EET96042 has been collected in 1996 by ANSMET and weighted 249.8 g (GROSSMAN 2009). The sample is moderately weathered (grade A/B) and shows a medium shock level (GROSSMAN 1998, RANKENBURG et al. 2008).

Olivine grains are up to 3 mm in size and show undulatory extinction (McCOY and McBRIDE 1998a). Olivine composition is  $fa_{18}$  (McCOY and McBRIDE 1998a, RANKENBURG et al. 2008). Reduction rims with  $fa_{14}$  are present (McCOY and McBRIDE 1998a).

## 6.6 Elephant Moraine 96331 (EET96331)

EET96331 has been collected in 1996 by ANSMET and weighted 121.9 g (GROSSMAN 2009). The sample is moderately weathered (grade B) (McCOY and McBRIDE 1998b). EET96331 consists of olivine, augite and pigeonite with abundant triple junctions (GROSSMAN 1999). The silicate grains show numerous signs of shock, such as undulatory extinction, polysynthetic twinning and kink banding (McCOY and McBRIDE 1998b).

Olivine grains are up to 1 mm in diameter and consist of  $fa_{12-13}$  with reduced rims with of  $fa_2$  (McCOY and McBRIDE 1998b).

Pigeonite is  $Wo_4$  and  $Fs_{11}$  and augite is  $Wo_{29}$ ,  $Fs_7$  (McCOY and McBRIDE 1998b).

## 6.7 Kenna

The Kenna ureilite was found near Kenna, New Mexico, USA in 1972 (BERKLEY et al. 1976). The original meteorite weighted 10.9 Kg (BERKLEY et al. 1976). The level of weathering is B (moderate) and the shock level is medium (GOODRICH 1992, MITTLEFEHLDT et al. 1998, RANKENBURG et al. 2008). Modal analyses give 11% Matrix material, 68% olivine and 21% pigeonite (BERKLEY et al. 1976). The equilibration temperature obtained from olivine-pyroxene-liquid thermometer (SINGLETARY and GROVE 2003) is 1227°C. Co concentrations in olivine and pyroxene grains range from 15-50 ppm and Ni concentrations range from 50-100 ppm (ASH et al. 2009).

Olivine grains are mostly anhedral and meet in triple junctions with size ranging from 0.2 – 2 mm and homogeneous composition with average  $fa_{21}$  (BERKLEY et al. 1976, BERKLEY et al. 1980, SINGLETARY and GROVE 2003, RANKENBURG et al. 2008). Olivines are rich in CaO (literature data for average concentrations ranging from 0.31 to 0.42 wt%, BERKLEY et al. 1976, BERKLEY et al. 1980, SINGLETARY and GROVE 2003) and  $Cr_2O_3$  (literature data for average concentrations ranging from 0.56 to 0.71 wt%, BERKLEY et al. 1976, BERKLEY et al. 1980, SINGLETARY and GROVE 2003). Ureilite olivine grains show thin reduction rims (BERKLEY et al. 1976). Modal proportions obtained from Mg x-ray maps show that reduced rims account for 38 % of the olivine (SINGLETARY and GROVE 2003). 13 of 100 analyzed olivine grains showed signs of shock (undulatory extinction and kink bands) (BERKLEY et al. 1976).

Pigeonite grains are anhedral and homogeneously distributed within the Kenna ureilite (BERKLEY et al. 1976). Their size ranges from 0.14 to 1.4 mm and reduction rims are absent

(BERKLEY et al. 1976). Pigeonite composition is homogeneous ranging from  $\text{En}_{73}\text{Wo}_9\text{Fs}_{17}$  to  $\text{En}_{72}\text{Wo}_{10}\text{Fs}_{19}$  (BERKLEY et al. 1976). Pigeonite grains show undulatory extinction and kink bands (BERKLEY et al. 1976).

The carbonaceous matrix contains metal, troilite and carbon polymorphs. Carbon polymorphs are graphite, diamond (1-3  $\mu\text{m}$  in diameter) and lonsdaleite (1-3  $\mu\text{m}$  in diameter). Hydrocarbons are absent (BERKLEY et al. 1976).

Three different types of metal occurrence have been distinguished by BERKLEY et al. (1976): Metal vein with a thickness of 6-20  $\mu\text{m}$  and 3.7 to up to 9 wt% Ni, irregular metal blebs within olivine and pyroxene grains and very thin networks of veins associated with the reduced rims. Metal in reduced rims contains <0.06 wt% Ni (BERKLEY et al. 1976).

The Kenna ureilite contains 2 wt% of carbon with a  $\delta^{13}\text{C}$  of -2.8 ‰ (GRADY et al. 1985). REE in Kenna show a V-shaped pattern in untreated samples and a LREE-depleted, HREE-enriched pattern in leached samples (BOYNTON et al. 1976). The  $\Delta^{17}\text{O}$  of bulk Kenna is -1.02 ‰ (CLAYTON and MAYEDA 1988).

## **6.8 Graves Nunataks 95205 (GRA95205)**

GRA95205 has been collected in 1995 by ANSMET and weighted 1460 g (GROSSMAN 2009). The sample is moderately weathered (grade B) and highly shocked (GROSSMAN 1998, RANKENBURG et al. 2008). GRA95205 consists of 94 % olivine and 5 % pigeonite (SINGLETARY and GROVE 2003). The olivine-pigeonite equilibration temperature is 1259°C (SINGLETARY and GROVE 2003).

Olivine grains are anhedral to subhedral, mosaicized and up to 6 mm in diameter (McCOY and McBRIDE 1998a). Their composition is  $fa_{18-21}$  with 0.27 wt% CaO and 0.6 - 0.67 wt%  $\text{Cr}_2\text{O}_3$  (SINGLETARY and GROVE 2003, WARREN and HUBER 2006).

In contrast to olivine, pigeonite grains are not mosaicized but show polysynthetic twinning (McCOY and McBRIDE 1998a). Reported compositions is  $\text{Wo}_4$  (McCOY and McBRIDE 1998a) -  $\text{Wo}_{7.6}$  (SINGLETARY and GROVE 2003) and  $\text{Fs}_{19}$  (McCOY and McBRIDE 1998a).

## **6.9 Lewis Cliff 85440 (LEW85440)**

LEW85440 is an augite-bearing ureilite and has been collected in 1985 by ANSMET and weighted 43.8 g (GROSSMAN 2009). The sample is moderately weathered (grade B) and low

shocked (GROSSMAN 1994, RANKENBURG et al. 2008). LEW85440 contains olivine, orthopyroxene and minor Augite (TAKEDA 1989). The olivine/orthopyroxene ratio is about 54/46 (TAKEDA 1989). SINHA et al. 1997 also report pigeonite compositions for LEW85440.

Olivine grains appear dusty due to the precipitation of fine metal particles (TAKEDA 1989). Grain sizes are up to 1.5 mm in diameter (TAKEDA 1989). The composition of olivine is  $fa_{8.7-15}$  with 0.32 - 0.33 wt% CaO and 0.5 wt%  $Cr_2O_3$  (TAKEDA 1989, SINHA et al. 1997, RANKENBURG et al. 2008). Olivines show reduction rims of 10 – 50  $\mu m$  (SINHA et al. 1997).

Orthopyroxene grains are up to 1.65 mm in diameter and consist of  $Wo_{4.9-5}$ ,  $Fs_{7.8-8}$  (TAKEDA 1989, SINHA et al. 1997). Augite composition is  $Wo_{35.5}$  and  $Fs_{4.9}$  (TAKEDA 1989). Pigeonite Composition is  $Wo_9$ ,  $Fs_{9.6}$  (SINHA et al. 1997).

## **7 Sample preparation and analytical procedures**

### **7.1 Sample preparation**

About 0.7 g of each meteorite sample was gently crushed in an agate mortar and sieved to obtain a fraction from 63  $\mu m$  to 200  $\mu m$ . The metal-grains were then separated with a strong hand magnet. A non-magnetic, silicate-rich fraction and a highly magnetic, metal-rich fraction of the sample material were obtained. From the silicate-rich fraction clear grains were handpicked under a binocular microscope and used for LA-ICP-MS and Ni-Isotope studies. The mineral grains for LA-ICP-MS analyzes and the obtained magnetic mineral fractions were embedded in EpoFix resin. After 24 hours of hardening at room temperature, the samples were ground and polished with a 3  $\mu m$  diamond polish.

### **7.2 Electron microprobe measurements**

Measurements were performed with a JEOL JXA 8900 electron beam microprobe analyzer (EPMA) operated at the Geowissenschaftliches Zentrum, University of Göttingen and at the Institute of Mineralogy, University of Cologne.

#### **7.2.1 Measurements at the Institute of mineralogy in Cologne**

In silicates,  $Na_2O$ ,  $Cr_2O_3$ ,  $Al_2O_3$ , CaO,  $TiO_2$ , MgO, FeO, MnO,  $SiO_2$  and  $TiO_2$  were measured.

Counting times were 5 s on the peak and 2.5 s on the backgrounds for  $Na_2O$ , 20 s on the peak and 10 s on the backgrounds for  $Cr_2O_3$ , CaO and MnO and 10 s on the peak and 5 s on

the backgrounds for Al<sub>2</sub>O<sub>3</sub>, TiO<sub>2</sub>, MgO, SiO<sub>2</sub> and FeO. Standards used were natural and synthetic oxides and silicates. For all elements, the K<sub>α</sub>-line was used. Na<sub>2</sub>O, Al<sub>2</sub>O<sub>3</sub>, MgO and SiO<sub>2</sub> were analyzed with a TAP-crystal, Cr<sub>2</sub>O<sub>3</sub>, MnO and FeO with a LIF-crystal, CaO with a PET J-crystal and TiO<sub>2</sub> with a LIF H-crystal. To account for matrix effects the ZAF-correction was applied. Measurements were performed at 20 nA beam current, 15 KeV acceleration voltage and with a focused beam. Backscattered electron imaging was used to ensure that the analyzed grains were free of cracks and inclusions.

In metals and sulfides, P, Si, Ni, Co, Fe, Cr, S and Mn were measured.

Counting times were 30 s on the peak and 15 s on the background for Si, 20 s on the peak and 10 s on the background for Mn and Cr and 10 s on the peak and 5 s on the background for P, Fe, S, Co and Ni. As standards we used 100 wt% Fe, 100 wt% Co, 100 wt% Ni and 100 wt% Si samples, apatite (8.0 wt% P), rhodonite (33.7 wt% Mn), chalcopyrite (34.9 wt% S) and synthetic Cr<sub>2</sub>O<sub>3</sub> (68.4 wt% Cr). For all elements, the K<sub>α</sub>-line was used. Si was analyzed with a TAP-crystal, Cr, Fe and Ni with a LIF-crystal, S and P with a PET J-crystal and Mn and Co with a LIF H-crystal. Measurements were performed at 20 nA beam current, 15 KV acceleration voltage and with a focused beam. Backscattered electron imaging was used to ensure that the analyzed grains were free of cracks and inclusions.

### **7.2.2 Measurements at the University of Göttingen**

In silicates, Na<sub>2</sub>O, Cr<sub>2</sub>O<sub>3</sub>, Al<sub>2</sub>O<sub>3</sub>, CaO, TiO<sub>2</sub>, MgO, FeO, MnO, SiO<sub>2</sub> and TiO<sub>2</sub> were measured.

Counting times were 15 s on the peak and 5 s on the backgrounds for Na<sub>2</sub>O, CaO, Al<sub>2</sub>O<sub>3</sub>, TiO<sub>2</sub>, MgO, SiO<sub>2</sub> and FeO and 30 s on the peak and 15 s on the background for Cr<sub>2</sub>O<sub>3</sub>. Standards used were olivine (Si, Mg), albite (Na), synthetic Ti, hematite (Fe), wollastonite (Ca), synthetic Cr and Rhodonite (Mn). For all elements, the K<sub>α</sub>-line was used. To account for matrix effects the Phi-Rho-Z-correction was applied. Measurements were performed at 15 nA beam current, 15 KV acceleration voltage and with a focused beam. Backscattered electron imaging was used to ensure that the analyzed grains were free of cracks and inclusions.

In metals and sulfides, P, Si, Ni, Co, Fe, Cr, S and Mn were measured.

Counting times were 15 s on the peak and 5 s on the background for P, Si, Ni, Fe, Cr, S and Mn and 30 s on the peak and 15 s on the background for Co. As standards we used 100 wt% Fe, 100 wt% Co, 100 wt% Ni, 100 wt% Mn, 100 wt% Cr and 100 wt% Si samples, apatite (8.0 wt% P), ZnS (32.9 wt% S). Measurements were performed at 20 nA beam current, 15 KV acceleration voltage and with a focused beam. Backscattered electron imaging was used to ensure that the analyzed grains were free of cracks and inclusions.

### **7.2.3 The Co-problem**

The Co  $K_{\alpha}$ -line used for Co-measurements overlaps with the flank of the Fe  $K_{\beta}$ -line, which results in a curvature of the underground below the Co-peak. The analytical software interpolates between the left and the right underground intensities. As a result, lower count rates and thus lower concentrations are detected for Co. To account for this overlap, an additional factor is added in the analytical software. The usage of different factors at the two microprobe analyzers caused different results in Co-measurements. In order to obtain the correct Co-values, both sets of data had to be corrected.

Synthetic metal standards (0.272 wt% Co, 8.055 wt% Ni, 91.67 wt% Fe and 0.562 wt% Co, 15.023 wt% Ni, 84.415 wt% Fe, Prof. A. Pack, pers. comm.), show a systematic difference of +0.193 wt% Co from the measurements (Fig. 23) performed in Cologne. The metal standards have been provided by Prof. Dr. Andreas Pack. The samples have been produced from a mixture of Fe-, Co- and Ni-metal powder, molten at 1600°C for 30 min. Their composition has been determined with a CAMECA SX-100 at Henry Poincaré University, Nancy.

Some metal grains (22 metal grains from ALHA77257, EET87517, ALH84136, LEW85440, EET96042 and GRA95205) have been measured both in Cologne and in Göttingen. Grains measured in Cologne are ~0.103 wt% higher in Co than those measured in Göttingen (Fig. 24). Fe-metal standards (100 wt% Fe), measured in Göttingen, give an excess of 0.064 wt% Co. As a result, the Co-data measured in Cologne have been corrected by subtracting 0.193 wt%, while Co-data measured in Göttingen have been corrected by subtracting 0.080 wt%.

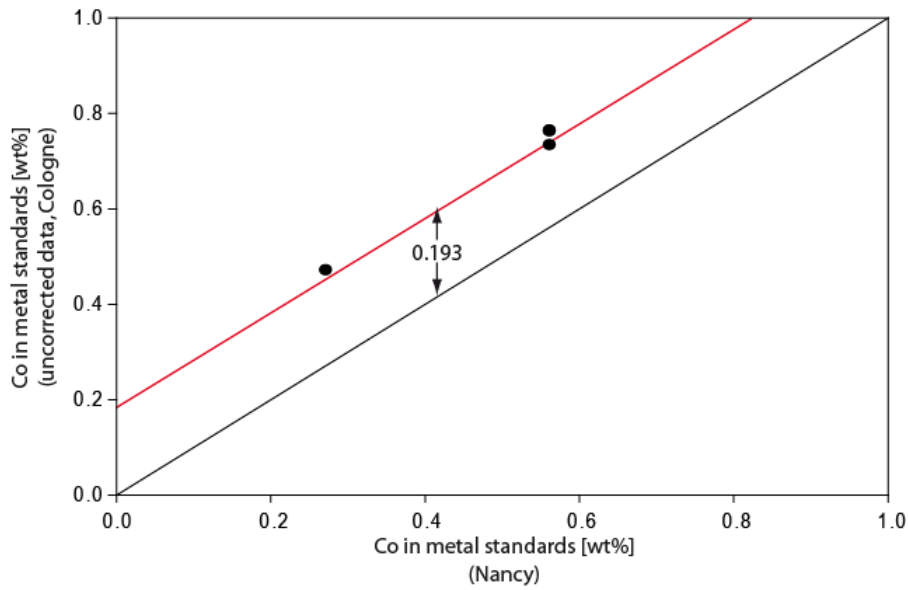


**Fig. 23** Systematic difference of Co in metal standards measured with a JEOL 8900 in Cologne and a CAMECA SX-100 in Nancy (Measurements in Nancy by Prof. A. Pack). Measured concentrations are  $\sim 0.193$  wt% higher with JEOL 8900 (Cologne).

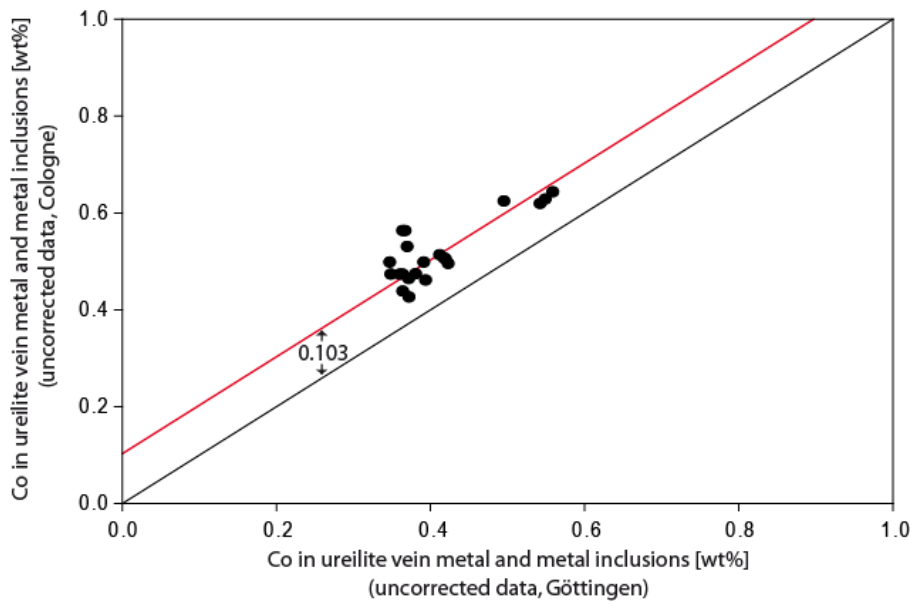


**Fig. 24** Systematic difference of Co in identical ureilite vein metal and metal inclusions (from ALHA77257, EET87517, ALH84136, LEW85440, EET96042 and GRA95205), measured in Cologne and in Göttingen. Measured concentrations are  $\sim 0.103$  wt% higher in Cologne than in Göttingen.

### 7.3 Laser-ablation-ICP-MS measurements of silicates

The concentrations of the trace elements Co and Ni in olivine and pyroxene were obtained using laser-ablation-ICP-MS. A 193 nm excimer-ArF-laserbeam with  $2 \frac{J}{cm^2}$  energy focused onto the sample surface with 40 to 60  $\mu\text{m}$  in diameter at a repetition pulse rate of 10 Hz (Compex110, Lambda Physik, GeoLas Optical Bench, MikroLas, Göttingen, Germany) was used. During 140 s of ablation four elements were analyzed with a fast scanning quadrupole ICPMS (Perkin Elmer DRC II, Sciex, Canada) at 20 ms dwell time for  $^{43}\text{Ca}$  (Ca was measured to distinguish pyroxene from olivine grains), 50 ms dwell time for  $^{57}\text{Fe}$  (Fe was measured as internal standard) and 200 ms dwell time for  $^{59}\text{Co}$  and  $^{60}\text{Ni}$ . The sample material is transported within an Ar-gas flow.

The absolute amounts of sample material in the gas flow vary, depending on the sample material and the ablation process. Concentrations of elements can therefore only be determined relatively to each other. Quantification is only possible if the concentration of at least one element in the unknown sample is known. Here we use Fe obtained from EPMA-analyses as an internal standardization element.

Each analyzed sample gives data sets consisting of 200 intensities with distinct time stamp for each element. The laser was activated 30-40 seconds after the start of each measurement to obtain the blank intensities. The mean blank intensities were subtracted from each data point.

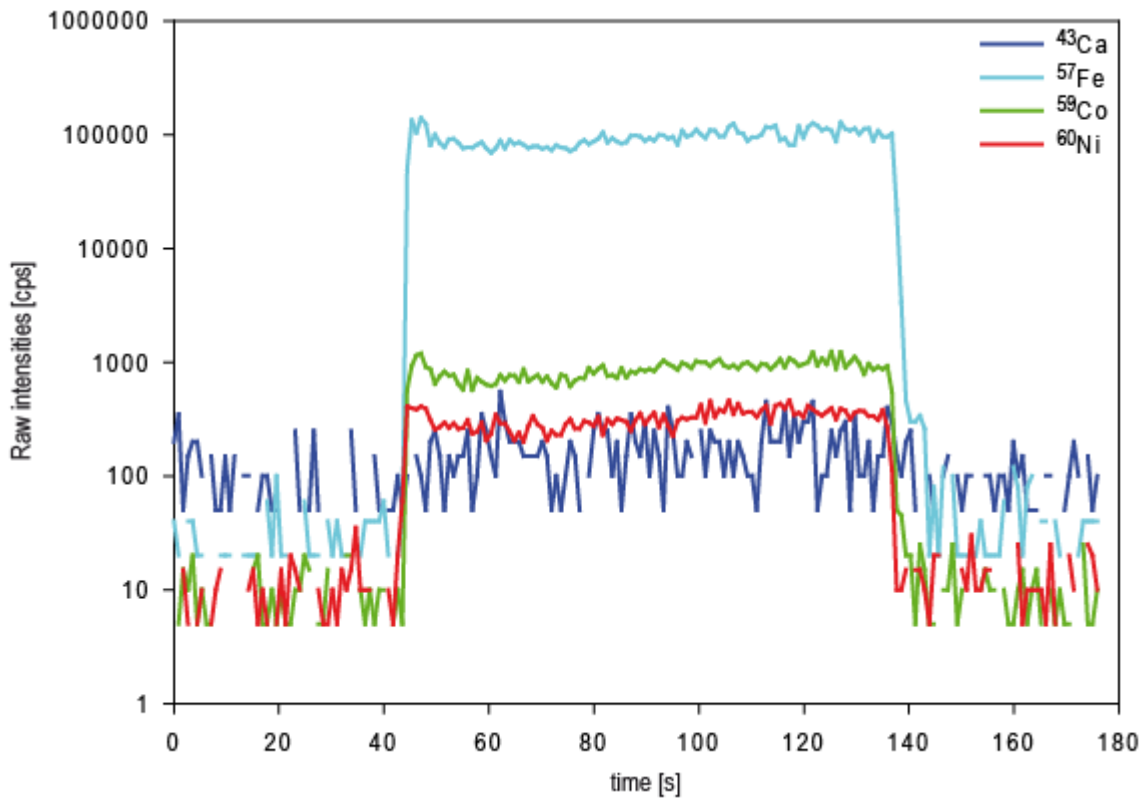


Fig. 25 Example for raw intensity data of a typical LA-ICP-MS measurement. The laser was activated after ~40 seconds and deactivated after ~135 seconds. Breaks in the line indicate 0 intensity (0 values can not be plotted on a logarithmic scale). The example is an olivine of ALHA77257 (ol-14).

To account for varying amounts of sample material in the gas flow, every data point is normalized by the intensity of  $^{57}\text{Fe}$ . Absolute concentrations can be calculated from calibration with standard materials:

$$\frac{\left(\frac{I_{\text{element}}}{I_{^{57}\text{Fe}}}\right)_{\text{sample}}}{\left(\frac{C_{\text{element}}}{C_{\text{Fe}}}\right)_{\text{sample}}} = \frac{\left(\frac{I_{\text{element}}}{I_{^{57}\text{Fe}}}\right)_{\text{standard}}}{\left(\frac{C_{\text{element}}}{C_{\text{Fe}}}\right)_{\text{standard}}} \quad \text{Eq. 47}$$

$$C_{\text{element}} = C_{\text{Fe}} \cdot \frac{\left(\frac{I_{\text{element}}}{I_{^{57}\text{Fe}}}\right)_{\text{sample}}}{\frac{\left(\frac{I_{\text{element}}}{I_{^{57}\text{Fe}}}\right)_{\text{standard}}}{\left(\frac{C_{\text{element}}}{C_{\text{Fe}}}\right)_{\text{standard}}}} \quad \text{Eq. 48}$$

The ratio of the average intensity ratio  $\left(\frac{I_{\text{element}}}{I_{^{57}\text{Fe}}}\right)_{\text{standard}}$  and the concentration ratio  $\left(\frac{C_{\text{element}}}{C_{\text{Fe}}}\right)_{\text{standard}}$  is termed sensitivity factor (SF). The sensitivity factor becomes more reliable the more different standards are used for calibration.

The calibration in this work (Table 10, Fig. 26 to Fig. 28) was done with the NBS 610 glass, doped with ~450 ppm of each element and seven MPI-Ding glasses (AtH0, GOR128, StHs6/80, T1, ML3B, GOR128 and KL2 in JOCHUM et al. 2006).

**Table 10 Sensitivity factors obtained for LA-ICP-MS measurements**

Element	Sensitivity factor	2 $\sigma$ error
<sup>43</sup> Ca	0.059	$\pm 0.003$
<sup>59</sup> Co	39.4	$\pm 1.1$
<sup>60</sup> Ni	7.74	$\pm 0.25$

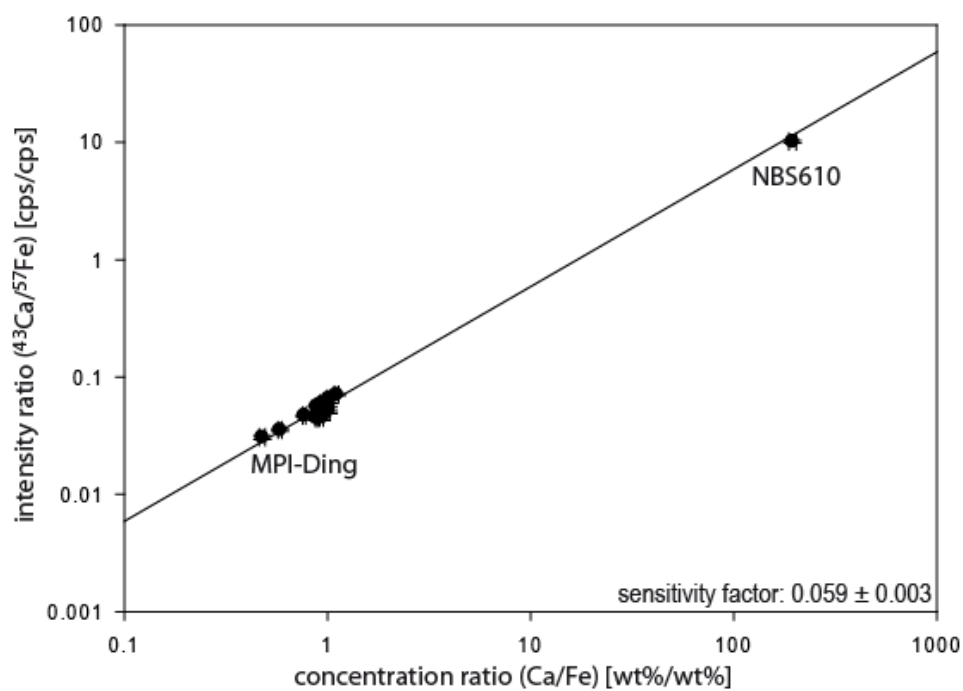


**Fig. 26** Plot of <sup>43</sup>Ca/<sup>57</sup>Fe intensity ratio against Ca/Fe concentration ratio. The sensitivity factor was obtained from a weighted average of seven MPI-Ding-glasses (Jochum et al. 2006) and NBS610.

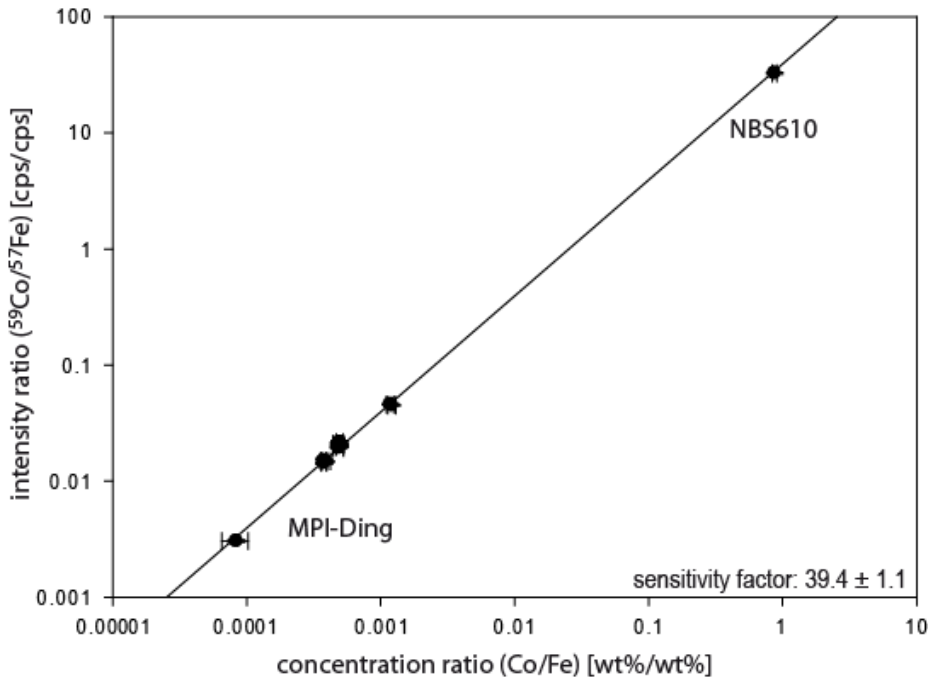


Fig. 27 Plot of  $^{59}\text{Co}/^{57}\text{Fe}$  intensity ratio against Co/Fe concentration ratio. The sensitivity factor was obtained from a weighted average of seven MPI-Ding-glasses (Jochum et al. 2006) and NBS610.

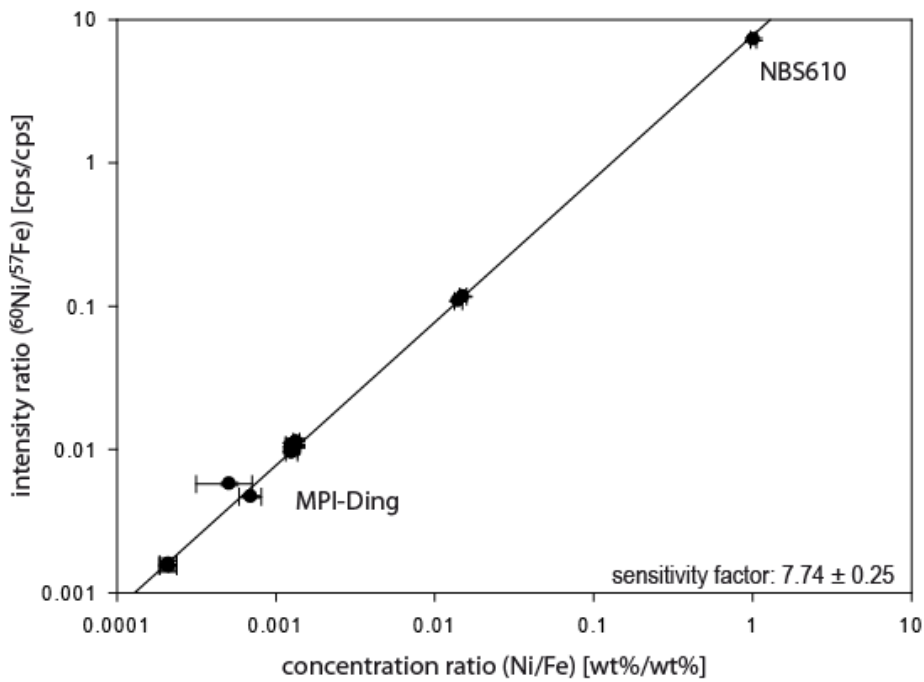


Fig. 28 Plot of  $^{60}\text{Ni}/^{57}\text{Fe}$  intensity ratio against Ni/Fe concentration ratio. The sensitivity factor was obtained from a weighted average of seven MPI-Ding-glasses (Jochum et al. 2006) and NBS610.

For each data point an absolute concentration was calculated with Eq. 47. The final concentration of an element in a sample is the average concentration of data points in a given range of data points. The range of data points is chosen manually for each sample (Fig. 29). In order to excluding spikes or shifts in intensities, a range is chosen that includes a maximum number of data points of approximately equal concentrations (plateau).

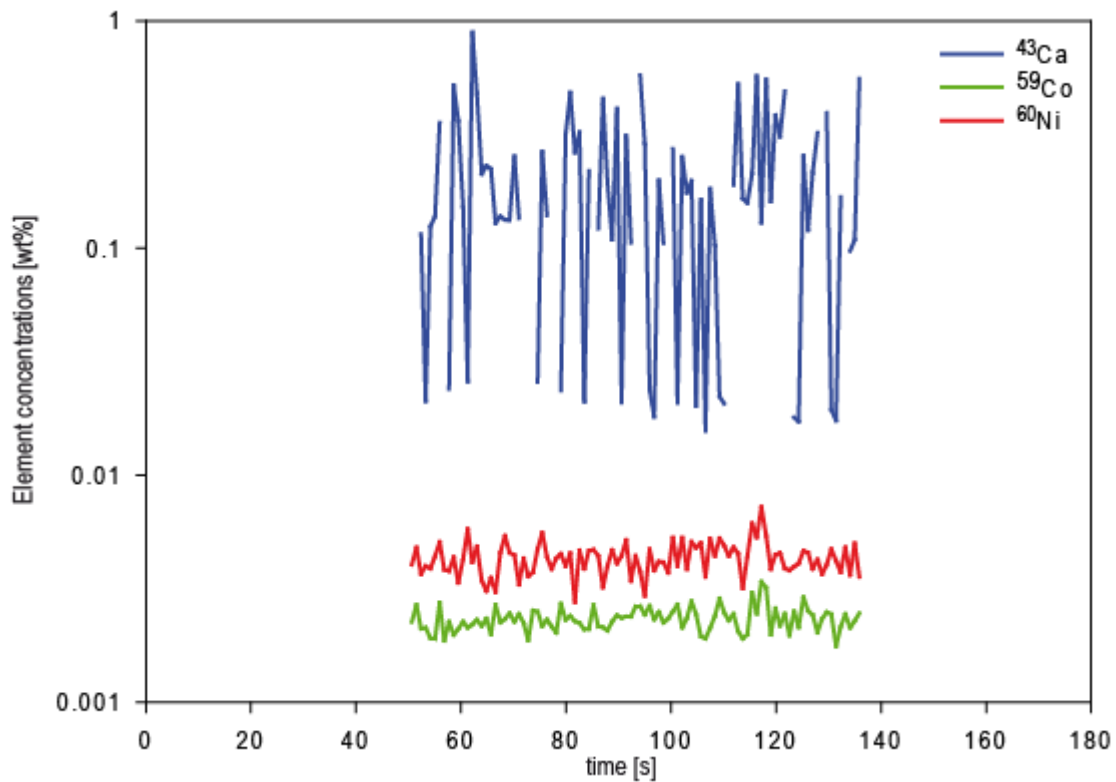


Fig. 29 Example of element concentrations in an olivine of ALHA77257 (ol-14). Raw intensities have been calculated into concentrations (Eq. 48). Time spans with deactivated lasers have been excluded. Although Ca-concentrations show a large scatter, the data is sufficient to distinguish olivine from pyroxene.

The error of the measurement was calculated as Gaussian error progression of Eq. 47:

$$\sigma_{c_{\text{element}}} = \sqrt{
 \left( \left( \frac{1}{SF} \cdot \left( \frac{I_{\text{element}}}{I_{57Fe}} \right)_{\text{sample}} \right) \cdot \sigma_{c_{57Fe}} \right)^2 +
 \left( \left( c_{Fe} \cdot \frac{1}{SF} \right) \cdot \sigma_{\left( \frac{I_{\text{element}}}{I_{57Fe}} \right)_{\text{sample}}} \right)^2 +
 \left( \left( c_{Fe} \cdot \frac{-1}{SF^2} \cdot \left( \frac{I_{\text{element}}}{I_{57Fe}} \right)_{\text{sample}} \right) \cdot \sigma_{SF} \right)^2
 }$$

Eq. 49

In Eq. 49, e represents the respective errors.

Ureilite silicates often contain fine metal inclusions. In order to prevent measurements to be compromised by these inclusions, only very clear grains were used for LA-ICP-MS. In some grains, however, metal inclusions were ablated and measured. Depending on the size of the inclusion, this may result in a spike of Ni- and Co-concentration or prevent the attaining of a clear plateau altogether. Spikes and outliers were manually removed.

Another problem arises from the relatively small grain sizes. In some cases, the silicate grains were penetrated after only a few seconds of ablation, resulting in very short plateaus and larger errors.

#### **7.4 Ni-Isotope analyses**

Sample dissolution, chemical Ni-separation and Ni isotope measurements were performed by Dr. Ghylaine Quitté at the ENS Lyon with a high resolution multicollection inductively coupled mass spectrometer (Nu1700 MC-ICP-MS, Nu Plasma Instruments).

The description of the sample dissolution and Ni-separation process has been taken from Dr. G. Quitté, pers. comm. and QUITTE and OBERLI (2006).

The sample material is dissolved in 6N HCl, 27N HF and 16N HNO<sub>3</sub>, evaporated and taken up in 6N HCl, evaporated again and then taken up in H<sub>2</sub>O<sub>2</sub> and HNO<sub>3</sub>. A 10% aliquot is now taken away to determine Ni- and Fe-concentrations. The remaining 90% are taken up in 6M HCl, dried and taken up in 1 ml of 0.5N HCl, 1 ml of citric acid and 0.4 ml of NH<sub>4</sub>OH. Now, 1 ml of 1% dimethylglyoxime (DMG) in ethanol is added to chelate Ni. To extract the Ni, the sample is washed with 3 ml CHCl<sub>3</sub> to remove traces of Co and Cu. The Ni-chelate complex is now back-extracted into 2 ml 2N HCl, and evaporated after adding one drop of HClO<sub>4</sub> to break the DMG-Ni-complex. The residue is taken up in 0.2 ml H<sub>2</sub>O and loaded onto a small-sized cation exchange column with 50 µl of Bio-Rad AG 50W-X8 resin. Matrix elements are eluted with 2.5 ml 0.2N HCl and the Ni-fraction is taken up in 0.5 ml of 3N HCl. After evaporation, the Ni-fraction is taken up into 0.1N HCl for ICP-MS-Measurements.

A MC-ICP mass spectrometer uses an inductively coupled plasma torch to produce positively charged ions from the sample material. Ionization efficiency is usually very high (close to 100 %). The ionized sample material accelerated with an electrical field gradient and focused into a narrow beam with several slits or electrostatically charged plates. The ion beam then passes through an energy filter to produce ions with approximately identical energies, which can then be separated in a magnetic field based on their mass to charge ratio. The ions can then be simultaneously measured in a series of faraday cups, which convert particle impacts to electrical current (VERVOORT and MUELLER 2008).

The Nu Plasma 1700 MC-ICPMS has a mass dispersion of 17% at zoom magnification 1 and is equipped with 16 faraday cups that allow simultaneous measurement of all Ni isotopes (<sup>58</sup>Ni,

$^{60}\text{Ni}$ ,  $^{61}\text{Ni}$ ,  $^{62}\text{Ni}$  and  $^{64}\text{Ni}$  (QUITTE and OBERLI 2006).

## 8 Results

### 8.1 Data of individual ureilites

As the respective grains are randomly chosen for analysis (in case of LA-ICP-MS, the clearest grains were preferred), the relative abundance of analyzed minerals does not reflect the relative abundance of minerals in the ureilite.

#### 8.1.1 ALH84136

Seven grains of olivine were analyzed in ALH84136 (Fig. 30) with EPMA. Olivine composition of all samples is  $fa_{0.7-2.5}$ . CaO ranges from 0.28 – 0.33, MnO ranges from 0.25 – 0.59 and  $Cr_2O_3$  ranges from 0.12 – 0.56. As reduction is extensive in ALH84136, only olivine with  $fa > 1.5$  was used as average composition for calculations (Table 11). Three olivine grains were analyzed with LA-ICP-MS. NiO-concentration range is 17.4 – 18.2  $\mu g \cdot g^{-1}$  and CoO-concentration range is 5.7 – 6.6  $\mu g \cdot g^{-1}$  (Fig. 32).

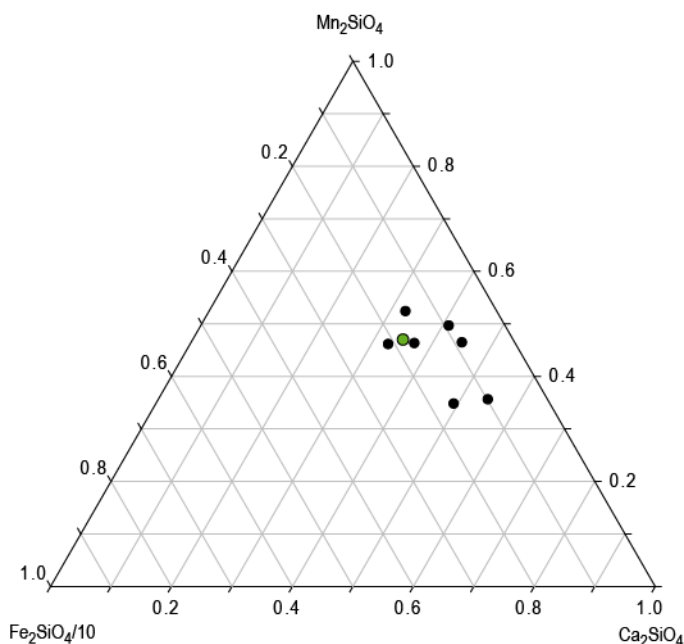


**Fig. 30 Ternary diagram of  $Fe_2SiO_4 \cdot 10^{-1}$ ,  $Ca_2SiO_4$  and  $Mn_2SiO_4$  in ALH84136 olivine. The green circle represents the composition used in calculations.**

Augite (6) and orthopyroxene grains (56) were analyzed in ALH84136 (Fig. 31) with EPMA. Orthopyroxene is  $Wo_{1.3-6.9}$ ,  $Fs_{1.4-5.8}$  and  $En_{88.9-96}$ .  $Cr_2O_3$ -concentrations range from 0.17 – 0.90 wt% (mean 0.79 wt%).  $Al_2O_3$ -concentrations range from 0.06 – 0.71 wt% (mean

0.44 wt%). TiO<sub>2</sub>-concentrations range from 0.04 – 0.17 wt% (mean 0.11 wt%). Two grains of orthopyroxene were analyzed with LA-ICP-MS. NiO-concentration range is 28.1 – 28.8 μg·g<sup>-1</sup> and CoO-concentration range is 6.7 – 9.0 μg·g<sup>-1</sup> (Table 11, Fig. 32).

Augite is Wo<sub>26.3-38</sub>, Fs<sub>1.9-3</sub> and En<sub>59.3-71</sub>. Cr<sub>2</sub>O<sub>3</sub>-concentrations range from 0.72 – 0.86 wt% (mean 0.80 wt%). Al<sub>2</sub>O<sub>3</sub>-concentrations range from 0.62 – 0.85 wt% (mean 0.76 wt%). TiO<sub>2</sub>-concentrations range from 0.18 – 0.26 wt% (mean 0.23 wt%).

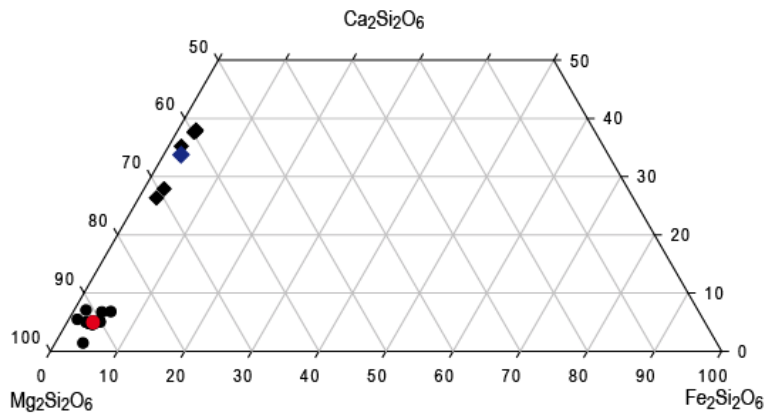


**Fig. 31** Composition of pyroxenes in ALH84136. Circles represent the composition of orthopyroxenes, with the red circle giving the average orthopyroxene composition. Diamonds give the composition of augite, with the blue diamond giving the average augite composition.

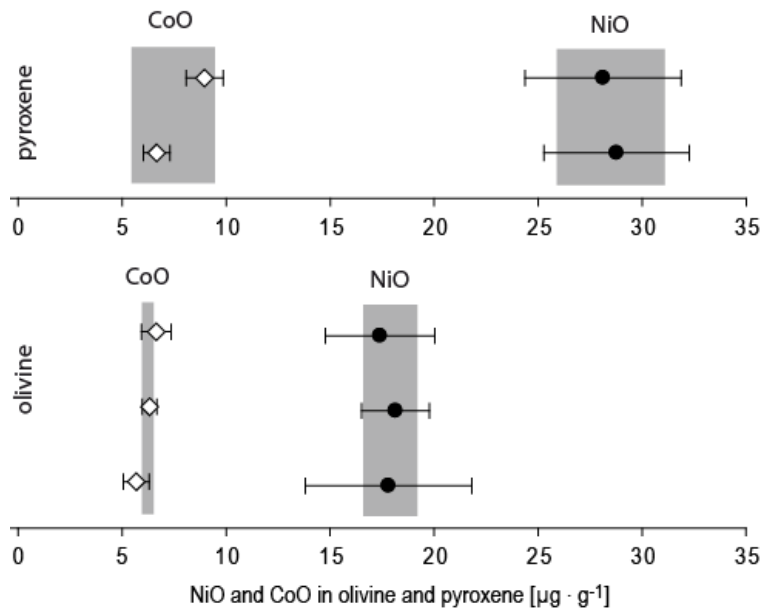


**Fig. 32** NiO and CoO concentrations in olivine and pyroxene in ALH84136. Diamonds give the concentrations of CoO and Circles give the concentration of NiO. Shaded areas give the weighted average of the measurements.

**Table 11 Composition of olivine, orthopyroxene and augite in ALH84136. Data obtained with EMPA, except for NiO and CoO, which was obtained with LA-ICP-MS. Number of grains included in average is given in parenthesis.**

	Olivine (3)		Orthopyroxene (56)		Augite (6)	
	wt%	2 $\sigma$	wt%	2 $\sigma$	wt%	2 $\sigma$
SiO <sub>2</sub>	41.99	0.21	57.82	0.17	55.48	0.25
TiO <sub>2</sub>	0.04	0.01	0.11	0.01	0.23	0.04
FeO	2.09	0.50	2.80	0.09	1.70	0.20
Al <sub>2</sub> O <sub>3</sub>	0.05	0.03	0.44	0.02	0.76	0.08
MgO	54.92	0.52	35.55	0.20	23.45	1.86
CaO	0.32	0.03	2.62	0.07	17.30	2.04
Cr <sub>2</sub> O <sub>3</sub>	0.51	0.05	0.79	0.02	0.80	0.04
MnO	0.56	0.03	0.51	0.01	0.38	0.02
	Olivine (3)		Orthopyroxene (2)			
	$\mu\text{g}\cdot\text{g}^{-1}$	2 $\sigma$	$\mu\text{g}\cdot\text{g}^{-1}$	2 $\sigma$		
NiO	17.9	1.3	28.5	2.6		
CoO	6.2	0.3	7.5	2.0		
Number of oxygen ions:	4		6		6	
Si	0.993		1.970		1.969	
Ti	0.000		0.003		0.006	
Fe	0.051		0.080		0.050	
Al	0.001		0.018		0.032	
Mg	1.936		1.805		1.240	
Ca	0.008		0.096		0.658	
Cr	0.010		0.021		0.022	
Mn	0.011		0.015		0.012	
T	1.000		1.996		2.020	
M	2.001		2.014		1.987	
Total	3.001		4.010		4.007	
<i>Fa</i>	2.1					
<i>En</i>			90.2		62.0	
<i>Wo</i>			4.8		32.9	
<i>Fs</i>			4.0		2.5	

The dominant metal phase in ALH84136 is FeNi vein metal. EPMA analyzes of 44 vein metal grains (Table 12) give Ni-concentrations ranging from 3.2 to 4.5 wt% (mean 4.1 wt%), Co-concentrations ranging from 0.20 to 0.33 wt% (mean 0.29 wt%), Cr-concentrations ranging from 0.05 to 0.32 wt% (mean 0.13 wt%) and Si-concentrations ranging from 0.01 to 1.31 wt% (mean 1.1 wt%).

Two cohenite spherule inclusions (90.25 – 91.82 wt% Fe, 1.96 - 1.99 wt% Ni, 0.22 – 0.25 wt% Co, 0.15 – 0.33 wt% Cr and 0.02 – 0.04 wt% Si) were analyzed.

Silicate grains contain inclusions of Fe-metal (8 grains) of varying composition (1.01 – 8.52 wt% Ni, 0.08 – 0.45 wt% Co, 0.05 – 0.15 wt% Cr and 0.05 – 0.95 wt% Si), troilite (5

grains, Ni and Co <0.02 wt%, 4.38 - 7.13 wt% Cr, 0.07 - 1.13 wt% Si, 0.34-0.49 wt% Mn) and daubreelite (2 grains, Ni and Co <0.02 wt%, 33.2 - 33.5 wt% Cr, 2.0 – 2.3 wt% Mn).

**Table 12 Composition of metal, sulfide phases and cohenite in ALH84136. Data obtained with EPMA. Values marked with ‘<’ are below detection limit.**

	Spherule inclusion		Vein metal (44)		Inclusions			
	Cohenite (2)				Troilite (5)		Daubreelite (2)	
	wt%	2 $\sigma$	wt%	2 $\sigma$	wt%	2 $\sigma$	wt%	2 $\sigma$
P	0.04	0.05	0.12	0.02	<0.02		<0.02	
Si	0.03	0.02	1.11	0.06	0.38	0.40	0.18	0.21
Cr	0.24	0.18	0.13	0.02	5.41	0.92	33.38	0.33
Fe	91.04	1.57	94.27	0.29	54.05	1.32	18.21	0.60
Co	0.23	0.03	0.29	0.01	<0.02		<0.02	
S	0.04	0.01	<0.02		37.91	0.56	43.66	1.00
Ni	1.98	0.03	4.15	0.06	<0.02		<0.02	
Mn	<0.02		<0.02		0.42	0.06	2.16	0.32

### 8.1.2 ALHA77257

Olivine and orthopyroxenes were analyzed in ALHA77257 with EPMA. Olivine (24 grains analyzed) is  $fa_{5.0-13.9}$  with an average of  $fa_{13}$ . CaO-concentrations are 0.29 – 0.35 wt% (mean 0.30 wt%),  $Cr_2O_3$ -concentrations are 0.63 – 0.81 wt% (mean 0.71 wt%), MnO-concentrations are 0.39 – 0.52 wt% (mean 0.45 wt%). NiO and CoO concentrations have been determined from 9 olivine grains with LA-ICP-MS (Fig. 35). NiO-concentrations range from 54.1 to 66.5  $\mu g \cdot g^{-1}$  (mean 56.8  $\mu g \cdot g^{-1}$ ) and CoO-concentrations range from 28.2 to 32.8  $\mu g \cdot g^{-1}$  (mean 29.8  $\mu g \cdot g^{-1}$ ).

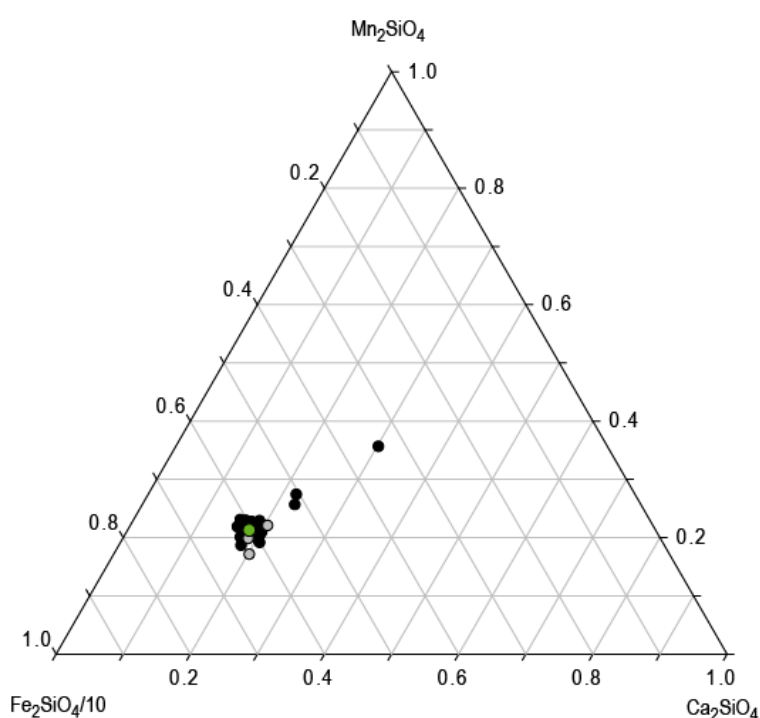


**Fig. 33 Ternary diagram of  $Fe_2SiO_4 \cdot 10^{-1}$ ,  $Ca_2SiO_4$  and  $Mn_2SiO_4$  in ALHA77257 olivine. The green circle represents the average composition. Grey circles are data taken from BERKLEY et al. (1980), TAKEDA (1987) and GOODRICH et al. (1987a).**

Orthopyroxene (60 grains analyzed) is  $Wo_{5.7-6.4}$  (mean  $Wo_{6.0}$ ),  $Fs_{11.0-12.4}$  (mean  $Fs_{11.8}$ ) and  $En_{78.2-82.7}$  (mean  $En_{80.8}$ ) with 0.03 - 0.13 wt%  $TiO_2$  (mean 0.08 wt%), 0.39 – 0.56 wt% MnO (mean 0.47) and 1.00 – 1.26 wt%  $Cr_2O_3$  (mean 1.11 wt%). Five grains of orthopyroxene were analyzed with LA-ICP-MS (Fig. 35), giving 14.5 – 18.2  $\mu g \cdot g^{-1}$  NiO (mean 17.1  $\mu g \cdot g^{-1}$ ) and 13.1 – 14.4  $\mu g \cdot g^{-1}$  CoO (mean 14.0  $\mu g \cdot g^{-1}$ ).

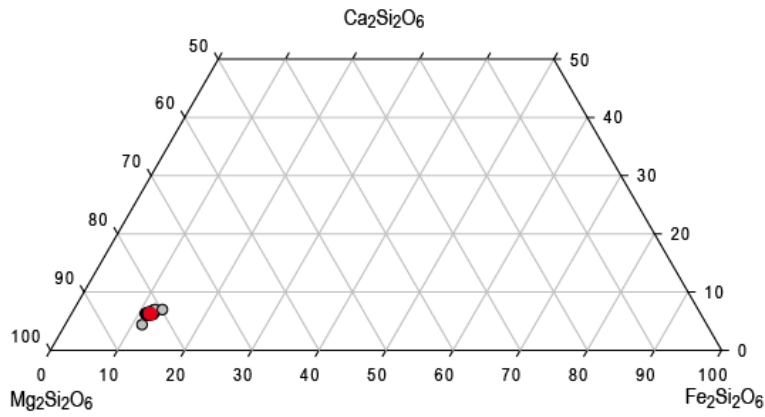


**Fig. 34** Composition of pyroxenes in ALHA77257. Circles represent the composition of orthopyroxenes (60 grains), with the red circle giving the average composition. Grey circles represent data taken from BERKLEY et al. (1980) and TAKEDA (1987).

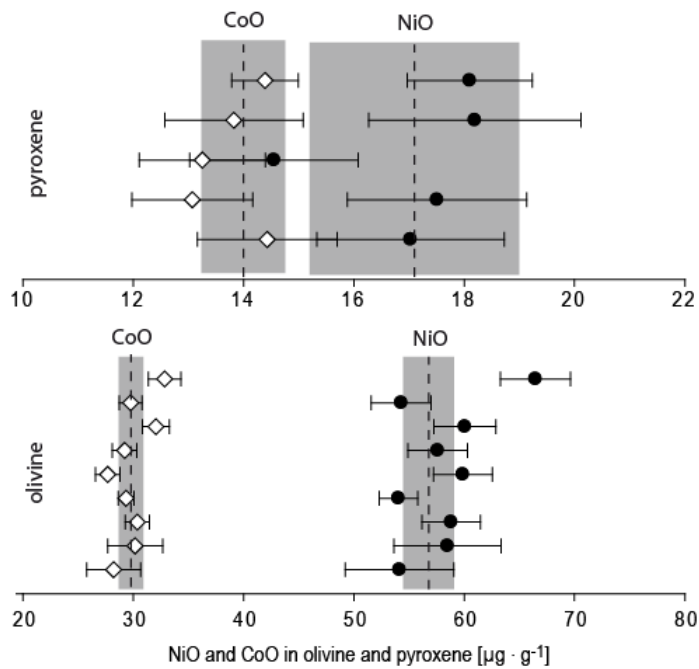


**Fig. 35** NiO and CoO concentrations in olivine and pyroxene in ALHA77257. Diamonds give the concentrations of CoO and Circles give the concentration of NiO. Shaded areas give the weighted average of the measurements.

**Table 13** Composition of olivine and orthopyroxene in ALHA77257. Data obtained with EMPA, except for NiO and CoO, which was obtained with LA-ICP-MS. Number of grains analyzed is given in parenthesis. Values marked with '<' are below detection limits.

	olivine (24)		orthopyroxene (60)	
	wt%	2 $\sigma$	wt%	2 $\sigma$
SiO <sub>2</sub>	40.46	0.23	57.27	0.18
TiO <sub>2</sub>	<0.02		0.08	0.01
FeO	12.96	0.15	8.20	0.06
Al <sub>2</sub> O <sub>3</sub>	0.03	0.01	0.60	0.01
MgO	47.47	0.49	31.60	0.17
CaO	0.30	0.01	3.26	0.01
Cr <sub>2</sub> O <sub>3</sub>	0.71	0.02	1.11	0.02
MnO	0.45	0.01	0.47	0.01
	olivine (9)		orthopyroxene (5)	
	$\mu\text{g}\cdot\text{g}^{-1}$	2 $\sigma$	$\mu\text{g}\cdot\text{g}^{-1}$	2 $\sigma$
NiO	56.8	2.3	17.1	1.9
CoO	29.8	1.1	14.0	0.8
Number of oxygen ions	4		6	
Si	0.986		1.964	
Na	0.001		0.003	
K	0.000		0.000	
Ti	0.000		0.002	
Fe	0.264		0.235	
Al	0.001		0.024	
Mg	1.724		1.615	
Ca	0.008		0.120	
Cr	0.014		0.030	
Mn	0.009		0.014	
T	0.986		1.964	
M	2.021		2.044	
Total	3.007		4.008	
<i>fa</i>	13.2			
En			80.8	
Wo			6.0	
Fs			11.8	

In ALHA77257 43 grains of vein metal were analyzed. Vein metal contains 3.31 - 4.29 wt% Ni (mean 3.86 wt%), 0.22 - 0.37 wt% Co (mean 0.27 wt%), 0.20 - 0.37 wt% Cr (mean 0.30 wt%) and <0.02 – 0.04 wt% Si (mean 0.03 Si).

As it has been reported in GOODRICH and BERKLEY (1986), ALHA77257 contains numerous spherule inclusions. Most spherules analyzed (7) are sulfide + FeNi-metal, 1 spherule is cohenite only. Cr-poor sulfide, with 0.76 – 2.52 wt% Cr, is more abundant (5 grains) than Cr-rich sulfide, with >7.1 wt% Cr (2 grains). The metal in spherule inclusions can also be distinguished into 2 types: A Ni-poor metal with 2.4 wt% Ni (2 grains) and a Ni-rich metal with 4.97 – 5.97 wt% Ni (7 grains). Ni-poor metal is not associated with Cr-poor metal.

Silicate grains in ALHA77257 also contain numerous metal inclusions of variable composition (0.44 – 4.16 wt% Ni, <0.02 – 0.31 wt% Co, <0.02 – 0.25 wt% Si and 0.13 – 0.34 wt% Cr).

**Table 14** Composition of vein metal and sulfide phases, metal and cohenite from spherule inclusions in ALHA77257. Data obtained with EPMA. Values marked with ‘<’ are below detection limit.

	Vein metal (43)		Spherule Inclusions									
			Cr-rich sulfide (2)		Sulfide (5)		Ni-rich metal (7)		Ni-poor metal (2)		Cohenite (1)	
	wt%	2σ	wt%	2σ	wt%	2σ	wt%	2σ	wt%	2σ	wt%	2σ
Si	0.03	0.01	0.16	0.12	0.13	0.07	<0.02		0.02	0.01	0.03	0.01
Cr	0.3	0.01	7.43	0.34	1.25	0.32	0.07	0.01	0.31	0	0.37	0.02
Fe	95.11	0.18	52.41	0.52	61.19	0.61	94.37	0.39	96.12	1.77	91.18	0.27
Co	0.27	0.01	<0.02		<0.02	0.02	0.4	0.02	0.15	0.01	0.13	0.01
S	<0.02		37.03	0.24	36.16	0.23	<0.02		<0.02		<0.02	
Ni	3.86	0.04	0.22	0.13	0.08	0.01	5.44	0.11	2.43	0.01	1.34	0.02
Mn	0.01	0	1.1	0.01	0.09	0.04	0.01	0	0.01	0	0.03	0.01

### 8.1.3 DaG340

In DaG340, 38 grains of olivine and 22 grains of orthopyroxene were analyzed with EPMA and 5 grains of olivine and 2 grains of orthopyroxene were analyzed with LA-ICP-MS (Table 15).

Olivine composition is  $fa_{17.3-20.3}$  (mean  $fa_{19.0}$ ) with 0.32 – 0.42 wt% CaO (mean 0.37 wt%), 0.70 – 0.88 wt%  $Cr_2O_3$  (mean 0.78 wt%) and 0.37 – 0.50 wt% MnO (mean 0.43 wt%) (Fig. 36). LA-ICP-MS measurements give 90.1 – 116.0  $\mu g \cdot g^{-1}$  (mean 105.0  $\mu g \cdot g^{-1}$ ) NiO and 42.1 – 57.4  $\mu g \cdot g^{-1}$  CoO (mean 52.1  $\mu g \cdot g^{-1}$ ).

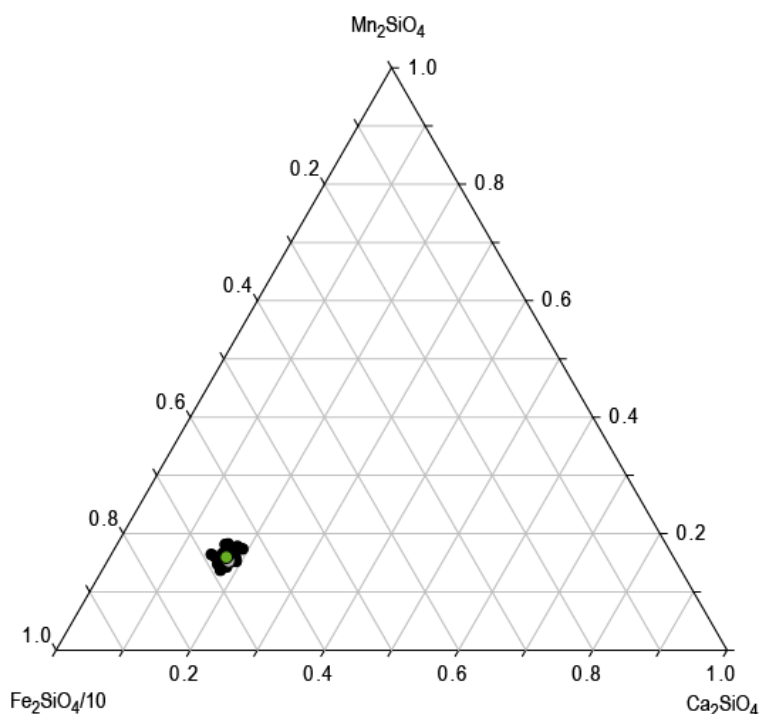
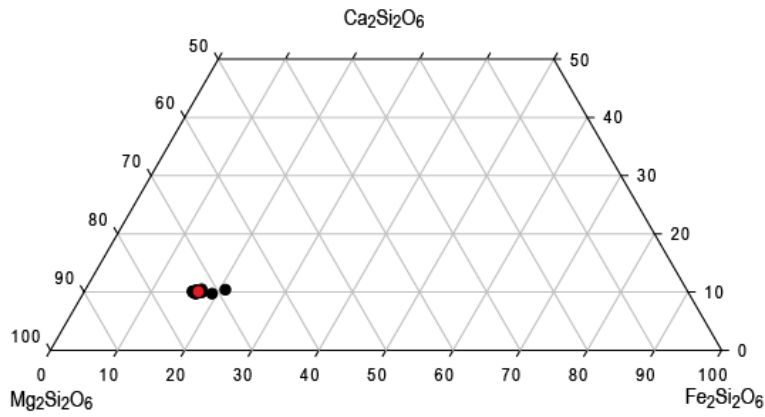
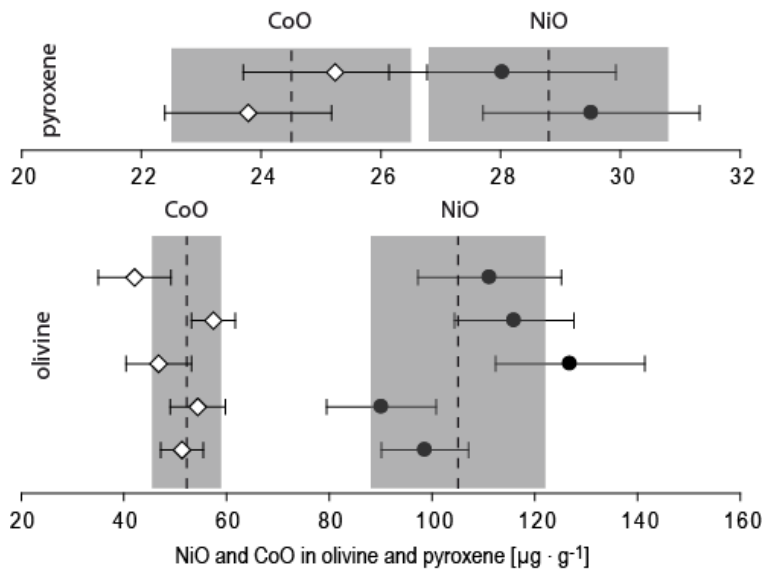


Fig. 36 Ternary diagram of  $Fe_2SiO_4 \cdot 10^{-1}$ ,  $Ca_2SiO_4$  and  $Mn_2SiO_4$  in DaG340 olivine (38 grains). The green circle represents the average composition. Grey circle is data taken from SINGLETARY and GROVE (2003).

Orthopyroxene composition is  $Wo_{9.2-10.3}$  (mean  $Wo_{9.5}$ ),  $Fs_{15.5-21.3}$  (mean  $Fs_{16.6}$ ) and  $En_{70.1-72.3}$  (mean  $En_{71.3}$ ) with 0.02 – 0.15 wt%  $TiO_2$  (mean 0.14 wt%), 1.13 – 1.38 wt%  $Cr_2O_3$  (mean 1.26 wt%) and 0.39 – 0.50 wt% MnO (mean 0.44 wt%) (Fig. 37). LA-ICP-MS measurements give 28.0 – 29.5  $\mu g \cdot g^{-1}$  (mean 28.8  $\mu g \cdot g^{-1}$ ) NiO and 23.8 – 25.2 CoO (mean 24.5  $\mu g \cdot g^{-1}$ ).



**Fig. 37** Composition of pyroxene in DaG340. Circles represent the composition of orthopyroxenes (22 grains), with the red circle giving the average composition. Literature data from SINGLETARY and GROVE (2003) is identical to the average composition and therefore not visible.



**Fig. 38** NiO and CoO concentrations in olivine and pyroxene in DaG340. Diamonds give the concentrations of CoO and Circles give the concentration of NiO. Shaded areas give the weighted average of the measurements.

**Table 15 Composition of olivine and orthopyroxene in DaG340. Data obtained with EMPA, except for NiO and CoO, which was obtained with LA-ICP-MS. Number of grains analyzed is given in parenthesis.**

	Olivine (38)		Orthopyroxene (22)	
	wt%	2 $\sigma$	wt%	2 $\sigma$
SiO <sub>2</sub>	39.58	0.08	55.50	0.29
TiO <sub>2</sub>	0.02	0.01	0.09	0.01
FeO	18.18	0.20	11.24	0.35
Al <sub>2</sub> O <sub>3</sub>	0.04	0.01	0.82	0.02
MgO	42.68	0.19	27.05	0.15
CaO	0.37	0.01	5.03	0.05
Cr <sub>2</sub> O <sub>3</sub>	0.78	0.02	1.26	0.03
MnO	0.43	0.01	0.43	0.01
	Olivine (5)		Orthopyroxene (2)	
	$\mu\text{g}\cdot\text{g}^{-1}$	2 $\sigma$	$\mu\text{g}\cdot\text{g}^{-1}$	2 $\sigma$
NiO	105.0	17.0	28.8	2.0
CoO	52.1	6.7	24.5	2.0
Number of oxygen ions	4		6	
Si	0.991		1.963	
Ti	0.000		0.002	
Fe	0.381		0.332	
Al	0.001		0.034	
Mg	1.592		1.426	
Ca	0.010		0.191	
Cr	0.015		0.035	
Mn	0.009		0.013	
T	1.001		2.004	
M	2.000		1.997	
Total	3.001		4.001	
<i>fa</i>	19.3			
En			71.3	
Wo			9.5	
Fs			16.6	

Due to the severe weathering of the sample, only 1 grain of vein metal was analyzed. It contains 3.79 wt% Ni, 0.24 wt% Co, 0.17 wt% Cr and 2.06 wt% Si.

Silicate grains in DaG340 contain inclusions of sulfide (2 grains) and Fe-metal (6 grains). The composition of troilite and metal is very variable in Ni- and Co-concentrations (troilite 0.09 – 1.04 wt% Ni, <0.02 wt% Co and Fe-metal 0.45 – 13.56 wt% Ni, 0.05 – 0.64 wt% Co).

### 8.1.4 EET87517

In EET87517, 17 grains of olivine, 63 grains of orthopyroxene and 1 grain of plagioclase were analyzed with EPMA. One grain of olivine and 4 grains of orthopyroxene were analyzed with LA-ICP-MS (Table 16).

Olivine composition is  $fa_{4.0-13.9}$  (mean  $fa_{7.8}$ ) with 0.27 – 0.41 wt% CaO (mean 0.31 wt%), 0.33 – 0.76 wt%  $Cr_2O_3$  (mean 0.37 wt%) and 0.36 – 0.40 wt% MnO (mean 0.47 wt%) (Fig. 39). LA-ICP-MS measurements (Fig. 41) give  $45.6 \mu\text{g}\cdot\text{g}^{-1}$  NiO and  $22.6 \mu\text{g}\cdot\text{g}^{-1}$  CoO.

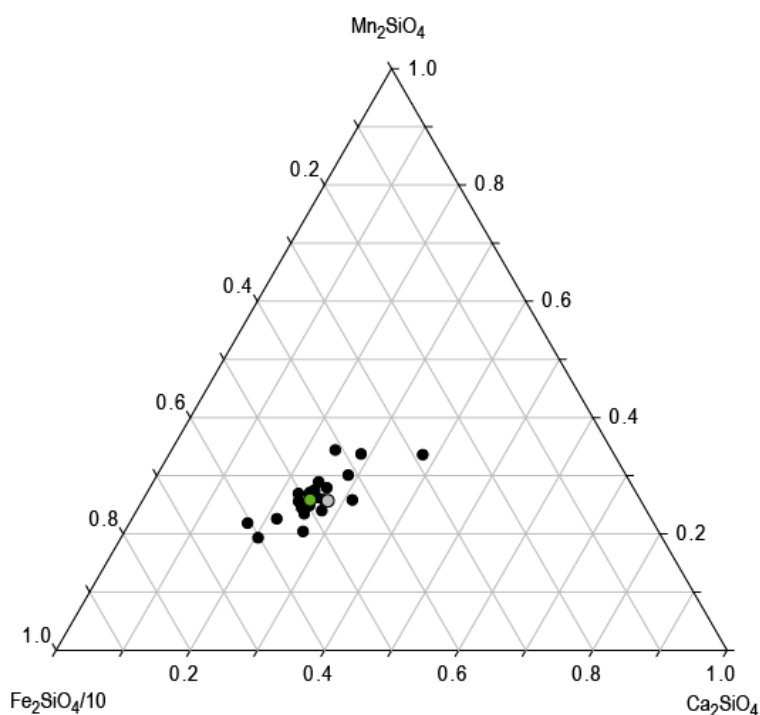


**Fig. 39 Ternary diagram of  $Fe_2SiO_4 \cdot 10^{-1}$ ,  $Ca_2SiO_4$  and  $Mn_2SiO_4$  in EET87517 olivine (17 grains). The green circle represents the average composition. Grey circle is data taken from SINGLETARY and GROVE (2003).**

Orthopyroxene (63 grains analyzed) is  $Wo_{4.3-4.9}$  (mean  $Wo_{4.6}$ ),  $Fs_{6.4-10.4}$  (mean  $Fs_{7.4}$ ) and  $En_{85.6-89.8}$  (mean  $En_{87.9}$ ) with 0.05 - 0.26 wt%  $TiO_2$  (mean 0.14 wt%), 0.27 – 0.49 wt% MnO (mean 0.39) and 0.47 – 0.66 wt%  $Cr_2O_3$  (mean 0.58 wt%). Four grains of orthopyroxene (Fig. 41) were analyzed with LA-ICP-MS, giving  $13.8 - 43.1 \mu\text{g}\cdot\text{g}^{-1}$  NiO (mean  $18.0 \mu\text{g}\cdot\text{g}^{-1}$ ) and  $10.1 - 12.6 \mu\text{g}\cdot\text{g}^{-1}$  CoO (mean  $11.6 \mu\text{g}\cdot\text{g}^{-1}$ ).

The plagioclase is  $Ab_{55.3}$  and  $An_{44.7}$  with 0.29 wt% FeO, 0.08 wt%  $TiO_2$  and  $<0.02$  wt% of MnO and MgO.

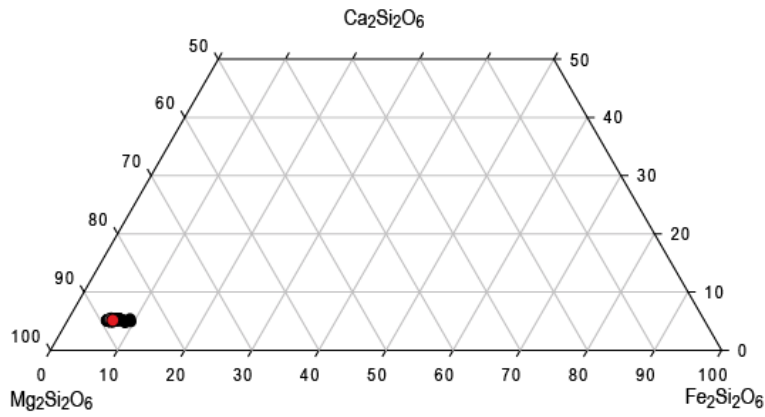


**Fig. 40** Composition of pyroxene in EET87517. Circles represent the composition of orthopyroxenes (63 grains), with the red circle giving the average composition. Literature data from SINGLETARY and GROVE (2003) is identical to the average composition of orthopyroxene (red circle) and therefore not visible.

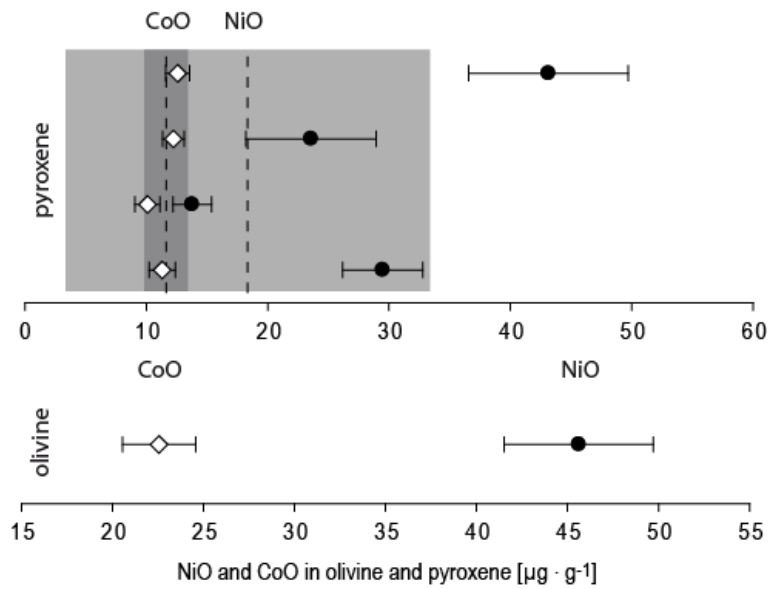


**Fig. 41** NiO and CoO concentrations in olivine and pyroxene in EET87517. Diamonds give the concentrations of CoO and Circles give the concentration of NiO. Shaded areas give the weighted average of the measurements.

**Table 16** Composition of olivine and orthopyroxene in EET87517. Data obtained with EMPA, except for NiO and CoO, which was obtained with LA-ICP-MS. Number of grains analyzed is given in parenthesis. Values marked with '<' are below detection limit.

	Olivine (17)		Orthopyroxene I (63)		Orthopyroxene II (3)		Plagioclase (1)	
	wt%	2 $\sigma$	wt%	2 $\sigma$	wt%	2 $\sigma$	wt%	2 $\sigma$
SiO <sub>2</sub>	41.17	0.14	57.97	0.21	56.71	0.88	56.84	0.16
Na <sub>2</sub> O	<0.02		0.05	0.01	0.05	0.02	6.70	0.50
TiO <sub>2</sub>	<0.02		0.14	0.01	0.11	0.03	0.08	0.03
FeO	7.92	0.11	5.21	0.15	8.29	0.13	0.29	0.00
Al <sub>2</sub> O <sub>3</sub>	0.04	0.01	0.55	0.01	0.59	0.05	27.55	1.01
MgO	51.52	0.24	34.84	0.21	30.59	0.80	0.00	0.00
CaO	0.31	0.01	2.53	0.02	3.36	0.12	9.80	0.14
Cr <sub>2</sub> O <sub>3</sub>	0.37	0.01	0.58	0.01	1.12	0.03	<0.02	
MnO	0.40	0.01	0.39	0.01	0.45	0.03	<0.02	
	Olivine (1)		Orthopyroxene (4)					
	$\mu\text{g}\cdot\text{g}^{-1}$	2 $\sigma$	$\mu\text{g}\cdot\text{g}^{-1}$	2 $\sigma$				
NiO	45.6	4.1	18.0	15.0				
CoO	22.6	2.0	11.6	1.8				
Number of oxygen ions	4		6		6		8	
Si	0.986		1.963		1.972		2.529	
Na	0.000		0.003		0.004		0.578	
Ti	0.000		0.004		0.003		0.003	
Fe	0.159		0.148		0.241		0.011	
Al	0.001		0.022		0.024		1.445	
Mg	1.839		1.758		1.586		0.000	
Ca	0.008		0.092		0.125		0.467	
Cr	0.007		0.015		0.031		0.000	
Mn	0.008		0.011		0.013		0.000	
T	0.989		1.992		2.003		3.977	
M	2.021		2.025		1.996		1.057	
Total	3.010		4.017		4.000		5.034	
<i>fa</i>	7.8							
Wo			4.6		6.3			
Fs			7.4		12.1			
En			87.9		79.3			
Ab							55.3	
An							44.7	

EET87517 contains two different types of vein metal. The first type (6 grains) is Si- and Ni-poor (<0.02 wt% Si, 3.62 – 4.09 wt% Ni (mean 3,88 wt%)) but Cr-rich (0.21 – 0.27 wt% Cr (mean 0.25 wt%)), the other (15 grains) is Si- and Ni- rich (1.14 – 4.74 wt% Si (mean 1.51), 4.93 – 5.72 wt% Ni (mean 5.45)) and Cr-poor (<0.02 – 0.10 wt% Cr (mean 0.05 wt%)).

EET87517 contains sulfide vein material (4 grains). The sulfide contains 0.05 – 0.14 wt% Ni (mean 0.11), <0.02 wt% Co, 0.59 – 0.92 wt% Mn (mean 0.71 wt%) and 5.25 – 8.14 wt% Cr (mean 6.40 wt%).

Eleven different spherule inclusions have been analyzed in EET87517. Spherule inclusions are FeNi-metal + troilite (1), troilite + cohenite (2), FeNi-metal (4), troilite (2), cohenite (1) or FeNi-metal + troilite + cohenite (1). Only the metal + troilite + cohenite spherule is

associated with Ni-rich metal (8.18 wt% Ni, 0.58 wt% Co, 0.05 wt% Cr and <0.02 wt% Si), while the metal in other spherules is similar to Ni-rich vein metal, but less abundant in Si (5.32 – 6.18 wt% Ni (mean 5.73), 0.39 – 0.53 wt% Co (mean 0.45 wt%), <0.02 wt% Cr and <0.02 – 1.24 wt% Si (mean 0.37 wt%)). Cohenite in spherule inclusions contains 1.66 – 1.78 wt% Ni (mean 1.71 wt%), 0.27 – 0.29 wt% Co (mean 0.28 wt%), 0.08 – 0.26 wt% Cr (mean 0.19) and <0.02 wt% Si.

**Table 17 Composition of vein metal, vein troilite and sulfide phases, metal and cohenite from spherule inclusions in EET87517. Data obtained with EPMA. Values marked with ‘<’ are below detection limit**

	Si-rich vein metal (15)		Si-poor vein metal II (6)		Vein troilite (4)			
	wt%	2 $\sigma$	wt%	2 $\sigma$	wt%	2 $\sigma$		
Si	1.51	0.46	0.04	0.02	0.09	0.05		
Cr	0.05	0.01	0.25	0.02	6.40	1.30		
Fe	92.48	0.53	94.69	1.13	53.58	2.45		
Co	0.45	0.03	0.27	0.04	<0.02			
S	<0.02		<0.02		37.27	0.47		
Ni	5.45	0.10	3.88	0.12	0.11	0.04		
Mn	<0.02		<0.02		0.71	0.15		
Spherule inclusions								
	Cohenite (4)		Ni-rich metal (1)		Ni-poor metal (5)		troilite (4)	
	wt%	2 $\sigma$	wt%	2 $\sigma$	wt%	2 $\sigma$	wt%	2 $\sigma$
Si	0.03	0.01	<0.02		0.37	0.44	0.04	0.02
Cr	0.19	0.09	0.05	0.02	0.04	0.02	3.13	1.84
Fe	90.10	0.32	90.91	1.64	93.38	1.16	58.45	2.50
Co	0.28	0.01	0.58	0.02	0.45	0.04	<0.02	
S	<0.02		<0.02		<0.02		36.89	0.55
Ni	1.71	0.05	8.19	0.14	5.73	0.27	0.12	0.02
Mn	<0.02		<0.02		<0.02		0.38	0.25

### 8.1.5 EET96042

In EET87517, 53 grains of olivine and 8 grains of orthopyroxene were analyzed with EPMA. Five grain of olivine and 3 grains of orthopyroxene were analyzed with LA-ICP-MS (Table 18).

Olivine composition is  $fa_{14.9-18.0}$  (mean  $fa_{17.2}$ ) with 0.28 – 0.56 wt% CaO (mean 0.34 wt%), 0.54 – 0.92 wt%  $Cr_2O_3$  (mean 0.80 wt%) and 0.38 – 0.54 wt% MnO (mean 0.45 wt%) (Fig. 42). LA-ICP-MS (Fig. 44) measurements give 59.6 – 77.2  $\mu g \cdot g^{-1}$  NiO (mean 73.2  $\mu g \cdot g^{-1}$ ) and 37.7 – 45.6  $\mu g \cdot g^{-1}$  CoO (mean 41.7  $\mu g \cdot g^{-1}$ ). Only grains with FeO > 14 wt% have been included into the calculation of mean values, as smaller FeO-concentrations probably represent reduced grains (Fig. 42).

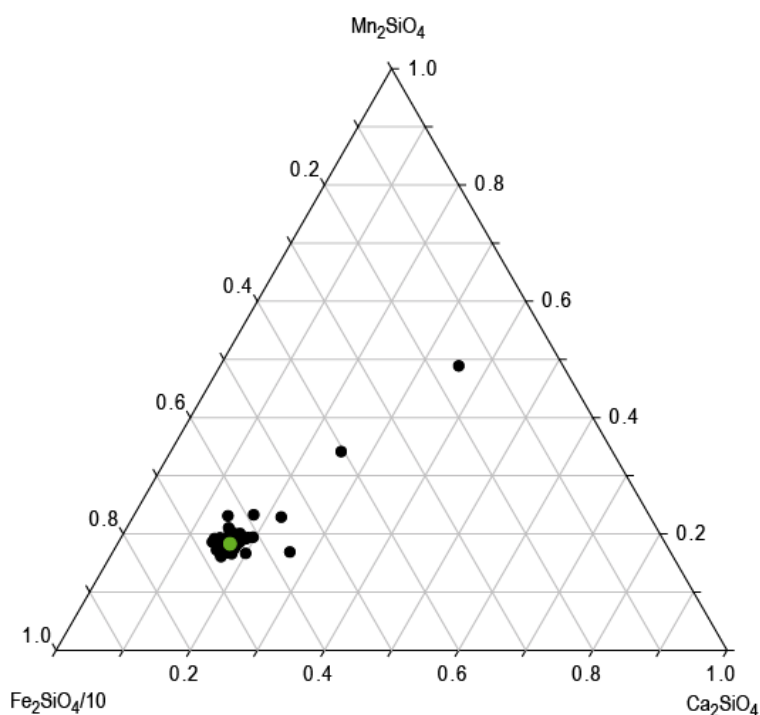


**Fig. 42 Ternary diagram of  $Fe_2SiO_4 \cdot 10^{-1}$ ,  $Ca_2SiO_4$  and  $Mn_2SiO_4$  in EET96042 olivine (53 grains). The green circle represents the average composition.**

Orthopyroxene composition is  $Wo_{8.7-9.2}$  (mean  $Wo_9$ ),  $Fs_{11.4-15.1}$  (mean  $Fs_{13.9}$ ) and  $En_{71.8-77.1}$  (mean  $En_{73.9}$ ) with 0.05 – 0.14 wt%  $TiO_2$  (mean 0.09 wt%), 1.30 – 1.40 wt%  $Cr_2O_3$  (mean 1.35 wt%) and 0.41 – 0.52 wt% MnO (mean 0.47 wt%) (Fig. 43). LA-ICP-MS measurements (Fig. 44) give 24.8 – 34.2  $\mu g \cdot g^{-1}$  (mean 28.0  $\mu g \cdot g^{-1}$ ) NiO and 16.5 – 18.7 CoO (mean 17.4  $\mu g \cdot g^{-1}$ ).

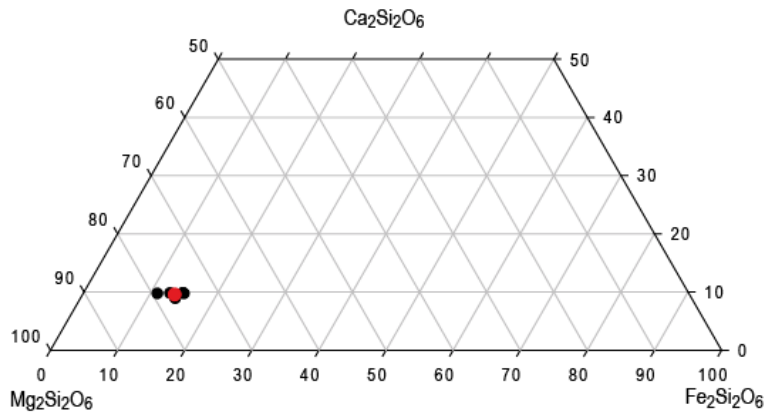


Fig. 43 Composition of pyroxene in EET96042. Circles represent the composition of orthopyroxenes (8 grains), with the red circle giving the average composition.

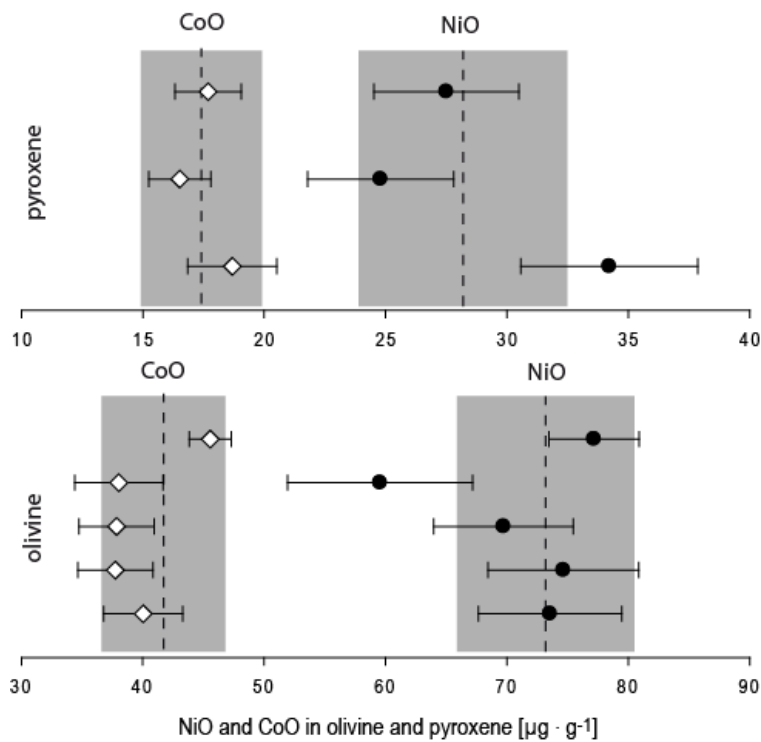


Fig. 44 NiO and CoO concentrations in olivine and pyroxene in EET96042. Diamonds give the concentrations of CoO and Circles give the concentration of NiO. Shaded areas give the weighted average of the measurements.

**Table 18** Composition of olivine and orthopyroxene in EET96042. Data obtained with EMPA, except for NiO and CoO, which were obtained with LA-ICP-MS. Number of grains analyzed is given in parenthesis.

	Olivine (46)		Orthopyroxene (8)	
	wt%	2 $\sigma$	wt%	2 $\sigma$
SiO <sub>2</sub>	39.12	1.87	55.32	0.54
TiO <sub>2</sub>	0.02	0.04	0.09	0.02
FeO	16.29	0.91	9.35	0.55
Al <sub>2</sub> O <sub>3</sub>	0.03	0.05	0.78	0.10
MgO	43.72	1.57	27.86	0.52
CaO	0.34	0.08	4.70	0.10
Cr <sub>2</sub> O <sub>3</sub>	0.80	0.13	1.35	0.03
MnO	0.45	0.07	0.47	0.03
	Olivine (5)		Orthopyroxene (3)	
	$\mu\text{g}\cdot\text{g}^{-1}$	2 $\sigma$	$\mu\text{g}\cdot\text{g}^{-1}$	2 $\sigma$
NiO	73.2	7.3	28.2	4.3
CoO	41.7	5.1	17.4	2.5
Number of oxygen ions	4		6	
Si	0.985		1.969	
Ti	0.000		0.002	
Fe	0.343		0.278	
Al	0.001		0.033	
Mg	1.641		1.477	
Ca	0.009		0.179	
Cr	0.016		0.038	
Mn	0.009		0.014	
T	0.985		1.969	
M	2.022		2.028	
Total	3.007		3.997	
<i>fa</i>	17.2			
En			73.9	
Wo			9.0	
Fs			13.9	

In EET96042, 14 grains of vein metal, 9 grains of vein troilite and 27 grains of metal and troilite inclusion in silicate grains were analyzed (Table 19).

The vein metal contains 3.36 – 5.57 wt% Ni (mean 4.75 wt%), 0.13 wt% - 0.36 wt% Co (mean 0.29 wt%) and 0 – 0.16 wt% Cr (mean 0.07 wt%). Of 14 grains, 12 contain 4.71 – 5.35 wt% Si (mean 4.88 wt%), while 2 grains contain <0.02 wt% Si. The vein troilite contains <0.02 – 0.27 wt% Ni, <0.02 Co, 0.05 – 0.45 wt% Mn (mean 0.24 wt%) and <0.02 – 0.30 wt% Si. Vein troilite is very variable in Cr, with concentrations ranging from 0.41 to 8.93 wt%. Three of 9 grains contain less than 1.4 wt% Cr, while the other grains contain >5.77 wt% Cr.

Sulfide inclusions in silicate grains (11 grains analyzed) are of similar composition as vein troilite, showing the same variability in Cr-concentrations (0.57 – 9.14 wt%). Metal inclusion in silicate grains (16 grains analyzed) contain 0.12 – 5.80 wt% Ni and <0.02 – 0.41 wt% Co.

The Ni- and Co-poor metal probably represents metal produced from silicate reduction. In contrast to vein metal, metal inclusions contain <0.02 – 1.18 wt% Si (mean 0.11 wt%).

**Table 19 Composition of vein metal, vein troilite, metal and troilite inclusions in EET96042. Data obtained with EPMA. Values marked with '<' are below detection limit. Elements with high variability are given as ranges.**

	Vein metal (12)		Vein troilite (11)		Metal inclusions (16)		Troilite inclusions (11)	
	wt%	2 $\sigma$	wt%	2 $\sigma$	wt%	2 $\sigma$	wt%	2 $\sigma$
Si	4.88	0.18	0.1	0.04	0.11	0.2	0.1	0.04
Cr	0.08	0.03	0.41 - 8.93		0.14	0.04	0.57 - 9.14	
Fe	90.8	0.72	58.82	3.72	97.55	1.77	58.82	3.72
Co	0.30	0.03	<0.02		<0.02 - 0.41		<0.02	
S	0.01	0.01	35.79	1.27	<0.02		35.79	1.27
Ni	4.89	0.23	0.36	0.42	0.12 - 5.80		0.36	0.42
Mn	0	0.01	0.29	0.11	0.02	0.01	0.29	0.11

### 8.1.6 EET96331

In EET96331, 27 grains of olivine, 32 grains of orthopyroxene and 3 grains of augite were analyzed with EPMA. Five grain of olivine and 5 grains of orthopyroxene were analyzed with LA-ICP-MS (Table 20).

Olivine composition is  $fa_{9.1-12.6}$  (mean  $fa_{11.8}$ ) with 0.23 – 0.30 wt% CaO (mean 0.27 wt%), 0.43 – 0.57 wt%  $Cr_2O_3$  (mean 0.48 wt%) and 0.47 – 0.66 wt% MnO (mean 0.55 wt%). LA-ICP-MS measurements (Fig. 47) give 18.5 – 28.4  $\mu g \cdot g^{-1}$  NiO (mean 20.1  $\mu g \cdot g^{-1}$ ) and 6.7 – 8.1  $\mu g \cdot g^{-1}$  CoO (mean 7.6  $\mu g \cdot g^{-1}$ ). Only grains with FeO > 10 wt% have been included into the calculation of mean values, as smaller FeO-concentrations probably represent reduced grains (Fig. 45).

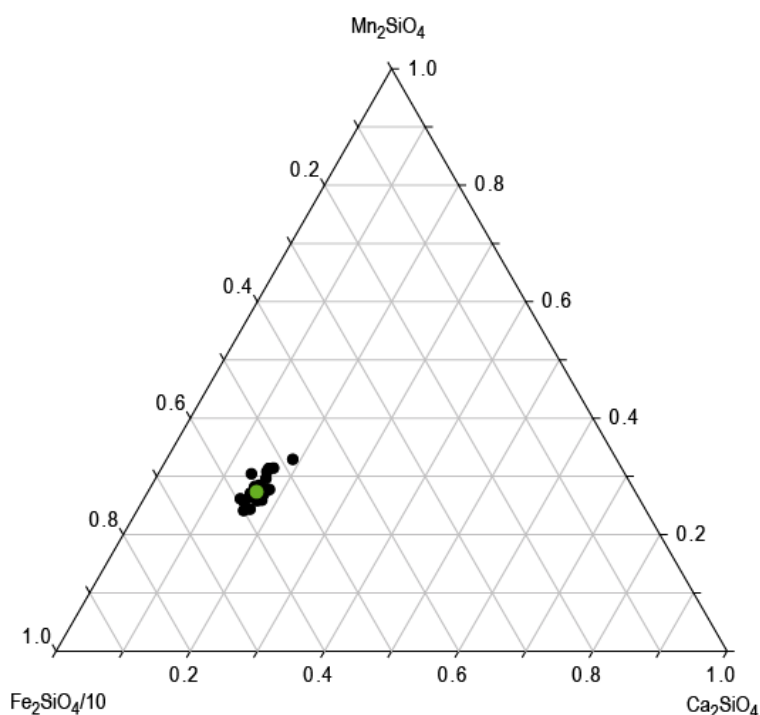


**Fig. 45 Ternary diagram of  $Fe_2SiO_4 \cdot 10^{-1}$ ,  $Ca_2SiO_4$  and  $Mn_2SiO_4$  in EET96331 olivine (27 grains). The green circle represents the average composition.**

Orthopyroxene composition is  $Wo_{4.3-4.6}$  (mean  $Wo_{4.5}$ ),  $Fs_{9.9-11.7}$  (mean  $Fs_{10.7}$ ) and  $En_{81.1-84.7}$  (mean  $En_{83.3}$ ) with 0.06 – 0.21 wt%  $TiO_2$  (mean 0.12 wt%), 0.88 – 1.13 wt%  $Cr_2O_3$  (mean 1.00 wt%) and 0.45 – 0.62 wt% MnO (mean 0.53 wt%). Augite composition is  $Wo_{34.6-35.2}$  (mean  $Wo_{35.0}$ ),  $Fs_{6.2-6.4}$  (mean  $Fs_{6.3}$ ) and  $En_{52.7-54.5}$  (mean  $En_{83.3}$ ) with 0.20 – 0.30 wt%  $TiO_2$  (mean 0.26 wt%), 1.13 – 1.31 wt%  $Cr_2O_3$  (mean 1.21 wt%) and 0.36 – 0.43 wt% MnO (mean 0.38

wt%) (Fig. 46). LA-ICP-MS measurements (Fig. 47) give 5.4 – 17.7  $\mu\text{g}\cdot\text{g}^{-1}$  (mean 9.9  $\mu\text{g}\cdot\text{g}^{-1}$ ) NiO and 3.2 – 4.2 CoO (mean 3.8  $\mu\text{g}\cdot\text{g}^{-1}$ ).

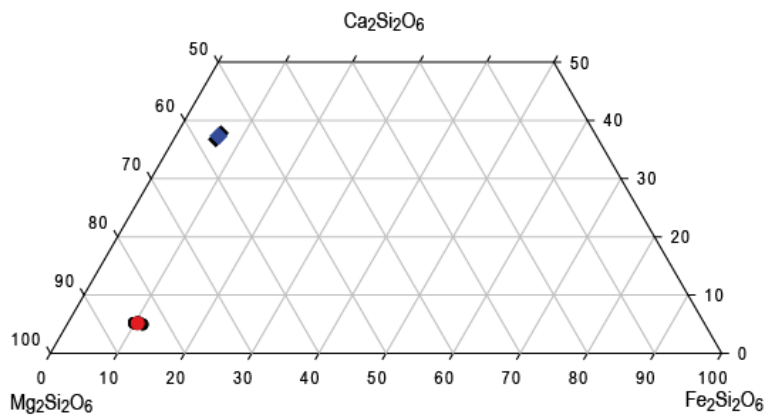


**Fig. 46** Composition of pyroxenes in EET96331. Circles represent the composition of orthopyroxenes (32), with the red circle giving the average orthopyroxene composition. Diamonds give the composition of augite (3), with the blue diamond giving the average augite composition.

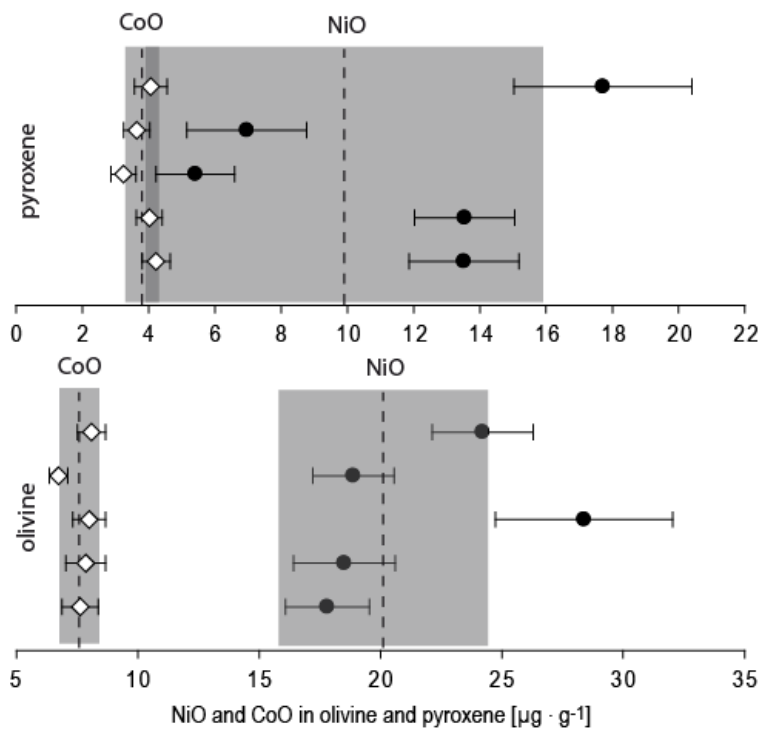


**Fig. 47** NiO and CoO concentrations in olivine and pyroxene in EET96331. Diamonds give the concentrations of CoO and Circles give the concentration of NiO. Shaded areas give the weighted average of the measurements.

**Table 20** Composition of olivine and pyroxenes in EET96331. Data obtained with EMPA, except for NiO and CoO, which was obtained with LA-ICP-MS. Number of grains analyzed is given in parenthesis. Values marked with '<' are below detection limit.

	Olivine (25)		Orthopyroxene (32)		Augite (3)	
	wt%	2 $\sigma$	wt%	2 $\sigma$	wt%	2 $\sigma$
SiO <sub>2</sub>	40.58	0.12	56.41	0.16	53.71	0.91
Na <sub>2</sub> O	<0.02		<0.02		0.24	0.08
TiO <sub>2</sub>	0.02	0.01	0.12	0.01	0.26	0.06
FeO	11.70	0.22	7.40	0.12	4.17	0.04
Al <sub>2</sub> O <sub>3</sub>	0.03	0.01	1.20	0.02	1.93	0.03
MgO	49.07	0.32	32.41	0.18	19.89	0.80
CaO	0.27	0.01	2.43	0.02	18.02	0.18
Cr <sub>2</sub> O <sub>3</sub>	0.48	0.01	1.00	0.02	1.23	0.11
MnO	0.55	0.02	0.53	0.02	0.38	0.05
	Olivine (5)		Orthopyroxene (5)			
	$\mu\text{g}\cdot\text{g}^{-1}$	2 $\sigma$	$\mu\text{g}\cdot\text{g}^{-1}$	2 $\sigma$		
NiO	20.1	4.3	9.9	6.0		
CoO	7.6	0.8	3.8	0.5		
Number of oxygen ions	4		6		6	
Si	0.981		1.947		1.945	
Na	0.000		0.003		0.017	
Ti	0.000		0.003		0.007	
Fe	0.236		0.213		0.126	
Al	0.001		0.049		0.083	
Mg	1.767		1.666		1.073	
Ca	0.007		0.090		0.699	
Cr	0.009		0.027		0.035	
Mn	0.011		0.015		0.012	
T	0.981		1.947		1.945	
M	2.034		2.067		2.052	
Total	3.014		4.014		3.997	
<i>fa</i>	11.8					
En			83.3		53.7	
Wo			4.5		35.0	
FS			10.7		6.3	

In EET96331, 6 grains of vein metal, 7 grains of troilite inclusions and 2 grains of metal inclusions were measured (Table 21).

The vein metal contains 4.78 – 5.11 wt% Ni (mean 4.91 wt%), 0.31 - 0.34 wt% Co (mean 0.32 wt%), 0.04 – 0.15 wt% Cr (mean 0.10 wt%) and 3.30 – 4.91 wt% Si (mean 4.20 wt%)

Metal inclusions in silicate grains contain 0.47 – 0.85 wt% Ni (mean 0.66 wt%), 0.04 wt% Co and 0.11 – 0.13 wt% Cr (mean 0.10 wt%), 0.05 wt% Si and probably represent metal derived from silicate reduction. Two types of troilite inclusions are present in EET96331, Cr-rich and Cr-poor troilite. Cr-poor troilite (4 grains) contains 0.05 – 0.21 wt% Ni (mean 0.12 wt%), <0.02 wt% Co, 0.08 – 0.16 wt% Mn (mean 0.14 wt%), 0.33 – 0.79 wt% Cr (mean 0.56 wt%) and <0.02 – 0.39 wt% Si (mean 0.16 wt%). Cr-rich troilite (3 grains) contains 0.03 – 0.08 wt%

Ni (mean 0.05 wt%), <0.02 wt% Co, 0.41 – 0.80 wt% Mn (mean 0.66 wt%), 4.57 – 13.38 wt% Cr and <0.02 – 0.49 wt% Si (mean 0.20 wt%).

**Table 21** Composition of vein metal, metal and troilite inclusions in EET96331. Data obtained with EPMA. Values marked with ‘<’ are below detection limit. Elements with high variability are given as ranges.

	Vein metal (6)		Metal inclusions (2)		Cr-poor troilite		Cr-rich troilite	
	wt%	2 $\sigma$	wt%	2 $\sigma$	wt%	2 $\sigma$	wt%	2 $\sigma$
Si	4.20	0.58	0.05	0.01	0.16	0.16	<0.02 - 0.49	
Cr	0.10	0.03	0.12	0.02	0.56	0.22	4.57 - 13.38	
Fe	89.85	0.57	97.54	1.44	61.36	0.60	44.71 - 54.94	
Co	0.32	0.01	0.04	0.00	<0.02		<0.02	
S	<0.02		0.09	0.15	36.09	1.03	38.27	1.42
Ni	4.91	0.14	0.66	0.38	0.12	0.08	0.05	0.03
Mn	<0.02		<0.02		0.14	0.04	0.66	0.25

### 8.1.7 GRA95205

In GRA95205, 70 grains of olivine, 4 grains of Ca-rich orthopyroxene and 7 grains of Ca-poor orthopyroxene were analyzed with EPMA. Ten grains of olivine and 5 grains of orthopyroxene were analyzed with LA-ICP-MS (Table 22).

Olivine composition is  $fa_{18.0-22.2}$  (mean  $fa_{19.7}$ ) with 0.17 – 0.50 wt% CaO (mean 0.28 wt%), 0.48 – 0.80 wt%  $Cr_2O_3$  (mean 0.64 wt%) and 0.33 – 0.56 wt% MnO (mean 0.42 wt%). LA-ICP-MS measurements (Fig. 50) give 74.1 – 111.2  $\mu g \cdot g^{-1}$  NiO (mean 88.3  $\mu g \cdot g^{-1}$ ) and 44.6 – 51.9  $\mu g \cdot g^{-1}$  CoO (mean 48.9  $\mu g \cdot g^{-1}$ ). Only grains with FeO > 16 wt% have been included into the calculation of mean values, as smaller FeO-concentrations probably represent reduced grains (Fig. 48).

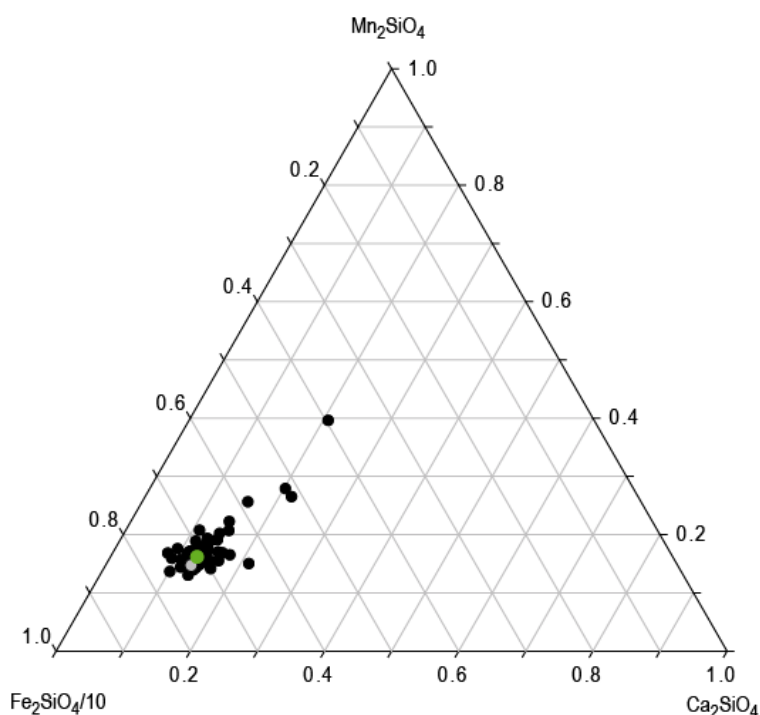


**Fig. 48 Ternary diagram of  $Fe_2SiO_4 \cdot 10^{-1}$ ,  $Ca_2SiO_4$  and  $Mn_2SiO_4$  in GRA95205 olivine (70 grains). The green circle represents the average composition. The grey circle represents data from SINGLETARY and GROVE (2003).**

The composition of Ca-rich orthopyroxene (4 grains) is  $Wo_{8.6-9.2}$  (mean  $Wo_{8.8}$ ),  $Fs_{14.1-14.8}$  (mean  $Fs_{14.5}$ ) and  $En_{74.9-76.5}$  (mean  $En_{75.6}$ ) with 0.07 – 0.10 wt%  $TiO_2$  (mean 0.09 wt%), 1.29 – 1.40 wt%  $Cr_2O_3$  (mean 1.39 wt%) and 0.43 – 0.48 wt% MnO (mean 0.45 wt%). The composition of Ca-poor orthopyroxene (7 grains) is  $Wo_{3.4-3.9}$  (mean  $Wo_{3.6}$ ),  $Fs_{14.5-16.6}$  (mean  $Fs_{15.6}$ ) and  $En_{78.8-81.8}$  (mean  $En_{80.3}$ ) with 0.03 – 0.10 wt%  $TiO_2$  (mean 0.07 wt%), 1.03 – 1.22 wt%  $Cr_2O_3$  (mean 1.11 wt%) and 0.35 – 0.44 wt% MnO (mean 0.38 wt%) (Fig. 49). LA-ICP-MS

measurements (Fig. 50) give  $24.7 - 50.0 \mu\text{g}\cdot\text{g}^{-1}$  (mean  $32.3 \mu\text{g}\cdot\text{g}^{-1}$ ) NiO and  $19.7 - 24.5 \text{CoO}$  (mean  $21.3 \mu\text{g}\cdot\text{g}^{-1}$ ).

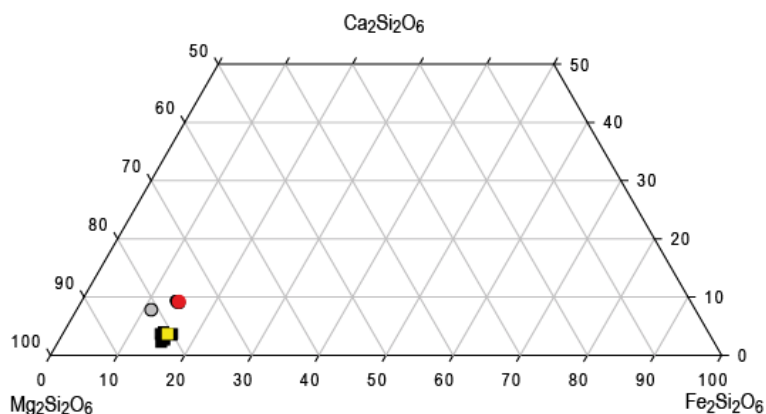


**Fig. 49** Composition of pyroxenes in GRA95205. Circles represent the composition of Ca-rich orthopyroxenes (4 grains), with the red circle giving the average composition. Squares give the composition Ca-poor orthopyroxene (7 grains), with the yellow square giving the average composition. Grey circles represent data taken from SINGLETARY and GROVE (2003).

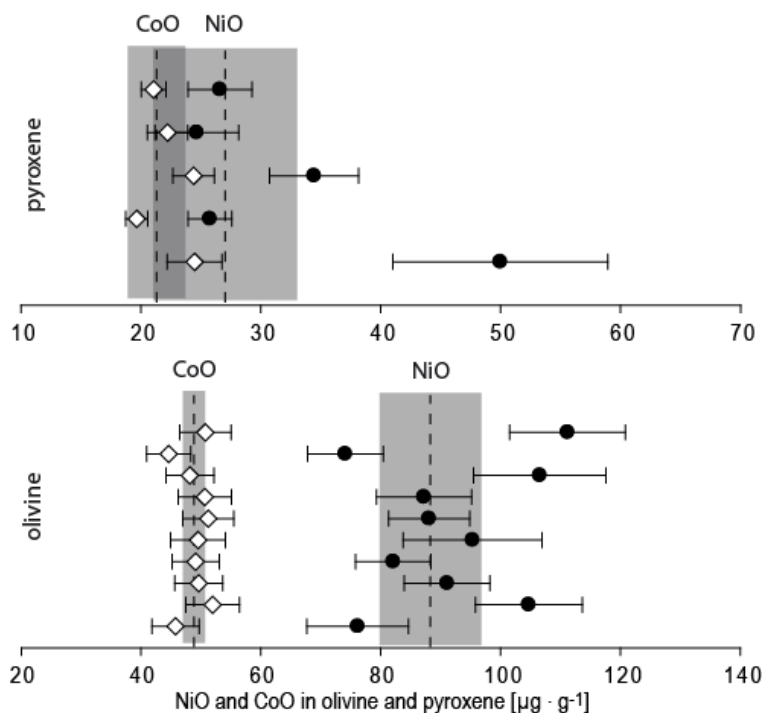


**Fig. 50** NiO and CoO concentrations in olivine and pyroxene in GRA95205. Diamonds give the concentrations of CoO and Circles give the concentration of NiO. Shaded areas give the weighted average of the measurements.

**Table 22 Composition of olivine and pyroxenes in GRA95205. Data obtained with EMPA, except for NiO and CoO, which was obtained with LA-ICP-MS. Number of grains analyzed is given in parenthesis.**

	Olivine (62)		Ca-rich orthopyroxene (4)		Ca-poor orthopyroxene (7)	
	wt%	2 $\sigma$	wt%	2 $\sigma$	wt%	2 $\sigma$
SiO <sub>2</sub>	39.15	0.12	55.28	0.88	55.83	0.71
Na <sub>2</sub> O	0.03	0.01	0.13	0.06	0.08	0.05
TiO <sub>2</sub>	0.01	0.00	0.09	0.01	0.07	0.02
FeO	18.91	0.14	9.81	0.20	10.63	0.33
Al <sub>2</sub> O <sub>3</sub>	0.04	0.01	0.69	0.04	0.74	0.22
MgO	43.39	0.20	28.75	0.38	30.95	0.40
CaO	0.28	0.01	4.66	0.16	1.74	0.23
Cr <sub>2</sub> O <sub>3</sub>	0.64	0.01	1.35	0.05	1.11	0.04
MnO	0.42	0.01	0.45	0.02	0.38	0.02
	Olivine (10)		Orthopyroxene (5)			
	$\mu\text{g}\cdot\text{g}^{-1}$	2 $\sigma$	$\mu\text{g}\cdot\text{g}^{-1}$	2 $\sigma$		
NiO	88.3	8.5	27.0	6.0		
CoO	48.9	1.8	21.3	2.4		
Number of oxygen ions	4		6			
Si	0.977		1.950		1.951	
Na	0.001		0.009		0.005	
Ti	0.000		0.002		0.002	
Fe	0.395		0.289		0.311	
Al	0.001		0.029		0.030	
Mg	1.613		1.512		1.612	
Ca	0.007		0.176		0.065	
Cr	0.013		0.038		0.031	
Mn	0.009		0.013		0.011	
T	0.977		1.950		1.951	
M	2.040		2.068		2.068	
Total	3.017		4.019		4.019	
<i>fa</i>	19.7					
En			75.6		80.3	
Wo			8.8		3.6	
Fs			14.5		15.6	

In GRA95205, 44 grains of vein metal and 20 grains of metal inclusions in silicate grains have been analyzed (Table 23).

The vein metal contains 2.56 – 4.64 wt% Ni (mean 3.63 wt%), 0.15 - 0.34 wt% Co (mean 0.26 wt%) and 0.03 – 0.41 wt% Cr (mean 0.20 wt%). Vein metal in GRA95205 is variable in Si-concentration, ranging from <0.02 to 1.55 wt% (mean 0.58 wt%).

Metal inclusions in silicate grains are similar to vein metal, except for a wider spread in Co and Ni concentrations (0.69 – 4.05 wt% Ni, 0.03 – 0.35 wt% Co). Ni- and Co-poor inclusions probably represent metal formed by silicate reduction.

**Table 23 Composition of vein metal and metal inclusions in GRA95205. Data obtained with EPMA. Values marked with '<' are below detection limit. Elements with high variability are given as ranges.**

	vein metal (44)		metal inclusions (20)	
	wt%	2 $\sigma$	wt%	2 $\sigma$
P	0.22	0.03	0.15	0.04
Si	<0.02 - 1.55		<0.02 - 1.65	
Cr	0.20	0.03	0.16	0.05
Fe	96.10	0.46	97.32	0.71
Co	0.26	0.01	0.16	0.04
S	<0.02		<0.02	
Ni	3.63	0.17	0.69 - 4.05	
Mn	<0.02		<0.02	

### 8.1.8 Kenna

In Kenna, 18 grains of olivine and 9 grains of orthopyroxene were analyzed with EPMA. Twelve grains of olivine and 3 grains of orthopyroxene were analyzed with LA-ICP-MS (Table 24).

Olivine composition is  $fa_{18.4-21.0}$  (mean  $fa_{20.0}$ ) with 0.36 – 0.44 wt% CaO (mean 0.41 wt%), 0.58 – 0.76 wt%  $Cr_2O_3$  (mean 0.72 wt%) and 0.37 – 0.49 wt% MnO (mean 0.43 wt%). LA-ICP-MS measurements (Fig. 53) give 83.2 – 113.9  $\mu g \cdot g^{-1}$  NiO (mean 91.6  $\mu g \cdot g^{-1}$ ) and 52.3 – 62.0  $\mu g \cdot g^{-1}$  CoO (mean 54.2  $\mu g \cdot g^{-1}$ ). Only grains with FeO > 16 wt% (11 of 18), have been included into the calculation of mean values, as smaller FeO-concentrations probably represent reduced grains (Fig. 51).

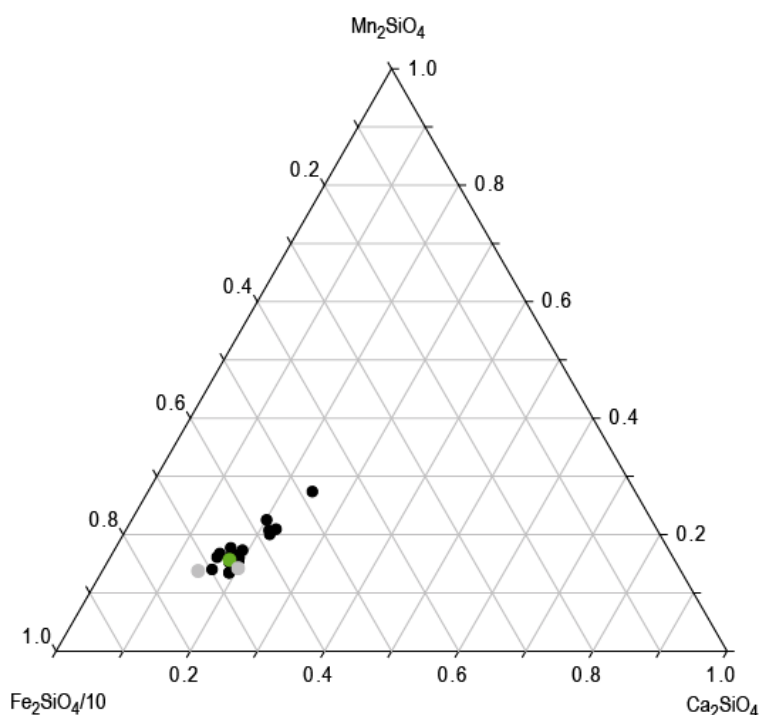


**Fig. 51 Ternary diagram of  $Fe_2SiO_4 \cdot 10^{-1}$ ,  $Ca_2SiO_4$  and  $Mn_2SiO_4$  in Kenna olivine (18 grains). The green circle represents the average composition. Grey circles represent data from BERKLEY et al. (1980) and SINGLETARY and GROVE (2003).**

The composition of orthopyroxene (9 grains) is  $Wo_{9.0-9.5}$  (mean  $Wo_{9.2}$ ),  $Fs_{16.4-17.5}$  (mean  $Fs_{17.0}$ ) and  $En_{70.1-73.2}$  (mean  $En_{71.3}$ ) with 0.04 – 0.12 wt%  $TiO_2$  (mean 0.08 wt%), 1.10 – 1.22 wt%  $Cr_2O_3$  (mean 1.14 wt%) and 0.36 – 0.45 wt% MnO (mean 0.41 wt%) (Fig. 52). LA-ICP-MS measurements (Fig. 53) give 23.8 – 29.9  $\mu g \cdot g^{-1}$  (mean 27.3  $\mu g \cdot g^{-1}$ ) NiO and 23.3 – 24.4 CoO (mean 24.0  $\mu g \cdot g^{-1}$ ).

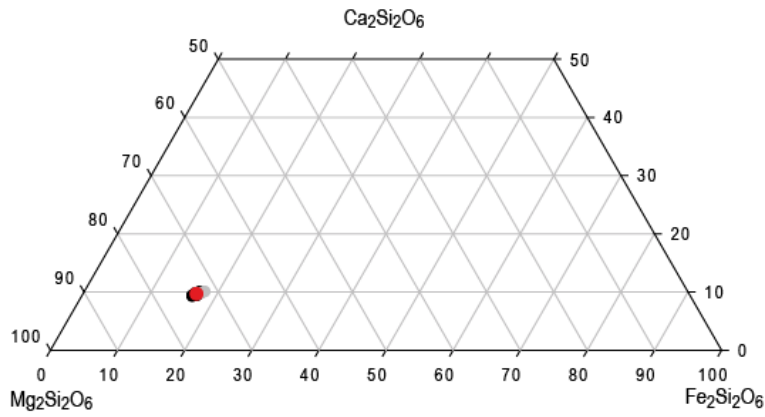


**Fig. 52** Composition of pyroxenes in Kenna. Circles represent the composition of orthopyroxenes (9 grains), with the red circle giving the average composition. Grey circles represent data taken from BERKLEY et al. (1980) and SINGLETARY and GROVE (2003).

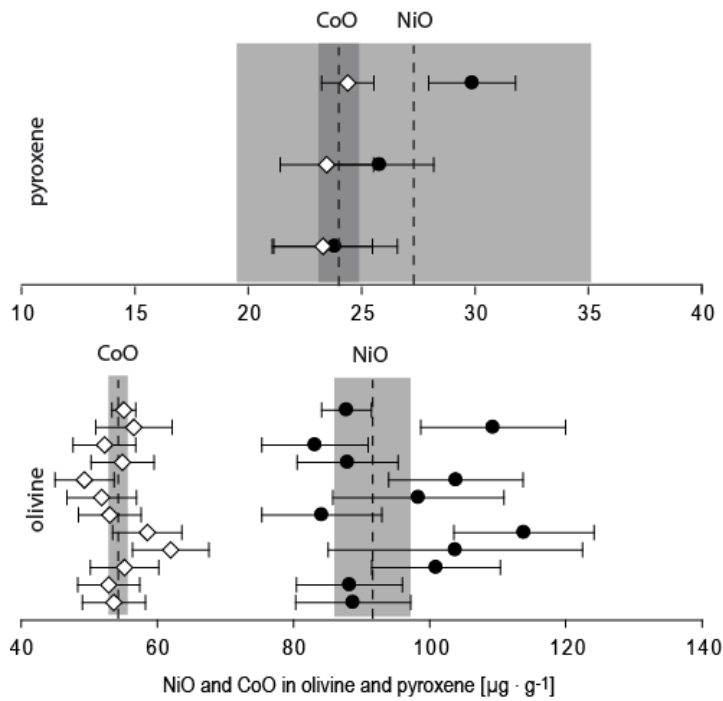


**Fig. 53** NiO and CoO concentrations in olivine and pyroxene in Kenna. Diamonds give the concentrations of CoO and Circles give the concentration of NiO. Shaded areas give the weighted average of the measurements.

**Table 24 Composition of olivine and pyroxenes in Kenna. Data obtained with EMPA, except for NiO and CoO, which was obtained with LA-ICP-MS. Number of grains analyzed is given in parenthesis. Values marked with '<' are below detection limit.**

	Olivine (11)		Orthopyroxene (9)	
	wt%	2 $\sigma$	wt%	2 $\sigma$
SiO <sub>2</sub>	38.90	0.22	55.51	0.24
Na <sub>2</sub> O	<0.02		0.06	0.01
TiO <sub>2</sub>	<0.02		0.08	0.01
FeO	18.73	0.42	11.43	0.06
Al <sub>2</sub> O <sub>3</sub>	0.04	0.01	0.66	0.01
MgO	41.19	0.54	26.97	0.18
CaO	0.41	0.02	4.85	0.03
Cr <sub>2</sub> O <sub>3</sub>	0.72	0.03	1.14	0.01
MnO	0.43	0.02	0.41	0.01
	Olivine (12)		Orthopyroxene (3)	
	$\mu\text{g}\cdot\text{g}^{-1}$	2 $\sigma$	$\mu\text{g}\cdot\text{g}^{-1}$	2 $\sigma$
NiO	91.6	5.6	27.3	7.8
CoO	54.2	1.4	24.0	0.9
number of oxygen ions	4		6	
Si	0.994		1.970	
Na	0.000		0.004	
Ti	0.000		0.002	
Fe	0.400		0.339	
Al	0.001		0.028	
Mg	1.568		1.427	
Ca	0.011		0.185	
Cr	0.015		0.032	
Mn	0.009		0.012	
T	0.994		1.970	
M	2.005		2.029	
Total	2.999		4.000	
<i>fa</i>	20.0			
En			71.3	
Wo			9.2	
Fs			17.0	

Due to severe weathering of the sample, only 1 grain of vein metal and 4 grains of metal inclusions in silicate grains could be measured in Kenna.

The vein metal grain contains 4.75 wt% Ni, 0.38 wt% Co, 0.50 wt% Cr and 0.95 wt% Si. The composition of metal inclusions is variable. Ranging from Ni-poor metal from reduction with 0.68 wt% Ni, 0.10 wt% Co and 0.08 wt% Si to Ni-rich metal similar to vein metal with 4.42 wt% Ni, 0.38 wt% Co and 0.752 wt% Si.

### 8.1.9 LEW85440

In LEW85440, 27 grains of olivine, 40 grains of orthopyroxene and 1 grain of augite were analyzed with EPMA. Seven grains of olivine and 4 grains of orthopyroxene were analyzed with LA-ICP-MS (Table 25).

Olivine composition is  $fa_{8.0-9.0}$  (mean  $fa_{8.6}$ ) with 0.27 – 0.33 wt% CaO (mean 0.30 wt%), 0.39 – 0.58 wt%  $Cr_2O_3$  (mean 0.49 wt%) and 0.40 – 0.55 wt% MnO (mean 0.46 wt%). LA-ICP-MS measurements (Fig. 56) give 28.1 – 50.6  $\mu g \cdot g^{-1}$  NiO (mean 36.1  $\mu g \cdot g^{-1}$ ) and 12.2 – 17.3  $\mu g \cdot g^{-1}$  CoO (mean 15.2  $\mu g \cdot g^{-1}$ ). Only grains with FeO > 6 wt% (19 of 27), have been included into the calculation of mean values, as smaller FeO-concentrations probably represent reduced grains (Fig. 54)

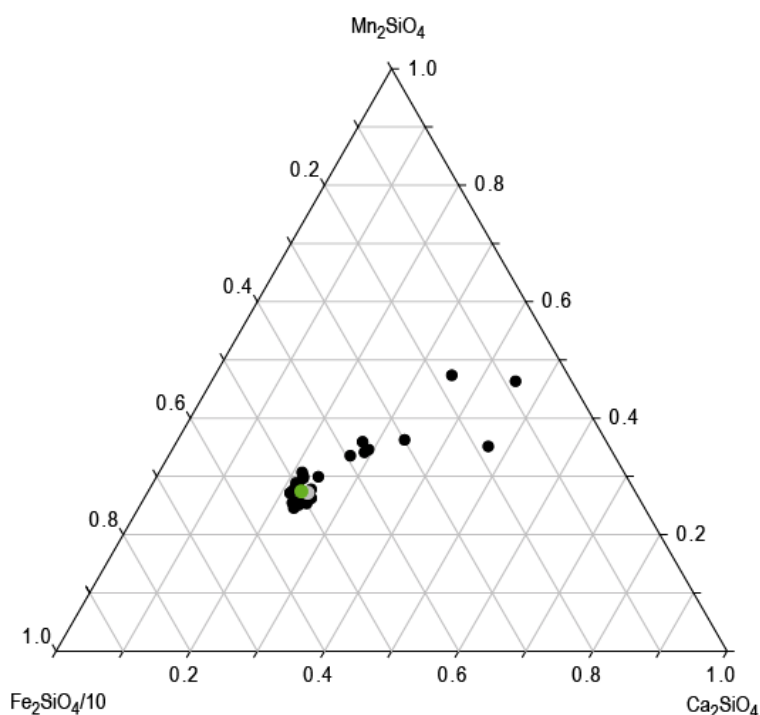


Fig. 54 Ternary diagram of  $Fe_2SiO_4 \cdot 10^{-1}$ ,  $Ca_2SiO_4$  and  $Mn_2SiO_4$  in LEW85440 olivine (27 grains). The green circle represents the average composition. The grey circle represents data from TAKEDA (1989).

Orthopyroxene composition is  $Wo_{4.6-5.7}$  (mean  $Wo_{4.8}$ ),  $Fs_{6.6-7.8}$  (mean  $Fs_{7.3}$ ) and  $En_{86.9-88.2}$  (mean  $En_{87.6}$ ) with 0.09 – 0.21 wt%  $TiO_2$  (mean 0.13 wt%), 0.72 – 1.00 wt%  $Cr_2O_3$  (mean 0.81 wt%) and 0.33 – 0.51 wt% MnO (mean 0.44 wt%). Augite composition is  $Wo_{33.4}$ ,  $Fs_{4.9}$  and  $En_{60.5}$  with 0.28 wt%  $TiO_2$ , 0.87 wt%  $Cr_2O_3$  and 0.36 wt% MnO. LA-ICP-MS measurements

(Fig. 56) in orthopyroxene give  $9.5 - 12.1 \mu\text{g}\cdot\text{g}^{-1}$  (mean  $10.6 \mu\text{g}\cdot\text{g}^{-1}$ ) NiO and  $6.8 - 7.0 \mu\text{g}\cdot\text{g}^{-1}$  CoO (mean  $6.9 \mu\text{g}\cdot\text{g}^{-1}$ ).

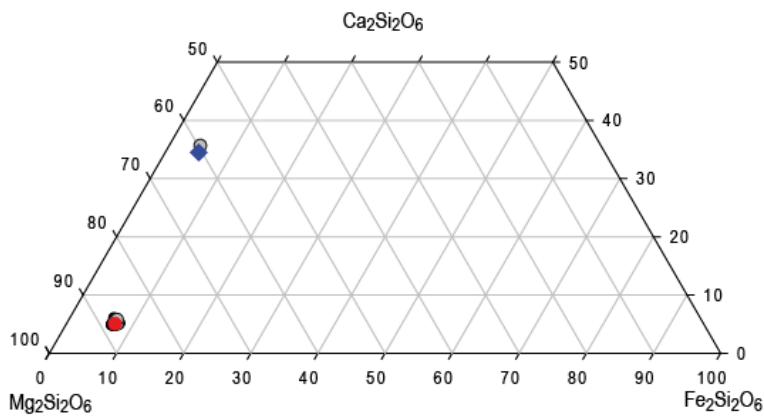


Fig. 55 Composition of pyroxenes in LEW85440. Circles represent the composition of orthopyroxenes (40), with the red circle giving the average orthopyroxene composition. The blue diamond gives the composition of augite. Grey circles represent orthopyroxene and augite data from TAKEDA (1989).

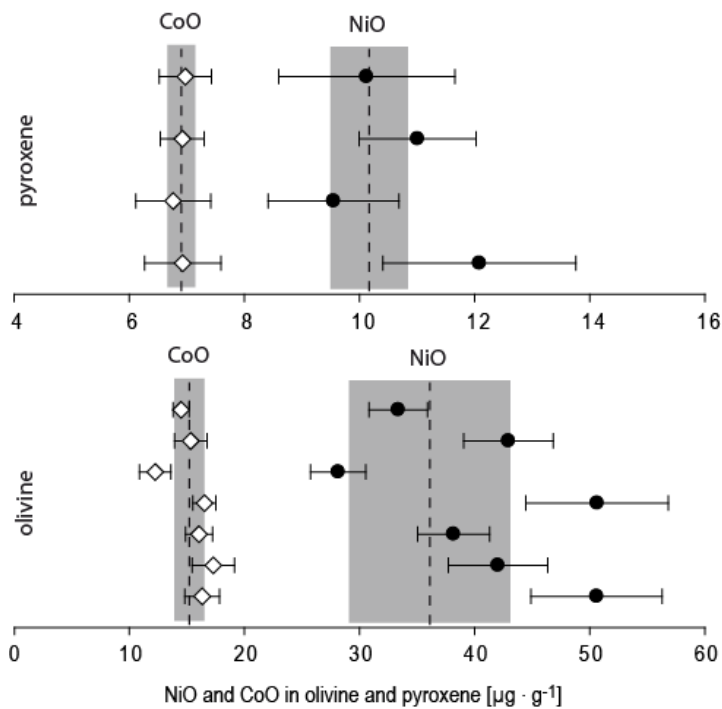


Fig. 56 NiO and CoO concentrations in olivine and pyroxene in LEW85440. Diamonds give the concentrations of CoO and Circles give the concentration of NiO. Shaded areas give the weighted average of the measurements.

**Table 25 Composition of olivine and pyroxenes in LEW85440. Data obtained with EMPA, except for NiO and CoO, which was obtained with LA-ICP-MS. Number of grains analyzed is given in parenthesis. Values marked with '<' are below detection limit.**

	Olivine (19)		Orthopyroxene (40)		Augite (1)	
	wt%	2 $\sigma$	wt%	2 $\sigma$	wt%	2 $\sigma$
SiO <sub>2</sub>	40.60	0.24	57.06	0.21	54.62	0.20
Na <sub>2</sub> O	<0.02		0.04	0.01	0.18	0.05
TiO <sub>2</sub>	0.03	0.01	0.13	0.01	0.28	0.02
FeO	8.40	0.13	5.05	0.06	3.28	0.04
Al <sub>2</sub> O <sub>3</sub>	0.05	0.01	0.78	0.03	1.23	0.05
MgO	50.02	0.38	33.38	0.16	22.00	0.11
CaO	0.30	0.01	2.60	0.03	17.42	0.21
Cr <sub>2</sub> O <sub>3</sub>	0.49	0.02	0.81	0.02	0.87	0.02
MnO	0.46	0.02	0.44	0.01	0.36	0.01
	Olivine (7)		Orthopyroxene (4)			
	$\mu\text{g}\cdot\text{g}^{-1}$	2 $\sigma$	$\mu\text{g}\cdot\text{g}^{-1}$	2 $\sigma$		
NiO	36.1	7	10.6	1.6		
CoO	15.2	1.3	6.9	0.24		
Number of oxygen ions	4		6		6	
Si	0.989		1.970		1.956	
Na	0.000		0.003		0.012	
Ti	0.001		0.003		0.007	
Fe	0.171		0.146		0.098	
Al	0.001		0.032		0.052	
Mg	1.816		1.717		1.174	
Ca	0.008		0.096		0.669	
Cr	0.009		0.022		0.024	
Mn	0.009		0.013		0.011	
T	0.989		1.970		1.956	
M	2.016		2.032		2.048	
Total	3.005		4.001		4.004	
<i>fa</i>	8.6					
En			87.6		60.5	
Wo			4.8		33.4	
Fs			7.3		4.9	

In LEW85440, 19 grains of vein metal, 2 grains of Cr-rich troilite vein and 2 grains of Cr-poor troilite vein were measured. Additionally 1 metal + troilite spherule inclusion and 23 metal and troilite inclusions in silicate grains were analyzed ().

The vein metal contains 3.35 – 4.94 wt% Ni (mean 3.98 wt%), 0.24 - 0.37 wt% Co (mean 0.29 wt%) and 0.05 – 0.41 wt% Cr (mean 0.22 wt%). Of 19 vein metal grains, 15 contain <0.1 wt% Si, 3 grains contain 0.84 – 1.11 wt% Si and 1 grains contains 4.97 wt% Si. Cr-rich troilite vein material contains <0.02 wt% Ni, <0.02 wt% Co, 5.41 wt% Cr and 0.24 wt% Mn. Cr-poor troilite vein contains 0.05 wt% Ni, <0.02 wt% Co, 1.52 wt% Cr and 0.05 wt% Mn.

The metal in the metal + troilite spherule inclusion contains 8.41 wt% Ni, 0.41 wt% Co, 0.07 wt% Cr and 0.03 wt% Si, while the troilite contains <0.02 Ni, <0.02 Co, 0.34 wt% Cr and 0.04 wt% Mn.

Metal inclusions in silicate grains are similar to vein metal, except for a wider spread in Co and Ni concentrations (0.65 – 4.25 wt% Ni, <0.02 – 0.28 wt% Co). Ni- and Co-poor inclusions probably represent metal formed by silicate reduction. Troilite inclusions in silicate grains contain <0.02 – 0.15 wt% Ni (mean 0.05), <0.02 wt% Co, 1.53 – 2.89 wt% Cr (mean 2.35) and 0.03 – 0.36 wt% Mn (mean 0.13).

**Table 26 Composition of vein metal, vein troilite and metal inclusions in LEW85440. Data obtained with EPMA. Values marked with '<' are below detection limit. For Si in vein metal, 1 measurement with >4 wt% Si was excluded. Elements with high variability are given as range**

	Vein metal (19)		Cr-rich vein troilite (2)		Cr-poor vein troilite(2)			
	wt%	2 $\sigma$	wt%	2 $\sigma$	wt%	2 $\sigma$		
P	0.14	0.03	<0.02		<0.02			
Si	0.19	0.16	0.02	0.01	0.24	0.41		
Cr	0.22	0.05	5.41	0.50	1.52	0.88		
Fe	94.52	0.73	55.56	0.02	59.82	2.70		
Co	0.29	0.02	<0.02		<0.02			
S	0.01	0.00	37.19	0.51	36.36	0.33		
Ni	3.98	0.19	<0.02		0.05	0.05		
Mn	<0.02		0.24	0.09	0.05	0.05		
	Spherule inclusion				Inclusion in silicate grains			
	metal (1)		troilite (1)		troilite (7)		metal (16)	
	wt%	2 $\sigma$	wt%	2 $\sigma$	wt%	2 $\sigma$	wt%	2 $\sigma$
P	0.14	0.03	<0.02		<0.02		0.12	0.03
Si	0.03	0.03	0.05	0.02	0.25	0.17	0.19	0.13
Cr	0.07	0.02	0.34	0.03	2.35	0.37	0.12	0.03
Fe	90.05	0.69	63.54	0.02	58.91	0.72	96.75	0.82
Co	0.41	0.02	<0.02	0.02	<0.02		0.11	0.04
S	0.03	0.02	36.60	0.50	36.57	0.25	<0.02	
Ni	8.41	0.40	<0.02		0.05	0.04	0.65 – 4.25	
Mn	<0.02		0.04	0.01	0.13	0.08	0.03	0.01

## 8.2 Ni and Co in ureilite silicates

Ni- and Co- concentrations in olivine are positively correlated with molar Fe/(Fe+Mg) (Fig. 57). Ni concentrations range from 15.2  $\mu\text{g}\cdot\text{g}^{-1}$  in ALH84136 to 82.5  $\mu\text{g}\cdot\text{g}^{-1}$  in DaG340 (Table 27). EET96331 olivine contains less Ni and Co than the trend would suggest.

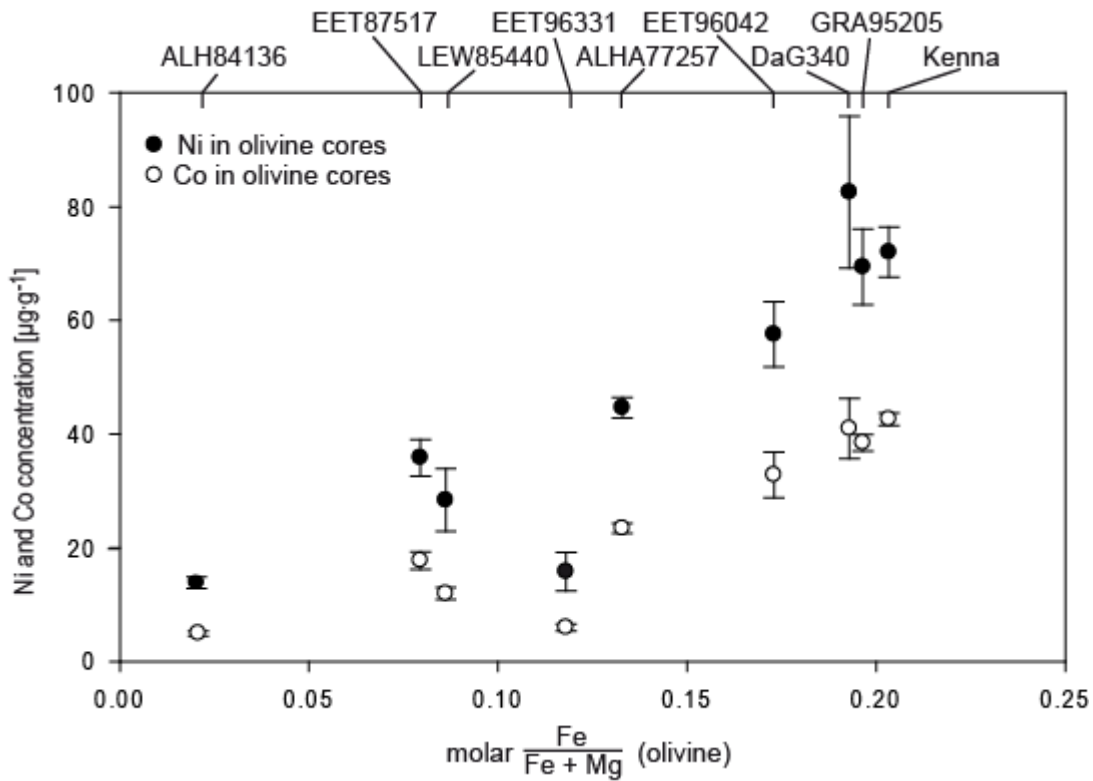


Fig. 57 Ni- and Co-concentrations in ureilite olivine cores. Ni and Co concentrations are positively correlated with molar Fe/(Fe+Mg). EET96331 gives lower values than the trend would suggest, while EET87517 appears to be slightly enriched.

EET87517 is slightly enriched in Ni and Co. As only 1 olivine grain of EET87517 was analyzed for Ni and Co, the enrichment might not be genuine, however, the orthopyroxene data shows a similar enrichment.

Ni- and Co-concentrations in orthopyroxenes give a similar positive correlation with molar Fe/(Fe+Mg) as in olivine (Fig. 58). Like in olivine, EET96331 gives lower Ni- and Co-concentrations than the trend would suggest, while EET87517 is slightly enriched. Ni-concentrations in ALH84136 are much higher than the trend defined by Ni-concentrations of orthopyroxenes of the other ureilites would suggest.

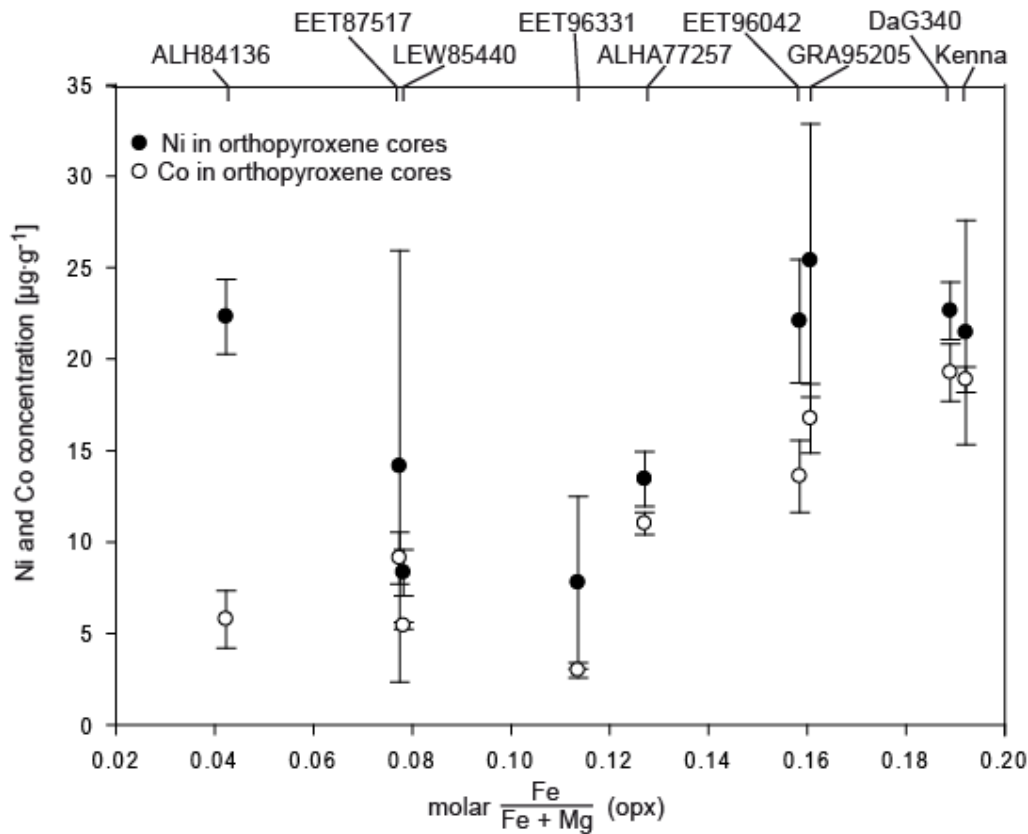


Fig. 58 Ni- and Co-concentrations in ureilite orthopyroxene cores. Ni and Co concentrations are positively correlated with molar  $\text{Fe}/(\text{Fe}+\text{Mg})$ . EET96331 gives lower values than the trend would suggest, while EET87517 appears to be slightly enriched and ALH84136 shows high Ni-concentrations.

The plot of molar Co/Fe in olivine vs. molar Co/Fe in orthopyroxene shows a very good linear correlation (Fig. 59). The data of ALH84136 do not lie on the trend, which might indicate a bias in Ni-measurements in orthopyroxene. EET96331 gives slightly lower ratios than other ureilites. The plot of molar Ni/Fe in olivine vs. molar Ni/Fe in orthopyroxene (Fig. 60) gives a result similar to Co. Most ureilites plot on a single regression line, with ALH84136 being off the trend and EET96331 showing lower ratios than the other ureilites.

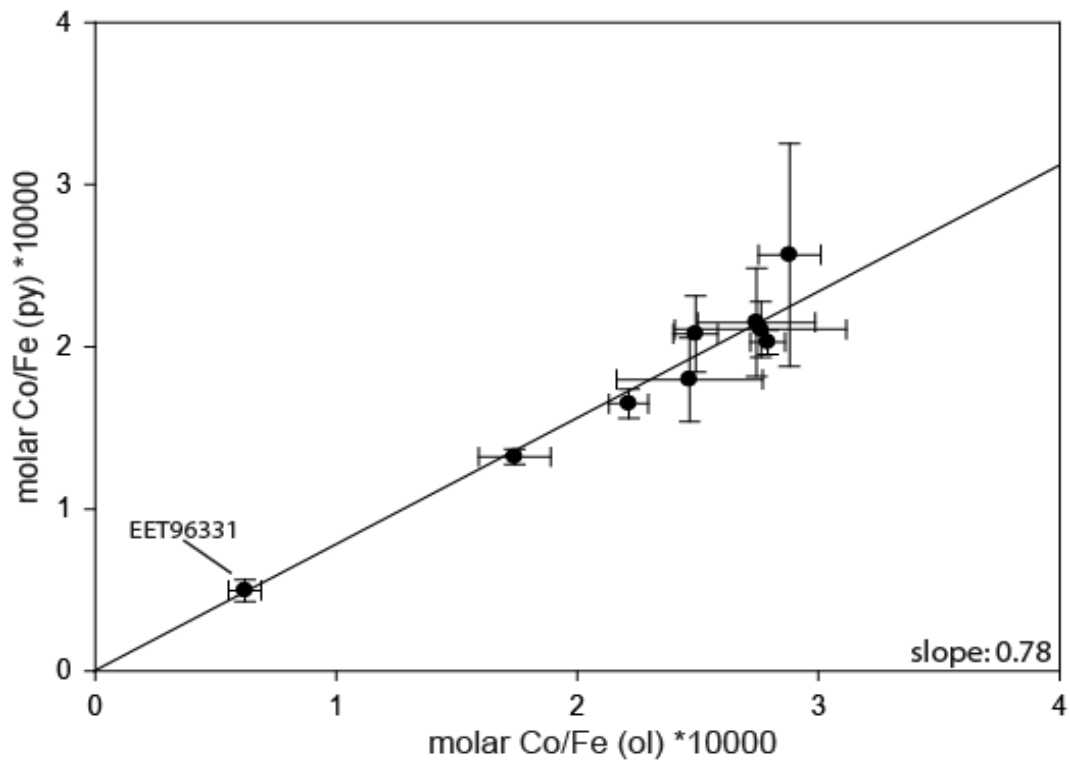


Fig. 59 Molar ratios of Co/Fe in olivine and pyroxenes. Most ureilites define a clear trend with a slope of  $\sim 0.78$ . EET96331 shows significantly lower ratios.

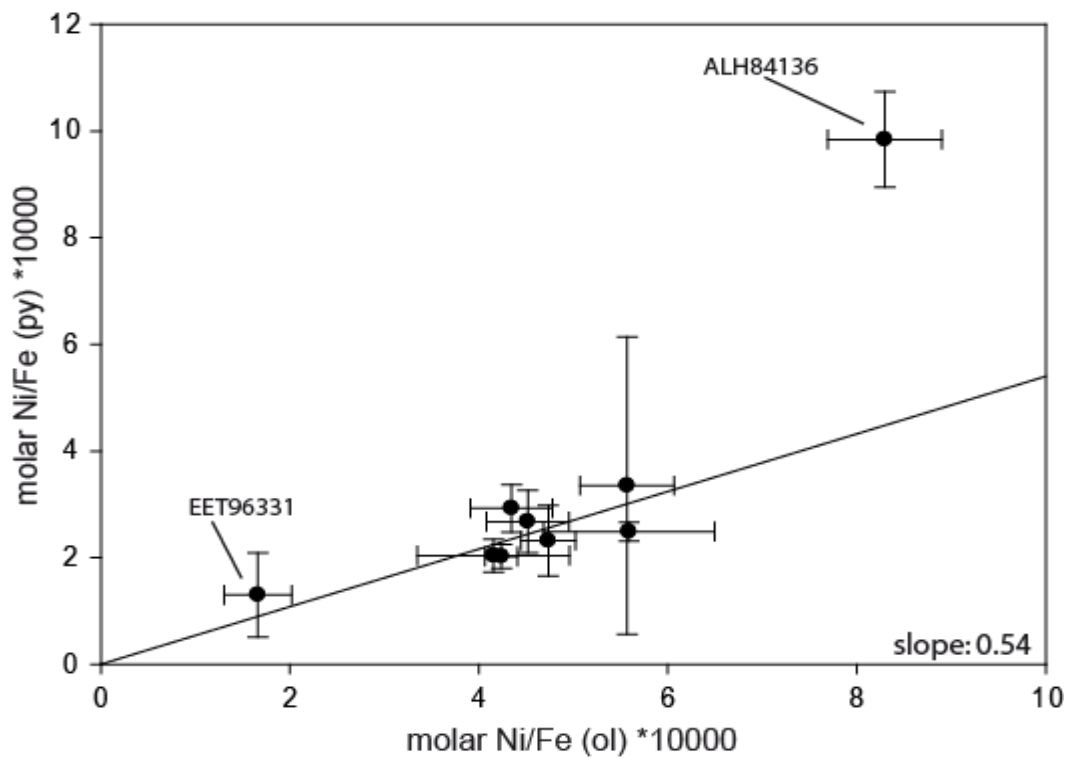


Fig. 60 Molar ratios of Ni/Fe in olivine and pyroxenes. EET96331 gives significantly lower values in Ni than the other ureilites and ALH84136 gives much higher ratios and is off the general trend.

**Table 27: Ni and Co in olivine and orthopyroxene cores obtained with LA-ICP-MS. Number of analyses shown in parenthesis. Errors are given as 2 $\sigma$  standard deviations.**

		Olivine									
		ALH84136 (3)		ALHA77257 (9)		DaG340 (5)		EET87517 (1)			
		$\mu\text{g}\cdot\text{g}^{-1}$	$2\sigma$	$\mu\text{g}\cdot\text{g}^{-1}$	$2\sigma$	$\mu\text{g}\cdot\text{g}^{-1}$	$2\sigma$	$\mu\text{g}\cdot\text{g}^{-1}$	$2\sigma$		
Ni		17.9	1.3	44.6	1.8	82.5	13.4	35.9	3.2		
Co		6.2	0.3	23.4	0.9	41.0	5.3	17.7	1.6		
		EET96042 (5)		EET96331 (5)		GRA95205 (10)		Kenna (12)		LEW85440 (7)	
		$\mu\text{g}\cdot\text{g}^{-1}$	$2\sigma$								
Ni		57.5	5.7	15.8	3.4	69.4	6.7	72.0	4.4	28.4	5.5
Co		32.8	4.0	6.0	0.6	38.5	1.4	42.6	1.1	12.0	1.0
		Orthopyroxene									
		ALH84136 (2)		ALHA77257 (5)		DaG340 (2)		EET87517 (4)			
		$\mu\text{g}\cdot\text{g}^{-1}$	$2\sigma$	$\mu\text{g}\cdot\text{g}^{-1}$	$2\sigma$	$\mu\text{g}\cdot\text{g}^{-1}$	$2\sigma$	$\mu\text{g}\cdot\text{g}^{-1}$	$2\sigma$		
Ni		25.5	2.6	13.4	1.5	22.6	1.6	14.1	11.8		
Co		7.5	2.0	11.0	0.6	19.3	1.6	9.1	1.4		
		EET96042 (3)		EET96331 (5)		GRA95205 (5)		Kenna (3)		LEW85440 (4)	
		$\mu\text{g}\cdot\text{g}^{-1}$	$2\sigma$								
Ni		22.0	8.6	7.8	4.7	25.4	7.5	21.5	6.1	8.3	1.3
Co		13.7	2.0	3.0	0.4	16.8	1.9	18.9	0.7	5.4	0.2

### 8.3 Ni and Co in vein metal

With respect to Ni- and Co-concentrations, ureilite vein metal is very homogeneous, except for EET87517 (Table 28). Ni concentrations range from 3.63 wt% in GRA95205 to 4.89 wt% in EET96042 and Co ranges from 0.24 wt% in DaG340 to 0.38 wt% in Kenna (Fig. 61). In EET87517, two types a vein metal are distinguished, a Si-rich vein metal with ~5.45 wt% Ni and 0.45 wt% Co and a Si-poor vein metal with 3.88 wt% Ni and 0.27 wt% Co.

Ni- and Co-concentrations in ureilite vein metal show no correlation with olivine *fa* of their respective ureilite (Fig. 67, Fig. 68, Fig. 69).

**Table 28 Ni and Co in ureilite vein metal. Data obtained by EPMA. Errors are given as 2 $\sigma$  of SD. Number of analyzes is given in parenthesis. For EET87517 2 types of vein metal are distinguished. EET87517 II represents the high-Si vein metal and EET87517 I represents the low-Si vein metal.**

Ureilite	Ni		Co		Ni/Co	
	[wt%]	2 $\sigma$	[wt%]	2 $\sigma$	-ratio	2 $\sigma$
ALH84136 (44)	4.15	0.06	0.29	0.01	14.31	0.54
ALHA77257 (43)	3.86	0.04	0.27	0.01	14.30	0.55
DaG340 (1)	3.79	0.19	0.24	0.01	15.79	1.03
EET87517 II (15)	5.45	0.10	0.45	0.03	12.11	0.84
EET87517 I (6)	3.88	0.12	0.27	0.04	14.37	2.17
EET96042 (12)	4.89	0.23	0.30	0.03	16.30	1.80
EET96331 (7)	4.78	0.29	0.30	0.05	15.93	2.83
GRA95205 (44)	3.63	0.17	0.26	0.01	13.96	0.85
Kenna (1)	4.75	0.24	0.38	0.02	12.50	0.91
LEW85440 (19)	3.98	0.19	0.29	0.02	13.72	1.15
weighted average	4.10	0.50	0.28	0.03	14.00	0.80

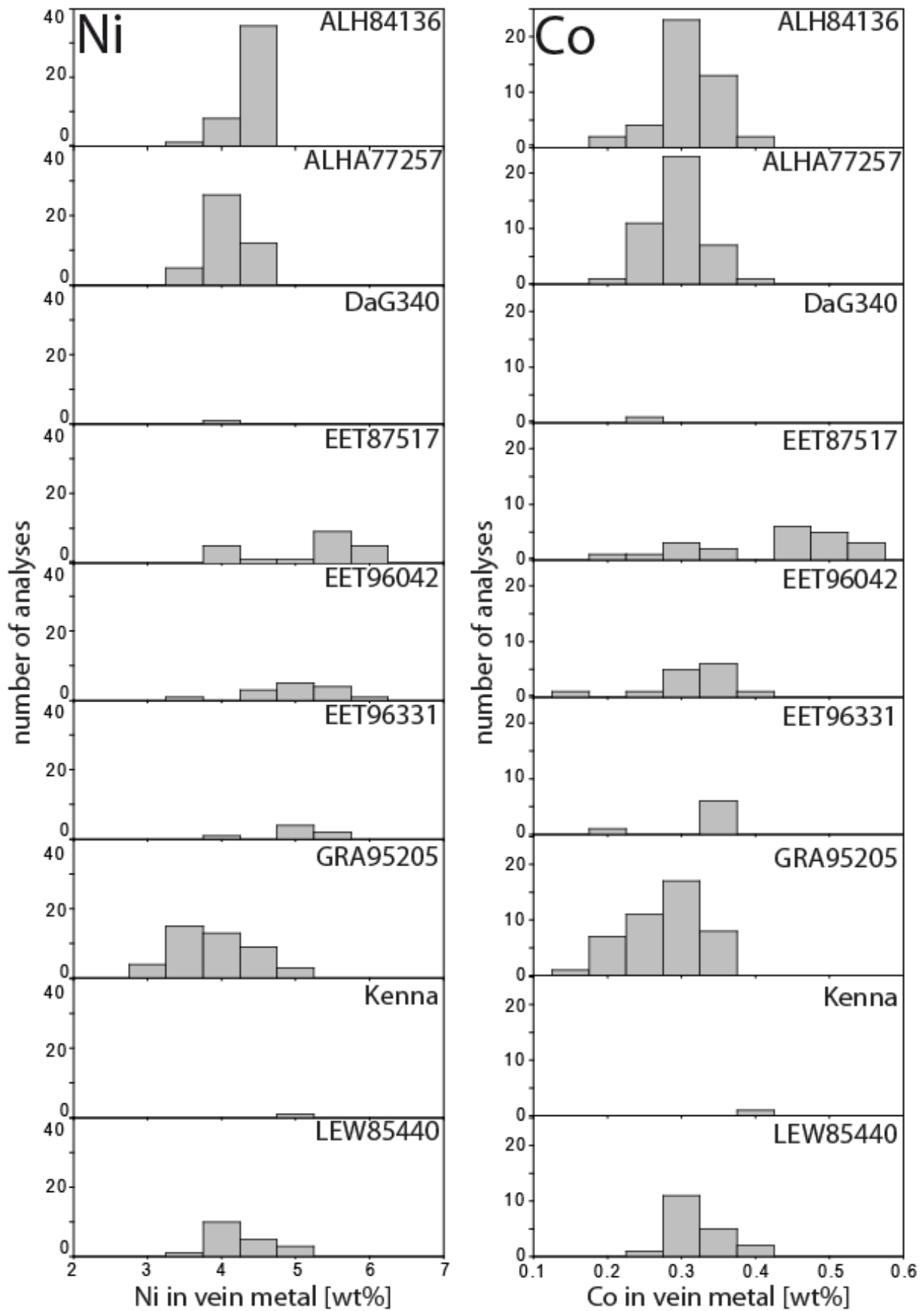


Fig. 61 Histograms of Ni- and Co-concentrations in ureilite vein metal.

## 8.4 Ni-isotope data

Ni-isotopes were measured in ALHA77257, Kenna, EET87517 and EET96042 by Dr. Ghylaine Quitté with MC-ICP-MS. From each ureilite, a silicate-rich- (handpicked clear silicate grains), a metal-rich- (separated via strong hand magnet) and a bulk fraction were analyzed (Table 29, Fig. 62). Fe and Ni-concentrations in each fraction have been determined by Dr. Ghylaine Quitté.

**Table 29** Fe, Ni, Fe/Ni and  $\epsilon^{60}\text{Ni}^*$  measured in Kenna, EET87517, ALHA77257 and EET96042

Ureilite	fraction	Fe [wt%]	Ni [wt%]	Fe/Ni-ratio	$2\sigma$	$\epsilon^{60}\text{Ni}^*$	$2\sigma$
Kenna	bulk	11.17	0.0193	86.4	1.8	0.08	0.12
Kenna	silicate-rich	12.90	0.2045	668	276	-0.77	0.31
Kenna	metal-rich	9.74	0.1293	47.6	3.0	0.11	0.16
EET87517	bulk	6.99	0.0758	45.6	0.7	-0.05	0.12
EET87517	silicate-rich	5.17	0.2702	68.2	1.9	-0.12	0.21
EET87517	metal-rich	8.38	0.1533	31.0	1.2	0.05	0.10
ALHA77257	bulk	10.99	0.0112	105.4	5.0	0.00	0.10
ALHA77257	silicate-rich	9.27	0.2172	827	139	-0.39	0.23
ALHA77257	metal-rich	12.87	0.1043	59.2	3.0	0.00	0.10
EET96042	bulk	11.62	0.0299	68.2	5.9	0.00	0.15
EET96042	silicate-rich	11.07	0.3216	370	106	-0.54	0.18
EET96042	metal-rich	12.82	0.1705	39.9	2.3	-0.05	0.13

For all four ureilites,  $\epsilon^{60}\text{Ni}^*$  of the bulk- and metal-rich component is 0 within analytical uncertainty.

In Kenna, the bulk fraction gives a Fe/Ni-ratio of  $86.4 \pm 1.8$  and  $\epsilon^{60}\text{Ni}^*$  of  $0.08 \pm 0.12$   $\epsilon$ -units, the metal-rich fraction gives a Fe/Ni-ratio of  $47.6 \pm 3.0$  and  $\epsilon^{60}\text{Ni}^*$  of  $0.11 \pm 0.16$   $\epsilon$ -units and the silicate-rich fraction gives a Fe/Ni-ratio of  $668 \pm 276$  and  $\epsilon^{60}\text{Ni}^*$  of  $-0.77 \pm 0.31$   $\epsilon$ -units. In EET87517, the bulk fraction gives a Fe/Ni-ratio of  $45.6 \pm 0.7$  and  $\epsilon^{60}\text{Ni}^*$  of  $-0.05 \pm 0.12$   $\epsilon$ -units, the metal-rich fraction gives a Fe/Ni-ratio of  $31.0 \pm 1.2$  and  $\epsilon^{60}\text{Ni}^*$  of  $0.05 \pm 0.10$   $\epsilon$ -units and the silicate-rich fraction gives a Fe/Ni-ratio of  $68.2 \pm 1.9$  and  $\epsilon^{60}\text{Ni}^*$  of  $-0.12 \pm 0.21$   $\epsilon$ -units. In ALHA77257, the bulk fraction gives a Fe/Ni-ratio of  $105.4 \pm 5.0$  and  $\epsilon^{60}\text{Ni}^*$  of  $0.00 \pm 0.10$   $\epsilon$ -units, the metal-rich fraction gives a Fe/Ni-ratio of  $59.2 \pm 3.0$  and  $\epsilon^{60}\text{Ni}^*$  of  $0.00 \pm 0.10$   $\epsilon$ -units and the silicate-rich fraction gives a Fe/Ni-ratio of  $827 \pm 139$  and  $\epsilon^{60}\text{Ni}^*$  of  $-0.39 \pm 0.23$   $\epsilon$ -units. In EET96042, the bulk fraction gives a Fe/Ni-ratio of  $68.2 \pm 5.9$  and

$\epsilon^{60}\text{Ni}^*$  of  $0.00 \pm 0.15$   $\epsilon$ -units, the metal-rich fraction gives a Fe/Ni-ratio of  $39.9 \pm 2.3$  and  $\epsilon^{60}\text{Ni}^*$  of  $-0.05 \pm 0.13$   $\epsilon$ -units and the silicate-rich fraction gives a Fe/Ni-ratio of  $370 \pm 106$  and  $\epsilon^{60}\text{Ni}^*$  of  $-0.05 \pm 0.13$   $\epsilon$ -units.

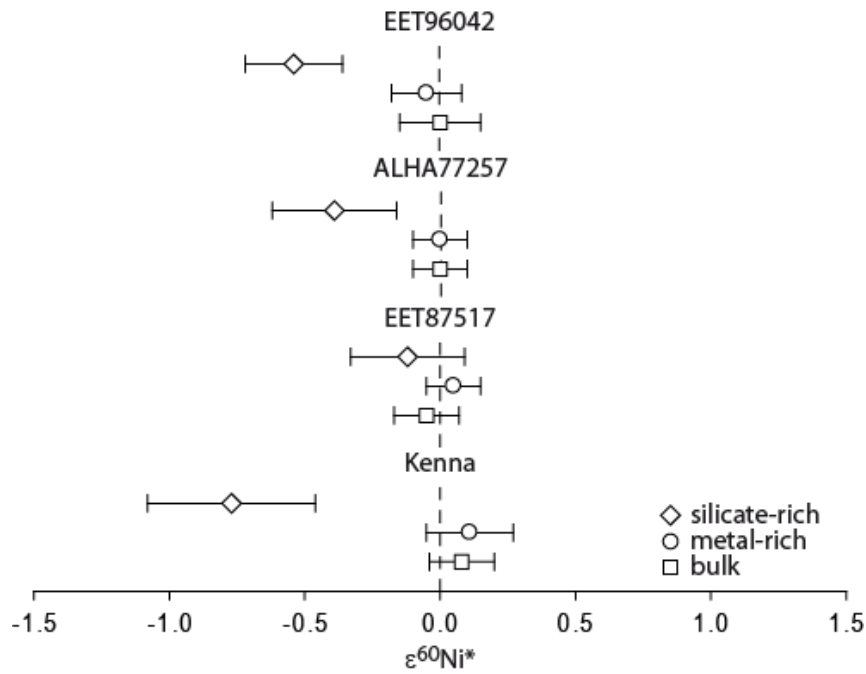


Fig. 62  $\epsilon^{60}\text{Ni}^*$  in silicate-rich, metal-rich and bulk fraction of EET96042, ALHA77257, EET87517 and Kenna. Metal-rich and bulk fraction are 0 within analytical uncertainty. Silicate-rich fraction is  $< 0$ , except for EET87517.

## 9 Discussion

### 9.1 Thermodynamic equilibrium between vein metal and ureilite olivine

#### 9.1.1 Calculation of Fe-Ni and Fe-Co-exchange equilibrium temperatures

To better understand the relation between vein metal and ureilite olivine, we first want to test the hypothesis that they are in thermodynamic equilibrium. If olivine and vein metal are in thermodynamic equilibrium, similar equilibration temperatures for Fe-Ni exchange and Fe-Co-exchange between solid metal and olivine would be expected. Equilibrium exchange temperatures for both Fe-Ni and Fe-Co exchange were calculated for solid metal/olivine-equilibration.

We used average vein metal compositions and average olivine core compositions for equilibrium calculations. The chemical composition of the vein metal with respect to Co and Ni is homogeneous within each ureilite (Fig. 61), except for EET87516 with 2 distinct vein metal types. The concentrations of Ni and Co in olivine cores are within analytical uncertainty homogeneous for each ureilite.

The Gibbs free energy of reaction  $\Delta G_{(Fe-Ni)}^0$  (see chapter 4.2) and activity models for  $Fe_2SiO_4$  (see chapter 4.4) and  $Co_2SiO_4$  (see chapter 4.5) have been taken from SEIFERT et al. (1988). The activity model for  $Ni_2SiO_4$  (see chapter 4.5) has been taken from HIRSCHMANN (2000). The activities of metallic Fe, Ni and Co have been taken from TOMISKA et al. (1979), RAMMENSEE and FRASER (1981) and FRASER and RAMMENSEE (1982) (see chapter 4.3).

The calculated equilibrium temperatures for the Fe-Ni-exchange reaction between olivine and solid metal range from  $886 \pm 66^\circ C$  in EET96331 to  $3013 \pm 606^\circ C$  in ALH84136 (Table 30, Fig. 63). The calculated equilibration temperatures for the Fe-Co-exchange reaction range from  $753 \pm 38^\circ C$  in EET87517 to  $1867 \pm 430^\circ C$  in DaG360.

Unfortunately, the used model does not permit calculation of  $K_D^{Ni(oliv)-Ni(met)}$  and  $K_D^{Co(oliv)-Co(met)}$  to a better precision than  $\pm 0.15$  resulting in large errors ( $38-606^\circ C$ ) for the calculated equilibration temperatures.

**Table 30** Calculated equilibration temperatures for Fe-Ni and Fe-Co exchange between ureilite olivine and vein metal. Errors are given as  $2\sigma$ . EET87517 (I) is the low-Si vein metal, EET87517 (II) the high-Si vein metal.

Ureilite	Fe-Ni-exchange		Fe-Co-exchange	
	$T_{\text{equilibration}}$ [°C]	$2\sigma$	$T_{\text{equilibration}}$ [°C]	$2\sigma$
ALH84136	3013	606	1720	321
ALHA77257	1706	182	1391	151
DaG340	2121	260	1867	430
EET87517 (I)	2018	256	1578	227
EET87517 (II)	1563	161	1134	91
EET96042	1516	143	1418	159
EET96331	886	66	753	38
GRA95205	1908	214	1619	239
Kenna	1841	198	1507	188
LEW85440	1605	168	1157	95

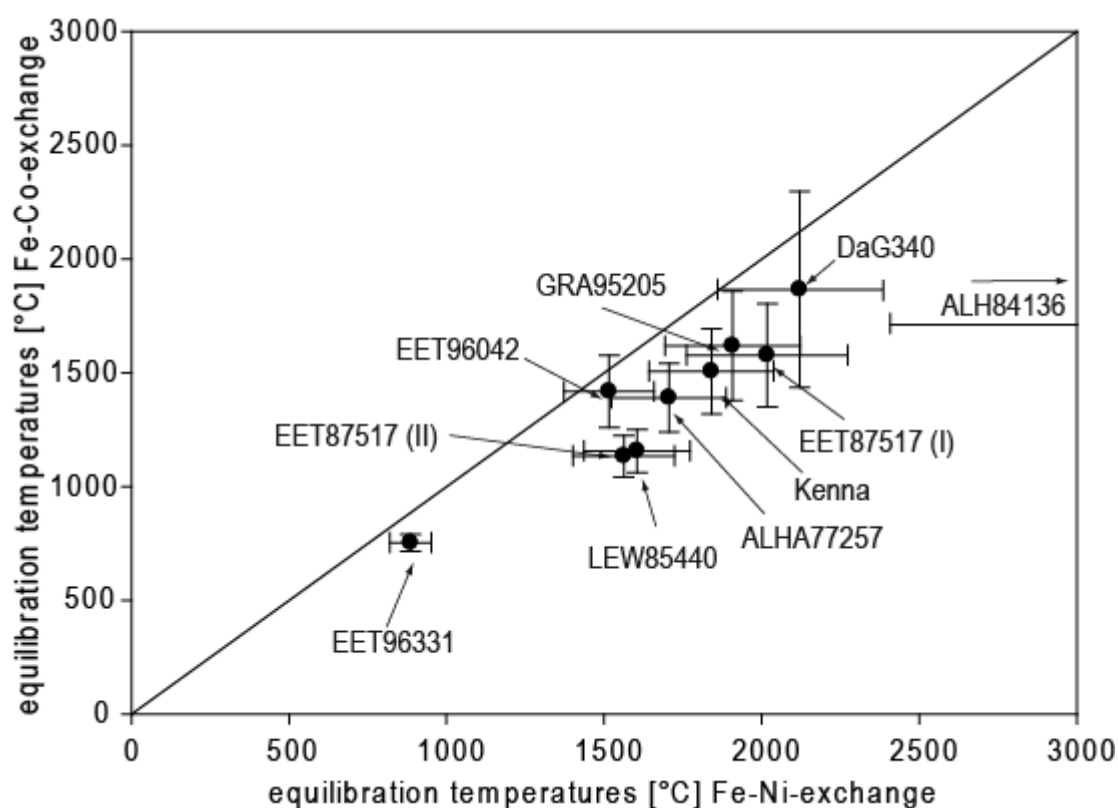


**Fig. 63** Calculated equilibration temperatures for the exchange of Fe-Ni and Fe-Co between ureilite vein metal and ureilite olivine for several ureilites. The equilibration temperature of ALH84136 is 3289°C and off the chart. EET87517 (I) represents low-Si vein metal whereas EET87517 (II) represents high-Si vein metal.

For the Ni-Fe-exchange, calculated equilibration temperatures of most ureilites are between 1500 and 2100°C. The Co-Fe-exchange equilibration temperatures of most ureilites are between 1100 and 1800°C. Two exceptions are ALH84136 and EET96331.

### 9.1.2 Equilibration temperatures for ALH84136

ALH84136 gives higher equilibration temperatures of  $3013 \pm 606$  °C. The high equilibration temperatures in ALH84136 are a result of a high Ni/Fe-ratio (Ni/Fe = 8.3, other ureilites Ni/Fe 4.2 – 5.6) in olivine (Fig. 60). In contrast to other ureilites, in ALH84136 the FeO-concentrations in measured olivine cores did not form a cluster (Fig. 30). The plot of molar Fe/(Fe+Mg) in olivine against molar Fe/(Fe+Mg) in orthopyroxene shows that most ureilites on a line with a slope of  $\sim 1$  line (Fig. 64). ALH84136 is off the trend, which might indicate that the measured olivines had no unreduced cores. FeO concentrations published in MASON and MARTINEZ (1986), give ranges of  $fa_0$  to  $fa_5$ . Olivine with  $fa_5$  plots exactly on the slope  $\sim 1$  line, which indicates that the  $fa$  of the unreduced olivine core is 5 rather than 2.1 (see chapter 8.1.1). We therefore conclude that ALH84136 is almost completely reduced and not suited for the calculation of equilibrium temperatures based on the Ni-Fe- or Co-Fe-exchange between olivine and metal.

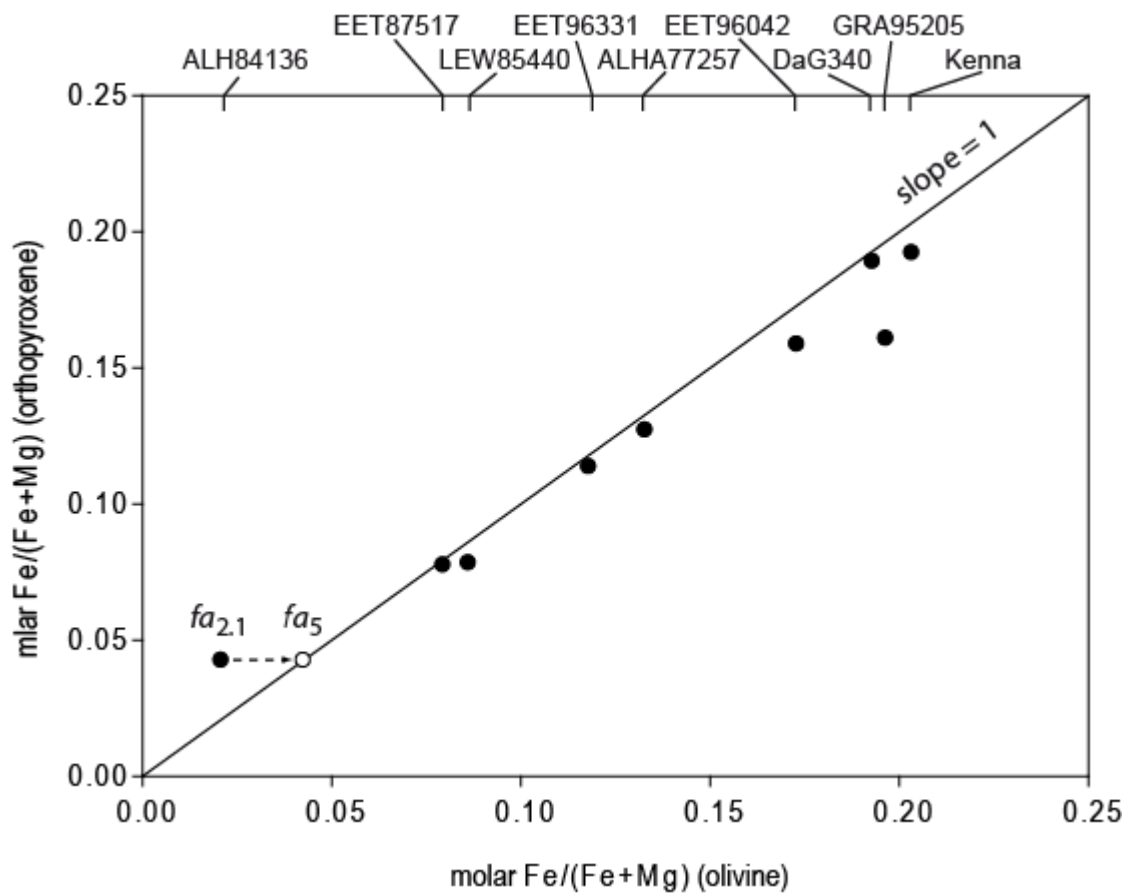


Fig. 64 Molar Fe/(Fe+Mg) of olivine against molar Fe/(Fe+Mg) of orthopyroxene in ureilites. Most ureilites plot on a slope  $\sim 1$  line. ALH8416 olivine with  $fa_{2.1}$  plots off the trend, while olivine with  $fa_5$  (as reported in MASON and MARTINEZ (1986), would plot on the trend.

### 9.1.3 Equilibration temperatures for EET96331

EET96331 gives low equilibrium temperatures of  $886 \pm 66$  °C for Ni-Fe-exchange and  $753 \pm 38$  °C for Co-Fe-exchange. This is a result of low Ni/Fe- and Co/Fe-ratios in EET96331 olivine (Ni/Fe = 1.66, other ureilites 4.2 – 5.6 and Co/Fe = 0.63, other ureilites 1.7 – 2.9). Olivine  $fa$  in EET96331 forms a cluster around  $fa_{11.8}$  (see chapter 8.1.6), which is consistent with data published in McCOY and McBRIDE (1998b) of  $fa_{12-13}$ . Molar Ni/Fe- and Co/Fe-ratios are similar in olivine and orthopyroxene (Fig. 59, Fig. 60). Six grains of vein metal have been analyzed in EET96331. The grains are very homogeneous in composition (4.8 – 5.1 wt% Ni, 0.31 – 0.34 wt% Co, 3.3 – 4.9 wt% Si). EET96331 olivine also has a low Ca/Mn-ratio of 0.61 (other ureilites ranging from 0.71 to 1.20), which also indicates lower temperatures. There is no indication that olivine or vein metal of EET96331 is not suited for equilibrium temperature calculations.

### 9.1.4 Is ureilite olivine and vein metal in equilibrium?

Calculations with MELTS (GHIORSO and SACK 1995, ASIMOW and GHIORSO 1998) suggest that the solidus phase in a CI1-chondritic parent body is olivine. Olivine crystallization starts between 1690°C and 1630°C depending on olivine  $fa$ . As the temperatures calculated for Fe-Ni and Fe-Co exchange in most ureilites (except for EET87517, EET96042 and EET96331) are above or close to the solidus temperature, they cannot represent actual equilibration temperatures.

For each ureilite sample the calculated equilibrium temperatures of Fe-Ni and Fe-Co exchange differ by 100°C (EET96042) to 448°C (LEW85440). In EET96042 and DaG340, equilibration temperatures overlap within uncertainties. If equilibrium had been attained, similar temperatures for both exchange reactions would be expected.

The calculated equilibration temperatures span a range of several hundred °C. While it is possible that each ureilite equilibrated at a different temperature, this is contradicted by px-px- and px-ol-thermometry, which yield similar temperatures of 1200-1300°C (TAKEDA 1987, SINHA et al. 1997, SINGLETARY and GROVE 2003) for each ureilite.

The calculated equilibration temperatures are too high, they are different for the Fe-Ni- and Fe-Co-exchange reaction and they are contradicted by px-px- and px-ol-thermometry data (TAKEDA 1987, SINHA et al. 1997, SINGLETARY and GROVE 2003). From that we conclude that vein metal is not in thermodynamic equilibrium with ureilite olivine.

Ureilites contain well equilibrated silicates (e.g. GOODRICH 1992), which equilibrated at 1200 – 1300°C. The question arises why no equilibrium was established between ureilite vein metal and olivine. One possibility is that the ureilite vein material was not present when the silicates equilibrated. The vein material could have intruded the silicate assemblage as melt from another part of the UPB or been injected from the impactor that disrupted the UPB. The other possibility is that the vein metal was present and equilibrium was established, but the composition of the vein metal changed at a later stage without reequilibration with the ureilite silicate.

In order to establish whether the vein material represents an altered primary metal component of the UPB or a material injected into the UPB, we modeled the composition of the primary metal component of an ureilite parent body of chondritic composition. In terms of asteroidal differentiation this metal component would correspond to the metal core of a parent body.

## **9.2 Relation between primary metal component of the ureilite parent body and the ureilite vein metal**

### **9.2.1 Initial bulk composition of the ureilite parent body**

Several starting compositions for the UPB are taken into consideration. GOODRICH et al. (2007) and KITA et al. (2004) prefer a CI1- or CM-chondritic precursor material due to the high amounts of C in ureilites. CLAYTON and MAYEDA (1996) suggested a more CV3-like parent body composition due to similarities in the oxygen isotopic composition of both meteorite groups. In this work, we use CI1-, CV3-, H-, L- and LL-chondritic starting compositions for our calculations.

In order to model the composition of the metal in each UPB, we assume that the ureilites represent restitic rocks that have lost a basaltic and a metal component. In terms of planetary differentiation, we consider ureilites to be depleted mantle rocks.

Another important simplification for our model is that we separately calculate the metal composition for each ureilite. The ureilites show a large variability of olivine FeO (e.g. MITTFELDT et al. 1998) and oxygen isotopic composition (e.g. CLAYTON and MAYEDA 1996), which normally suggests multiple parent bodies. A similar temperature history (e.g. TAKEDA 1987, SINHA et al. 1997) and the presence of clasts of multiple monomict ureilites in polymict ureilites (e.g. GOODRICH et al. 2004) suggest a single parent body. It has therefore been suggested that ureilites represent remnants of a single heterogeneous parent body (e.g. GOODRICH (1992), MITTFELDT et al. 1998). For our modeling, we assume that the ureilite parent body consists of domains of homogeneous compositions and our ureilite samples originate from different domains. These domains can either form layers, similar to an onion shell (e.g. WALKER and GROVE 1993) or are randomly mixed as proposed in SINGLETARY and GROVE (2006).

### **9.2.2 Calculation of the composition of the undepleted mantle**

To calculate the composition of the primary metal component, the amounts of FeO, NiO and CoO in the undepleted mantle (depleted mantle + basalt) must be determined. In this work, the estimate of FeO in the undepleted mantle is based on the FeO abundance in olivine of the depleted mantle, the ureilite.

Starting from chondritic compositions (CI1, CV3, H, L, LL), 6 sets of data were each created by removing 40 wt%, 50 wt%, 60 wt%, 70 wt%, 80 wt% and 95 wt% Fe to account for different degrees of Fe-removal during core formation. The crystallization of these compositions with different Fe was modeled with the software MELTS (GHIORSO and SACK 1995, ASIMOW and GHIORSO 1998). Following the suggestions in KITA et al. (2004) and GOODRICH et al. (2007), a degree of partial melting of 25% was assumed for the basaltic component. The composition and abundance of olivine and pyroxene at 25% melting was determined for every set of data (an example for CI1 is given in Fig. 65).

With this data, the amount of FeO in the undepleted mantle can be determined indirectly from the FeO of ureilite olivine.

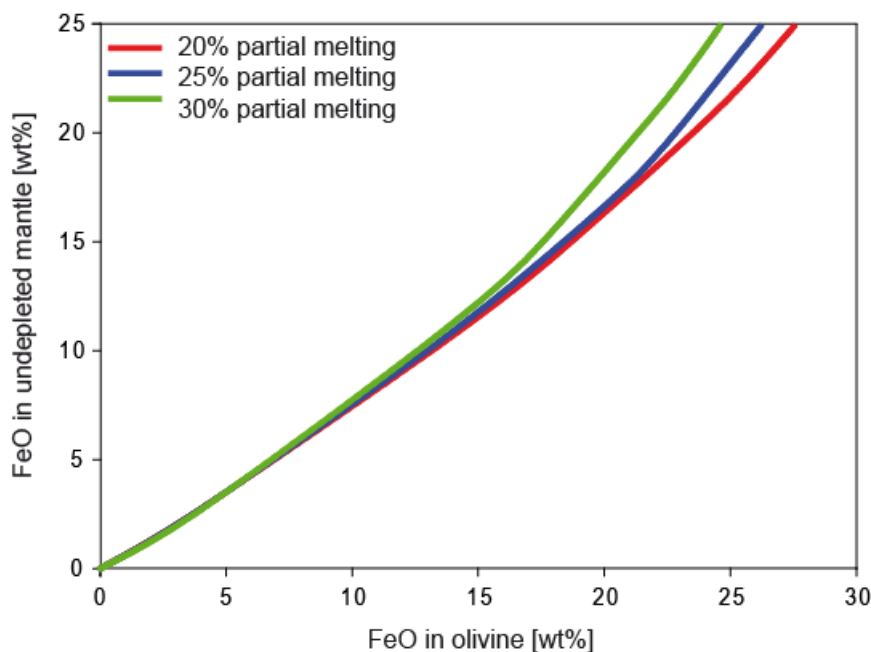


Fig. 65 Amount of FeO in the undepleted mantle against FeO in olivine at different degrees of partial melting. Modeling was done with MELTS starting from a CI1-chondritic composition with different amounts of FeO removed into a core.

The estimate of the amounts of NiO and CoO in the undepleted mantle is based on the measurements of NiO and CoO in ureilite silicates. Relative abundances of orthopyroxene and olivine taken from the MELTS calculations give the abundances of NiO and CoO in the depleted mantle. The distribution coefficients between terrestrial depleted mantle (SALTERS and STRACKE 2004) and terrestrial middle ocean ridge basalt (MORB, KELEMEN et al. 2004) are

$$\frac{D_{\text{mantle}}^{\text{basalt}}}{D_{\text{mantle}}^{\text{Ni}}} = 0.07 \quad \text{and} \quad \frac{D_{\text{mantle}}^{\text{basalt}}}{D_{\text{mantle}}^{\text{Co}}} = 0.39$$

. NiO and CoO in the basaltic component are calculated

from the distribution coefficients, NiO and CoO in ureilite silicates and assuming 25% of partial melting (an example for CI1 is given in Table 31).

**Table 31 FeO, NiO and CoO in the undepleted mantle based on a CI1-chondritic starting composition. Estimates of FeO are based on MELTS-calculations and olivine FeO in ureilites. Estimated of NiO and CoO are based on relative orthopyroxene and olivine abundances as calculated with MELTS and LA-ICP-MS-measurements in ureilite silicates.**

Ureilite	FeO [wt%]	NiO [wt%]	CoO [wt%]
ALH84136	1.26	0.0017	0.0006
ALHA77257	10.02	0.0038	0.0023
DaG340	14.86	0.0077	0.0043
EET87517	5.93	0.0029	0.0016
EET96042	13.06	0.0052	0.0033
EET96331	8.99	0.0014	0.0006
GRA95205	15.61	0.0065	0.0040
Kenna	15.68	0.0068	0.0045
LEW85440	6.32	0.0022	0.0011

### 9.2.3 Calculation of the composition of the primary metal component in the ureilite parent body

With the composition of the undepleted mantle, the composition of the primary metal complementary to the respective ureilite can be established by mass balance calculation (see chapter 5.1). The calculations were done for each chondritic starting composition and each ureilite (an example for CI1 is given in Table 32).

**Table 32 Fe, Ni and Co of model metal in a UPB of CI1-chondritic starting composition and the percentage of model metal in each ureilite parent body.**

Ureilite	Ni (core) [wt%]	Co (core) [wt%]	Fe (core) [wt%]	percentage of metal in bulk UPB [wt%]
ALH84136	5.8	0.27	93.9	44.5
ALHA77257	7.0	0.32	92.6	36.7
DaG340	8.1	0.36	91.5	31.7
EET87517	6.4	0.29	93.3	40.6
EET96042	7.7	0.34	92.0	33.7
EET96331	6.9	0.31	92.8	37.7
GRA95205	8.3	0.37	91.3	30.9
Kenna	8.4	0.37	91.3	30.8
LEW85440	6.4	0.29	93.3	40.2

The higher the extent of oxidation, the more FeO is incorporated into the UPB's mantle. Ureilites like Kenna, GRA95205 and DaG340 with  $fa_{\sim 19}$  are typical examples for an oxidized parent body, whereas ureilites like ALH84136 and EET87517 show lower fayalite contents (down to  $fa_2$  wt% in ALH84136), representing more reduced parent bodies. The more FeO is incorporated into the mantle, the less Fe is left for the primary metal. As a result, the concentrations of Ni and Co in the metal component increase with the degree of oxidation, while the relative amount of metal decreases (Fig. 66).

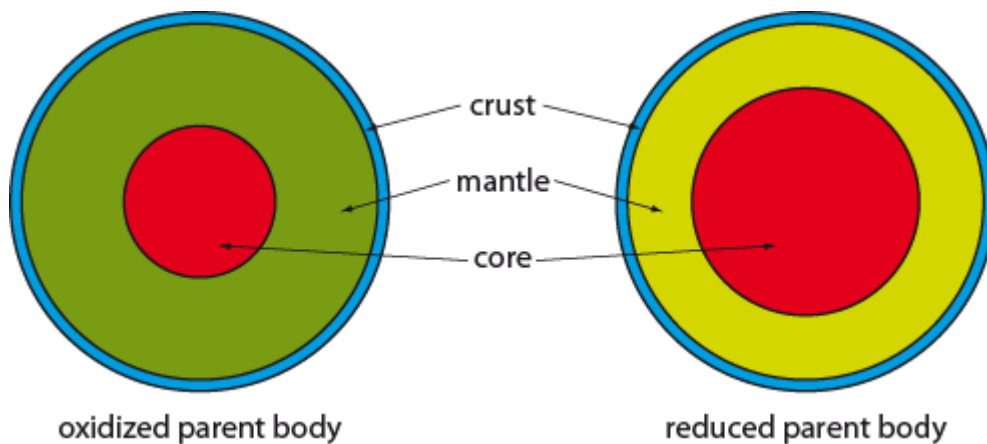


**Fig. 66** Illustration of differentiation in an oxidized parent body (left side) and a reduced parent body (right side). The blue layer represents the basaltic component (which is lost for the ureilite parent body), the green layer represents the depleted mantle (the ureilites) and the red layer represents the metal core. The different shades of green illustrate the fact that the fayalite-content of the olivine in an oxidized parent body is greater than in a reduced parent body. Note that the amount of metal in the reduced parent body (right side) is larger than in the oxidized parent body.

## 9.2.4 Comparison of vein metal and the modeled primary metal component

### Nickel

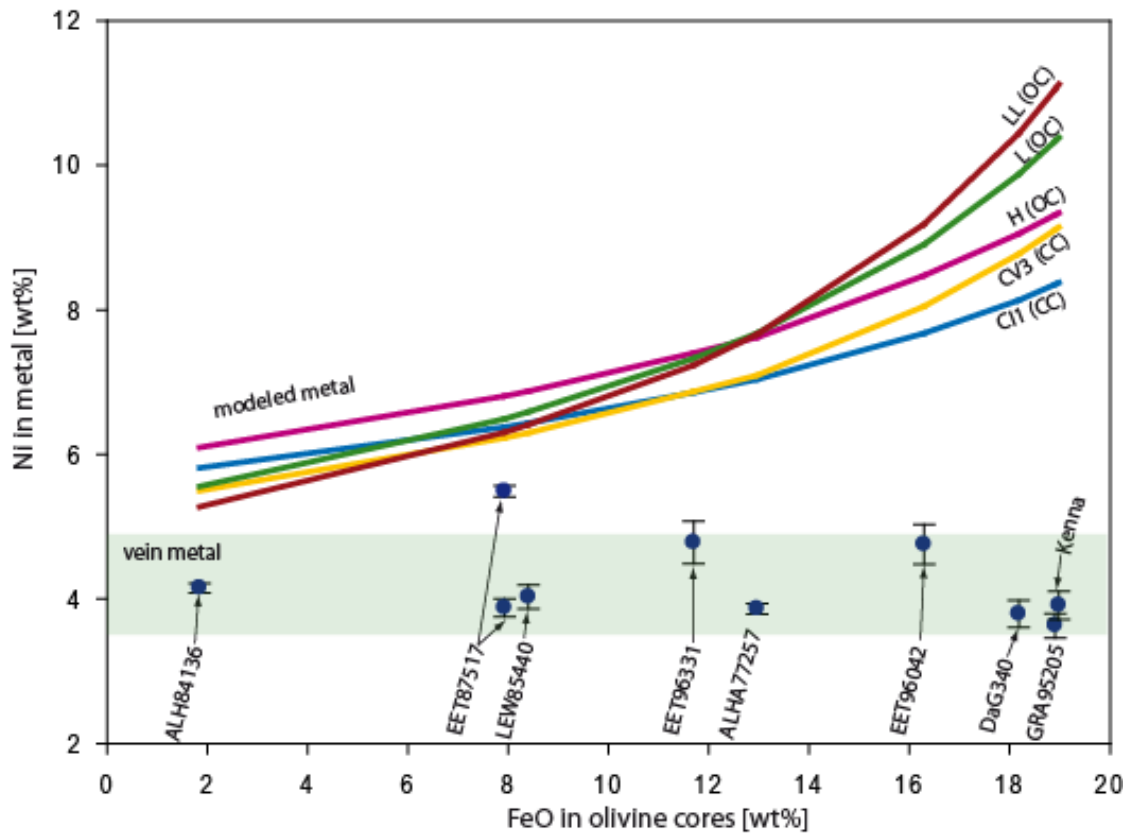


Fig. 67 Plot of calculated Ni-concentrations in the primary metal component of a parent body of different chondritic starting compositions and different amounts of FeO in the parent body's mantle. The blue symbols are measured concentrations of Ni in the vein metal of the respective Ureilites. The Ni concentrations in vein metal are lower than the calculated concentrations for the metal portion of a chondritic parent body composition. The increase in Ni with increasing FeO in olivine is not observed in vein metal.

The modeled Ni-concentrations of the metal range from 5.3 wt% in a highly reduced parent body to up to 11.2 wt% in an oxidized parent body with low bulk FeO (e.g. LL-chondrites). All Ni-concentrations calculated for the primary metal component are higher (between ~1 wt% for reduced parent bodies to ~8 wt% in more oxidized parent bodies) than those observed in the vein metal. The concentrations of Ni in the model core increase with increasing degree of oxidation (represented by an increasing FeO in olivine), while concentrations of Ni in the vein metal show no such correlation (Fig. 67).

## Cobalt

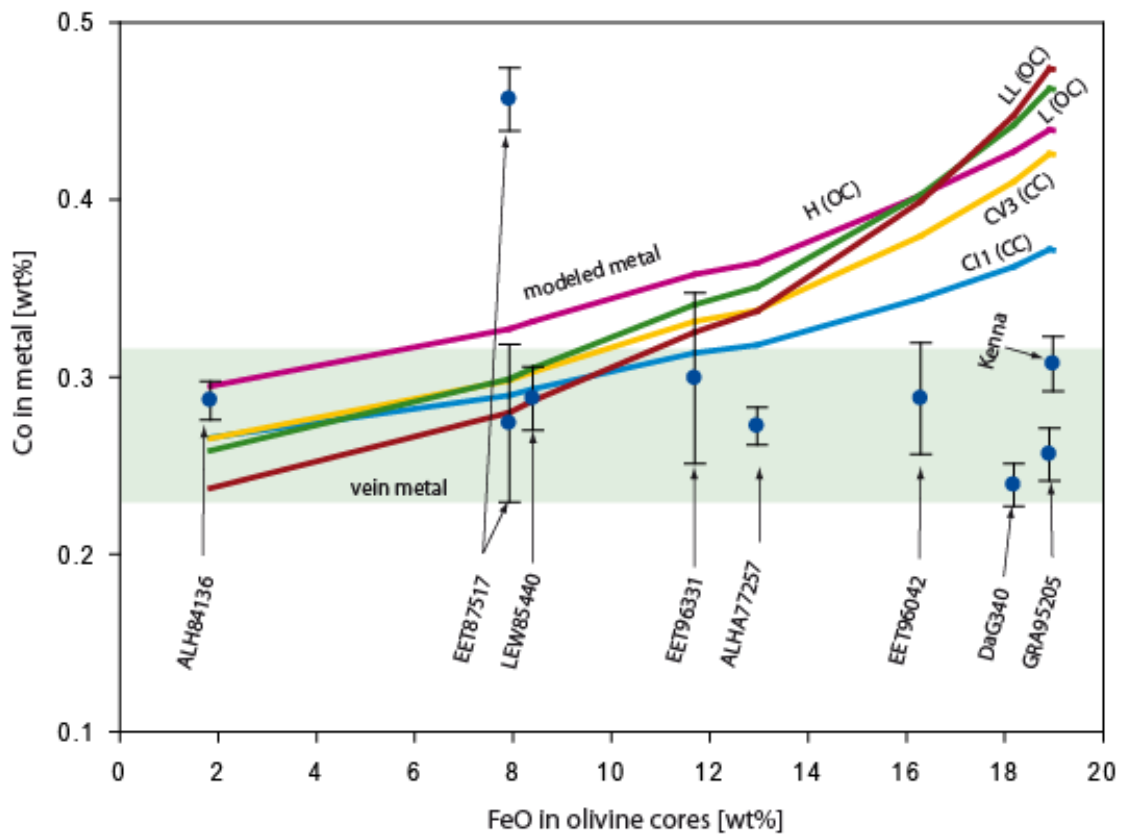


Fig. 68 plot of calculated Co-concentrations in the primary metal component of a parent body of different chondritic starting compositions and different amounts of FeO in the parent body's mantle. The blue symbols are measured concentrations of Co in the vein metal of the respective Ureilites. The Co concentrations in vein metal are lower than the calculated concentrations for olivine FeO > 13 wt%. The increase in Co with increasing FeO in olivine is not observed in vein metal.

The calculated concentrations of Co in the modeled metal core are similar to Co concentrations observed in ureilite vein metal for ureilites with low  $fa$  ( $fa_{<13}$ ). The calculated concentrations for high  $fa$  ( $fa_{>13}$ ) ureilites are larger than the observed concentrations in vein metal. Similar to Ni, Co concentration in the modeled primary metal component increase with increasing degree of oxidization, while Co concentrations in the vein metal show no such correlation (Fig. 68).

## Nickel/Cobalt - ratio

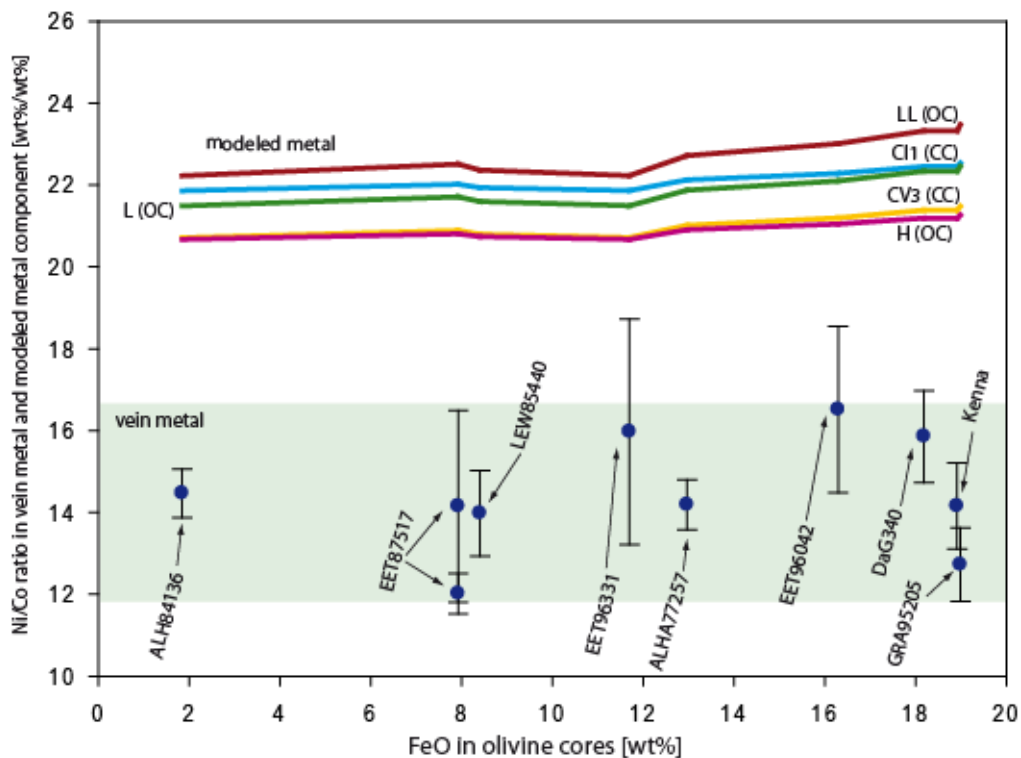


Fig. 69 Plot of the calculated Ni/Co-ratio in the metal core of a parent body of different chondritic starting compositions and different amounts of FeO in the parent body's mantle. The blue symbols are measured ratios of Ni/Co in the vein metal of the respective Ureilites. The Ni/Co ratios in vein metal are lower than the calculated concentrations.

The Ni/Co-ratio in all calculated primary metal compositions is > 20. Over the whole range of olivine FeO-compositions, the Ni/Co ratio increases only by ~1. The observed Ni/Co ratio of the vein metal ranges from 12.72 (Kenna) to 16.51 (EET96042) with an average of 14.4 (Fig. 69) and is lower than in the modeled metal by at least 4.

The Ni/Co-ratios of the calculated metals are similar to the Ni/Co-ratios of the bulk chondritic compositions. All known chondrite groups show a Ni/Co-ratio of >20 (LODDERS and FEGLEY 1998). We therefore assume that all chondritic parent body composition produce a metal core with a Ni/Co-ratio of ~20 or higher and none would produce a metal with a Ni/Co-ratio similar to that measured in ureilite vein metal.

### 9.2.5 Equilibration between the primary metal component and ureilite olivine

In order to establish if ureilite olivine was in equilibrium with the primary metal component of the UPB, equilibration temperatures for Fe-Ni and Fe-Co-exchange were calculated similar to the calculations in chapter 9.1. An example for equilibrium between ureilite olivine and the primary metal component of a CI1-chondritic parent body is given in Table 33 (Fig. 70).

**Table 33** Calculated equilibration temperatures for Fe-Ni and Fe-Co exchange between ureilite olivine and the primary metal component of a CI1-chondritic parent body. Errors are given as  $2\sigma$ .

Ureilite	Fe-Ni-exchange		Fe-Co-exchange	
	$T_{\text{equilibration}} [^{\circ}\text{C}]$	$2\sigma$	$T_{\text{equilibration}} [^{\circ}\text{C}]$	$2\sigma$
ALH84136	2087	284	1732	331
ALHA77257	1157	95	1201	104
DaG340	1270	105	1271	117
EET87517	1389	133	1425	165
EET96042	1141	91	1226	107
EET96331	741	53	731	36
GRA95205	1124	87	1182	98
Kenna	1149	89	1253	113
LEW85440	1176	102	1103	85

Except for EET96331, ALHA84136 and EET87517, all ureilites show similar equilibration temperatures between  $1100^{\circ}\text{C}$  and  $1300^{\circ}\text{C}$  for both exchange reactions. EET96331 gives very low equilibration temperatures of  $\sim 740 \pm 50^{\circ}\text{C}$  due to the lower Ni- and Co-concentrations in the olivine (Fig. 57). ALH84136 gives very high and inconsistent equilibration temperatures ( $2087 \pm 284^{\circ}\text{C}$  for Fe-Ni and  $1732 \pm 331^{\circ}\text{C}$  for Fe-Co-exchange) due to its unusually low FeO in the olivine. EET87517 gives slightly higher equilibration temperatures ( $1389 \pm 133^{\circ}\text{C}$  for Fe-Ni and  $1425 \pm 165^{\circ}\text{C}$  for Fe-Co-exchange) due to the slight enrichment of Ni and Co in EET87517 silicates (Fig. 57).

Calculations were also performed for the other chondritic compositions (i.e. H-, L-, LL- and CV3-chondritic). The calculated temperatures are similar to those calculated for the CI1-composition and only differ up to  $75^{\circ}\text{C}$  from CI1 depending on the chondritic composition used, except for the anomalous ALH84136 which gives much larger differences of  $\sim 200^{\circ}\text{C}$ .

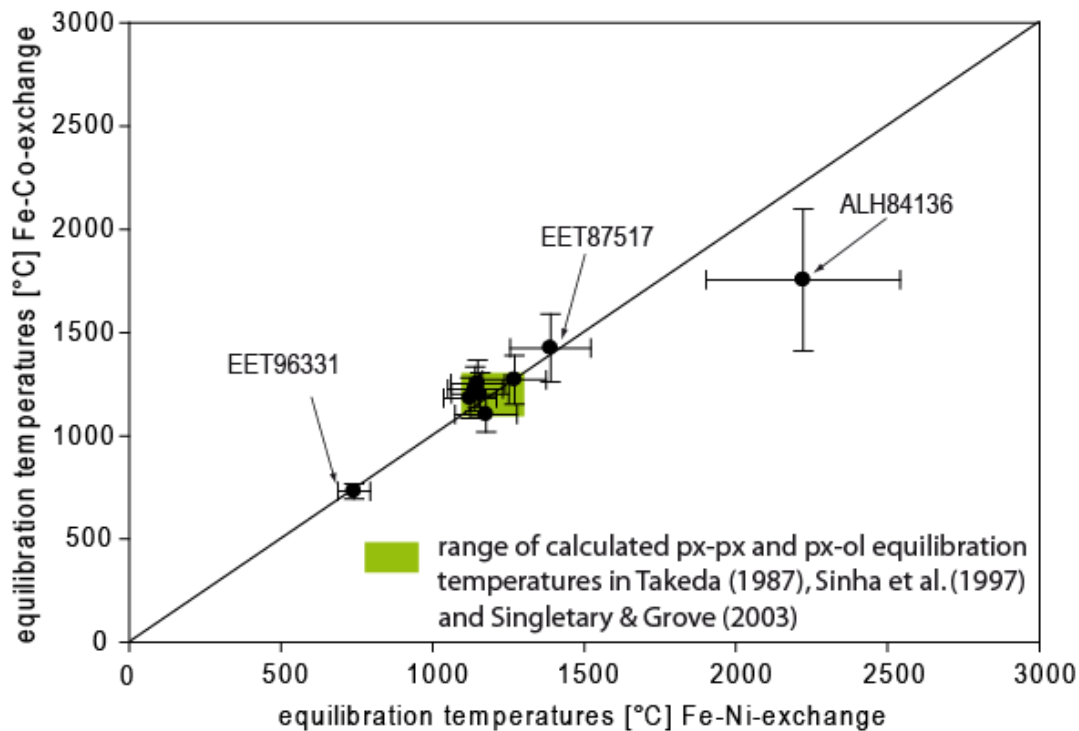


Fig. 70 Calculated equilibration temperatures for the exchange of Fe-Ni and Fe-Co between olivine and modeled metal of a CI1-chondritic parent body. The range of published pyroxene-pyroxene equilibration temperatures (TAKEDA 1987, SINHA et al. 1997, SINGLETARY and GROVE 2003) has been plotted for comparison. Calculations were performed for all nine ureilite samples.

The good agreement between inferred temperatures of both exchange reactions indicates that Ni and Co in olivine have been attained from a component with a Ni/Co-ratio similar to the primary chondritic metal component.

The metal/olivine equilibration temperatures agree well with the temperature range calculated by the px-px- and px-ol-thermometer of 1170-1300°C (TAKEDA 1987, SINHA et al. 1997, SINGLETARY and GROVE 2003). This indicates that equilibrium between the component of chondritic Ni/Co-ratio and ureilite olivine had been established shortly before the disruption of the ureilite parent body. The metal component with chondritic Ni/Co is no longer present in the ureilite. It was either altered or removed, most likely shortly before the impact.

### 9.2.6 Metal depletion in ureilites

The calculated percentage of metal in the ureilite parent body range from 45 wt% for a very reduced parent body (like for ALH84136) and a relatively iron rich starting composition (e.g. CI1 carbonaceous chondrite) to 16 wt% for an oxidized parent body (like for GRA95205) and a relatively iron poor starting composition (e.g. LL-ordinary chondrites), (Fig. 71).

The amounts of metal in published ureilite data are generally lower than 2 wt% (JAROSEWICH 1990, TAKEDA 1987, WIIK 1972). An exception is Haverö, containing 3.5 wt% Fe (WIIK 1972). Since it is assumed that the composition of the UPB was of approximately chondritic, at least 95 wt% of the metal was removed.

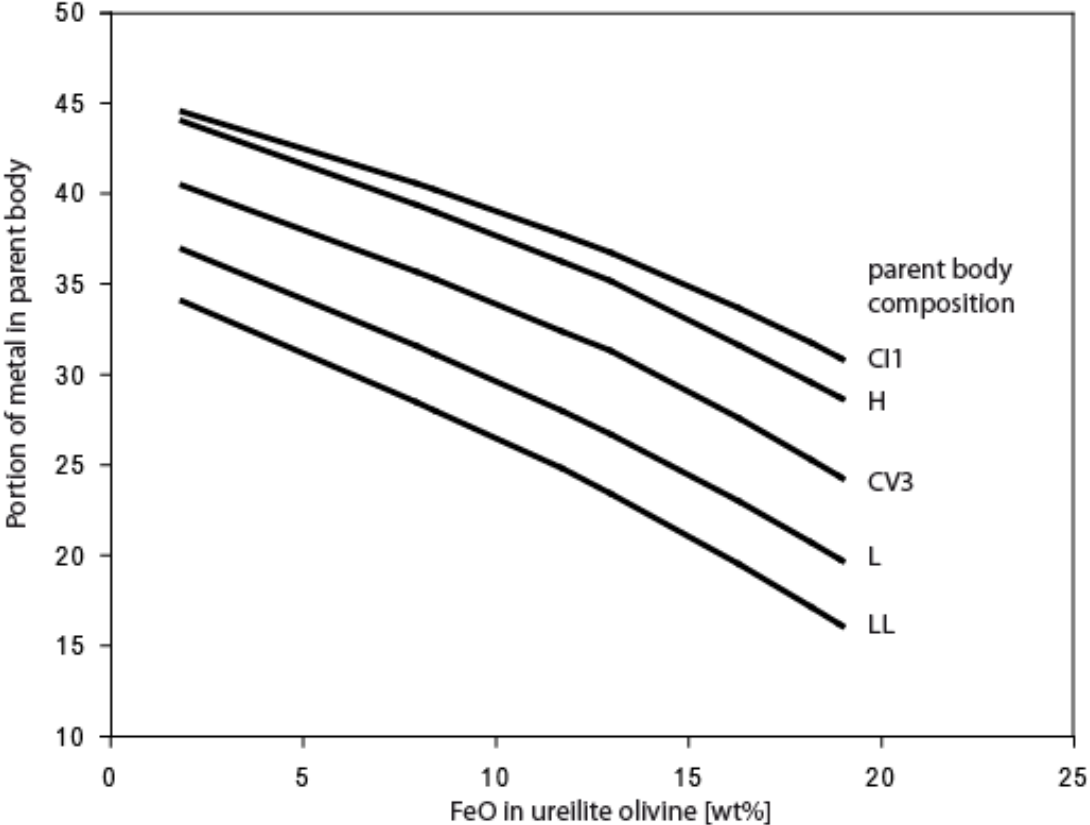


Fig. 71 Percentage of metal in parent body (Fe, Ni and Co only), calculated for different chondritic parent body compositions and different ureilites. The amount of metal decreases with increasing degree of oxidization and decreasing amount of FeO in the starting composition.

### 9.2.7 Scenarios for vein metal generation

Mass balance calculations show that the Ni and Co concentrations and the Ni/Co-ratio of ureilite vein metal is different from that of metal formed from a chondritic starting composition. As at least 95% of the original metal content of the ureilite parent body has been removed, such a difference is to be expected. Any process that removes most of the metal will significantly change the composition of the residual metal with respect to Ni and Co. For the source of the vein metal, we propose three principal scenarios:

1. Ureilite vein metal is a primary component. The vein metal represents a residual metal or a melt fraction of the primary chondritic metal budget of the ureilite parent body. This can either happen by fractional or by batch melting of the original metal component.
2. Ureilite vein metal is a secondary component. The primary metal component was completely lost, either by batch melting or fractional melting. The vein metal represents metal from an external source (e.g. metal-rich impactor) or metal from reduction of silicates.
3. Ureilite vein metal represents a mixture of primary and secondary components. The primary metal was not completely lost and either a residue or a partial melt mixed with metal from an external source or metal from silicate reduction.

In order to clarify which of the three scenarios might be responsible for the formation of the vein metal, batch melting and fractional melting of the primary metal component was modeled. The Ni and Co concentrations of the resulting residues and melts were compared to the measured composition of the ureilite vein metal.

## 9.3 Ureilite vein metal as a primary component

### 9.3.1 Constraints for metal fractionation processes on the ureilite parent body

#### *Fractionation mechanisms – batch and fractional melting*

If ureilite vein metal constitutes a primary component, it represents either a residue or a partial melt from the primary chondritic metal component. The responsible melting mechanism can either be fractional melting, where the melt is gradually removed as it forms, or batch melting, where the whole melt stays in equilibrium with the solid residuum and is removed entirely at a certain stage of the melting process.

The removal of a liquid metal fraction needs a pathway, as well as a driving force. The migration of the melt is triggered, when the porosity of the mantle reaches a certain threshold (WARREN et al. 2006). The first melts will be formed at the Fe-FeS eutectic point at  $\sim 950^{\circ}\text{C}$  (RAGHAVAN 1988). In order to allow the migration of melt within solid silicate material, an interconnected network must be formed.

LEBEDEV et al. (1999) concluded that 5-10% melting of silicate phases would be necessary for a sulfide melt to be removed effectively. HERPFER and LARIMER (1993) reported experimental results implying 1-2 vol% to be sufficient, while experiments in YOSHINO et al. (2004) suggest that the percolation threshold of Fe-S melts is  $\sim 13 \pm 2$  vol.% and that small amounts of silicate melt could actually inhibit segregation. WALKER and AGEE (1988) conducted melting experiments with Allende (CV). According to their observations, S-rich melt is very reluctant to form interconnected networks. Instead, the S-rich melt bonded well to graphite. Several other studies observed a similar reluctance of S-rich melt to form interconnected networks (McCoy et al. (2006) and references therein). It is suggested that for the formation of such a network, a dihedral angle  $\Theta$  of  $< 60^{\circ}$  is necessary. If  $\Theta$  is  $> 60^{\circ}$  isolated melt pockets are formed. According to McCoy et al. (2006) only anion-dominated melts exhibit  $\Theta < 60^{\circ}$ , thus an FeS-eutectic melt (Anion/Cation  $\sim 0.8$ ), would not migrate under static conditions.

The calculations of KEIL and WILSON (1993) show that small amounts of volatiles (possibly CO-gas derived from a smelting process as discussed in BERKLEY and JONES (1982), SINHA et al. (1997) or SINGLETARY and GROVE (2003)) can cause the negatively buoyant FeNi-S-melts to be

driven to the surface. Similar to the model proposed in WILSON and KEIL (1991), these melts could be lost by explosive volcanism.

Our thermodynamic calculations showed that ureilite olivine is not in equilibrium with ureilite vein metal but with the primary metal component of the UPB. This primary component is no longer present. The question arises which melting mechanism could have removed the primary metal component without reequilibration with the ureilite olivine.

In a fractional melting process, the composition of the residual metal component is continuously changed. Even if equilibrium had been attained prior to the onset of melting, new equilibria should be established during the fractionation process, unless the fractionation process was very rapid.

In a batch melting process, neither the Ni/Co-ratio nor the Ni and Co-concentrations of the bulk system change during the melting process. When the whole metal component was molten, it could have been rapidly removed. The impact and the subsequent disruption of the ureilite parent body could have prevented re-equilibration with the vein metal.

Neither batch melting nor fractional melting can be ruled out as suitable fractionation process although the missing silicate/metal reequilibration appears to favor batch melting.

### ***Temperature considerations***

All proposed scenarios for the formation of the vein metal start with a chondritic parent body (Fig. 72). The degree of partial melting on the ureilite parent body is still subject to discussion, however most authors assume a degree of partial melting of 20 to up to 30% (e.g. KITA et al. 2004, WARREN and HUBER 2006 , GOODRICH et al. 2007).

Calculations performed with the MELTS for CI1-, CV3-, H-, L- and LL-chondritic compositions indicate that a partial melting of ~30% requires temperatures of ~1300°C, which would give an upper temperature limit of the ureilite parent body. However, even if ~30 wt% of basaltic melt have been removed from the undepleted mantle, the degree of melting might have been higher. According to our modeling with MELTS (GHIORSO and SACK 1995, ASIMOW and GHIORSO 1998), at ~1500°C, which is the liquidus temperature of pure FeNi-metal (RAGHAVAN 1988), more than 70% of most parent body compositions would be molten. Heterogeneities in oxygen isotopes (CLAYTON and MAYEDA 1996) suggest that igneous processing did not occur

on large scale on the ureilite parent body. Carbon phases in ureilite vein material contain unfractionated noble gases. If the vein material constitutes a primary component, their presence also argues against such extensive melting processes on the UPB. We therefore assume that the peak temperature of the UPB was  $\sim 1300^{\circ}\text{C}$ .

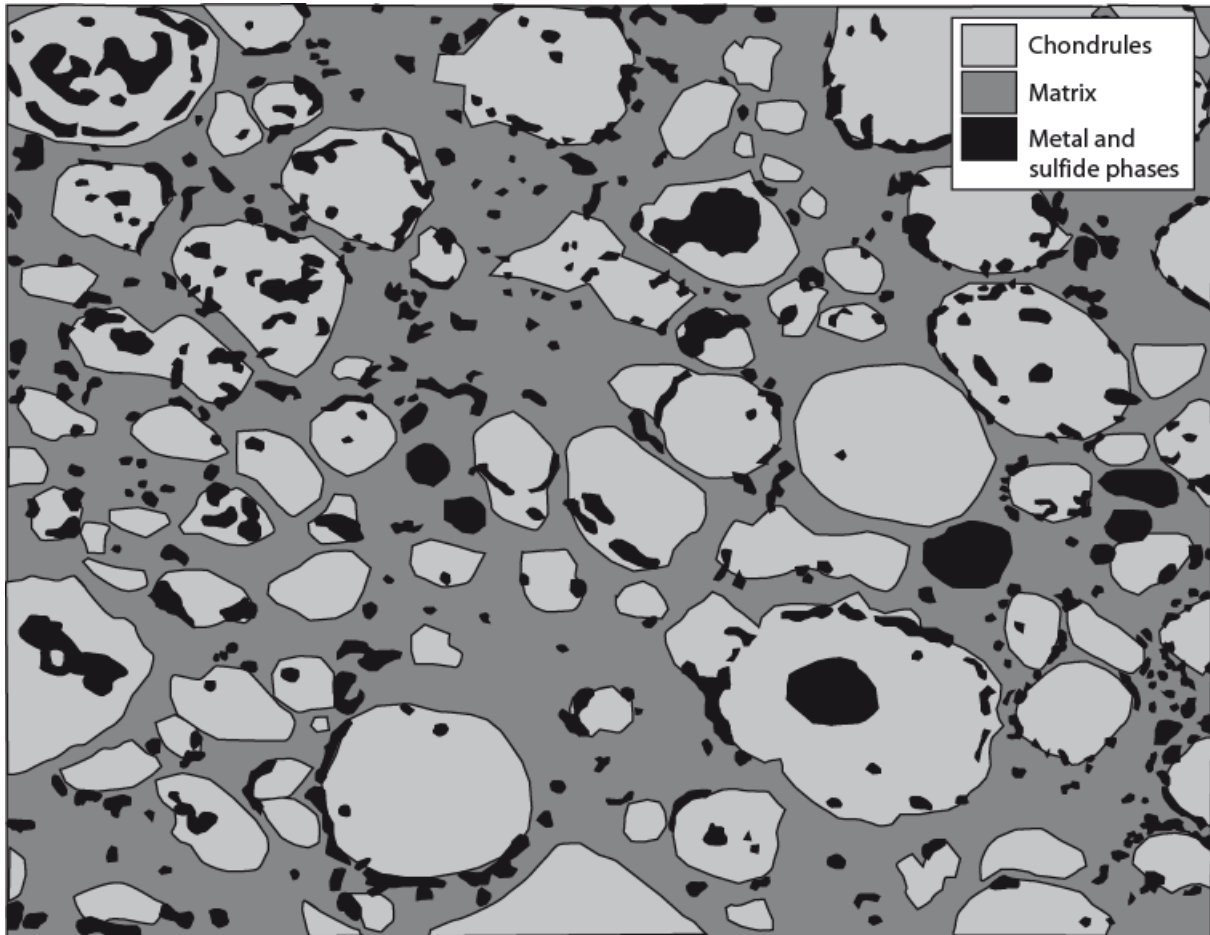


**Fig. 72 Schematic picture of a chondrite. Chondrules (light grey) within matrix material (dark grey) with finely dispersed and compact metal phases.**

Several authors have published px-px- and px-ol-equilibration temperatures for a number of ureilites (i.e. TAKEDA 1987, SINHA et al. 1997, SINGLETARY and GROVE 2003). These temperatures range from 1170 to  $\sim 1300^{\circ}\text{C}$ . After the ureilite parent body disrupted, as indicated by its temperature history (see chapter 2.4.2), silicate equilibration stopped. The equilibration temperatures therefore record the temperatures at the impact event and provide a lower limit to the temperatures in the ureilite parent body.

Both, the upper temperature limit given by the degree of partial melting and the lower temperature limit given by the silicate equilibration temperature give a similar temperature of  $\sim 1300^{\circ}\text{C}$ . This indicates that the UPB was at its peak temperature when it was disrupted,

which means that the heating process was either still active or had barely stopped, at the time of impact.

The solidus temperature of a pure Fe-Ni-metal is  $\sim 1500^{\circ}\text{C}$  (RAGHAVAN 1988). Assuming a maximum temperature of  $\sim 1300^{\circ}\text{C}$  in the UPB, the metal could not have been removed without the presence of other components that lower the metal's solidus temperature. Suitable components that are present in ureilites are sulfur and carbon.

### ***Sulfur in the ureilite parent body***

Bulk FeS concentrations in ureilites range from 0.01 to 1.95 wt% with an average of 0.68 wt% ( $n=10$ ) (MCGALL and CLEVERLY 1968, WIIK 1972, TAKEDA 1987, JAROSEWICH 1990). Assuming that FeS is the major sulfide component within the ureilite, this corresponds to a bulk S content of 0.25 wt%. CV-, H-, L-, and LL-chondrites contain  $\sim 2$  wt% sulfur while the CI1 group contains  $\sim 5$  wt% of sulfur (LODDERS and FEGLEY 1998). This means that the ureilites have also lost between 85 and 95 wt% of their initial sulfur content.

The solidus temperature of an S-rich melt in a pure Fe-S-System is about  $988^{\circ}\text{C}$  (RAGHAVAN 1988) but the Ni-content might lower it by  $\sim 40^{\circ}\text{C}$  (RANKENBURG et al. 2008). Considering the loss of most sulfur from the initial chondritic system, metal removal in form of a S-rich melt appears to be a viable explanation as has been proposed by many authors (e.g. GOODRICH et al. 1987a, WARREN et al. 2006, RANKENBURG et al. 2008).

The maximum amounts of S in the initial chondritic metal portion have been calculated from mass balance calculations similar to the calculation of Ni- and Co-concentrations (Fig. 73). The calculated S-contents range from 7 wt% in a reduced H-chondritic parent body to up to 29 wt% in an oxidized parent body with CI1-chondritic composition. For any combination of degree of oxidization and chondritic parent body composition, the S-concentrations in the metal are on the iron-rich side of the Fe-S eutectic point at  $\sim 31$  wt% S (RAGHAVAN 1988).

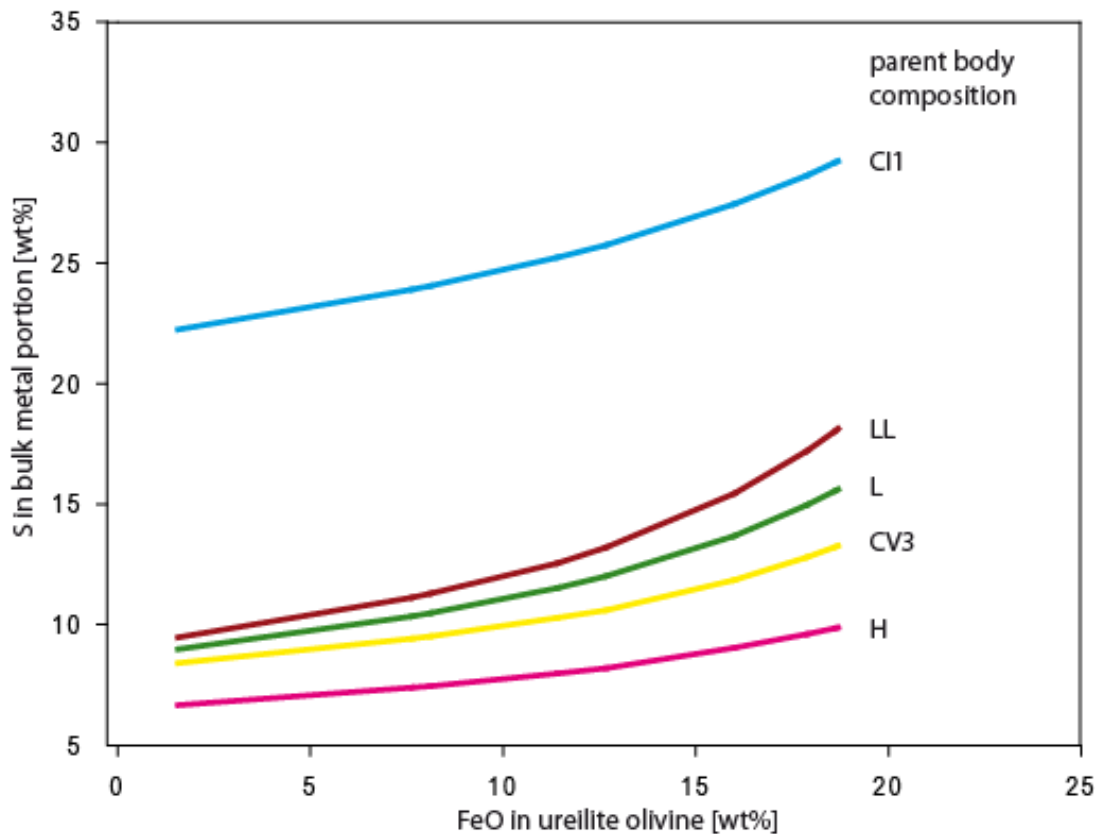


Fig. 73 Theoretical maximum amount of S in the metal component of a given parent body with chondritic composition and for different amounts of FeO in the corresponding ureilite olivine. Calculations have been done for the Fe-Ni-Co-S-System.

As sulfur belongs to the more volatile elements (WARREN et al. 2006), part of it might have been lost prior to the accretion of the ureilite parent body.

### ***Carbon in the ureilite parent body***

Carbon concentrations in ureilites range from 0.2 to 5.9 wt% with an average of 2.9 (n=20) (MCGALL and CLEVERLY 1968, WIIK 1972, GRADY et al. 1985, TAKEDA 1987). While early models for ureilite petrogenesis assumed that carbon was injected into the parent body (e.g. WASSON et al. 1976, HIGUCHI et al. 1976), more recent studies assume carbon represents a primary component (GOODRICH and BERKLEY 1986). Carbon concentrations of the chondritic compositions are 3.45 wt% C in a CI1 chondrite, 0.53 wt% C in a CV3 chondrite and ~0.2 wt% C in H, L and LL-chondrites (LODDERS and FEGLEY 1998).

Mass balance calculations show that the maximum portion of metal that could have been removed from bulk ureilites into a core is <45 wt% (Fig. 71). The amount of basaltic component lost from the undepleted mantle is estimated to be 20-30 wt% (e.g. KITA et al. 2004, GOODRICH et al. 2007). As a result, the maximum factor by which carbon can be

enriched within bulk ureilites is ~3. If carbon was a primary component in ureilites, only CI1 contains sufficient carbon, to produce an ureilite with ~3 wt% carbon.

The maximum amounts of carbon in the ureilite metal can be calculated by mass balance calculation (Fig. 74). As, it is possible that at least some of the carbon had been injected into the UPB by an impactor as proposed by WASSON et al. (1976), we also include CV3-, H-, L- and LL-chondritic compositions into mass balance calculations. The eutectic point of the Fe-C-System is at 4.5 wt% C and at a temperature of ~1150°C (RAGHAVAN 1988).

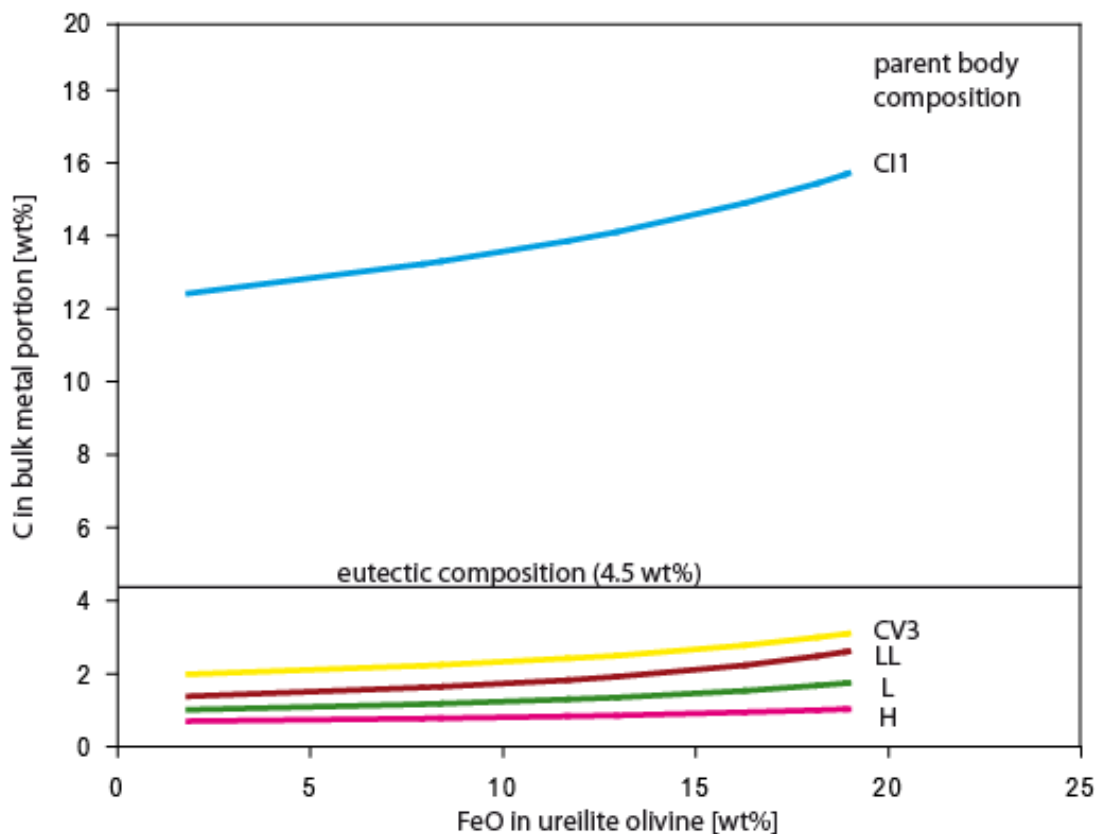


**Fig. 74** Maximum amount of C in the metal component of a given parent body with chondritic composition and for different amounts of FeO in the corresponding ureilite olivine. Calculations have been done for the Fe-Ni-Co-S-C-System.

For the 'low-C' chondritic compositions (CV3, H, L, LL) the amounts of C in the metal phase range from 1 - 3 wt%. All of those compositions plot on the iron-rich side of the eutectic point. The metal generated from the 'C-rich' CI1 chondritic composition contains 12 to 16 wt% C and plots on the carbon-rich side of the eutectic point.

Mass balance calculation only gives a maximum amount of C for the ureilite metal component. WARREN and HUBER (2006) argue that considerable amounts of carbon could already be lost during early heating and accretion processes. But high bulk carbon

concentrations (McGALL and CLEVERLY 1968, WIIK 1972, GRADY et al. 1985, TAKEDA 1987) in ureilites suggest that even if some amount of carbon depletion occurred, most of the carbon was retained in the ureilite parent body.

### ***Starting compositions***

Depending on the type of chondritic parent body, different starting compositions can be considered. H-chondrites generally have the lowest carbon- and sulfur-contents, while CI1-chondrites have the highest carbon- and sulfur-contents. The CV3-chondrite was chosen to represent an intermediate starting composition with respect to carbon and sulfur concentration.

The starting composition also depends on the degree of oxidation on the UPB. The majority of known ureilites contain olivines with  $fa_{>18}$  (MITTFEHLDT et al. 1998). Our ureilite samples cover a wide range of oxidation states with  $fa$  ranging from  $fa_2$  to  $fa_{20}$ . It is also possible that the vein metal represents a metal from a very reduced domain of the UPB. For our model of metal differentiation during core formation, we therefore consider oxidized parent bodies similar to the UPB of GRA9505 ( $fa_{\sim 20}$ ) and very reduced parent bodies similar to the UPB of ALH84136 ( $fa_{\sim 3}$ ).

As a result, 6 different starting compositions with different degrees of oxidation and different carbon and sulfur concentrations were used to model metal fractionation processes on the UPB (Table 34).

**Table 34 Starting compositions of core metal for fractionation calculations. Metal compositions are given for a very reduced UPB ( $fa_{\sim 3}$ ) and a oxidized UPB ( $fa_{\sim 20}$ ) of H-, CV3-, or CI1-chondritic composition.**

Composition [wt%]	Reduced UPB (ALH84136)			Oxidized UPB (GRA95205)		
	H	CV3	CI1	H	CV3	CI1
Ni	5.65	4.94	3.96	8.31	7.66	4.99
Co	0.27	0.24	0.18	0.39	0.36	0.22
Fe	86.77	84.61	63.97	80.53	76.09	54.51
S	6.61	8.23	19.47	9.74	12.81	24.59
C	0.69	1.98	12.42	1.02	3.09	15.68

### 9.3.2 Modeling of fractional melting on the ureilite parent body

#### *Starting compositions rich in carbon and sulfur*

When the ureilite parent body is heated up, the first metal melts will form at the Fe-FeS eutectic point at  $\sim 950^\circ\text{C}$  (RAGHAVAN 1988, RANKENBURG et al. 2008). We assume that the eutectic melt in the Fe-S-C-System is similar to the eutectic melt in the Fe-S-System as the solubility of carbon in sulfide melts is very limited (RAGHAVAN 1988). As proposed in RANKENBURG et al. (2008), it is assumed that the presence of carbon does not lead to major changes of the solid metal/liquid metal distribution coefficients.

The composition of the modeled core metal is on the iron rich side of the Fe-FeS eutectic point, thus eutectic melts are removed until S is depleted in the system. The solid metal/liquid metal distribution coefficients of Ni and Co for the eutectic composition are  $D_{Ni}^f = 2$  and  $D_{Co}^f = 4$  (CHABOT et al. 2003), thus Ni and Co are enriched in the residual metal while melting progresses. The first melt shows low Ni- and Co-concentrations and becomes gradually enriched in Ni and Co as melting progresses. When sulfur is exhausted, melting stops until temperature rises to the Fe-C eutectic point at  $\sim 1153^\circ\text{C}$ , and the system can then be treated as a pure Fe-C (+Ni)-system.

In a carbon-rich system (CI1-chondritic starting composition) the sulfur-depleted metal residue is on the carbon-rich side of the eutectic point in the Fe-C-system. Eutectic metal melt formed is in equilibrium with graphite. The melting process continues until Fe is exhausted in the system. Similar to the Fe-S-system, the residual metal and the liquid metal become progressively enriched in Ni and Co (CHABOT et al. 2006), leaving residual carbon (Fig. 75, Fig. 76). The solid metal/liquid metal distribution coefficients of Ni and Co for the eutectic composition are  $D_{Ni}^f = 1.8$  and  $D_{Co}^f = 1.4$ . The distribution coefficient of Ni remains similar to the Fe-S-System, while the distribution coefficient for Co is lowered by 2.6. As a result, the Ni/Co-ratio in the C-rich liquid much lower than in the S-rich liquid.

In the case of a more oxidized parent body (Fig. 76), Fe is almost completely depleted by the removal of S-rich melts alone. The amount of C-rich melt that can be removed before Fe is completely depleted in the system is very small ( $\sim 2$  wt%).

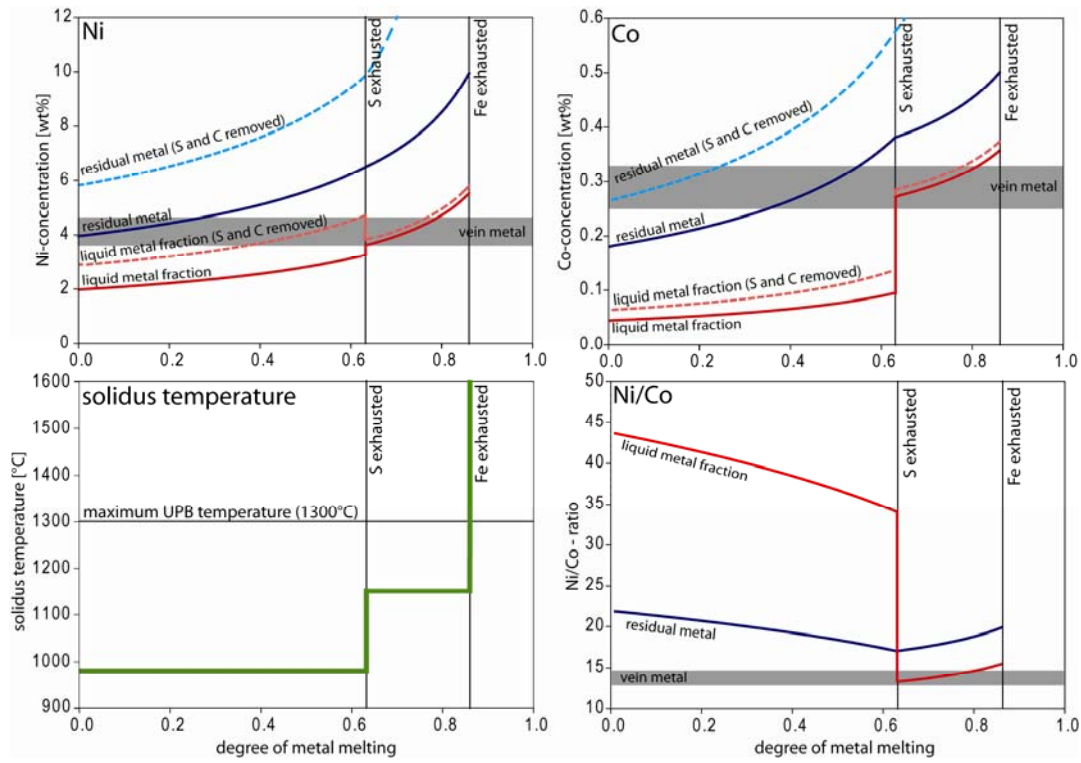


**Fig. 75** Concentrations of Ni and Co, solidus temperatures and Ni/Co-ratio during fractional melting of the metal fraction (Fe-Ni-S-C-Co) of a reduced parent body (e.g. ALH84136) with a carbon- and sulfur-rich CI1 chondritic composition.

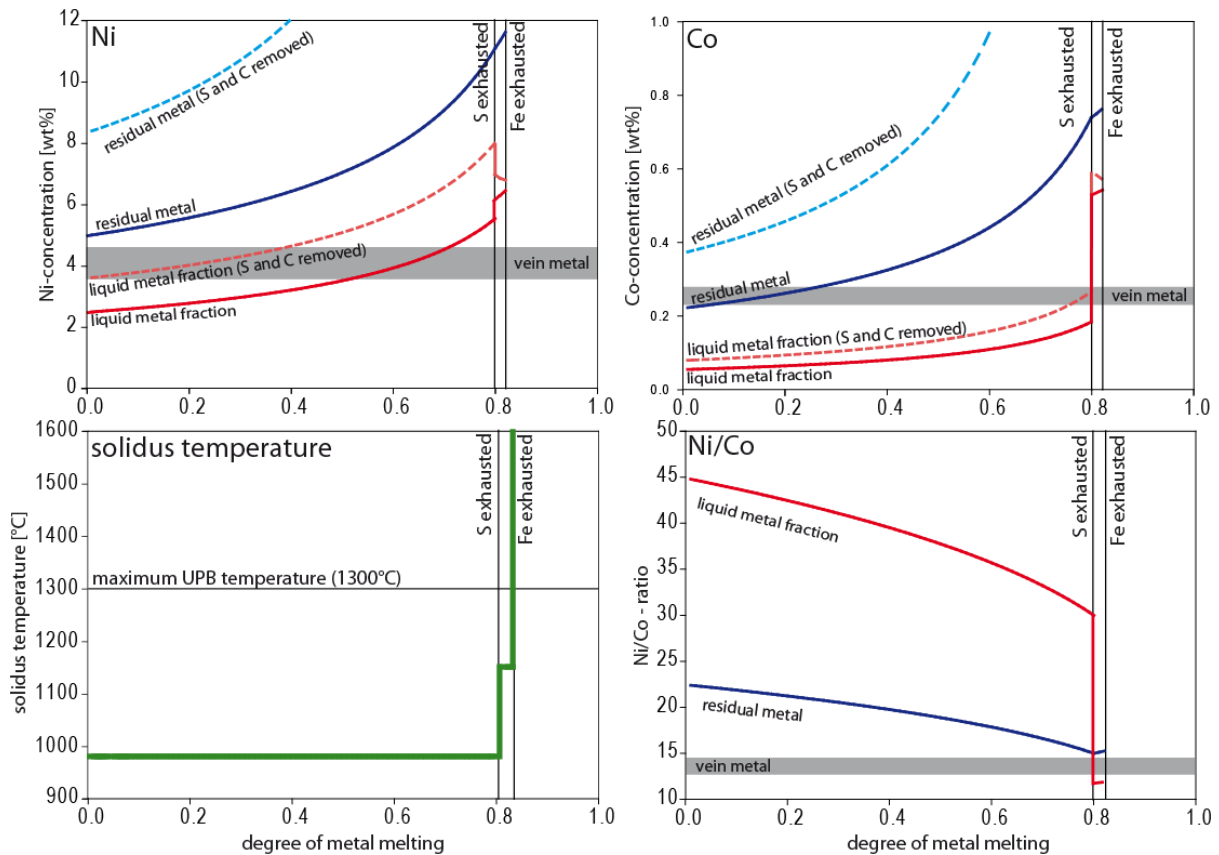


**Fig. 76** Concentrations of Ni and Co, solidus temperatures and Ni/Co-ratio during fractional melting of the metal fraction (Fe-Ni-S-C-Co) of an oxidized parent body (e.g. GRA95205) with a carbon- and sulfur-rich CI1 chondritic composition.

Unlike the vein metal, the modeled metal residue and the liquid metal fraction contain considerable amounts of sulfur and carbon. To directly compare vein metal with modeled residual metals and metal liquids, Ni and Co were also plotted as carbon- and sulfur-free metal (dotted lines).

### ***Starting compositions with moderate sulfur- and carbon-contents***

In a system with moderate carbon and sulfur-concentrations (e.g. CV3 chondritic parent body composition), the result of the modeling depends on the amount of Fe in the primary metal component.

In a reduced parent body (Fig. 77) with high amounts of Fe (~85 wt%) in the primary metal component, S is exhausted after ~30 % of melting. After S is depleted, the solidus temperature increases until carbon-rich melt begins to form at ~1150°C. The removal of the C-rich melt leads to a depletion of C at ~70 % of melting, leaving a Ni- and Co-rich FeNi-metal residuum. During both stages, Ni and Co are enriched in the residual metal. A further melting of the FeNi-residuum requires temperatures of ~1500°C, which is higher than the estimated UPB's peak temperature. If the estimate of UPB's peak temperature is wrong and the UPB was hot enough to permit the melting of pure FeNi-metal, the concentrations of Ni and Co decrease in the residual metal as melting progresses.

Fractional melting of an oxidized parent body (~75 wt% Fe) will result in a different scenario. Sulfur is exhausted after ~40% of the primary metal component is molten. The subsequent formation and removal of a carbon rich liquid leads to a depletion of Fe at close to ~98 % of melting and the formation of a carbon residual. Ni and Co are enriched in the residual and the liquids during both stages.

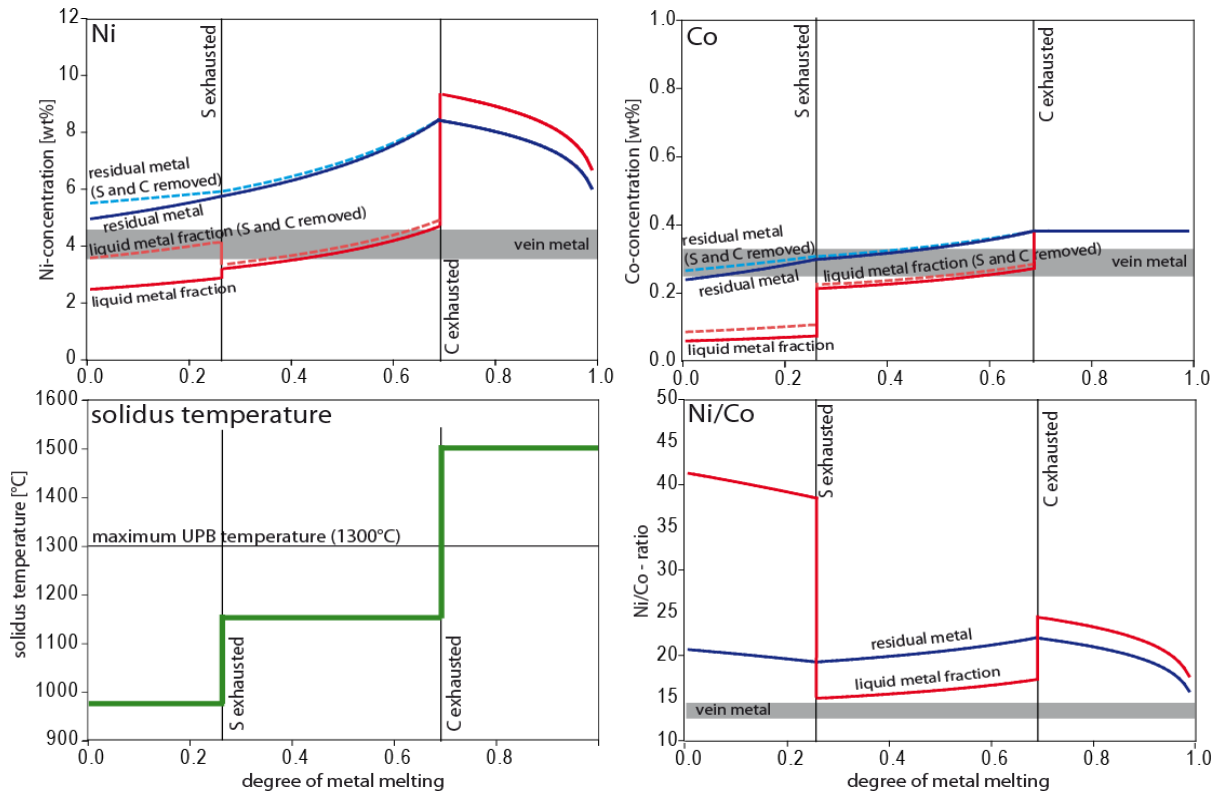


**Fig. 77** Concentrations of Ni and Co, solidus temperatures and Ni/Co-ratio during fractional melting of the metal fraction (Fe-Ni-S-C-Co) of a reduced parent body (e.g. ALH84136) with intermediate carbon- and sulfur-concentrations (CV3 chondritic starting composition).

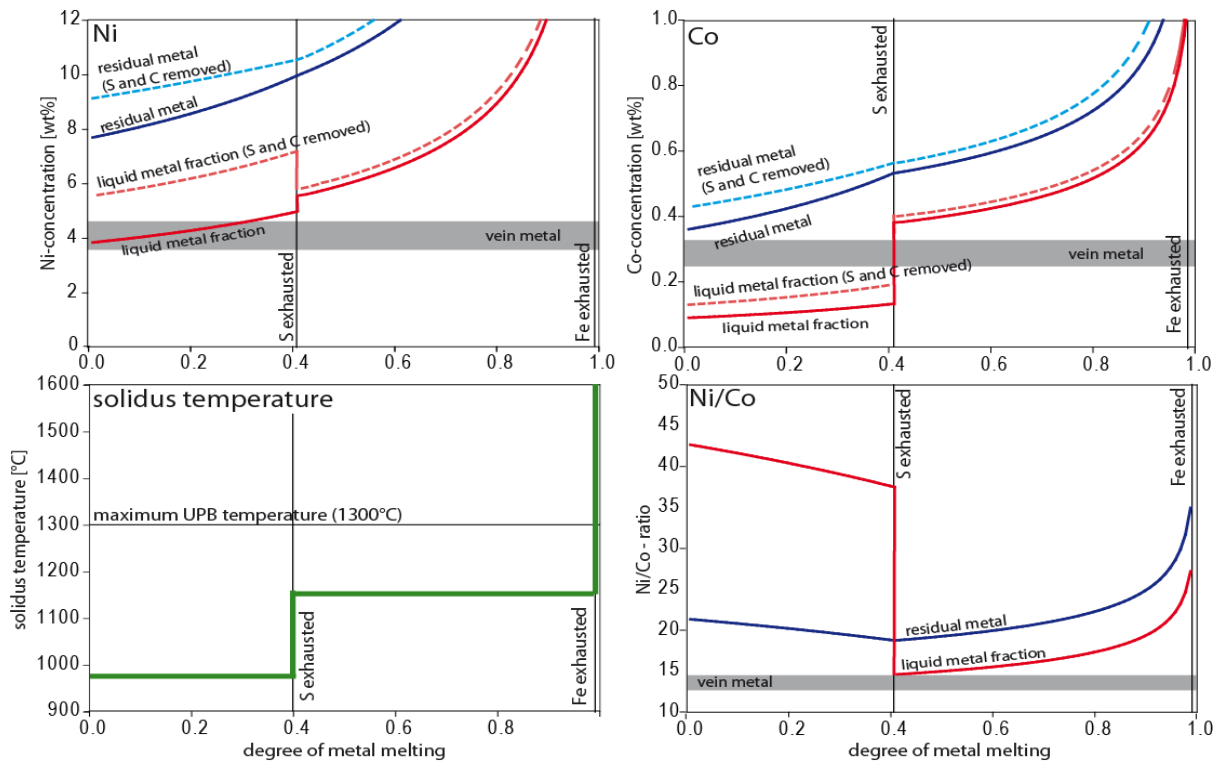


**Fig. 78** Concentrations of Ni and Co, solidus temperatures and Ni/Co-ratio during fractional melting of the metal fraction (Fe-Ni-S-C-Co) of an oxidized parent body (e.g. GRA95205) with intermediate carbon- and sulfur-concentrations (CV3 chondritic starting composition).

### Starting compositions with low sulfur- and carbon-contents

In a carbon-poor system, with an H-, L- or LL-chondritic composition, the composition of the primary metal component is on the Fe-rich side of the Fe-C eutectic point and the Fe-S eutectic point. This is true for a reduced as well as an oxidized parent body composition (Fig. 79, Fig. 80).

The first melts formed are S-rich eutectic melts in equilibrium with FeNi-metal, which are removed until S is depleted in the system. The solidus temperature increases until eutectic C-rich melts start to form at 1150 °C. Removing these eutectic melts reduces the amount of carbon in the system until carbon is exhausted. Similar to the other model's calculations, the distribution coefficient of Co will be reduced to 1.4 in the C-rich melt, which results in an inversion of the Ni/Co-ratios.

Melting will then cease as the solidus temperature increases to ~1500°C. During both stages of melting, Ni and Co are enriched in the residual metal and in the liquid metal melt.

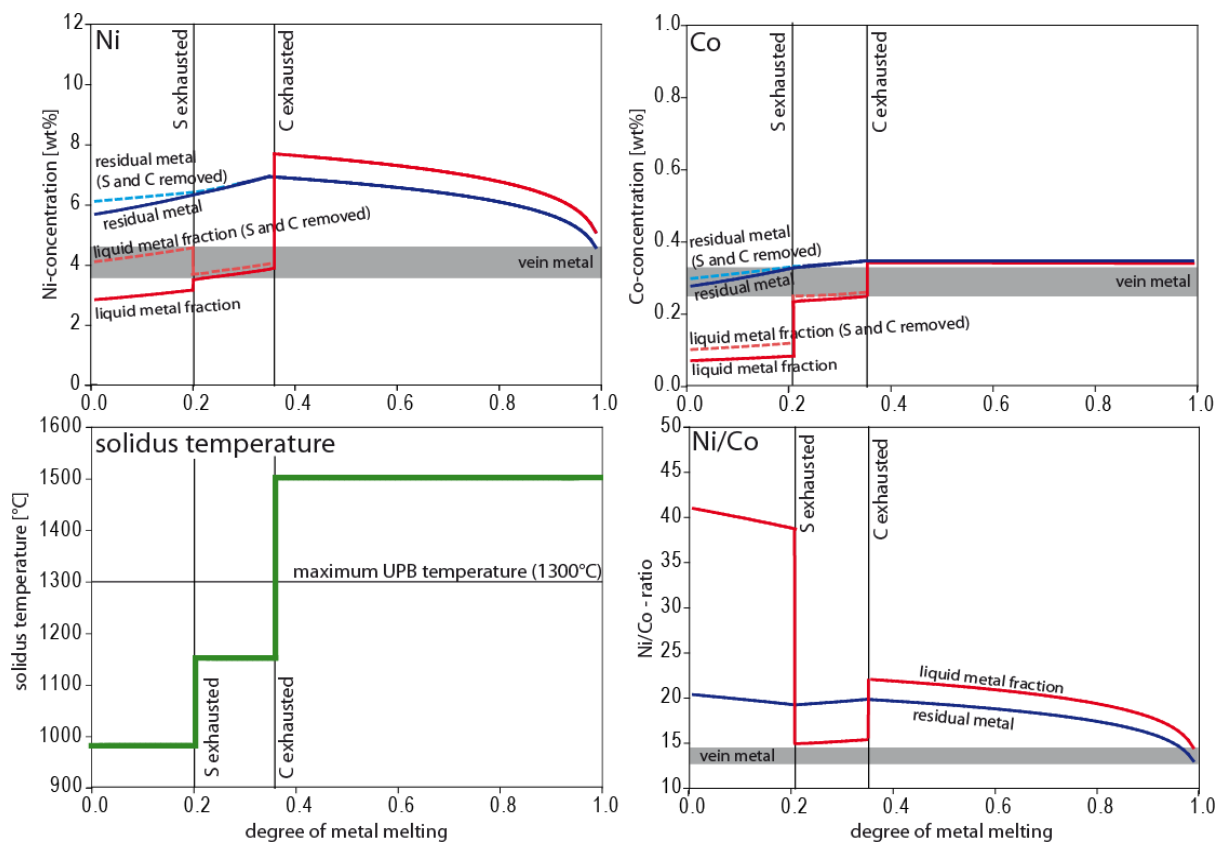


**Fig. 79** Concentrations of Ni and Co, solidus temperatures and Ni/Co-ratio during fractional melting of the metal fraction (Fe-Ni-S-C-Co) of a reduced parent body (e.g. ALH84136) with a carbon- and sulfur-poor H chondritic composition.

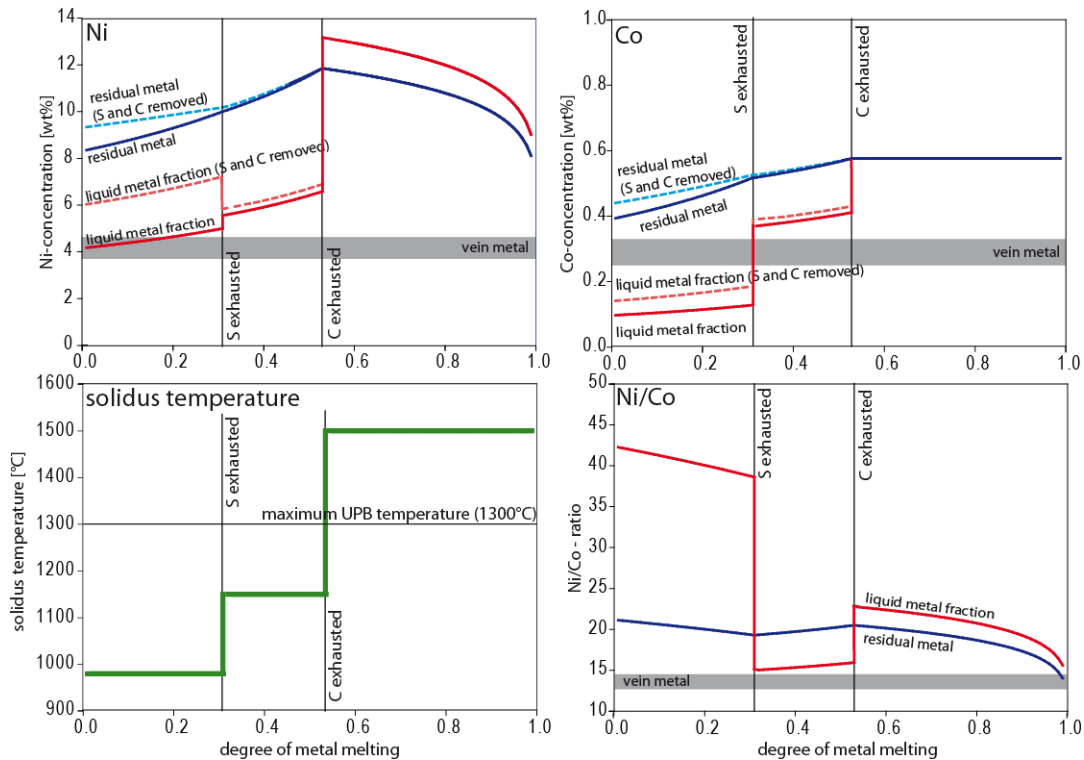


**Fig. 80** Concentrations of Ni and Co, solidus temperatures and Ni/Co-ratio during fractional melting of the metal fraction (Fe-Ni-S-C-Co) of an oxidized parent body (e.g. GRA95205) with a carbon- and sulfur-poor H-chondritic composition.

### ***Is the vein metal the result of a fractional melting process on the UPB?***

Depending on the starting composition, the models of the fractional melting process produce different types of residues and melts. Scenarios with high amounts of sulfur (>20 wt%) and carbon (>10 wt%) in the primary metal component produce a carbon-rich residuum, while Fe-metal is entirely removed. Scenarios with intermediate sulfur and carbon concentrations (>10 wt% S and ~3 wt% C) produce either a carbon rich residuum or a FeNi-metal residuum. Scenarios with low amounts of sulfur and carbon (<10 wt% S and ~2 wt% C) produce a FeNi-metal residuum.

**Residual metal:** The scenarios that produced a residual FeNi-metal did produce large quantities of it (between 30 and 70% of the initial metal portion). This is inconsistent with a > 95 wt% metal removal observed in ureilites. The metal residues are richer in Ni (factor 2 - 3) and Co (factor 1 - 2) than the ureilite vein metal. The Ni/Co-ratio of the metal residues is a factor ~2 higher than in the vein metal.

If we assume that the maximum temperatures on the UPB were higher than 1300°C, a pure FeNi-metal residue can be removed. A reduced, carbon- and sulfur-poor starting composition could then produce a metal residuum that closely resembles the vein metal

(Fig. 79) when ~95% of the initial metal are removed. But, as neither the required low amounts of carbon nor the high temperature are consistent with observations in ureilites, this scenario is not very plausible. In addition, the majority of ureilites does not appear to be highly reduced (MITTFELDT et al. 1998).

*Residual Carbon:* Residual carbon is produced from fractional melting of a C11-chondritic parent body and (in very low quantities) from fractional melting of an oxidized CV3-chondritic parent body. The primary metal component comprises between ~30 and 54 wt% of the original parent body. Carbon concentrations in ureilites are ~3 wt% with peak carbon concentrations of ~6 wt% (e.g. GRADY et al. 1985). An carbon residuum that represents 18 wt% of the original metal component, like it has been calculated for a C11-chondritic starting composition in an oxidized parent, would correspond to 7.7 wt% carbon in the bulk ureilite. While this is not a perfect match, it demonstrates that minor variations of the initial model carbon concentrations (which were estimated maximum concentrations), could account for the carbon concentrations in bulk ureilites. If, for example, the initial carbon-concentration was lowered to 9 wt% (from 16 wt%), the residual carbon content of bulk GRA95205 would be 3.8 wt%.

*Metal melts.* Due to the difference of  $D_{Ni}^f$  and  $D_{Co}^f$ , the Ni/Co-ratio in S-rich melts is always >30, effectively ruling out those melts as a source of the vein metal. Moreover, eutectic melts contain ~31 wt% of S, which is not observed in actual ureilite vein metal either.

The Ni/Co-ratio observed in C-rich melts is generally lower due to the shift in  $D_{Co}^f$  from 4 to 1.4. As a result, at least some quantities of partial C-melt produced by reduced parent bodies (regardless of the chondritic starting composition) show similarities to ureilite vein metal with respect to Ni- and Co-concentrations as well as Ni/Co-ratio (Fig. 75, Fig. 77, Fig. 79).

Eutectic, carbon-rich melts contain ~4.5 wt% of carbon. If such a melt crystallizes slowly, carbon crystallizes as graphite in equilibrium with FeNi-metal (HORSTMANN 2004). Graphite and FeNi-metal are commonly observed in ureilite vein material. The disequilibrium between vein metal and olivine suggests that the vein metal was emplaced shortly before the impact or when the UPB had already cooled, thus preventing equilibration. If the vein metal would represent a melt fraction, it should have been quenched by the impact, which would result

in the crystallization of cohenite instead of graphite (HORSTMANN 2004). While cohenite has been observed in spherule inclusions, it has not been found in ureilite vein metal.

Only a fraction of the modeled C-rich liquid is similar to the vein metal and the complementary C-rich melts have also not been found in the ureilite. Carbon-rich melts resembling vein metal have only been modeled for very reduced parent body compositions. It is imaginable that oxidized ureilite assemblages have been swept clean of their own initial metal portion and then injected with such a carbon-rich melt from a more reduced assemblage. But it appears unlikely that such a process would produce ureilites with similar metal content and composition.

Fractional melting alone does therefore not provide a suitable explanation for the origin of the ureilite vein metal. Fractional melting does, however, represent a way to completely remove the primary metal component of the ureilite parent body using a combination of S-rich and C-rich melts and leaving a carbon residue behind.

### 9.3.3 Modeling of batch melting on the ureilite parent body

#### *Description of the batch melting process*

In contrast to fractional melting, batch melting requires simultaneous monitoring of sulfur and carbon in the system. Unfortunately, little information is available on the behavior of carbon and sulfur-rich systems at temperatures below 1100°C (RAGHAVAN 1988, WANG et al. 1991, OHTANI and NISHIZAWA 1987). The available data agree on the presence of a carbon-rich and a sulfur-rich immiscible liquid at temperatures above ~1100°C. GOODRICH and BERKLEY (1986) have adapted a ternary Fe-FeS-Fe<sub>3</sub>C-diagram from VOGEL and RITZAU (1931) that is also used in this study.

It is assumed that melting commences near the eutectic temperature of the Fe-S-System at about ~950°C (GOODRICH and BERKLEY 1986, RANKENBURG et al. 2008, VAN ORMAN et al. 2009). The first melt formed is a eutectic sulfur-rich melt with ~31 wt% S. Melt generation continues until sulfur is exhausted in the residual metal. At that point, the solidus temperature of the system increases, as the amount of S in the melt decreases.

At ~1100°C, the formation of a C-rich melt starts. The composition of the C- and the S-rich melt has been taken directly from the ternary Fe-FeS-Fe<sub>3</sub>C-diagram in GOODRICH and BERKLEY (1986). The S-rich melt contains ~28 wt% S and ~0.3 wt% C, while the C-rich melt contains ~1 wt% S and ~4 wt% C. As most of the S of the system is contained in the S-rich melt, the C-rich melt is formed partly at the expense of the S-rich melt. The formation of the C-rich eutectic melt will continue until C is depleted in the residual metal.

At that point, the solidus temperature increases again, while S- and C-concentrations in the respective liquids decrease. The solidus temperature will increase until the whole system is molten, or the estimated peak temperature of ~1300°C for the ureilite parent body is reached. As ureilites have lost >95 wt% of their initial metal component, it is assumed that the melt is removed when 95% of the primary metal component is molten.

### ***Starting compositions rich in carbon and sulfur***

In a C- and S-rich parent body (Fig. 81, Fig. 82), similar to a CI1-chondrite, partitioning behavior is dominated by S as has been proposed by a number of authors (e.g. WARREN et al. 2006, RANKENBURG et al. 2008). In case of a reduced parent body (Fig. 81), only small amounts of C-rich melts are formed (~15 wt%) until Fe is exhausted, leaving a carbon residue. An oxidized parent body (Fig. 82) might not produce a C-rich melt at all, as the system contains sufficient S to completely melt all of the metal at temperatures lower than 1100°C.

In both modeled systems the inferred Ni and Co concentrations of the residual metal are far greater than those observed in our ureilite vein metal. The calculated Ni/Co-ratios argue against S-rich melt as origin for the vein metal. The C-rich liquid is, although not a perfect fit, similar to the vein metal with respect to Ni- and Co-concentrations as well as Ni/Co-ratio.

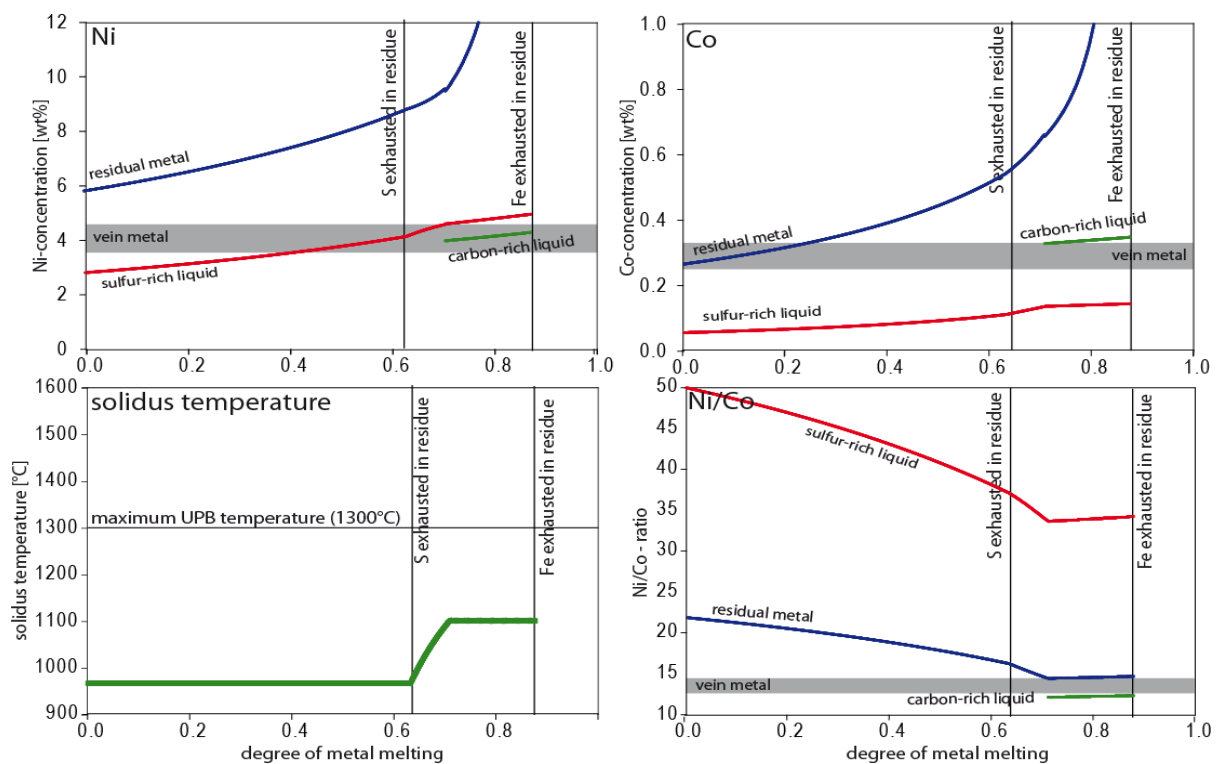


**Fig. 81** Concentrations of Ni and Co, solidus temperatures and Ni/Co-ratio during batch melting of the metal fraction (Fe-Ni-S-C-Co) of a reduced parent body (e.g. ALH84136) with a carbon- and sulfur-rich CI1 chondritic composition. The concentrations of Ni and Co have been normalized to pure Fe-Ni-Co-metal.

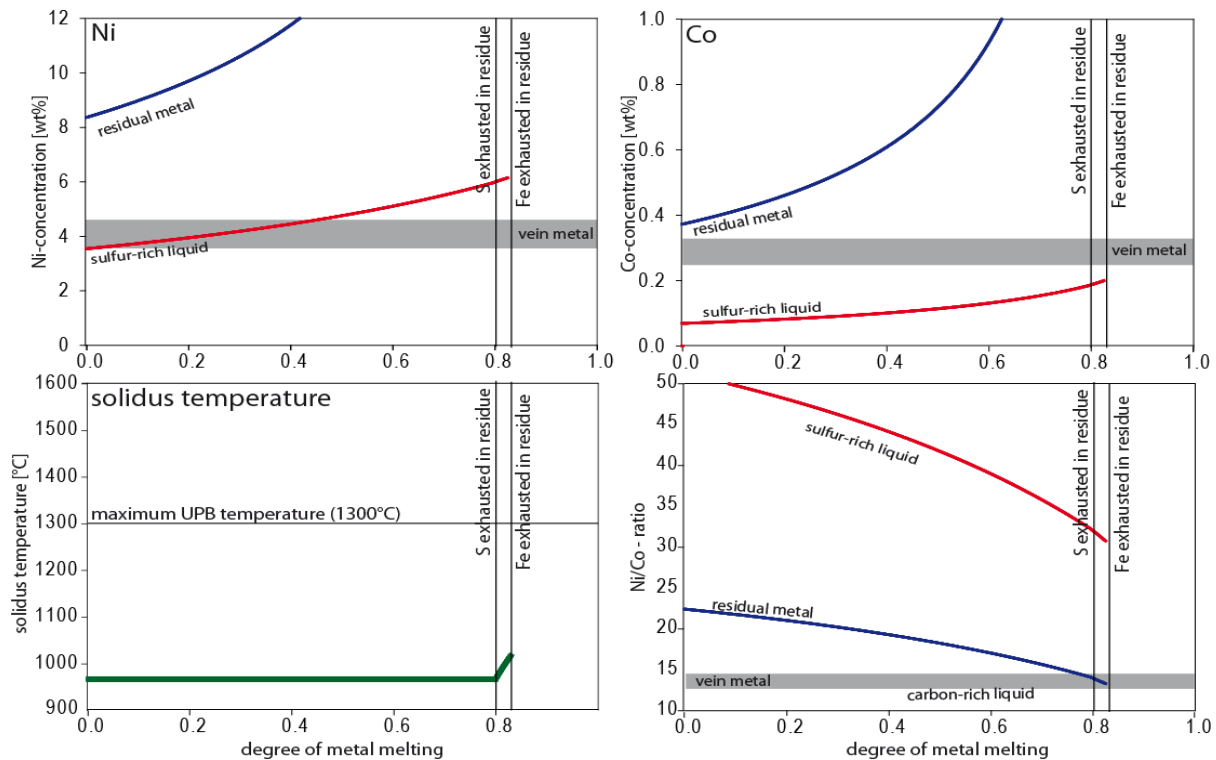


**Fig. 82** Concentrations of Ni and Co, solidus temperatures and Ni/Co-ratio during batch melting of the metal fraction (Fe-Ni-S-C-Co) of an oxidized parent body (e.g. GRA95205) with a carbon- and sulfur-rich CI1 chondritic composition. The concentrations of Ni and Co have been normalized to pure Fe-Ni-Co-metal.

### *Starting compositions with moderate sulfur- and carbon-contents*

Models based on a CV3-chondritic parent body with intermediate sulfur and carbon-concentrations produce different results based on the degree of oxidation assumed. On a reduced parent body (Fig. 83), a Fe-S eutectic melt is formed until S is exhausted in the residual metal at ~25% melting. The solidus temperature of the system increases, while S becomes depleted in the melt, until it reaches ~1100°C. At this temperature the eutectic C-rich melt is formed. Formation of the Fe-C-eutectic melt persists until C is depleted in the residue at ~88% melting. At that point, the solidus temperature of the system increases again, until the whole system is molten at ~1270°C.

In contrast, a more oxidized parent body contains higher relative amounts C and S in the metal portion. After the formation of the Fe-S-eutectic melt, Fe-C eutectic melt is generated and Fe is exhausted at ~99% of melting, generating a carbon rich residue.

This starting composition does not produce a metal residue or a metal liquid that constitutes a suitable candidate for the ureilite vein metal.

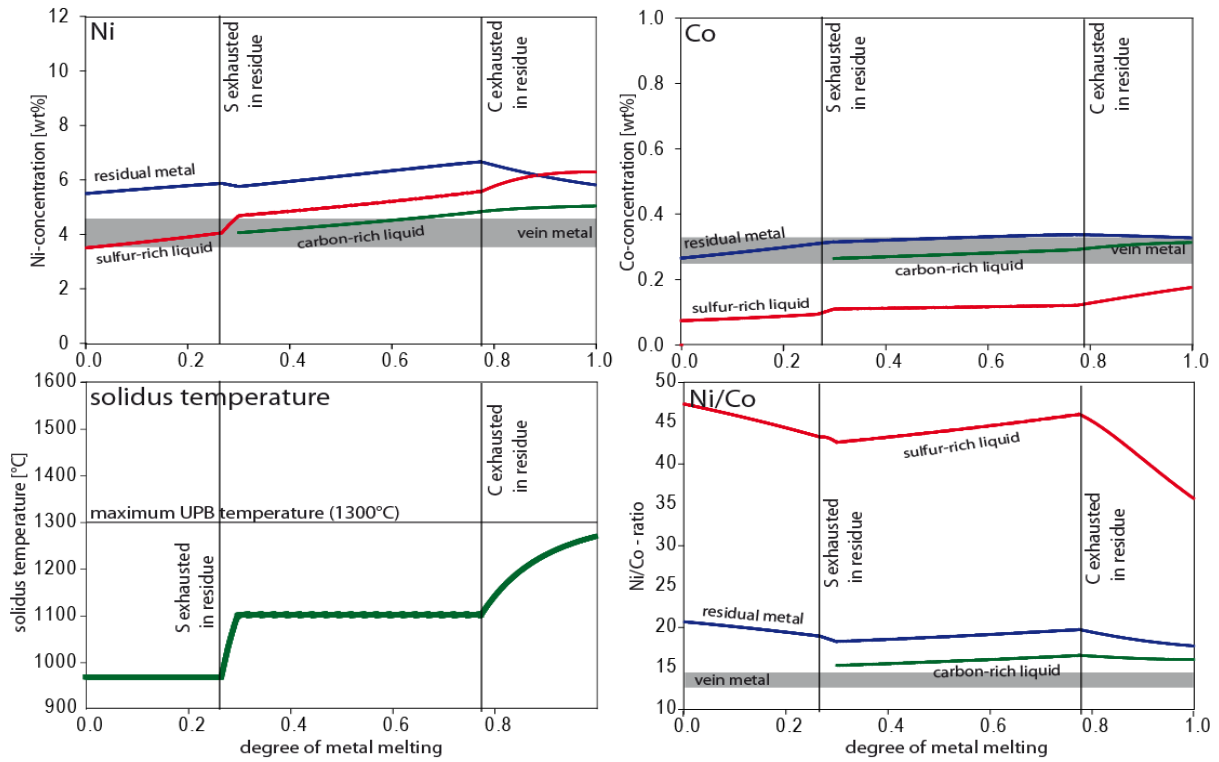


**Fig. 83** Concentrations of Ni and Co, solidus temperatures and Ni/Co-ratio during batch melting of the metal fraction (Fe-Ni-S-C-Co) of a reduced parent body (e.g. ALH84136) with intermediate carbon- and sulfur-concentrations similar to a CV3-chondritic composition. The concentrations of Ni and Co have been normalized to pure Fe-Ni-Co-metal.

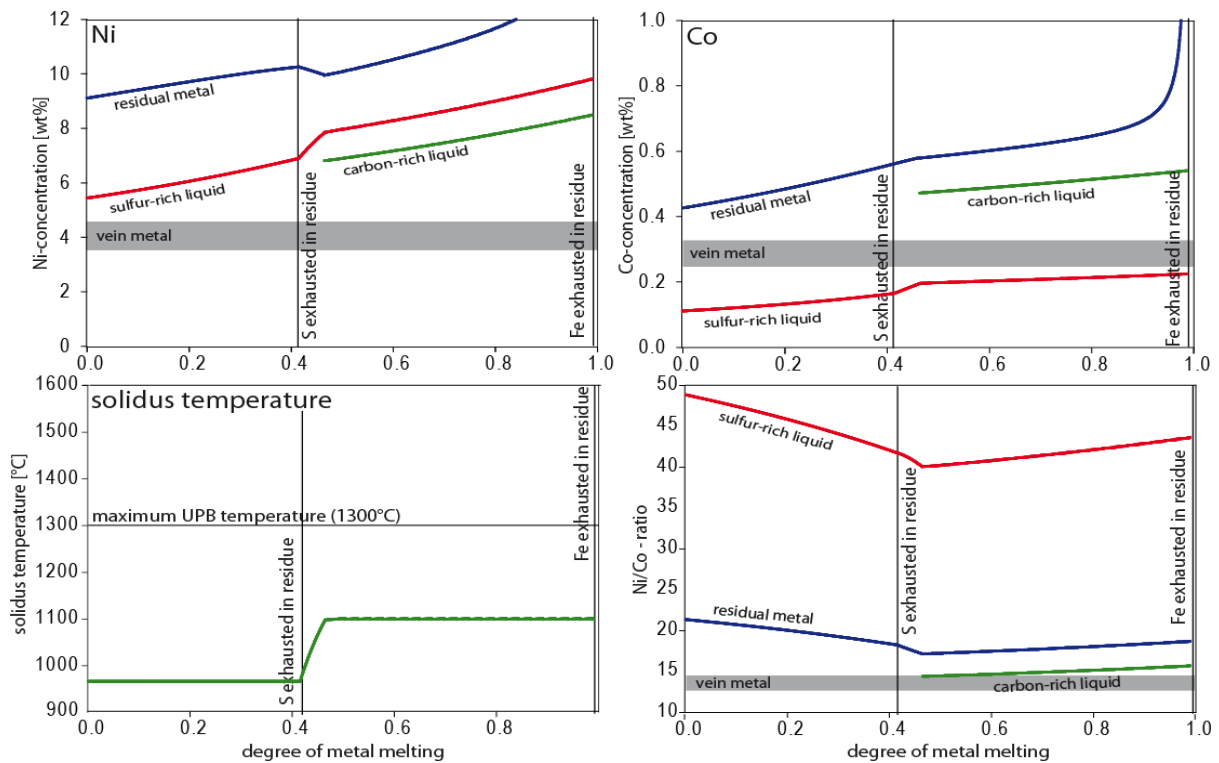


**Fig. 84** Concentrations of Ni and Co, solidus temperatures and Ni/Co-ratio during batch melting of the metal fraction (Fe-Ni-S-C-Co) of an oxidized parent body (e.g. GRA95205) with intermediate carbon- and sulfur-concentrations similar to a CV3-chondritic composition. The concentrations of Ni and Co have been normalized to a pure Fe-Ni-Co-metal.

### ***Starting compositions with low sulfur- and carbon-contents***

Batch melting on a parent body of H-chondritic composition will produce similar results, regardless of the degree of oxidation (Fig. 85, Fig. 86). At ~980°C, the Fe-S-eutectic melt forms, followed by the Fe-C-eutectic melt at ~1100°C. Both liquids will become progressively depleted in carbon and sulfur as the solidus temperature rises, until the whole metal is molten. The calculated solidus temperatures of the more reduced system are slightly above the estimated maximum temperature of the ureilite parent body. Neither the melts nor the metal residues resemble the ureilite vein metal.

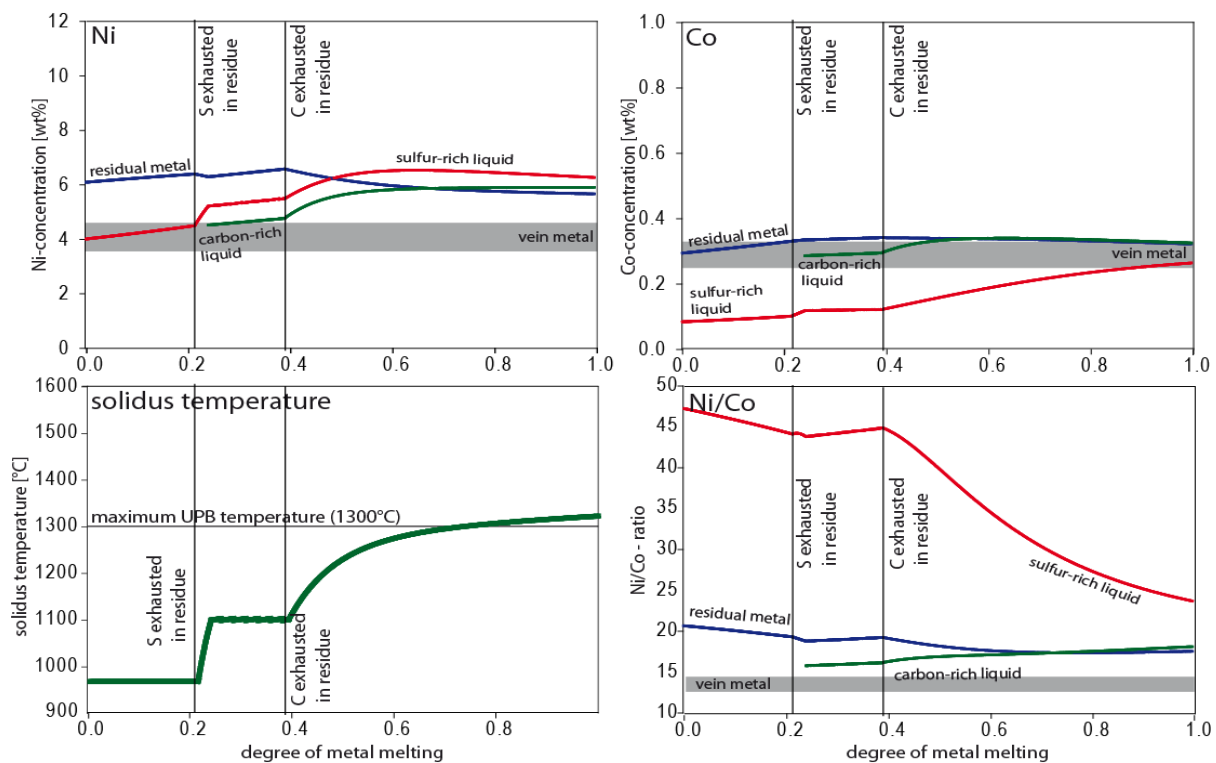


**Fig. 85** Concentrations of Ni and Co, solidus temperatures and Ni/Co-ratio during batch melting of the metal fraction (Fe-Ni-S-C-Co) of a reduced parent body (e.g. ALH84136) with low carbon- and sulfur-concentrations similar to a H-chondritic composition. The concentrations of Ni and Co have been normalized to pure Fe-Ni-Co-metal.

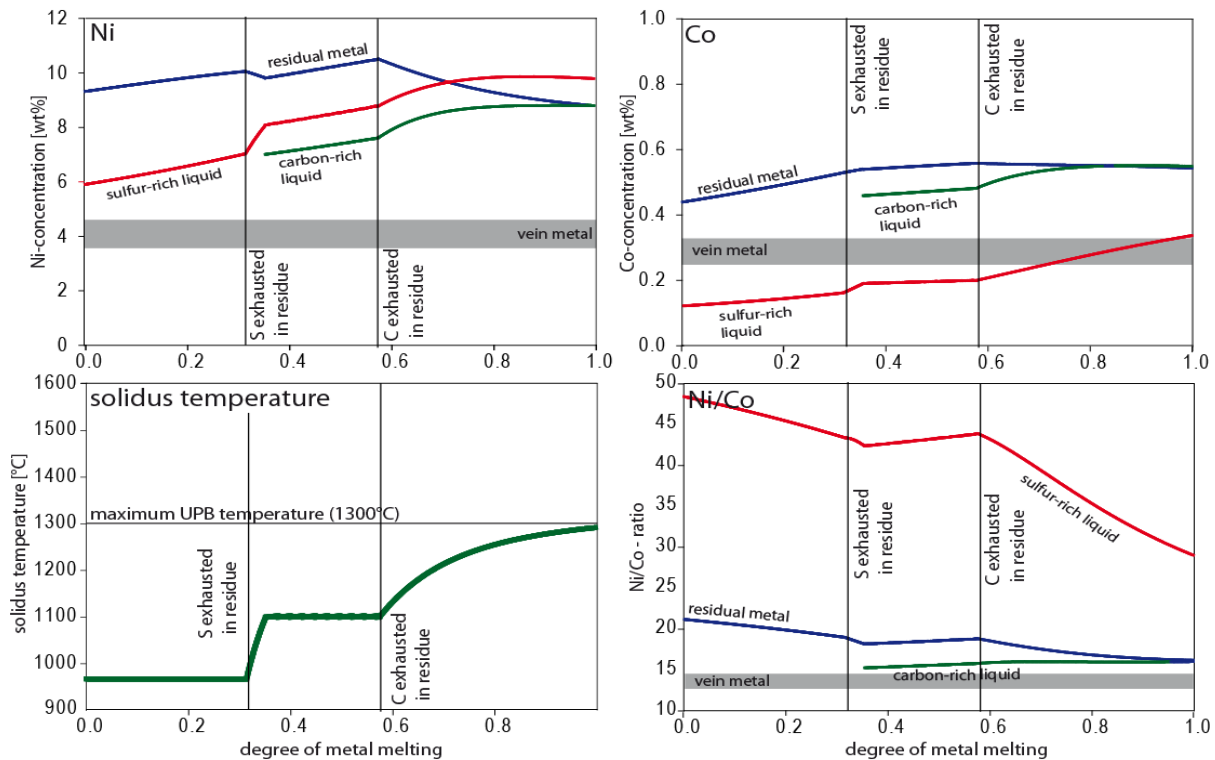


**Fig. 86** Concentrations of Ni and Co, solidus temperatures and Ni/Co-ratio during batch melting of the metal fraction (Fe-Ni-S-C-Co) of an oxidized parent body (e.g. GRA95205) with low carbon- and sulfur-concentrations similar to a H-chondritic composition. The concentrations of Ni and Co have been normalized to pure Fe-Ni-Co-metal.

### ***Is the vein metal the result of a batch melting process on the UPB?***

**Residual metal:** Similar to fractional melting, batch melting will not produce residual metal that resembles the ureilite vein metal. In all calculated scenarios, Ni concentrations of residual metal were higher (factor ~1.5-3+) than observed in ureilite vein metal. Similarly, Co-concentrations are too high for most scenarios, except scenarios with low to moderate sulfur- and carbon-concentrations and a reduced parent body (Fig. 83, Fig. 85). Ni/Co ratios of the residual metal are generally higher than observed ratios, except for very carbon- and sulfur-rich parent body compositions (Fig. 81, Fig. 82). In order to represent a suitable model for the origin of ureilite vein metal, all three conditions (Ni and Co-concentrations and Ni/Co-ratio) must be met.

**Residual carbon:** Both oxidized and reduced parent bodies produce large carbon residues of 10-20 wt% of the initial model core metal, for sulfur- and carbon-rich starting compositions.

An oxidized parent body with moderate concentrations of carbon and sulfur would produce a small carbon residue of 1-3 wt%, which is consistent with carbon concentrations observed in bulk ureilites.

*Sulfur-rich metal melt:* Generated sulfur-rich melts are generally too high in Ni and too low in Co to be suitable candidates for ureilite vein metal. The calculated Ni/Co-ratio is generally a factor of 2 – 4 higher than in vein metal.

*Carbon-rich metal melt:* Calculated carbon-rich melts are generally too high in Ni as well as Co and Ni/Co-ratio. An exception is a reduced parent body with high sulfur- and carbon-concentrations. The composition of calculated carbon-rich melts in such a UPB are close to the composition of vein metal (Fig. 81). Although not a perfect fit, fine tuning of sulfur and carbon-concentrations in the starting composition can produce a carbon-rich melt that fits the ureilite vein metal. Decreasing the assumed sulfur-concentrations by ~4 wt% would, for example, result in a perfect fit for the Ni- and Co-concentrations and Ni/Co-ratios. Such a melt contains ~4 wt% of carbon which is consistent with ureilite vein metal.

Again, carbon-rich melts that resemble ureilite vein metal are only produced on reduced parent bodies. They therefore do not represent an explanation for the origin of vein metal in the majority of ureilites with  $f_{a_{>18}}$ .

## 9.4 Ureilite vein metal as a secondary component

### 9.4.1 The complete removal of the initial chondritic metal portion

If the vein metal represents a secondary component in the UPB, the original metal from the chondritic parent body has been removed, possibly into a metal core.

The initial metal component can be completely molten either by batch melting or by fractional melting. For a fractional melting process, this would require a parent body with at least moderate sulfur- and carbon-concentrations (~3 wt% carbon, 8-13 wt% sulfur). In scenarios modeled for these starting compositions all metal is removed leaving behind only residual carbon.

In batch melting the metal component of sulfur- and carbon-poor starting compositions are completely molten at the assumed ureilite peak temperatures of ~1300°C. In case of carbon- and sulfur-rich starting compositions a carbon residual is left behind.

The original metal component represents 30 - 55 wt%, and thus 15 - 30 vol% of the parent body, providing pathways for segregation. A complete loss of the metal component either by fractional or by batch melting therefore is a possible scenario.

### 9.4.2 Secondary addition of metal from silicate reduction

If the ureilite parent body had been swept clean of its initial metal component, a possible source of metal in the ureilite is the reduction of silicates in the presence of carbon (i.e. “smelting”). It has been proposed that smelting is responsible for the different *f<sub>a</sub>* of ureilite olivine (e.g. BERKLEY and JONES 1982) and the source of vein metal (GOODRICH et al. 2004).

Trace element studies of ureilite silicates (this work, ASH et al. 2009) show that Ni and Co concentrations in ureilite silicates are <150 µg·g<sup>-1</sup>. A Fe-rich metal produced from reduction contains only ~0.04 wt% of Ni and ~0.02 wt% of Co. The amount of metal produced depends on the degree of reduction in the ureilite. The reduction of an iron-rich olivine with ~20 wt% of FeO (similar to olivine in GRA95205 or Kenna) to an iron-poor olivine with ~2 wt% of FeO (similar to olivine in ALH84136) produces ~11 wt% of Fe-rich metal (WARREN et al. 2006). As a result, metal concentrations in ureilites would be negatively correlated with olivine FeO,

which is not observed. It can therefore be concluded that the ureilite vein metal could not have been produced from reduction of silicate material.

### **9.4.3 Secondary addition of metal from an metal-rich impactor**

Several authors have proposed the presence of two components: One that is refractory poor and associated with the vein material and one that is refractory-rich (BOYNTON et al. 1976, HIGUCHI et al. 1976, JANSSENS et al. 1987). Shock features, thermal history and the reduced rims suggest that the ureilite parent body was catastrophically disrupted by impact of another asteroid (e.g. GOODRICH et al. 2004). It was therefore suggested that the ureilite carbon and part of the siderophile elements had been injected through an impactor into the ureilite parent body (e.g. WASSON et al. 1976, RANKENBURG et al. 2008). The presence of carbon rich spherule inclusions, on the other hand, indicates that at least a part of the carbon was a primary component (GOODRICH and BERKLEY 1986).

Assuming that the ureilite parent body material had been swept clean of its initial metal portion, it is possible that the vein metal represents metal introduced into the system by the impactor. Such a metal rich impactor could have been similar to one of the known iron meteorites. Fig. 87 therefore shows Ni/Co-ratio and Ni concentrations in iron meteorites and ureilite vein metal.

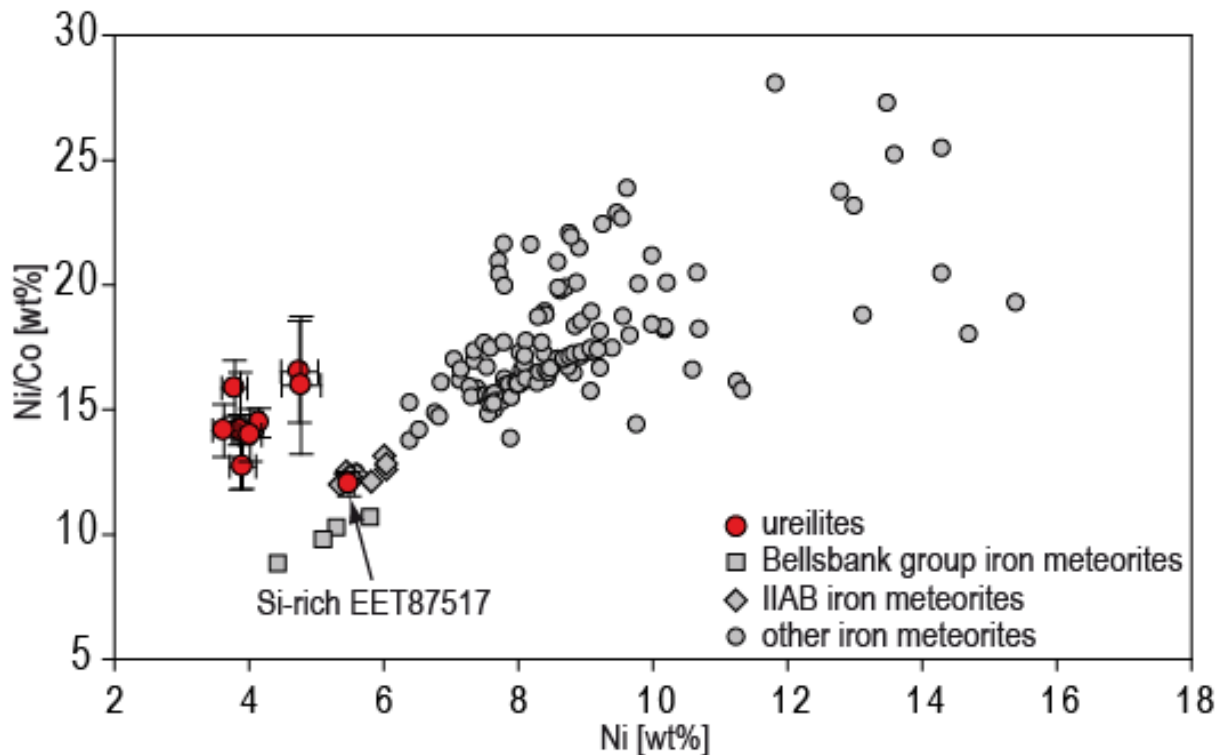


Fig. 87 Ni concentrations in several iron meteorites and ureilite vein metal plotted against bulk Ni/Co-ratios. Iron meteorite data from KRACHER et al. (1980), MALVIN et al. (1984b), MALVIN et al. (1984a), WASSON et al. (1989), WASSON et al. (1998) and RUSSELL et al. (2004). Iron meteorites show a linear trend, pointing towards the origin. Except for the Si-rich vein metal in EET87517, ureilites are clearly off the trend.

According to published iron meteorite data (KRACHER et al. 1980, MALVIN et al. 1984b, MALVIN et al. 1984a, WASSON et al. 1989, WASSON et al. 1998, RUSSELL et al. 2004), most iron meteorites show higher Ni-concentrations than ureilite vein metal. The iron meteorites of the Bellsbank-group resemble the ureilite vein metal most closely with respect to Ni concentrations. However, the Bellsbank-group meteorites exhibit high P-concentrations of  $\sim 2$  wt% (MALVIN et al. 1984a), while P is  $< 0.25$  wt% in ureilite vein metal. It has been suggested that the Bellsbank-group iron meteorites formed from an immiscible P-rich liquid on the IIAB-parent body (MALVIN et al. 1984b).

Iron meteorites show a positive correlation of Ni/Co-ratio and Ni concentrations. Although this correlation becomes less pronounced at higher Ni-concentrations, ureilites clearly define a singular group outside the trend of the iron meteorites (Fig. 87). IIAB-Irons, which show similar Ni/Co-ratios to ureilites, exhibit  $\sim 2$  wt% higher Ni-concentrations. One exception is the Si-rich vein metal portion of the EET87517 ureilite, which shows a Ni/Co-ratio and Ni-concentrations very similar to IIAB-irons. This might indicate a connection between IIAB

irons and ureilites. However, only one of nine examined ureilites shows a IIAB-like metal component.

Although no group of iron meteorites can be clearly linked to ureilite vein metal, it is possible that such an iron-rich meteorite exists and has not been sampled yet. In CHABOT (2004), mass balance calculations have been performed in order to infer the initial sulfur-content in the IIAB metallic melt. According to these calculations the IIAB-iron meteorites might have formed by fractional crystallization from a parental core composition with ~17 wt% S.

In a similar way, we modeled fractional crystallization of an extremely reduced (all Fe in metal) and Ni-poor parent body (Fig. 88). The chosen starting composition was the Ni-poor LL-chondrite Manych (JAROSEWICH 1990). The metal core of an extremely reduced Manych-like composed parent body contains 4.54 wt% Ni and 0.28 wt% Co. Other LL-chondritic compositions such as Greenwell Springs, Cherokee Springs and Karatu give similar low-Ni and low-Co starting compositions.

The sulfur-dependent distribution coefficients  $D_{Ni}^f$  and  $D_{Co}^f$  were taken from CHABOT et al. (2003).

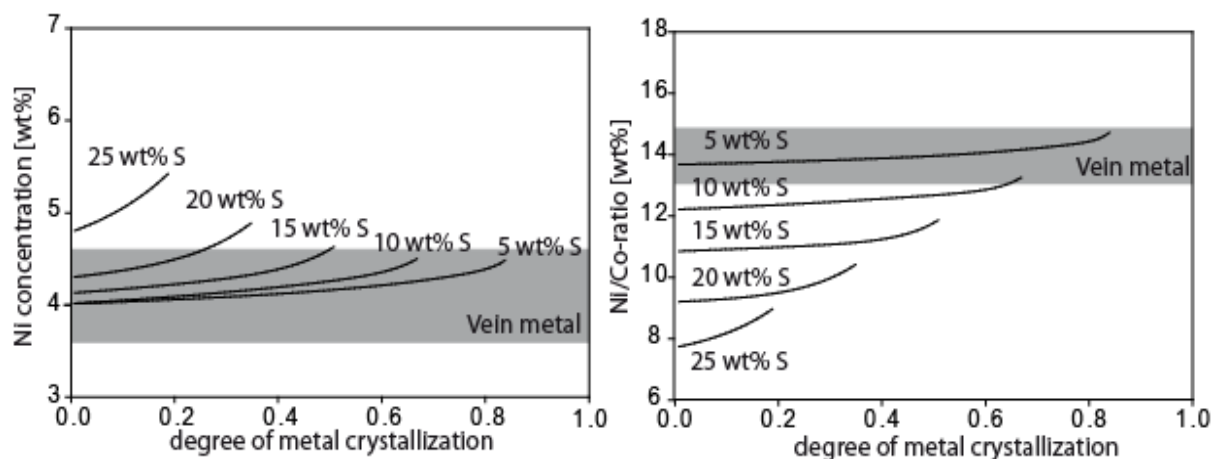


**Fig. 88** Ni concentrations and Ni/Co-ratio in modeled metal produced from fractional crystallization of a Ni- and Fe-poor LL-chondritic starting composition. Calculations were performed for different sulfur-concentrations in the initial metal portion.

The calculations were performed for 5 %, 10 %, 15 %, 20 % and 25% of S in the starting composition. Crystallization persists until sulfur in the residual melt approaches the eutectic composition at 31 wt% S.

A fractional crystallization of a Ni-poor metal core with 5-10 wt% S can produce metal similar to ureilite vein metal. With respect to Ni- and Co-concentrations as well as Ni/Co-ratios, ureilite vein metal could represent metal from such a metal-rich impactor.

Such a metal-rich impactor would explain, why the ureilite siderophile elements show no correlation with olivine  $f_a$  of each ureilite. It would also explain why the ureilite vein metal is not in equilibrium with adjacent olivine grains.

## 9.5 Ureilite vein metal as mixture of primary and secondary components

### 9.5.1 Batch and fractional melting and addition of Ni-poor metal from silicate reduction

Most calculated scenarios produced melts and metal residues that were higher in Ni and Co than ureilite vein metal. The addition of Ni- and Co-poor metal from reduction might represent a mechanism to explain low Ni- and Co-concentrations in the vein metal. The metal produced from smelting is added either during the fractionation process or to the respective FeNi-metal or carbon residue at the end of the fractionation process.

The addition of Ni- and Co-poor metal from reduction to a carbon residue is no explanation for the formation of ureilite vein metal as the composition of the added metal does not change during this process.

The addition of metal from smelting during a batch melting process before the metal liquid is removed is already accounted for through the starting compositions of the batch melting models. If, for example, a FeO-rich, oxidized parent body (e.g. GRA95205) was almost completely reduced, the resulting composition would be identical to that assumed for a FeO-poor reduced parent body (e.g. ALH84136). As batch melting is considered to be a continuous process where equilibrium between liquid metal and solid metal is maintained, the addition of Ni-poor Fe from reduction would produce result similar to the model calculations for a reduced parent body.

The addition of metal from smelting during a fractional melting process is hampered by temperature. The estimated temperatures, at which smelting starts, are  $\sim 1040^{\circ}\text{C}$  at low pressures of  $\sim 3$  MPa in the shallowest regions of the UPB and up to  $1280^{\circ}\text{C}$  at  $\sim 12.6$  MPa at greater depth (SINGLETARY and GROVE 2006, GOODRICH et al. 2007). It has been suggested (e.g. SINGLETARY and GROVE 2003) that 'normal' ureilites with  $f_{a \sim 20}$  represent assemblages from greater depth in the UPB, while reduced ureilites with  $f_{a < 20}$  represent assemblages from a more shallow position in the UPB.

In a fractional melting process of reduced starting composition, smelting starts at temperatures of  $\sim 1040^{\circ}\text{C}$ . Sulfur would already be completely exhausted in such a system

and the metal from smelting is added to the carbon-rich liquid. The composition of the carbon-rich-liquid would, depending on the amount of added Ni-poor metal, resemble the composition of ureilite vein metal. Such a vein-metal like C-rich liquid is only produced from reduced starting compositions and does therefore not represent a viable source of ureilite vein metal for the majority of ureilites.

The majority of ureilites show  $f_{a \sim 20}$  (MITTLEFEHLDT et al. 1998). For those ureilites, smelting is not assumed to start at temperatures lower than 1200°C (GOODRICH et al. 2007). At that temperature, in the fractional melting model, S-rich and C-rich melts have already been removed, leaving either a FeNi-metal residue or a carbon residue.

The addition of a Ni- and Co-poor metal to a Ni- and Co-rich FeNi-metal residue produced either from batch or from fractional melting lowers the concentrations of Ni and Co, while leaving the Ni/Co-ratio of the metal unchanged. The Ni/Co-ratio of the residual metal in all modeled scenarios is  $\sim 20$  and higher than the observed Ni/Co-ratio in ureilite vein metal of  $\sim 14$ . A further differentiation of the residual metal can lower the Ni/Co-ratio, but would require temperatures higher than the estimated peak temperature of  $\sim 1300^\circ\text{C}$ .

Smelting would also result in a pronounced correlation of the vein metal composition with olivine  $f_a$  which is not observed in our data. It can therefore be concluded that there is no evidence for the addition of metal from reduction to the vein metal.

Ni-poor metal could have been added through the secondary reduction process that produced the reduced rims in olivine and pyroxene grains. However, small Ni-poor metal speckles are abundant within the reduced rims and it appears not likely that the Ni-poor metal has left the silicate grains in large quantities.

### **9.5.2 Batch and fractional melting and addition of metal from an impactor**

The px-px- or ol-px-equilibration temperatures calculated for several ureilites (SINHA et al. 1997, SINGLETARY and GROVE 2003) record the temperatures at the impact at 1300°C. At this temperature, the fractionation processes of most fractional and batch melting models are finished. The metal from the impactor would be injected into a FeNi-residue, a carbon residue or into a melt fraction that has migrated into a silicate assemblage.

The FeNi-metal residues calculated in the models are higher in Ni and Co than the vein metal. If the vein metal represents a mixture of a FeNi-metal residue and a metal-rich impactor, that impactor must have been even poorer in Ni than previously calculated for extremely Ni-poor starting compositions. This is also the case when such a metal-rich impactor is injected into a melt fraction. The necessary almost Ni- and Co-free impactor cannot have formed from a chondritic starting composition by fractional crystallization.

If, however, an impactor of approximately vein metal-like composition would be injected into a carbon-residue, the result would be very similar to the ureilite vein material. This scenario presents the most viable explanation for the formation of the ureilite vein metal.

## 9.6 Ni-Isotope systematics

The Fe/Ni-ratios measured in the silicate fractions of Kenna (Fe/Ni = 668), EET87517 (Fe/Ni = 68.2), ALHA77257 (Fe/Ni = 827) and EET96042 (Fe/Ni = 370) are much lower than the Fe/Ni-ratios of pure olivine and orthopyroxene. Fe/Ni-ratios range from ~1718 (EET87517) to ~2023 (Kenna) in olivine and from ~2864 (EET87517) to ~4741 (ALHA77257) in orthopyroxene. Depending on the respective olivine/pyroxene ratio, the Fe/Ni-ratio of a pure silicate fraction is in between the Fe/Ni-ratio of olivine and the Fe/Ni-ratio of orthopyroxene.

The low Fe/Ni-ratios of the silicate-rich fraction indicate that traces of vein metal and metal inclusions have been included in the measurements. In order to calculate the respective amounts of the three components, a set of equations was used (Eq. 50 - Eq. 52).

$$c_{\text{sample}}^{\text{Fe}} = X_{\text{ol}} \cdot c_{\text{ol}}^{\text{Fe}} + X_{\text{opx}} \cdot c_{\text{opx}}^{\text{Fe}} + X_{\text{met}} \cdot c_{\text{met}}^{\text{Fe}} \quad \text{Eq. 50}$$

$$c_{\text{sample}}^{\text{Ni}} = X_{\text{ol}} \cdot c_{\text{ol}}^{\text{Ni}} + X_{\text{opx}} \cdot c_{\text{opx}}^{\text{Ni}} + X_{\text{met}} \cdot c_{\text{met}}^{\text{Ni}} \quad \text{Eq. 51}$$

$$X_{\text{ol}} + X_{\text{opx}} + X_{\text{met}} = 1 \quad \text{Eq. 52}$$

X represents the weight fraction, while c represents the concentration of the respective elements in different components. The Fe-concentrations in silicates and vein metal as well as Ni in vein metal has been determined with EPMA. Ni concentrations in silicates have been determined with LA-ICP-MS. In this work, the Excel solver-function was used to determine  $X_{\text{ol}}$ ,  $X_{\text{opx}}$  and  $X_{\text{met}}$ , based on Eq. 50 - Eq. 52. The weight fraction of Ni from vein metal ( $X_{\text{vein}}^{\text{Ni}}$ ) in the silicate-rich sample can be calculated (Eq. 53).

$$X_{\text{vein}}^{\text{Ni}} = \frac{X_{\text{met}} \cdot c_{\text{vein}}^{\text{Ni}}}{c_{\text{sample}}^{\text{Ni}}} \quad \text{Eq. 53}$$

The  $c_{\text{vein}}^{\text{Ni}}$  of the pure silicate portion is calculated as mass balance from  $X_{\text{vein}}^{\text{Ni}}$  (Eq. 54, Eq. 55).

$$(\epsilon_{60}^{Ni*})_{sample} = [(\epsilon_{60}^{Ni*})_{pure\ silicate} \cdot (1 - X_{vein}^{Ni})] + (\epsilon_{60}^{Ni*})_{met} \cdot X_{vein}^{Ni} \quad \text{Eq. 54}$$

$$(\epsilon_{60}^{Ni*})_{pure\ silicate} = \frac{[(\epsilon_{60}^{Ni*})_{sample} - (\epsilon_{60}^{Ni*})_{met} \cdot X_{vein}^{Ni}]}{(1 - X_{vein}^{Ni})} \quad \text{Eq. 55}$$

The corrected  $\epsilon^{60}Ni^*$  values range from  $-1.19 \pm 0.31$  to  $-9.19 \pm 5.36 \epsilon u$  (Table 35). The  $2\sigma$ -errors were calculated assuming an error of 10% for the solver-model. The very low  $\epsilon^{60}Ni^*$  of EET87517 is a result of the very low Fe/Ni-ratio (Fe/Ni = 68.2) of the silicate sample. This indicates a high degree of vein metal contamination. The extrapolation of data to pure silicate material is therefore significantly less reliable for this sample.

ureilite	Ni-contribution from vein metal [wt%]	Fe/Ni-ratio (pure silicate)	$\epsilon^{60}Ni^*$ (corrected values)	$2\sigma$
Kenna	72.4	3173	-3.08	0.54
EET87517	98.2	3858	-9.19	5.36
ALHA77257	67.3	3342	-1.19	0.31
EET96042	85.3	3241	-3.41	0.80
Weighted average	-/-	3404	-2.24	0.89

Table 35 vein metal-contamination, calculated Fe/Ni-ratios of pure silicate and corrected  $\epsilon^{60}Ni^*$ -values.

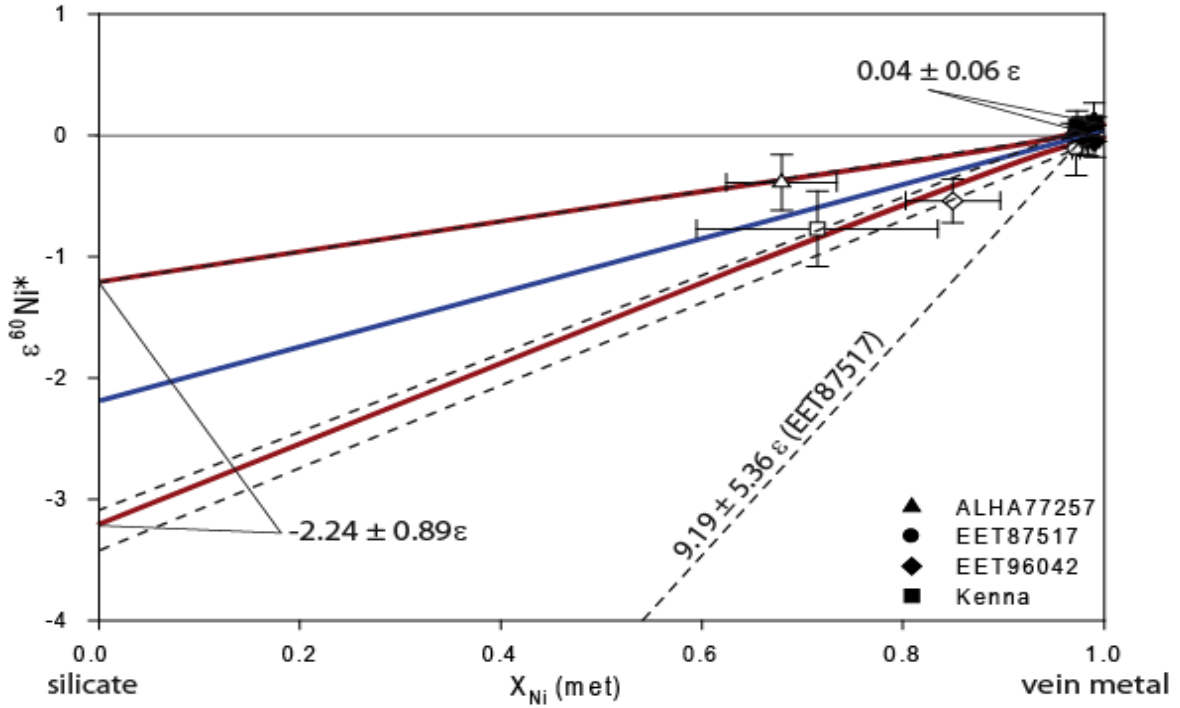


Fig. 89 Weight fraction of vein metal in the ureilite samples. Silicate-rich fractions contain 67.3 – 98.2 wt% of vein metal Ni. Extrapolation to pure silicate gives -1.19  $\epsilon$ -units for ALHA77257, -3.08  $\epsilon$ -units for Kenna, -3.41  $\epsilon$ -units for EET96042 and -9.19  $\epsilon$ -units for EET87517. The weighted average of all four samples gives  $-2.24 \pm 0.89 \epsilon$ -units.

Ni-concentrations in ureilite metal and silicates suggest considerable fractionation. If both components are co-genetic, this fractionation might have led to variations in  $^{60}\text{Ni}$  that can be used to obtain relative age information for the formation and the evolution of the ureilite parent body. However, as the isochron-diagram (Fig. 90) indicates, the ureilite data do not represent an isochron.

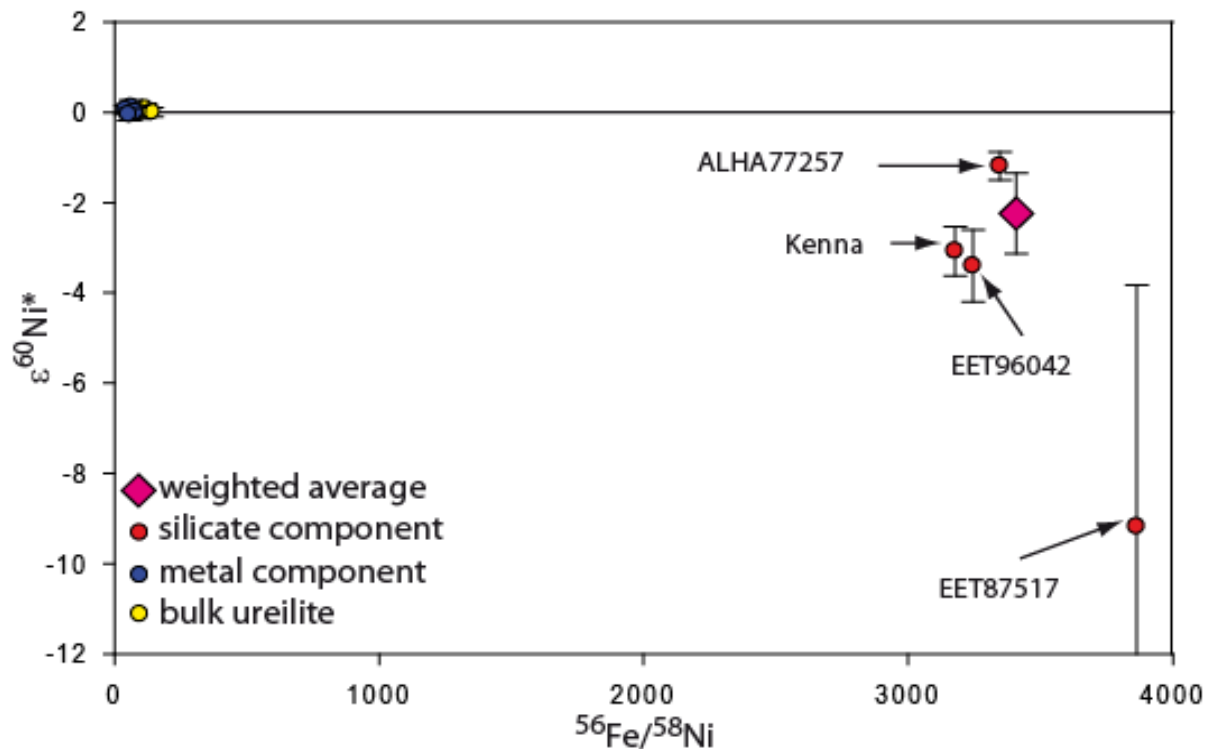


Fig. 90 Isochron diagram showing ureilite bulk, metal and silicate components.

Ni concentrations in vein metal and silicates indicate that vein metal is the principal Ni-carrier within the ureilite. Metal component and bulk ureilite have to yield similar values. Both components display, within uncertainty,  $\epsilon^{60}\text{Ni}^*$  of 0 relative to terrestrial standards, while the silicate-rich fraction has an  $\epsilon^{60}\text{Ni}^*$  of  $-1.19 \pm 0.35$  to  $-9.19 \pm 5.36$ . These data do not confirm the data in BIZZARRO et al. (2007b), where deficits in  $\epsilon^{60}\text{Ni}^*$  of  $\sim 0.25 \epsilon$  were reported for bulk ureilites. Assuming that earth acquired  $^{60}\text{Fe}$ ,  $\epsilon^{60}\text{Ni}^*$  of 0 indicates the presence of  $^{60}\text{Fe}$  on the ureilite parent body. During metal/silicate fractionation, most Ni is removed along with Fe into the core, leaving only small amounts ( $<150$ ) ppm behind in the silicate mantle. If  $^{60}\text{Fe}$  was present on the ureilite parent body, this would result in large positive excesses in  $^{60}\text{Ni}$  (Fig. 91).

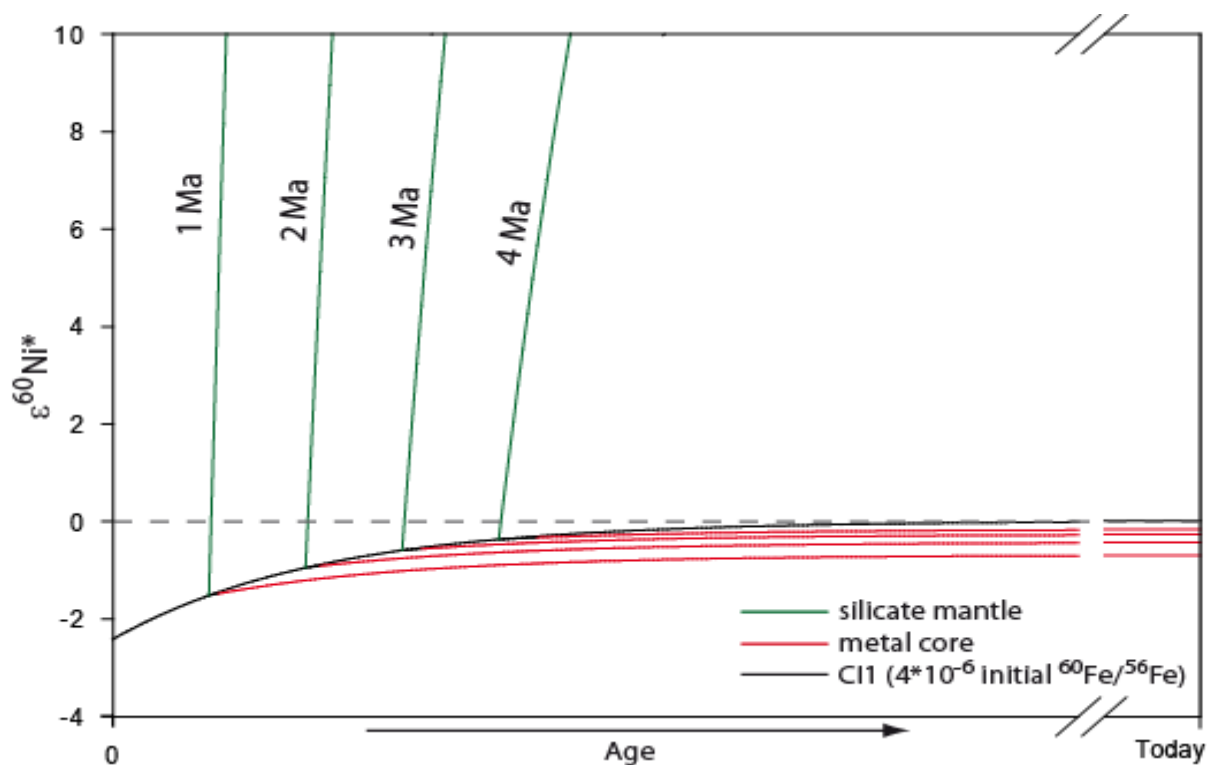


Fig. 91 Model calculations for metal/silicate fractionation at different time steps (1 Ma – 4 Ma), based on a CI1-chondritic composition (LODDERS and FEGLEY 1998) and an initial  $^{60}\text{Fe}/^{56}\text{Fe}$  of  $4 \cdot 10^{-6}$ . An initial  $^{60}\text{Fe}/^{56}\text{Fe}$  of  $4 \cdot 10^{-6}$  is consistent with a  $\epsilon^{60}\text{Ni}^*$  of -2.24 measured in ureilite silicate and the estimated initial  $^{60}\text{Fe}/^{56}\text{Fe}$  given in GOSWAMI et al. (2007). The fractionation model assumes 20 wt% FeO and 0.01 wt% Ni in the silicate mantle. For the silicate fraction, large positive excesses in  $^{60}\text{Ni}$  are modeled, while the metal fraction plots lower than the bulk composition.

The Ni-isotope data therefore indicate that ureilite vein metal and ureilite silicates are not cogenetic and formed from two isotopically distinct reservoirs. Ureilite silicate and vein metal might have formed on two distinct parent bodies. It is possible that the ureilite parent body accreted prior to the injection of  $^{60}\text{Fe}$  into the early solar system, while the source of the vein metal accreted after this event. Another explanation is that both parent bodies formed at similar times in different regions and that  $^{60}\text{Fe}$  was heterogeneously distributed within the early solar system.

Deficits in  $^{60}\text{Ni}$  relative to terrestrial standards are consistent with an ureilite parent body formation prior to the injection of  $^{60}\text{Fe}$  into the solar system. Several authors have proposed different initial  $^{60}\text{Fe}/^{56}\text{Fe}$ -ratios for the early solar system (e.g. MOSTEFAOUI et al. 2005, TACHIBANA et al. 2006, GOSWAMI et al. 2007). Among the highest suggested initial  $^{60}\text{Fe}/^{56}\text{Fe}$ -ratios is  $2.31 \pm 1.8 \cdot 10^{-6}$  from GOSWAMI et al. (2007), which is, within uncertainty, consistent with average negative  $\epsilon^{60}\text{Ni}^*$  of  $-2.24 \pm 0.89 \epsilon$  in ureilite silicates. Type II supernovae could produce even higher initial  $^{60}\text{Fe}/^{56}\text{Fe}$ -ratios up to  $>1 \cdot 10^{-5}$  (TACHIBANA et al. (2006) and references therein).

Negative excesses in  $^{60}\text{Ni}$  can also be caused by nucleosynthetic anomalies in Ni-isotopes. If Ni-isotopes were heterogeneously distributed in the early solar system, excesses or deficits in  $^{60}\text{Ni}$  would not provide significant information. Anomalies in  $^{60}\text{Ni}$ ,  $^{61}\text{Ni}$  and  $^{64}\text{Ni}$  have been reported for troilite from iron meteorites (QUITTÉ et al. 2006, COOK et al. 2008). COOK et al. (2008) suggested that these anomalous Ni-isotopic compositions are a result of mixing of two different stellar sources. CHEN et al. (2008) were unable to confirm the anomalies reported in QUITTÉ et al. (2006), COOK et al. (2008) and BIZZARRO et al. (2007b).

Correlated anomalies in  $^{60}\text{Ni}$  and  $^{62}\text{Ni}$  have been reported in CAIs by QUITTÉ et al. (2007). BIZZARRO et al. (2007a) suggested that the anomalies in  $^{60}\text{Ni}$  in CAIs could stem from the incorporation of presolar  $^{60}\text{Ni}^*$ . Heterogeneities in the early solar system are also known for other elements, including chromium (e.g. ROTARU et al. 1992), barium, samarium or neodymium (ANDREASEN and SHARMA 2007).

## 10 Conclusions

1. Ureilite vein metal is not co-genetic with ureilite silicates. Ni isotope studies suggest that ureilite vein metal and thus bulk ureilites show no excesses or deficits in  $^{60}\text{Ni}$ , while ureilite silicate shows deficits in  $^{60}\text{Ni}$ . This difference cannot be the result of a differentiation process from a single isotopic reservoir. This conclusion is further backed up by the thermodynamic disequilibrium between vein metal and silicates with respect to the exchange of Fe and Ni that is suggested by different equilibration temperatures.
2. Ureilite vein metal is not a residual metal from metal/silicate fractionation on the ureilite parent body. In contrast to the conclusions of other authors (WARREN et al. 2006, RANKENBURG et al. 2008), low concentrations of Ni and Co in the vein metal strongly argue against vein metal representing a metal residue of a parent body with initially chondritic composition. Mass balance calculations show that the primary metal component of a chondritic parent body is richer in Ni and Co than the vein metal. Temperatures within the ureilite parent body were likely not high enough to permit melting of pure FeNi-metal, which is indicated by missing equilibration of oxygen isotopes as well as high abundances of noble gases (provided that carbon is a primary component). Fractionation of >95 wt% of the initial metal component was therefore only possible as S-rich or C-rich liquid. Distribution coefficients for Ni and Co (CHABOT et al. 2003, CHABOT et al. 2006) indicate that, if S or C are present, Ni and Co become enriched in the residual metal during solid metal/liquid metal fractionation. In contrast, ureilite vein metal is depleted in Ni and Co relative to the primary metal component.
3. A complete clean sweep of metal on the ureilite parent body is possible. The presence of sufficient amounts of sulfur and carbon permits the complete melting of the initial metal portion of the ureilite parent body at  $\sim 1300^\circ\text{C}$ . The required amounts depend on the mode of melting. Fractional melting requires relatively high amounts of sulfur and carbon (>3 wt% C and >12 wt% S), while batch melting requires less carbon and sulfur ( $\sim 1$  wt% and  $\sim 7$  wt% S). Depending on the composition of the parent body, the metal fraction constitutes 18 – 30 vol% of the parent body. The

metal melt could have been removed either by a batch melting process under static conditions (HERPFER and LARIMER 1993, YOSHINO et al. 2004) or by a buoyancy driven explosive volcanism (KEIL and WILSON 1993). Due to the missing re-equilibration between initial metal component and silicate, which would be expected during a fractional melting process, batch melting appears to be the most likely mode of melting.

4. Ureilite vein metal could represent a partial or batch melt from metal/silicate fractionation. Ignoring the problems arising from the Ni-isotopic data, carbon-rich melts produced in either a fractional melting or a batch melting process on a reduced parent body resemble ureilite vein metal with respect to Ni and Co concentrations as well as Ni/Co-ratio. Most ureilites (> 70%, MITTFELDT et al. 1998), however, do not stem from a reduced parent body.

A scenario that circumvents that problem is one where the more oxidized ureilite assemblages were swept clean of their initial metal portion and then injected with a carbon-rich melt from a reduced ureilite assemblage. It appears, however, unlikely that such a process would lead to similar amounts of metal in all ureilites. Another possible problem arising from that scenario is that complementary melts which are Ni-richer than vein metal, for example the sulfur-rich melt from a batch melting process or the succeeding carbon rich melts, are not observed in our ureilite samples.

5. Ureilite vein metal could represent metal from an iron-rich impactor. Metal crystallizing from a reduced, Ni-poor LL-chondritic parent body shows Ni- and Co-concentrations and Ni/Co-ratios similar to ureilite vein metal. Such an impactor would explain the discrepancies between vein metal and ureilite silicate Ni-isotopes. Either the metal-rich impactor formed after the injection of  $^{60}\text{Fe}$  in the early solar system, or  $^{60}\text{Fe}$  was heterogeneously distributed in the early solar system and the ureilite parent body and the impactor's parent body formed in different regions. If the ureilite vein metal was formed by such an impactor it would also explain the missing metal/olivine equilibration and the similarities in ureilite vein metal composition in each ureilite.
6. Based on the other conclusions, it is proposed that ureilites formed as restites on a parent body of initially chondritic composition. The primary metal component established equilibrium with ureilite olivine at  $\sim 1300^\circ\text{C}$  and was then removed by a

batch melting process. The primary metal component segregated into a metal core and left a carbon rich residue behind. The vein metal was injected into the parent body by the impact of a metal-rich asteroid which was poor in Ni and Co.

## 11 References

- Andreasen, R. and Sharma, M., 2007. Mixing and homogenization in the early solar system: Clues from Sr, Ba, Nd and Sm isotopes in meteorites. *The Astrophysical Journal* **665**, 874 - 883.
- Ash, R. D., Goodrich, C. A., McDonough, W. F., and Van Orman, J. A., 2009. Metal in ureilites: Siderophile elements from LA-ICP-MS. *40th Lunar and Planetary Science Conference*, Houston, USA.
- Asimow, P. D. and Ghiorso, M. S., 1998. Algorithmic modifications extending MELTS to calculate subsolidus phase relations. *AM* **83**, 1127-1132.
- Berkley, J. L., 1986. 4 Antarctic Ureilites - Petrology and Observations on Ureilite Petrogenesis. *Meteoritics* **21**, 169-189.
- Berkley, J. L., Brown VI, H. G., and Keil, K., 1976. The Kenna ureilite: an ultramafic rock with evidence for igneous, metamorphic, and shock origin. *GCA* **40**, 1429-1437.
- Berkley, J. L. and Jones, J. H., 1982. Primary Igneous Carbon in Ureilites - Petrological Implications. *Journal of Geophysical Research* **87**, A353-A364.
- Berkley, J. L., Taylor, G. J., Keil, K., Harlow, G. E., and Prinz, M., 1980. The Nature and Origin of Ureilites. *GCA* **44**, 1579-1597.
- Bizzarro, M., Chen, J. H., Huss, G. R., Lugmair, G. W., S., M., Papanastasiou, D. A., Shukolyukov, A., Quitté, G., Tachibana, S., and Wadhwa, M., 2007a. Nickel isotope anomalies in meteorites and the  $^{60}\text{Fe}$ - $^{60}\text{Ni}$  clock *Workshop on Chronology of Meteorites*.
- Bizzarro, M., Ulfbeck, D., Trinquier, A., Thrane, K., Connelly, J. N., and Meyer, B. S., 2007b. Evidence for a late supernova injection of Fe-60 into the protoplanetary disk. *Science* **316**, 1178-1181.
- Bogard, D. D. and Johnson, P., 1983. Martian gases in an antarctic meteorite? *Science* **221**, 651 - 654.
- Boynton, W. V., Starzyk, P. M., and Schmitt, R. A., 1976. Chemical Evidence for Genesis of Ureilites, Achondrite Chassigny and Nakhilites. *GCA* **40**, 1439-1447.
- Brearley, A. J. and Jones, R. H., 1998. Chondritic Meteorites. *Planetary Materials* **36**, 3-2 - 3-398.
- Chabot, N. L., 2004. Sulfur contents of the parental metallic cores of magmatic iron meteorites. *GCA* **68**, 3607-3618.
- Chabot, N. L., Campbell, A. J., Jones, J. H., Humayun, M., and Agee, C. B., 2003. An experimental test of Henry's Law in solid metal-liquid metal systems with implications for iron meteorites. *Meteoritics & Planetary Science* **38**, 181-196.
- Chabot, N. L., Campbell, A. J., Jones, J. H., Humayun, M., and Lauer, H. V., 2006. The influence of carbon on trace element partitioning behavior. *GCA* **70**, 1322-1335.
- Chen, J. H., Papanastasiou, D. A., and Wasserburg, G. J., 2007. High precision Nickel isotopic analysis in meteorites *38th Lunar and Planetary Science Conference*.
- Chen, J. H., Papanastasiou, D. A., and Wasserburg, G. J., 2008. A search for nickel isotopic anomalies in iron meteorites and chondrites. *GCA* **73**, 1461 - 1471.
- Clayton, R. N. and Mayeda, T. K., 1988. Formation of ureilites by nebular processes. *GCA* **52**, 1313-1318.

- Clayton, R. N. and Mayeda, T. K., 1996. Oxygen isotope studies of achondrites. *GCA* **60**, 1999-2017.
- Cook, D. L., Clayton, R. N., Wadhwa, M., Janney, P. E., and Davis, A. M., 2008. Nickel isotopic anomalies in troilite from iron meteorites. *Geophysical Research Letters* **35**, L01203.
- Dauphas, N. and Cook, D. L., 2008. Iron-60 evidence for solar injection and efficient mixing of stellar debris in the protosolar nebular. *The Astrophysical Journal* **686**, 560 - 569.
- Ebel, D. S., 2006. Condensation of Rocky Material in Astrophysical Environments. In: Lauretta, D. S. and McSween, H. Y. J. Eds.), *Meteorites and the Early Solar System II*. The University of Arizona Press, Houston.
- Ebihara, M., Shinonaga, T., and Takeda, H., 1990. Trace element composition of Antarctic ureilites and some implications to their origin. *Meteoritics* **25**, 359 - 360.
- Fedkin, A. V. and Grossman, J. N., 2006. The Fayalite Content of Chondritic olivine: Obstacle to Understanding the Condensation of Rocky Material. In: Lauretta, D. S. and McSween, H. Y. J. Eds.), *Meteorites and the Early Solar System II*. The University of Arizona Press, Houston.
- Franchi, I. A., Baker, L., Bridges, J. C., Wright, I. P., and Pillinger, C. T., 2001. Oxygen isotopes in the early solar system. *Philosophical Transactions of the Royal Society of London A* **359**, 2019 - 2035.
- Franchi, I. A., Sexton, A. S., Wright, I. P., and Pillinger, C. T., 1997. Resolved subgroups within the ureilite population. *Meteoritics & Planetary Science* **32**, A44.
- Fraser, D. G. and Rammensee, W., 1982. Activity Measurements by Knudsen Cell Mass-Spectrometry - the System Fe-Co-Ni and Implications for Condensation Processes in the Solar Nebula. *Geochimica Et Cosmochimica Acta* **46**, 549-556.
- Ghiorso, M. S. and Sack, R. O., 1995. Chemical Mass-Transfer in Magmatic Processes .4. A Revised and Internally Consistent Thermodynamic Model for the Interpolation and Extrapolation of Liquid-Solid Equilibria in Magmatic Systems at Elevated-Temperatures and Pressures. *Contributions to Mineralogy and Petrology* **119**, 197-212.
- Goodrich, C. A., 1992. Ureilites - a Critical-Review. *Meteoritics* **27**, 327-352.
- Goodrich, C. A. and Berkley, J. L., 1986. Primary Magmatic Carbon in Ureilites - Evidence from Cohenite-Bearing Metallic Spherules. *GCA* **50**, 681-691.
- Goodrich, C. A., Fioretti, A. M., Tribaudino, M., and Molin, G., 2001. Primary trapped melt inclusions in olivine in the olivine-augite-orthopyroxene ureilite Hughes 009. *GCA* **65**, 621-652.
- Goodrich, C. A., Jones, J. H., and Berkley, J. L., 1987a. Origin and Evolution of the Ureilite Parent Magmas - Multistage Igneous Activity on a Large Parent Body. *GCA* **51**, 2255-2273.
- Goodrich, C. A., Keil, K., Berkley, J. L., Laul, J. C., Smith, M. R., Wacker, J. F., Clayton, R. N., and Mayeda, T. K., 1987b. Roosevelt County-027: A Low-Shock Ureilite with Interstitial Silicates and High Noble-Gas Concentrations. *Meteoritics* **22**, 191-218.
- Goodrich, C. A., Lugmair, G. W., Drake, M. J., and Patchett, P. J., 1995. U-Th-Pb and Sm-Nd Isotopic Systematics of the Goalpara Ureilite - Resolution of Terrestrial Contamination - Comment. *GCA* **59**, 4083-4085.
- Goodrich, C. A., Patchett, P. J., Lugmair, G. W., and Drake, M. J., 1991. Sm-Nd and Rb-Sr Isotopic Systematics of Ureilites. *GCA* **55**, 829-848.
- Goodrich, C. A., Scott, E. R. D., and Fioretti, A. M., 2004. Ureilitic breccias: clues to the petrographic structure and impact disruption of the ureilite parent asteroid. *Chemie der Erde* **64**, 283 - 327.

- Goodrich, C. A., Van Orman, J. A., and Wilson, L., 2007. Fractional melting and smelting on the ureilite parent body. *GCA* **71**, 2876-2895.
- Goswami, J. N., Mishra, R., and Rudraswami, N. G., 2007.  $^{60}\text{Fe}$  and  $^{26}\text{Al}$  records in chondrules from unequilibrated ordinary chondrites of low petrologic type. *28th Lunar and Planetary Science Conference*, Leage City, USA.
- Grady, M. M. and Wright, I. P., 2003. Elemental and isotopic abundances of carbon and nitrogen in meteorites. *Space Science Reviews* **106**, 231-248.
- Grady, M. M. and Wright, I. P., 2006. Types of extraterrestrial material available for study. In: Lauretta, D. S. and McSween, H. Y. J. Eds.), *Meteorites and the Early Solar System II*. The University of Arizona Press, Houston.
- Grady, M. M., Wright, I. P., Swart, P. K., and Pillinger, C. T., 1985. The Carbon and Nitrogen Isotopic Composition of Ureilites - Implications for Their Genesis. *GCA* **49**, 903-915.
- Grossman, J. N., 1994. The Meteoritical Bulletin, No. 76, 1994 January: The U.S. Antarctic Meteorite Collection. *Meteoritics* **29**, 100 - 143.
- Grossman, J. N., 1998. The Meteoritical Bulletin, No. 82, 1998 July. *Meteoritics & Planetary Science* **33**, A221 - A239.
- Grossman, J. N., 1999. The Meteoritical Bulletin, No. 83, 1999 July. *Meteoritics & Planetary Science* **34**, A169 - 186.
- Grossman, J. N., 2009. Meteoritical Bulletin Database. The Meteoritical Society.
- Guan, Y. and Leshin, L. A., 2001. Oxygen Isotopes of Mineral and Lithic Clasts in the Polymict Ureilite EET 83309: an Ion Microprobe Study. *meteoritics & Planetary Science* **36**, A74.
- Heger, A., Hoffman, R. D., Rauscher, T., and Woosley, S. E., 2000. Nucleosynthesis in massive stars including all stable isotopes. In: Müller, E. and Hillebrandt, W. Eds.) *10th Workshop on Nuclear Astrophysics*, Ringburg Castle.
- Herpfer, M. A. and Larimer, J. W., 1993. Core formation: an experimental study of metallic melt-silicate segregation. *Meteoritics* **28**, 362.
- Higuchi, H., Morgan, J. W., Ganapathy, R., and Anders, E., 1976. Chemical Fractionations in Meteorites .10. Ureilites. *GCA* **40**, 1563-1571.
- Hirschmann, M., 1991. Thermodynamics of Multicomponent Olivines and the Solution Properties of  $(\text{Ni,Mg,Fe})_2\text{SiO}_4$  and  $(\text{Ca,Mg,Fe})_2\text{SiO}_4$  Olivines. *AM* **76**, 1232-1248.
- Hirschmann, M. M., 2000. Thermodynamics of multicomponent olivines and the solution properties of  $(\text{Ni,Mg,Fe})_2\text{SiO}_4$  and  $(\text{Ca,Mg,Fe})_2\text{SiO}_4$  olivine - Reply. *AM* **85**, 1548-1555.
- Hirschmann, M. M. and Ghiorso, M. S., 1994. Activities of Nickel, Cobalt, and Manganese Silicates in Magmatic Liquids and Applications to Olivine Liquid and to Silicate Metal Partitioning. *GCA* **58**, 4109-4126.
- Horstmann, D., 2004. *Das Zustandsschaubild Eisen-Kohlenstoff*. Verlag Stahleisen mbH, Düsseldorf.
- Hudon, P., Romanek, C., Paddock, L., and Mittlefehldt, D. W., 2004. Evolution of the ureilite parent body. *25th Lunar and Planetary Science Conference*, Houston, USA.
- Humayun, M., Rushmer, T., Rankenburg, K., and Brandon, A. D., 2005. A model for siderophile element distribution in planetary differentiation. *36th Lunar and Planetary Science Conference*, Houston, USA.
- Janssens, M. J., Hertogen, J., Wolf, R., Ebihara, M., and Anders, E., 1987. Ureilites - Trace-Element Clues to Their Origin. *GCA* **51**, 2275-2283.
- Jarosewich, E., 1990. Chemical-Analyses of Meteorites - a Compilation of Stony and Iron Meteorite Analyses. *Meteoritics* **25**, 323-337.

- Jochum, K. P., Stoll, B., Herwig, K., Willbold, M., Hofmann, A. W., Amini, M., Aarburg, S., Abouchami, W., Hellebrand, E., Mocek, B., Raczek, I., Stracke, A., Alard, O., Bouman, C., Becker, S., Dücking, M., Bratz, H., Klemd, R., de Bruin, D., Canil, D., Cornell, D., de Hoog, C. J., Dalpe, C., Danyushevsky, L., Eisenhauer, A., Gao, Y. J., Snow, J. E., Goschopf, N., Gunther, D., Latkoczy, C., Guillong, M., Hauri, E. H., Hofer, H. E., Lahaye, Y., Horz, K., Jacob, D. E., Kasemann, S. A., Kent, A. J. R., Ludwig, T., Zack, T., Mason, P. R. D., Meixner, A., Rosner, M., Misawa, K. J., Nash, B. P., Pfander, J., Premo, W. R., Sun, W. D., Tiepolo, M., Vannucci, R., Vennemann, T., Wayne, D., and Woodhead, J. D., 2006. MPI-DING reference glasses for in situ microanalysis: New reference values for element concentrations and isotope ratios. *Geochemistry Geophysics Geosystems* **7**, -.
- Jones, J. H. and Goodrich, C. A., 1989. Siderophile Trace-Element Partitioning in the Fe-Ni-C System - Preliminary-Results with Application to Ureilite Petrogenesis. *Meteoritics* **24**, 281-282.
- Kallemeyn, G. W., Rubin, A. E., and Wasson, J. T., 1996. The compositional classification of chondrites: VII. The R chondrite group. *GCA* **60**, 2243 - 2256.
- Kawasaki, T. and Matsui, Y., 1983. Thermodynamic Analyses of Equilibria Involving Olivine, Ortho-Pyroxene and Garnet. *GCA* **47**, 1661-1679.
- Keil, K., Berkley, J. L., and Fuchs, L. H., 1982. Suessite, Fe<sub>3</sub>Si - a New Mineral in the North Haig Ureilite. *AM* **67**, 126-131.
- Keil, K., Stoffler, D., Love, S. G., and Scott, E. R. D., 1997. Constraints on the role of impact heating and melting in asteroids. *Meteoritics & Planetary Science* **32**, 349-363.
- Keil, K. and Wilson, L., 1993. Explosive Volcanism and the Compositions of Cores of Differentiated Asteroids. *EPSL* **117**, 111-124.
- Kelemen, P. B., Hangohj, K., and Greene, A. R., 2004. One View of the Geochemistry of Subduction-related Magmatic Arcs, with an Emphasis on Primitive Andesite and Lower Crust. In: Holland, H. D. and Turekian, K. K. Eds.), *Treatise on Geochemistry*. Elsevier, Amsterdam.
- Kennedy, A. K., Lofgren, G. E., and Wasserburg, G. J., 1993. An experimental study of trace element partitioning between olivine, orthopyroxene and melt in chondrules: Equilibrium values and kinetic effects. *EPSL* **115**, 177 - 195.
- Kita, N. T., Ikeda, Y., Togashi, S., Liu, Y. Z., Morishita, Y., and Weisberg, M. K., 2004. Origin of ureilites inferred from a SIMS oxygen isotopic and trace element study of clasts in the Dar al Gani 319 polymict ureilite. *GCA* **68**, 4213-4235.
- Kita, N. T., Togashi, S., and Morishita, Y., 1998. Search for <sup>60</sup>Ni Excess in MET-78008 Ureilite: An ion microprobe study. *Antarctic Meteorite Research* **11**, 103-121.
- Kracher, A., Willis, J., and Wasson, J. T., 1980. Chemical Classification of Iron-Meteorites .9. A New Group (IIF), Revision of IAB and IIICD, and Data on 57 Additional Irons. *GCA* **44**, 773-787.
- Lebedev, E. B., Kadik, A. A., Kuskov, O. L., Dorfman, A. M., and Lukanin, O. A., 1999. The motion of sulfide phases in a partially molten silicate material: application to the problem of formation of planetary cores. *Solar System Research* **33**, 346 - 356.
- Lindsley, D. H. and Andersen, D. J., 1983. A Two-pyroxene thermometer. *Proceedings of the 13th Lunar and Planetary Science Conference Part 2* **88**, A887 - A906.
- Lodders, K. and Fegley, B., 1998. *The planetary scientist's companion*. Oxford University Press, Oxford.

- Malvin, D. J., Wang, D., and Wasson, J. T., 1984a. Chemical classification of iron meteorites-X. Multielement studies of 43 irons, resolution of group IIIE from IIIAB, and evaluation of Cu as taxonomic parameter. *GCA* **48**, 785-804.
- Malvin, D. J., Zong, P., and Wasson, J. T., 1984b. Formation of the Bellsbank Trio iron meteorite as immiscible, P-rich liquid Pockets on the crystallizing floor of the IIAB core. *15th Lunar and Planetary Science Conference*, Houston, USA.
- Marvin, U. B. and Wood, J. A., 1972. The Haverö ureilite: Petrographic notes *Meteoritics* **7**, 601 - 610.
- Mason, B., 1981. ALHA77257. *Antarctic Meteorite Newsletter* **4**.
- Mason, B. and Martinez, R., 1986. ALH84136. *Antarctic Meteorite Newsletter* **9**.
- Mason, B. and Score, R., 1988. EET87517. *Antarctic Meteorite Newsletter* **11**, 20.
- McCoy, T. and McBride, K., 1998a. EET96042, GRA95205. *Antarctic Meteorite Newsletter* **21**.
- McCoy, T. and McBride, K., 1998b. EET96331. *Antarctic Meteorite Newsletter* **21**.
- McCoy, T., Mittlefehldt, D. W., and Wilson, L., 2006. Asteroid Differentiation. In: Lauretta, D. S. and McSween, H. Y. J. Eds.), *Meteorites and the Early Solar System II*. The University of Arizona Press, Houston.
- McGill, G. J. H. and Cleverly, W. H., 1968. New stony meteorite finds including two ureilites from the Nullarbor Plain, Western Australia. *Mineralogical Magazine*, 691-695.
- McSween, H. Y. J. and Treiman, A. H., 1998. Martian Meteorites. *Planetary Materials* **36**, 6-1 - 6-53.
- Meyer, B. S. and Zinner, E., 2006. Nucleosynthesis. In: Lauretta, D. S. and McSween, H. Y. J. Eds.), *Meteorites and the Early Solar System II*. The University of Arizona Press, Houston.
- Mittlefehldt, D. W., McCoy, T. J., Goodrich, C. A., and Kracher, A., 1998. Non-chondritic meteorites from asteroidal bodies. *Planetary Materials* **36**, D1-D195.
- Mostefaoui, S., Lugmair, G. W., and Hoppe, P., 2005. Fe-60: A heat source for planetary differentiation from a nearby supernova explosion. *Astrophysical Journal* **625**, 271-277.
- Norton, O. R., 2002. *The cambridge encyclopedia of meteorites*. Cambridge University Press, Cambridge.
- O'Neill, H. S., 1987a. Free-Energies of Formation of NiO, CoO, Ni<sub>2</sub>SiO<sub>4</sub>, and Co<sub>2</sub>SiO<sub>4</sub>. *AM* **72**, 280-291.
- O'Neill, H. S., 1987b. Quartz-Fayalite-Iron and Quartz-Fayalite-Magnetite Equilibria and the Free-Energy of Formation of Fayalite (Fe<sub>2</sub>SiO<sub>4</sub>) and Magnetite (Fe<sub>3</sub>O<sub>4</sub>). *AM* **72**, 67-75.
- Ohtani, H. and Nishizawa, T., 1987. Calculation of Fe-C-S Ternary Phase-Diagram. *Tetsu to Hagane-Journal of the Iron and Steel Institute of Japan* **73**, 152-159.
- Prinz, M., Weisberg, M. K., Nehru, C. E., and Delaney, J. S., 1986. North Haig and Nilpena: Paired polymict ureilites with Angra Dos Reis-related and other clasts. *17th Lunar and Planetary Science Conference*, Houston, USA.
- Quitté, G., Halliday, A. N., Meyer, B., Markowski, A., Latkoczy, C., and Günther, D., 2007. Correlated Iron 60, Nickel 62 and Zirconium 96 in refractory inclusions and the origin of the solar system. *The Astrophysical Journal* **655**, 678 - 684.
- Quitté, G., Meier, M., Latkoczy, C., Halliday, A. N., and Gunther, D., 2006. Nickel isotopes in iron meteorites-nucleosynthetic anomalies in sulphides with no effects in metals and no trace of Fe-60. *EPSL* **242**, 16-25.
- Quitte, G. and Oberli, F., 2006. Quantitative extraction and high precision isotope measurements of nickel by MC-ICPMS. *Journal of Analytical Atomic Spectrometry* **21**, 1249 - 1255.

- Raghavan, V., 1988. *Phase diagrams of ternary iron alloys*. The Indian Institute of Metals, Calcutta.
- Rai, V. K., Murty, S. V. S., and Ott, U., 2003. Noble gases in ureilites: Cosmogenic, radiogenic, and trapped components. *GCA* **67**, 4435 - 4456.
- Rammensee, W. and Fraser, D. G., 1981. Activities in Solid and Liquid Fe-Ni and Fe-Co Alloys Determined by Knudsen Cell Mass-Spectrometry. *Berichte Der Bunsen-Gesellschaft-Physical Chemistry Chemical Physics* **85**, 588-592.
- Rankenburg, K., Brandon, A. D., and Humayun, M., 2007. Osmium isotope systematics of ureilites. *GCA* **71**, 2402-2413.
- Rankenburg, K., Humayun, M., Brandon, A. D., and Herrin, J. S., 2008. Highly siderophile elements in ureilites. *GCA* **72**, 4642-4659.
- Robie, R. A. and Hemingway, B. S., 1995. *Thermodynamic properties of minerals and related substances at 298.15 K and 1 Bar (10<sup>5</sup> Pascals) pressure and at higher temperatures*. U.S. geological Survey, Denver.
- Rotaru, M., Birck, J. L., and Allègre, C. J., 1992. Clues to early solar system history from chromium isotopes in carbonaceous chondrites. *Nature* **358**, 465 - 470.
- Rubin, A. E., 1988. Formation of Ureilites by Impact-Melting of Carbonaceous Chondritic Material. *Meteoritics* **23**, 333-337.
- Rubin, A. E., 2006. Shock, post-shock annealing, and post-annealing shock in ureilites. *Meteoritics & Planetary Science* **41**, 125-133.
- Rubin, A. E. and Scott, E. R. D., 1997. Shock metamorphism of enstatite chondrites. *GCA* **61**, 847 - 858.
- Russell, S. S., Folco, L., Grady, M. M., Zolensky, M. E., Jones, R., Righter, K., Zipfel, J., and Grossman, J. N., 2004. The Meteoritical Bulletin, No. 88, 2004 July. *Meteoritics & Planetary Science* **39**, A215 - A272.
- Sack, R. O. and Ghiorso, M. S., 1989. Importance of Considerations of Mixing Properties in Establishing an Internally Consistent Thermodynamic Database - Thermochemistry of Minerals in the System Mg<sub>2</sub>SiO<sub>4</sub>-Fe<sub>2</sub>SiO<sub>4</sub>-SiO<sub>2</sub>. *Contributions to Mineralogy and Petrology* **102**, 41-68.
- Sack, R. O. and Ghiorso, M. S., 1994. Thermodynamics of multi-component pyroxene: II. Phase relation in the quadrilaterak. *Contributions to Mineralogy and Petrology* **116**, 287 - 300.
- Salters, V. and Stracke, A., 2004. Composition of the depleted mantle. *Geochemistry Geophysics Geosystems* **5**, 1525 - 2027.
- Scott, E. R. D., Taylor, G. J., and Keil, K., 1993. Origin of Ureilite Meteorites and Implications for Planetary Accretion. *Geophysical Research Letters* **20**, 415-418.
- Seifert, S. and O'Neill, H. S., 1987. Experimental-Determination of Activity-Composition Relations in Ni<sub>2</sub>SiO<sub>4</sub>-Mg<sub>2</sub>SiO<sub>4</sub> and Co<sub>2</sub>SiO<sub>4</sub>-Mg<sub>2</sub>SiO<sub>4</sub> Olivine Solid-Solutions at 1200 K and 0.1 Mpa and 1573 K and 0.5 Gpa. *GCA* **51**, 97-104.
- Seifert, S., O'Neill, H. S., and Brey, G., 1988. The Partitioning of Fe, Ni and Co between Olivine, Metal, and Basaltic Liquid - an Experimental and Thermodynamic Investigation, with Application to the Composition of the Lunar Core. *GCA* **52**, 603-616.
- Shukolyukov, A. and Lugmair, G. W., 1993. Fe-60 in Eucrites. *EPSL* **119**, 159-166.
- Singletary, S. and Grove, T. L., 2006. Experimental constraints on ureilite petrogenesis. *GCA* **70**, 1291-1308.
- Singletary, S. J. and Grove, T. L., 2003. Early petrologic processes on the ureilite parent body. *Meteoritics & Planetary Science* **38**, 95-108.

- Sinha, S. K., Sack, R. O., and Lipschutz, M. E., 1997. Ureilite meteorites: Equilibration temperatures and smelting reactions. *GCA* **61**, 4235-4242.
- Sonett, C. P., Colburn, D. S., Schwartz, K., and Keil, K., 1970. The melting of asteroidal-sized bodies by unipolar dynamo induction from a primitive T Tauri sun. *Astrophysics and Space Science* **7**, 446 - 488.
- Stöffler, D., Keil, K., and Scott, E. R. D., 1991. Shock metamorphism of ordinary chondrites. *GCA* **55**, 3845 - 3867.
- Tachibana, S. and Huss, G. R., 2003. The initial abundance of  $^{60}\text{Fe}$  in the solar system. *The Astrophysical Journal* **588**, L41 - L44.
- Tachibana, S., Huss, G. R., Kita, N. T., Shimoda, G., and Morishita, Y., 2006.  $^{60}\text{Fe}$  in chondrites: Debris from a nearby supernova in the early solar system? *The Astrophysical Journal* **639**, L87-L90.
- Takahashi, K. and Masuda, A., 1990. The Rb-Sr and Sm-Nd dating and REE measurements of ureilites. *Meteoritics* **25**, 413.
- Takeda, H., 1987. Mineralogy of Antarctic Ureilites and a Working Hypothesis for Their Origin and Evolution. *EPSL* **81**, 358-370.
- Takeda, H., 1989. Mineralogy of Coexisting Pyroxenes in Magnesian Ureilites and Their Formation Conditions. *EPSL* **93**, 181-194.
- Tomiska, J. and Neckel, A., 1985. Thermodynamics of Solid Fe-Ni Alloys - Mass-Spectrometric Determination of Thermodynamic Mixing Effects and Calculation of the Phase-Diagram. *Ber Bunsen Phys Chem* **89**, 1104-1109.
- Tomiska, J., Nowotny, H., Erdelyi, L., and Neckel, A., 1979. Thermodynamical Investigations on the System Cobalt-Nickel - Mass-Spectrometric Measurements of the Activities in the Liquid and the Solid-Phase and the Calculation of the Phase-Diagram. *Berichte Der Bunsen-Gesellschaft-Physical Chemistry Chemical Physics* **83**, 1035-1042.
- Torigoye-Kita, N., Misawa, K., and Tatsumoto, M., 1995a. U-Th-Pb and Sm-Nd Isotopic Systematics of the Goalpara Ureilite - Resolution of Terrestrial Contamination. *GCA* **59**, 381-390.
- Torigoye-Kita, N., Misawa, K., and Tatsumoto, M., 1995b. U-Th-Pb and Sm-Nd Isotopic Systematics of the Goalpara Ureilite - Resolution of Terrestrial Contamination - Reply. *GCA* **59**, 4087-4091.
- Torigoye-Kita, N., Tatsumoto, M., Meeker, G. P., and Yanai, K., 1995c. The 4.56 Ga U-Pb Age of the Met-78008 Ureilite. *GCA* **59**, 2319-2329.
- Treiman, A. H. and Berkley, J. L., 1994. Igneous petrology of the new ureilites Nova 001 and Nullarbor 010. *Meteoritics* **29**, 843 - 848.
- Van Orman, J. A., Goodrich, C. A., and Wilson, L., 2009. Metal and siderophile elements in ureilites: reconciliation with smelting *40th Lunar and Planetary Science Conference*, Houston, USA.
- Van Schmus, W. R. and Wood, J. A., 1967. A chemical-petrologic classification for the chondrite meteorites. *GCA* **31**, 747 - 765.
- Vdovykin, G. P., 1972. Forms of carbon in the new Haverö Ureilite of Finland. *Meteoritics* **7**, 447 - 552.
- Vdovykin, G. P., 1975. The Haverö Meteorite. *Space Science Reviews*, 749 - 776.
- Vervoort, J. and Mueller, P., 2008. Multicollector-Inductively Coupled Plasma Mass Spectrometer (MC-ICPMS). Science Education Resource Center (SERC) at Carleton College.
- Vogel, R. and Ritzau, G., 1931. Über das ternäre System Eisen-Schwefel-Kohlenstoff. *Archiv für das Hüttenwesen* **4**, 459 - 556.

- Wacker, J. F., 1986. Noble-Gases in the Diamond-Free Ureilite, ALHA 78019 - the Roles of Shock and Nebular Processes. *GCA* **50**, 633-642.
- Walker, D. and Agee, C. B., 1988. Ureilite Compaction. *Meteoritics* **23**, 81-91.
- Walker, D. and Grove, T., 1993. Ureilite Smelting. *Meteoritics* **28**, 629-636.
- Wang, C., Hiramata, J., Nagasaka, T., and Shiro, B. Y., 1991. Phase-Equilibria of Liquid Fe-S-C Ternary-System. *Isij International* **31**, 1292-1299.
- Wänke, H., Baddenhausen, H., Spettel, B., Teschke, F., Quijano-Rico, M., Dreibus, G., and Palme, H., 1972. The chemistry of the Haverö ureilite. *Meteoritics* **7**, 579 - 590.
- Warren, P. H. and Huber, H., 2006. Ureilite petrogenesis: A limited role for smelting during anatexis and catastrophic disruption. *Meteoritics & Planetary Science* **41**, 835-849.
- Warren, P. H., Jerde, E., and Kallemeyn, G. W., 1989. Lunar meteorites - Siderophile element contents, and implications for the composition and origin of the moon. *EPSL* **91**, 245 - 260.
- Warren, P. H. and Kallemeyn, G. W., 1992. Explosive Volcanism and the Graphite Oxygen Fugacity Buffer on the Parent Asteroid(S) of the Ureilite Meteorites. *Icarus* **100**, 110-126.
- Warren, P. H., Ulf-Moller, F., Huber, H., and Kallemeyn, G. W., 2006. Siderophile geochemistry of ureilites: A record of early stages of planetesimal core formation. *GCA* **70**, 2104-2126.
- Wasson, J. T., Choi, B., Jerde, E., and Ulf-Moller, F., 1998. Chemical classification of iron meteorites: XII. New members of the magmatic groups. *GCA* **62**, 715-724.
- Wasson, J. T., Chou, C. L., Bild, R. W., and Baedeker, P. A., 1976. Classification of and Elemental Fractionation among Ureilites. *GCA* **40**, 1449-&.
- Wasson, J. T., Ouyang, X., Wang, J., and Jerde, E., 1989. Chemical classification of iron meteorites: XI. Multi-element studies of 38 new irons and the high abundance of ungrouped irons from Antarctica. *GCA* **53**, 735-744.
- Weber, H. W., Begemann, F., and Hintenbe.H, 1971. Noble-Gases in Haverö Ureilite. *EPSL* **13**, 205-&.
- Weber, H. W., Begemann, F., and Hintenberger, H., 1976. Primordial Gases in Graphite-Diamond-Kamacite Inclusions from Haverö Ureilite. *EPSL* **29**, 81-90.
- Weber, I., Bischoff, A., and Weber, D., 2003. TEM investigations on the monomict ureilites Jalanash and Hammadah al Hamra 064. *Meteoritics & Planetary Science* **38**, 145-156.
- Weisberg, M. K., McCoy, T. J., and Krot, A. N., 2006. Systematics and Evaluation of Meteorite Classification. In: Lauretta, D. S. and McSween, H. Y. J. Eds.), *Meteorites and the Early Solar System II*. The University of Arizona Press, Houston.
- Wiik, H. B., 1972. The chemical composition of the Haverö meteorite and the genesis of ureilites. *Meteoritics* **7**, 553-557.
- Wilkening, L. L. and Marti, K., 1976. Rare-Gases and Fossil Particle Tracks in Kenna Ureilite. *GCA* **40**, 1465-&.
- Will, T. M., 1998. *Phase Equilibria in metamorphic rocks: thermodynamic background and petrological applications*. Springer, Berlin Heidelberg.
- Wilson, L. and Keil, K., 1991. Consequences of Explosive Eruptions on Small Solar-System Bodies - the Case of the Missing Basalts on the Aubrite Parent Body. *EPSL* **104**, 505-512.
- Wlotzka, F., 1972. Haverö ureilite: Evidence for recrystallization and partial reduction. *Meteoritics* **7**, 591 - 600.
- Wlotzka, F., 1993. A weathering scale for the ordinary chondrites. *Meteoritics* **28**, 460.

- Wood, B. J. and Kleppa, O. J., 1981. Thermochemistry of Forsterite-Fayalite Olivine Solutions. *GCA* **45**, 529-534.
- Yamaguchi, A., Takeda, H., and Kuskabe, M., 2005. Mineralogy and Oxygen isotopic composition of an augite-orthopyroxene bearing ureilite. *Meteoritics & Planetary Science* **40**, 5085.
- Yoshino, T., Walter, M. J., and Katsura, T., 2003. Core formation in planetesimals triggered by permeable flow. *Nature* **422**, 154 - 157.
- Yoshino, T., Walter, M. J., and Katsura, T., 2004. Connectivity of molten Fe alloy in peridotite based on in situ electrical conductivity measurements: implications for core formation in terrestrial planets. *EPSL* **222**, 625-643.

## 12 Appendix

### 12.1 Ureilite data

#### 12.1.1 ALHA84136

##### *Silicates (EPMA)*

Mineral	SiO <sub>2</sub> [wt%]	TiO <sub>2</sub> [wt%]	FeO [wt%]	Al <sub>2</sub> O <sub>3</sub> [wt%]	MgO [wt%]	CaO [wt%]	Cr <sub>2</sub> O <sub>3</sub> [wt%]	MnO [wt%]	wt-total	EPMA <sup>a</sup>
Olivine	42.35	0.05	0.70	0.03	56.17	0.24	0.32	0.37	100.30	Gö
Olivine	42.23	0.00	0.75	0.05	56.16	0.30	0.24	0.40	100.14	Gö
Olivine	42.50	0.01	0.76	0.03	56.87	0.33	0.12	0.27	100.91	Gö
Olivine	42.44	0.00	1.16	0.03	56.80	0.28	0.20	0.25	101.23	Gö
Olivine	42.16	0.03	1.73	0.02	55.40	0.29	0.47	0.59	100.72	Gö
Olivine	41.79	0.08	1.96	0.07	54.86	0.34	0.50	0.54	100.15	Gö
Olivine	42.01	0.02	2.57	0.05	54.50	0.31	0.56	0.55	100.57	Gö
Opx	57.85	0.19	1.35	0.32	35.85	3.79	0.84	0.43	100.71	Co
Opx	59.13	0.14	1.01	0.42	36.60	2.91	0.72	0.53	101.54	Co
Opx	57.90	0.05	3.09	0.06	37.93	0.72	0.17	0.43	100.50	Gö
Opx	58.72	0.13	2.49	0.48	35.19	2.67	0.69	0.45	100.91	Gö
Opx	58.45	0.11	2.68	0.53	35.45	2.65	0.77	0.54	101.21	Gö
Opx	58.30	0.13	3.47	0.47	34.66	2.62	0.84	0.52	101.01	Gö
Opx	57.56	0.09	2.88	0.42	35.61	2.44	0.86	0.55	100.39	Co
Opx	57.22	0.07	2.85	0.46	35.38	2.46	0.73	0.52	99.77	Co
Opx	57.58	0.15	2.86	0.44	35.80	2.49	0.75	0.54	100.66	Co
Opx	57.34	0.09	2.82	0.43	35.85	2.50	0.76	0.48	100.32	Co
Opx	57.22	0.10	2.71	0.48	34.73	2.50	0.90	0.48	99.13	Co
Opx	58.67	0.15	2.82	0.44	35.37	2.50	0.84	0.47	101.32	Co
Opx	57.92	0.08	2.87	0.50	36.27	2.51	0.85	0.47	101.47	Co
Opx	57.99	0.14	2.71	0.43	36.31	2.52	0.81	0.48	101.46	Co
Opx	57.88	0.08	2.78	0.42	35.25	2.52	0.80	0.59	100.33	Co
Opx	57.32	0.07	2.69	0.44	35.60	2.52	0.73	0.42	99.80	Co
Opx	57.31	0.12	2.93	0.45	35.92	2.54	0.76	0.52	100.55	Co
Opx	57.61	0.05	2.88	0.41	35.51	2.54	0.78	0.54	100.36	Co
Opx	57.89	0.11	2.96	0.43	35.76	2.54	0.81	0.48	101.08	Co
Opx	57.54	0.16	3.02	0.42	35.85	2.55	0.74	0.53	100.90	Co
Opx	57.40	0.10	2.80	0.44	35.85	2.55	0.79	0.46	100.45	Co
Opx	57.58	0.12	2.82	0.50	35.60	2.55	0.77	0.49	100.42	Co
Opx	57.46	0.12	2.92	0.44	35.71	2.56	0.72	0.49	100.54	Co
Opx	58.14	0.09	2.45	0.46	36.33	2.56	0.80	0.48	101.40	Co
Opx	57.74	0.11	2.87	0.40	36.08	2.56	0.80	0.57	101.18	Co
Opx	58.77	0.15	2.55	0.44	35.18	2.56	0.77	0.48	100.95	Co
Opx	57.08	0.09	2.77	0.44	35.34	2.57	0.73	0.57	99.66	Co
Opx	58.39	0.09	2.81	0.43	35.65	2.57	0.75	0.51	101.24	Co
Opx	57.88	0.15	2.78	0.49	35.86	2.58	0.65	0.51	100.92	Co
Opx	57.80	0.12	2.51	0.46	35.84	2.59	0.73	0.53	100.68	Co
Opx	58.14	0.13	2.45	0.46	36.00	2.59	0.75	0.48	101.10	Co
Opx	57.98	0.17	2.77	0.43	35.99	2.59	0.79	0.44	101.30	Co
Opx	58.60	0.08	2.98	0.42	35.80	2.60	0.77	0.53	101.83	Co
Opx	58.88	0.10	2.71	0.43	34.61	2.61	0.84	0.52	100.83	Co
Opx	58.52	0.08	2.55	0.42	35.53	2.62	0.84	0.49	101.04	Co
Opx	57.42	0.10	2.62	0.45	35.70	2.62	0.82	0.55	100.39	Co
Opx	58.16	0.09	2.54	0.41	36.12	2.62	0.79	0.48	101.29	Co
Opx	57.47	0.11	2.76	0.42	35.49	2.63	0.79	0.53	100.26	Co

Opx	58.71	0.11	2.86	0.45	34.56	2.64	0.85	0.49	100.66	Co
Opx	57.56	0.16	2.70	0.41	35.80	2.65	0.85	0.47	100.64	Co
Opx	58.28	0.06	2.93	0.49	35.81	2.65	0.84	0.62	101.67	Co
Mineral	SiO <sub>2</sub>	TiO <sub>2</sub>	FeO	Al <sub>2</sub> O <sub>3</sub>	MgO	CaO	Cr <sub>2</sub> O <sub>3</sub>	MnO	wt-total	EPMA <sup>a</sup>
	[wt%]	[wt%]	[wt%]	[wt%]	[wt%]	[wt%]	[wt%]	[wt%]		
Opx	57.85	0.14	2.10	0.44	36.28	2.65	0.70	0.55	100.85	Co
Opx	57.35	0.12	2.13	0.44	36.12	2.67	0.79	0.51	100.18	Co
Opx	56.95	0.13	3.42	0.31	35.19	2.73	0.78	0.53	100.22	Co
Opx	56.43	0.15	3.81	0.71	32.55	3.45	0.83	0.55	98.75	Co
Opx	57.13	0.12	3.12	0.30	35.01	3.62	0.87	0.48	100.76	Co
CPx	54.99	0.26	1.76	0.82	21.63	19.30	0.84	0.40	100.31	Gö
CPx	55.45	0.23	1.78	0.80	21.51	19.01	0.83	0.38	100.28	Gö
CPx	55.51	0.20	1.67	0.85	21.72	19.01	0.86	0.40	100.49	Gö
CPx	55.34	0.23	1.75	0.62	26.65	13.75	0.72	0.36	99.66	Co
CPx	55.80	0.18	1.98	0.66	25.80	14.50	0.78	0.41	100.32	Co
CPx	55.80	0.31	1.24	0.82	23.37	18.21	0.77	0.36	101.19	Co

<sup>a</sup> place of measurements: Co = Cologne, Gö = Göttingen

### **Silicates (LA-ICP-MS)**

Mineral	NiO		CoO	
	[ $\mu\text{g}\cdot\text{g}^{-1}$ ]	2 $\sigma$	[ $\mu\text{g}\cdot\text{g}^{-1}$ ]	2 $\sigma$
Olivine	17.8	4.0	5.7	0.6
Olivine	18.2	1.6	6.3	0.4
Olivine	17.4	2.6	6.6	0.7
Opx	28.1	3.8	9.0	0.9
Opx	28.8	3.5	6.7	0.6

### **Vein material and inclusions (EPMA)**

phase <sup>a</sup>	loc <sup>b</sup>	wt-%										EPMA <sup>c</sup>
		P	Si	Cr	Fe	Co	S	Ni	Mn	wt-total		
Coh	Sph	0.06	<0.02	0.15	90.25	0.22	0.03	1.99	<0.02	92.72	Co	
Coh	Sph	<0.02	0.04	0.33	91.82	0.25	0.04	1.96	<0.02	94.46	Co	
Met	Inc	0.09	0.15	0.11	95.16	0.08	<0.02	2.88	0.07	98.62	Gö	
Met	Inc	0.07	1.47	0.14	92.78	0.32	<0.02	4.21	<0.02	98.99	Co	
Met	Inc	0.24	0.13	0.05	98.26	0.08	<0.02	1.01	0.04	99.77	Co	
Met	Inc	0.08	0.13	0.10	90.10	0.26	<0.02	8.52	0.03	99.21	Co	
Met	Inc	0.07	0.05	0.12	92.57	0.38	<0.02	5.99	<0.02	99.18	Co	
Met	Inc	0.17	0.95	0.10	93.62	0.28	0.05	4.12	0.03	99.28	Co	
Met	Inc	0.13	1.30	0.13	94.11	0.31	<0.02	4.27	<0.02	100.26	Co	
Met	Inc	0.08	0.05	0.14	92.33	0.45	<0.02	6.85	0.03	99.89	Co	
Met	Vein	0.22	1.04	0.13	93.35	0.28	<0.02	4.15	<0.02	99.28	Gö	
Met	Vein	0.24	1.06	0.15	92.63	0.28	<0.02	4.22	<0.02	98.67	Gö	
Met	Vein	0.23	1.03	0.32	94.38	0.31	0.04	4.15	0.06	100.59	Gö	
Met	Vein	0.21	1.04	0.16	94.75	0.30	<0.02	4.34	<0.02	100.91	Gö	
Met	Vein	0.23	1.10	0.17	94.03	0.30	<0.02	4.29	<0.02	100.23	Gö	
Met	Vein	0.21	1.03	0.12	93.22	0.31	<0.02	4.08	0.04	99.08	Gö	
Met	Vein	0.23	1.10	0.08	93.20	0.30	<0.02	3.96	<0.02	98.94	Gö	
Met	Vein	0.10	1.18	0.12	93.46	0.25	<0.02	4.30	<0.02	99.41	Co	
Met	Vein	0.08	1.25	0.05	93.70	0.29	<0.02	4.13	<0.02	99.51	Co	
Met	Vein	0.12	1.07	0.05	95.02	0.24	<0.02	4.23	<0.02	100.75	Co	
Met	Vein	0.09	1.03	0.07	95.81	0.27	<0.02	4.20	<0.02	101.49	Co	
Met	Vein	0.09	1.31	0.14	93.38	0.28	<0.02	4.47	<0.02	99.67	Co	
Met	Vein	0.11	1.07	0.16	94.65	0.37	<0.02	4.08	<0.02	100.44	Co	
Met	Vein	0.09	1.26	0.10	93.19	0.27	<0.02	3.96	<0.02	98.87	Co	
Met	Vein	0.10	1.12	0.15	93.77	0.26	<0.02	4.22	<0.02	99.62	Co	
Met	Vein	0.09	1.20	0.15	95.29	0.26	<0.02	4.39	0.03	101.38	Co	
Met	Vein	0.11	1.13	0.11	93.78	0.31	<0.02	4.21	<0.02	99.64	Co	
Met	Vein	0.05	1.10	0.11	94.05	0.27	<0.02	3.91	<0.02	99.49	Co	
Met	Vein	0.10	1.14	0.19	94.89	0.18	0.03	4.17	<0.02	100.70	Co	

Met	Vein	0.11	1.06	0.12	94.20	0.31	<0.02	4.07	<0.02	99.87	Co
Met	Vein	0.12	0.98	0.12	94.06	0.33	<0.02	4.13	0.03	99.75	Co
Met	Vein	0.07	1.02	0.12	94.18	0.30	<0.02	4.32	<0.02	100.02	Co
phase <sup>a</sup>	loc <sup>b</sup>	P	Si	Cr	Fe	Co	S	Ni	Mn	wt-total	EPMA <sup>c</sup>
		[wt%]									
Met	Vein	0.09	1.21	0.13	94.80	0.37	<0.02	3.99	<0.02	100.58	Co
Met	Vein	0.11	1.10	0.20	94.48	0.29	<0.02	4.21	<0.02	100.38	Co
Met	Vein	0.09	1.08	0.07	93.07	0.31	<0.02	4.30	<0.02	98.91	Co
Met	Vein	0.08	1.02	0.14	93.10	0.24	<0.02	4.13	0.03	98.72	Co
Met	Vein	0.11	1.23	0.15	93.55	0.22	<0.02	4.06	<0.02	99.33	Co
Met	Vein	0.13	1.00	0.06	93.39	0.28	<0.02	4.13	<0.02	98.99	Co
Met	Vein	0.11	1.19	0.09	94.79	0.29	<0.02	4.34	0.04	100.82	Co
Met	Vein	0.11	1.14	0.24	94.84	0.30	<0.02	4.26	<0.02	100.88	Co
Met	Vein	0.12	1.35	0.03	93.65	0.32	<0.02	3.81	<0.02	99.28	Co
Met	Vein	0.08	1.09	0.14	94.74	0.31	<0.02	3.96	0.03	100.32	Co
Met	Vein	0.13	1.27	0.21	93.62	0.27	<0.02	4.05	<0.02	99.54	Co
Met	Vein	0.11	1.16	0.19	95.61	0.30	<0.02	4.30	<0.02	101.67	Co
Met	Vein	0.07	1.32	0.08	92.47	0.29	<0.02	3.90	<0.02	98.12	Co
Met	Vein	0.14	1.19	0.13	93.93	0.31	<0.02	4.14	<0.02	99.83	Co
Met	Vein	0.14	1.32	0.11	95.31	0.30	<0.02	4.00	<0.02	101.17	Co
Met	Vein	0.13	1.13	0.14	94.66	0.25	<0.02	4.20	0.04	100.51	Co
Met	Vein	0.08	1.13	0.15	95.23	0.30	0.03	4.28	<0.02	101.19	Co
Met	Vein	0.13	1.19	0.14	95.36	0.33	<0.02	4.40	<0.02	101.55	Co
Met	Vein	0.12	1.31	0.16	94.63	0.31	<0.02	4.32	0.03	100.84	Co
Met	Vein	0.19	0.08	0.12	97.33	0.20	0.03	3.18	<0.02	101.12	Co
Met	Vein	0.13	1.05	0.15	95.04	0.31	<0.02	4.39	<0.02	101.10	Co
Met	Vein	0.16	1.00	0.15	95.47	0.31	<0.02	4.26	0.04	101.34	Co
Dau	Inc	<0.02	0.07	33.21	18.51	<0.02	43.16	0.06	2.32	97.36	Gö
Dau	Inc	<0.02	0.29	33.54	17.91	<0.02	44.16	<0.02	2.00	97.93	Gö
Troi	Inc	<0.02	0.13	5.37	54.35	<0.02	38.58	<0.02	0.34	98.81	Gö
Troi	Inc	<0.02	0.07	7.13	52.06	<0.02	38.48	0.03	0.43	98.24	Gö
Troi	Inc	<0.02	1.13	5.02	53.05	<0.02	37.32	<0.02	0.49	97.09	Gö
Troi	Inc	<0.02	0.45	4.38	55.29	<0.02	37.90	<0.02	0.46	98.54	Gö
Troi	Inc	<0.02	0.12	5.13	55.51	<0.02	37.26	<0.02	0.36	97.96	Co

<sup>a</sup> phases: Met = metal, Coh = cohenite, Dau = daubreelite, Troi = troilite

<sup>b</sup> locations: Sph = spherule inclusion, Vein = vein material, Inc = inclusion in silicate

<sup>c</sup> place of measurements: Co = Cologne, Gö = Göttingen

## 12.1.2 ALHA77257

### *Silicates (EPMA)*

Mineral	SiO <sub>2</sub> [wt%]	TiO <sub>2</sub> [wt%]	FeO [wt%]	Al <sub>2</sub> O <sub>3</sub> [wt%]	MgO [wt%]	CaO [wt%]	Cr <sub>2</sub> O <sub>3</sub> [wt%]	MnO [wt%]	wt-total	EPMA <sup>a</sup>
Olivine	41.55	<0.02	5.02	0.05	52.04	0.35	0.71	0.52	100.3	Gö
Olivine	40.62	<0.02	9.28	0.04	49.41	0.32	0.63	0.46	100.8	Gö
Olivine	40.23	0.03	9.68	0.07	48.63	0.33	0.74	0.52	100.3	Gö
Olivine	40.96	<0.02	11.26	0.01	50.13	0.29	0.74	0.44	103.9	Co
Olivine	41.16	<0.02	11.88	0.03	49.50	0.30	0.73	0.45	104.0	Co
Olivine	40.15	0.04	12.29	<0.02	48.08	0.30	0.78	0.44	102.1	Co
Olivine	41.21	0.02	12.34	0.03	47.69	0.29	0.64	0.44	102.7	Co
Olivine	40.15	<0.02	12.37	0.03	46.51	0.32	0.69	0.47	100.6	Gö
Olivine	41.42	0.02	12.42	0.02	47.51	0.30	0.67	0.43	102.8	Co
Olivine	40.04	0.05	12.59	0.04	48.39	0.29	0.69	0.45	102.6	Co
Olivine	40.95	<0.02	12.70	0.01	47.70	0.26	0.81	0.47	102.9	Co
Olivine	39.74	<0.02	12.76	0.04	46.44	0.34	0.70	0.43	100.5	Gö
Olivine	40.75	<0.02	12.78	0.04	48.81	0.30	0.66	0.48	103.8	Co
Olivine	40.08	0.03	12.79	0.03	45.66	0.34	0.76	0.45	100.2	Gö
Olivine	39.72	<0.02	12.81	0.05	46.06	0.33	0.72	0.47	100.2	Gö
Olivine	39.86	<0.02	12.94	0.04	45.88	0.31	0.72	0.46	100.2	Gö
Olivine	40.00	0.07	12.95	0.02	45.33	0.35	0.69	0.41	99.9	Gö
Olivine	40.97	<0.02	13.04	<0.02	49.04	0.28	0.73	0.49	104.6	Co
Olivine	39.67	0.03	13.11	0.05	45.69	0.30	0.68	0.46	100.0	Gö
Olivine	41.17	<0.02	13.11	0.07	48.85	0.29	0.75	0.42	104.7	Co
Olivine	39.94	<0.02	13.18	0.03	47.83	0.29	0.66	0.42	102.4	Co
Olivine	41.05	<0.02	13.23	0.01	48.56	0.30	0.72	0.42	104.3	Co
Olivine	39.73	<0.02	13.26	0.08	45.97	0.35	0.72	0.43	100.6	Gö
Olivine	40.22	<0.02	13.29	0.02	47.82	0.29	0.77	0.47	102.9	Co
Olivine	40.97	<0.02	13.32	0.01	48.91	0.30	0.73	0.50	104.7	Co
Olivine	41.15	<0.02	13.40	0.04	48.61	0.30	0.63	0.39	104.5	Co
Olivine	40.86	<0.02	13.43	0.03	48.42	0.29	0.71	0.43	104.2	Co
Olivine	40.54	<0.02	13.48	0.03	48.12	0.29	0.67	0.49	103.6	Co
Olivine	40.74	0.03	13.52	0.04	47.44	0.28	0.73	0.47	103.2	Co
Opx	56.40	0.07	8.01	0.60	30.07	3.38	1.09	0.41	100.1	Gö
Opx	55.99	0.07	7.94	0.60	29.60	3.36	1.12	0.42	99.2	Gö
Opx	56.27	0.12	8.13	0.57	30.11	3.36	1.10	0.42	100.1	Gö
Opx	56.34	0.12	8.26	0.62	30.08	3.31	1.13	0.48	100.4	Gö
Opx	55.62	0.09	8.16	0.59	30.10	3.23	1.08	0.50	99.5	Gö
Opx	56.53	0.07	7.93	0.59	31.14	3.17	0.93	0.47	100.8	Co
Opx	57.54	0.08	8.12	0.58	31.63	3.17	1.13	0.48	102.7	Co
Opx	57.96	0.08	8.15	0.63	32.13	3.18	1.08	0.50	103.7	Co
Opx	56.36	0.06	8.09	0.57	31.31	3.18	1.11	0.46	101.1	Co
Opx	57.96	0.10	8.29	0.63	32.95	3.18	1.03	0.42	104.6	Co
Opx	57.55	0.08	8.39	0.58	32.38	3.19	1.12	0.50	103.8	Co
Opx	56.23	0.10	8.51	0.57	31.50	3.20	1.10	0.49	101.7	Co
Opx	57.60	0.09	8.35	0.62	31.91	3.20	1.01	0.45	103.2	Co
Opx	57.08	0.02	8.20	0.66	31.67	3.21	1.17	0.42	102.4	Co
Opx	57.81	0.15	7.69	0.62	31.72	3.21	1.05	0.42	102.7	Co
Opx	57.31	0.07	8.45	0.61	31.89	3.21	1.10	0.47	103.1	Co
Opx	56.75	0.06	8.12	0.56	31.43	3.22	1.15	0.53	101.8	Co
Opx	56.93	0.06	7.91	0.58	31.56	3.22	1.13	0.47	101.9	Co
Opx	57.24	0.08	7.90	0.65	31.90	3.22	1.22	0.43	102.6	Co
Opx	57.65	0.09	8.04	0.61	31.53	3.22	1.12	0.41	102.7	Co
Opx	57.61	0.10	8.28	0.61	32.31	3.23	1.14	0.50	103.8	Co
Opx	57.13	0.09	8.72	0.62	32.12	3.23	1.17	0.45	103.5	Co
Opx	57.73	0.06	7.93	0.57	31.05	3.23	1.17	0.47	102.2	Co

Opx	57.68	0.10	8.19	0.57	31.78	3.24	1.05	0.41	103.0	Co
Opx	57.71	0.04	8.30	0.62	31.68	3.24	1.18	0.50	103.3	Co
Mineral	SiO <sub>2</sub> [wt%]	TiO <sub>2</sub> [wt%]	FeO [wt%]	Al <sub>2</sub> O <sub>3</sub> [wt%]	MgO [wt%]	CaO [wt%]	Cr <sub>2</sub> O <sub>3</sub> [wt%]	MnO [wt%]	wt-total	EPMA <sup>a</sup>
Opx	57.70	0.09	8.14	0.57	32.47	3.24	1.07	0.55	103.8	Co
Opx	57.49	0.10	8.29	0.58	31.83	3.24	1.07	0.43	103.0	Co
Opx	57.39	0.11	8.34	0.58	31.59	3.24	1.13	0.47	102.8	Co
Opx	57.56	0.06	8.09	0.61	31.79	3.24	1.00	0.52	102.9	Co
Opx	57.41	0.05	8.43	0.58	31.90	3.24	1.06	0.48	103.1	Co
Opx	57.42	0.10	7.94	0.54	31.51	3.25	1.05	0.54	102.3	Co
Opx	57.40	0.07	8.61	0.66	32.16	3.25	1.18	0.45	103.8	Co
Opx	57.01	0.03	8.36	0.64	31.94	3.25	1.12	0.50	102.8	Co
Opx	57.40	0.09	8.33	0.63	31.19	3.26	1.05	0.54	102.5	Co
Opx	57.75	0.07	8.43	0.61	32.19	3.26	1.03	0.41	103.7	Co
Opx	57.83	0.06	8.19	0.58	31.31	3.26	1.15	0.48	102.9	Co
Opx	57.94	0.05	8.34	0.58	32.37	3.26	1.06	0.45	104.1	Co
Opx	58.16	0.12	8.30	0.65	32.19	3.26	1.17	0.49	104.3	Co
Opx	56.85	0.10	8.24	0.63	31.54	3.26	1.09	0.39	102.1	Co
Opx	57.64	0.10	8.52	0.63	32.24	3.27	1.08	0.54	104.0	Co
Opx	55.79	0.06	8.03	0.59	31.08	3.27	1.16	0.55	100.5	Co
Opx	55.48	0.05	7.78	0.65	31.71	3.27	1.18	0.53	100.7	Co
Opx	57.66	0.11	7.94	0.54	32.22	3.28	1.26	0.49	103.5	Co
Opx	57.85	0.05	8.05	0.63	31.92	3.28	1.01	0.45	103.2	Co
Opx	57.42	0.11	8.11	0.63	31.63	3.28	1.04	0.46	102.7	Co
Opx	56.96	0.06	8.21	0.60	32.36	3.28	1.16	0.51	103.1	Co
Opx	57.45	0.07	8.47	0.57	31.40	3.28	1.03	0.42	102.7	Co
Opx	57.73	0.09	7.92	0.58	32.43	3.28	1.12	0.45	103.6	Co
Opx	58.01	0.02	8.08	0.57	32.13	3.28	1.25	0.46	103.8	Co
Opx	57.16	0.07	8.14	0.64	31.57	3.28	1.10	0.39	102.3	Co
Opx	57.76	0.10	8.24	0.66	31.83	3.29	1.12	0.44	103.4	Co
Opx	57.61	0.09	8.50	0.58	31.86	3.29	1.08	0.43	103.4	Co
Opx	58.27	0.07	7.79	0.59	30.66	3.29	1.17	0.45	102.3	Co
Opx	58.27	0.13	8.19	0.52	31.01	3.30	1.07	0.43	102.9	Co
Opx	57.14	0.09	7.96	0.56	31.22	3.30	1.12	0.51	101.9	Co
Opx	55.51	0.11	8.43	0.68	31.71	3.30	1.17	0.48	101.4	Co
Opx	57.58	0.12	8.25	0.59	31.82	3.30	1.16	0.47	103.3	Co
Opx	57.79	0.10	8.60	0.63	31.80	3.30	1.03	0.48	103.7	Co
Opx	57.60	0.09	8.36	0.56	31.00	3.32	1.12	0.43	102.5	Co
Opx	57.04	0.04	8.16	0.60	30.88	3.34	1.20	0.56	101.8	Co

<sup>a</sup> place of measurements: Co = Cologne, Gö = Göttingen

### ***Silicates (LA-ICP-MS)***

Mineral	NiO	2 $\sigma$	CoO	2 $\sigma$
	[ $\mu\text{g}\cdot\text{g}^{-1}$ ]		[ $\mu\text{g}\cdot\text{g}^{-1}$ ]	
Olivine	54.1	4.9	28.2	2.5
Olivine	58.5	4.8	30.2	2.5
Olivine	58.8	2.7	30.4	1.1
Olivine	54.0	1.8	29.3	0.7
Olivine	59.9	2.7	27.7	1.1
Olivine	57.6	2.7	29.2	1.1
Olivine	60.1	2.8	32.1	1.2
Olivine	54.3	2.7	29.8	1.0
Olivine	66.5	3.2	32.8	1.5
Opx	17.0	1.7	14.4	1.3
Opx	17.5	1.6	13.1	1.1
Opx	14.6	1.5	13.3	1.1
Opx	18.2	1.9	13.8	1.3
Opx	18.1	1.1	14.4	0.6

### ***Vein material and inclusions (EPMA)***

Phase <sup>a</sup>	Loc <sup>b</sup>	P	Si	Cr	Fe	Co	S	Ni	Mn	wt-total	EPMA <sup>c</sup>
		[wt%]									
Met	Inc	0.03	0.07	0.13	99.40	<0.02	<0.02	0.44	<0.02	100.07	Co
Met	Inc	0.07	0.17	0.28	97.40	0.07	<0.02	0.59	0.04	98.57	Co
Met	Inc	0.04	0.25	0.21	96.57	<0.02	0.04	0.78	<0.02	97.87	Co
Met	Inc	0.04	0.23	0.22	96.94	<0.02	<0.02	0.96	0.03	98.42	Co
Met	Inc	0.13	<0.02	0.28	97.19	0.08	<0.02	1.64	<0.02	99.34	Co
Met	Inc	0.12	0.04	0.19	96.66	0.07	<0.02	1.75	0.04	98.84	Co
Met	Inc	0.15	<0.02	0.17	94.84	0.25	<0.02	3.35	<0.02	98.78	Co
Met	Inc	0.13	<0.02	0.33	94.78	0.28	<0.02	3.76	<0.02	99.30	Co
Met	Inc	0.14	0.03	0.34	96.02	0.31	<0.02	3.97	<0.02	100.81	Co
Met	Inc	0.09	0.04	0.29	95.00	0.28	<0.02	4.16	<0.02	99.85	Co
Met	Vein	0.09	<0.02	0.28	96.04	0.22	<0.02	3.31	<0.02	99.96	Co
Met	Vein	0.23	<0.02	0.30	93.04	0.25	<0.02	3.34	<0.02	97.29	Gö
Met	Vein	0.08	<0.02	0.30	95.95	0.24	0.04	3.50	<0.02	100.12	Co
Met	Vein	0.14	0.03	0.28	96.27	0.21	<0.02	3.50	<0.02	100.42	Co
Met	Vein	0.23	<0.02	0.35	94.20	0.27	<0.02	3.50	0.03	98.57	Co
Met	Vein	0.13	0.04	0.27	96.26	0.27	<0.02	3.53	<0.02	100.53	Co
Met	Vein	0.28	0.03	0.27	93.55	0.28	<0.02	3.62	<0.02	98.11	Gö
Met	Vein	0.15	0.03	0.32	95.84	0.24	<0.02	3.62	<0.02	100.20	Co
Met	Vein	0.05	0.03	0.36	95.58	0.28	<0.02	3.63	<0.02	99.94	Co
Met	Vein	0.18	<0.02	0.21	93.85	0.20	<0.02	3.67	<0.02	98.13	Co
Met	Vein	0.12	<0.02	0.20	96.29	0.27	<0.02	3.75	<0.02	100.67	Co
Met	Vein	0.40	0.03	0.30	93.82	0.26	<0.02	3.79	0.03	98.72	Gö
Met	Vein	0.38	0.05	0.28	92.83	0.28	<0.02	3.79	<0.02	97.73	Gö
Met	Vein	0.14	0.03	0.32	96.31	0.25	<0.02	3.81	0.03	100.86	Co
Met	Vein	0.09	<0.02	0.32	96.52	0.28	<0.02	3.81	<0.02	101.03	Co
Met	Vein	0.14	<0.02	0.31	96.42	0.28	<0.02	3.82	<0.02	100.98	Co
Met	Vein	0.13	0.05	0.32	94.07	0.25	<0.02	3.85	<0.02	98.66	Co
Met	Vein	0.16	0.03	0.29	95.11	0.25	<0.02	3.86	<0.02	99.70	Co
Met	Vein	0.10	0.21	0.28	94.93	0.27	<0.02	3.88	<0.02	99.67	Co
Met	Vein	0.32	0.04	0.32	92.93	0.29	<0.02	3.90	0.04	97.93	Gö

Phase <sup>a</sup>	Loc <sup>b</sup>	P [wt%]	Si [wt%]	Cr [wt%]	Fe [wt%]	Co [wt%]	S [wt%]	Ni [wt%]	Mn [wt%]	wt-total	EPMA <sup>c</sup>
Met	Vein	0.12	<0.02	0.28	95.84	0.25	<0.02	3.90	<0.02	100.41	Co
Met	Vein	0.13	<0.02	0.26	95.68	0.30	<0.02	3.91	<0.02	100.30	Co
Met	Vein	0.12	<0.02	0.34	94.92	0.21	<0.02	3.91	<0.02	99.53	Co
Met	Vein	0.30	0.03	0.35	93.70	0.30	<0.02	3.92	0.03	98.73	Gö
Met	Vein	0.07	<0.02	0.31	95.19	0.28	<0.02	3.92	<0.02	99.78	Co
Met	Vein	0.10	0.05	0.31	94.56	0.21	<0.02	3.92	<0.02	99.14	Co
Met	Vein	0.13	<0.02	0.37	96.04	0.32	<0.02	3.94	<0.02	100.83	Co
Met	Vein	0.13	<0.02	0.29	96.42	0.28	<0.02	3.95	<0.02	101.10	Co
Met	Vein	0.08	<0.02	0.29	94.35	0.31	<0.02	3.96	<0.02	99.00	Co
Met	Vein	0.11	<0.02	0.29	95.59	0.36	<0.02	3.96	<0.02	100.34	Co
Met	Vein	0.15	<0.02	0.24	96.42	0.34	<0.02	4.00	<0.02	101.17	Co
Met	Vein	0.13	0.04	0.25	95.24	0.28	<0.02	4.01	<0.02	99.96	Co
Met	Vein	0.14	0.03	0.32	95.91	0.30	<0.02	4.02	<0.02	100.72	Co
Met	Vein	0.10	0.03	0.32	94.42	0.24	<0.02	4.02	<0.02	99.14	Co
Met	Vein	0.11	<0.02	0.30	95.21	0.27	<0.02	4.04	<0.02	99.95	Co
Met	Vein	0.15	<0.02	0.35	95.35	0.28	<0.02	4.05	<0.02	100.18	Co
Met	Vein	0.12	0.17	0.29	94.64	0.27	<0.02	4.09	<0.02	99.58	Co
Met	Vein	0.08	0.03	0.36	95.75	0.32	<0.02	4.09	<0.02	100.63	Co
Met	Vein	0.07	0.04	0.27	96.57	0.29	<0.02	4.13	0.05	101.37	Co
Met	Vein	0.13	0.03	0.33	96.70	0.28	<0.02	4.13	<0.02	101.61	Co
Met	Vein	0.11	0.04	0.24	92.87	0.32	<0.02	4.15	<0.02	97.74	Co
Met	Vein	0.12	0.04	0.32	95.59	0.28	<0.02	4.28	<0.02	100.63	Co
Met	Vein	0.11	0.03	0.30	93.00	0.32	<0.02	4.29	<0.02	98.06	Co
troi	Sph	0.00	0.28	7.09	51.89	<0.02	37.27	0.09	1.10	97.77	Gö
troi	Sph	0.04	0.04	7.76	52.92	<0.02	36.79	0.35	1.09	97.83	Co
troi	Sph	0.02	<0.02	1.08	61.45	<0.02	36.96	0.06	0.06	99.71	Gö
troi	Sph	0.01	0.41	0.76	59.92	<0.02	36.22	0.06	0.07	97.47	Gö
troi	Sph	0.00	0.05	0.82	62.48	<0.02	35.70	0.13	0.05	99.08	Co
troi	Sph	0.00	0.03	1.07	62.46	<0.02	36.21	0.10	0.03	99.78	Co
troi	Sph	0.00	0.16	2.52	59.62	<0.02	35.72	0.05	0.26	97.96	Co
Met	Sph	0.24	0.03	0.11	92.91	0.35	<0.02	5.17	<0.02	98.93	Gö
Met	Sph	0.11	<0.02	0.10	94.87	0.33	<0.02	5.79	<0.02	101.23	Co
Met	Sph	0.35	<0.02	<0.02	95.60	0.43	<0.02	5.36	<0.02	101.85	Gö
Met	Sph	0.29	<0.02	0.08	93.10	0.42	<0.02	5.48	<0.02	99.48	Gö
Met	Sph	0.12	<0.02	0.08	95.22	0.41	<0.02	5.61	<0.02	101.47	Co
Met	Sph	0.08	<0.02	0.08	94.16	0.38	<0.02	4.97	<0.02	99.70	Co
Met	Sph	0.35	<0.02	0.31	94.35	0.17	<0.02	2.42	<0.02	97.71	Gö
Met	Sph	0.17	0.03	0.32	97.89	0.14	<0.02	2.44	<0.02	100.98	Co
Coh	Sph	0.07	0.03	0.37	91.18	0.13	<0.02	1.34	0.03	93.13	Co

<sup>a</sup> phases: Met = metal, Coh = cohenite, Troi = troilite

<sup>b</sup> locations: Sph = spherule inclusion, Vein = vein material, Inc = inclusion in silicate

<sup>c</sup> place of measurements: Co = Cologne, Gö = Göttingen

### 12.1.3 DaG340

#### *Silicates (EPMA)*

Mineral	SiO <sub>2</sub> [wt%]	TiO <sub>2</sub> [wt%]	FeO [wt%]	Al <sub>2</sub> O <sub>3</sub> [wt%]	MgO [wt%]	CaO [wt%]	Cr <sub>2</sub> O <sub>3</sub> [wt%]	MnO [wt%]	wt-total	EPMA <sup>a</sup>
Olivine	39.61	0.04	16.69	< 0.02	44.49	0.33	0.82	0.44	102.45	Co
Olivine	39.07	0.04	17.30	0.06	41.91	0.37	0.74	0.46	100.03	Co
Olivine	39.62	0.03	17.41	0.05	43.07	0.40	0.70	0.40	101.67	Co
Olivine	39.67	< 0.02	17.45	0.04	43.49	0.39	0.80	0.48	102.34	Co
Olivine	39.89	< 0.02	17.49	0.05	43.07	0.39	0.76	0.46	102.21	Co
Olivine	40.18	< 0.02	17.65	0.03	42.96	0.38	0.75	0.40	102.40	Co
Olivine	39.81	0.07	17.82	0.03	42.43	0.42	0.73	0.48	101.80	Co
Olivine	39.80	< 0.02	17.90	0.05	42.38	0.34	0.78	0.41	101.72	Co
Olivine	39.32	< 0.02	17.98	< 0.02	43.03	0.36	0.80	0.42	101.93	Co
Olivine	39.67	0.03	17.99	< 0.02	42.39	0.35	0.78	0.40	101.63	Co
Olivine	39.80	< 0.02	18.17	0.03	42.49	0.36	0.76	0.50	102.11	Co
Olivine	39.81	< 0.02	18.27	0.08	42.42	0.37	0.80	0.44	102.26	Co
Olivine	39.88	< 0.02	18.39	0.03	42.48	0.39	0.82	0.40	102.46	Co
Olivine	39.55	< 0.02	18.39	0.03	42.86	0.41	0.78	0.43	102.48	Co
Olivine	39.68	0.03	18.47	0.04	42.15	0.37	0.80	0.42	102.01	Co
Olivine	39.65	0.03	18.61	< 0.02	42.85	0.36	0.71	0.46	102.68	Co
Olivine	39.79	< 0.02	18.67	0.08	42.62	0.42	0.80	0.45	102.83	Co
Olivine	39.45	< 0.02	18.84	0.07	41.81	0.39	0.75	0.47	101.86	Co
Olivine	39.57	< 0.02	18.90	< 0.02	41.88	0.39	0.74	0.42	102.01	Co
Olivine	39.52	< 0.02	18.91	< 0.02	42.61	0.34	0.70	0.44	102.58	Co
Olivine	40.10	0.03	18.98	0.03	42.13	0.36	0.73	0.43	102.91	Co
Olivine	39.02	< 0.02	19.22	0.05	41.59	0.41	0.85	0.40	101.54	Co
Olivine	39.50	< 0.02	18.54	0.03	42.70	0.32	0.84	0.44	102.42	Co
Olivine	39.92	< 0.02	17.68	< 0.02	43.06	0.34	0.84	0.38	102.25	Co
Olivine	39.40	< 0.02	17.81	< 0.02	42.90	0.35	0.78	0.42	101.67	Co
Olivine	39.60	< 0.02	18.10	< 0.02	42.79	0.35	0.80	0.49	102.17	Co
Olivine	39.65	0.03	18.51	< 0.02	42.64	0.36	0.83	0.42	102.50	Co
Olivine	39.49	< 0.02	18.51	0.05	42.15	0.37	0.78	0.41	101.75	Co
Olivine	38.98	< 0.02	18.34	< 0.02	42.54	0.37	0.77	0.47	101.49	Co
Olivine	39.25	< 0.02	19.28	0.04	42.58	0.37	0.70	0.40	102.68	Co
Olivine	39.53	0.03	17.17	0.04	43.56	0.38	0.73	0.41	101.84	Co
Olivine	39.61	< 0.02	18.85	< 0.02	42.05	0.38	0.76	0.37	102.07	Co
Olivine	39.42	< 0.02	19.09	0.08	42.83	0.38	0.88	0.40	103.18	Co
Olivine	39.41	0.04	18.05	0.03	42.13	0.38	0.84	0.40	101.29	Co
Olivine	39.41	< 0.02	17.16	0.05	44.08	0.39	0.78	0.39	102.28	Co
Olivine	39.50	0.03	18.20	0.05	42.62	0.39	0.76	0.39	101.93	Co
Olivine	39.39	< 0.02	17.98	0.04	43.19	0.39	0.88	0.41	102.32	Co
Olivine	39.73	< 0.02	18.07	< 0.02	42.73	0.40	0.74	0.44	102.15	Co
Opx	55.89	0.08	10.70	0.87	27.23	5.02	1.32	0.50	101.65	Co
Opx	55.65	0.08	10.76	0.79	27.42	5.07	1.31	0.44	101.55	Co

Mineral	SiO <sub>2</sub> [wt%]	TiO <sub>2</sub> [wt%]	FeO [wt%]	Al <sub>2</sub> O <sub>3</sub> [wt%]	MgO [wt%]	CaO [wt%]	Cr <sub>2</sub> O <sub>3</sub> [wt%]	MnO [wt%]	wt-total	EPMA <sup>a</sup>
Opx	55.79	0.12	10.84	0.86	27.15	5.10	1.25	0.39	101.49	Co
Opx	55.85	0.13	10.88	0.86	26.72	5.06	1.20	0.44	101.14	Co
Opx	55.88	0.10	10.95	0.80	26.97	5.02	1.23	0.48	101.54	Co
Opx	54.80	0.11	10.97	0.81	26.96	4.78	1.16	0.39	99.98	Co
Opx	55.72	0.09	11.12	0.78	26.78	5.11	1.25	0.40	101.30	Co
Opx	56.19	0.15	11.19	0.86	27.62	5.07	1.32	0.44	102.88	Co
Opx	55.23	0.13	11.23	0.82	26.73	5.00	1.31	0.42	100.95	Co
Opx	55.39	< 0.02	11.38	0.86	26.74	5.22	1.32	0.41	101.37	Co
Opx	55.54	0.10	11.53	0.85	27.35	5.09	1.24	0.48	102.26	Co
Opx	55.14	0.10	11.76	0.85	27.21	5.03	1.13	0.43	101.65	Co
Opx	54.71	0.08	12.89	0.79	26.83	4.93	1.26	0.47	102.12	Co
Opx	55.44	0.10	10.97	0.73	27.24	4.90	1.34	0.43	101.17	Co
Opx	55.89	0.07	10.66	0.82	27.19	4.93	1.20	0.49	101.25	Co
Opx	55.97	0.08	11.18	0.74	27.10	4.96	1.24	0.39	101.70	Co
Opx	55.68	0.12	10.99	0.89	26.53	4.99	1.38	0.42	101.08	Co
Opx	55.57	0.04	11.02	0.74	27.50	5.00	1.22	0.45	101.61	Co
Opx	55.63	0.03	10.66	0.75	27.10	5.01	1.29	0.42	100.88	Co
Opx	56.29	0.07	10.55	0.86	27.16	5.01	1.36	0.47	101.78	Co
Opx	55.83	0.07	10.84	0.82	27.42	5.09	1.21	0.40	101.73	Co
Opx	52.99	0.11	14.13	0.95	26.19	5.34	1.31	0.42	101.58	Co

<sup>a</sup> place of measurements: Co = Cologne, Gö = Göttingen

### ***Silicates (LA-ICP-MS)***

Mineral	NiO [µg·g <sup>-1</sup> ]	2σ	CoO [µg·g <sup>-1</sup> ]	2σ
Olivine	98.6	8.5	51.3	4.1
Olivine	90.1	10.7	54.4	5.4
Olivine	126.9	14.5	46.8	6.4
Olivine	116.0	11.6	57.4	4.2
Olivine	111.2	14.0	42.1	7.1
Opx	29.5	1.8	23.8	1.4
Opx	28.0	1.9	25.2	1.5

### ***Vein material and inclusions***

Phase <sup>a</sup>	Loc <sup>b</sup>	P [wt%]	Si [wt%]	Cr [wt%]	Fe [wt%]	Co [wt%]	S [wt%]	Ni [wt%]	Mn [wt%]	wt-total	EPMA <sup>c</sup>
Metal	Inc	0.32	0.88	0.19	84.33	0.49	1.72	9.41	0.05	97.34	Co
Metal	Inc	< 0.02	0.38	0.15	98.46	0.06	0.03	0.45	0.03	99.53	Co
Metal	Inc	0.03	0.43	0.09	97.81	0.05	0.04	0.57	0.04	99.01	Co
Metal	Inc	0.09	0.05	0.16	98.43	0.14	< 0.02	1.68	< 0.02	100.55	Co
Metal	Inc	0.09	0.03	0.12	92.61	0.31	0.05	7.53	< 0.02	100.74	Co
Metal	Inc	0.04	0.06	0.19	84.09	0.64	0.53	13.56	0.04	99.11	Co
Metal	Vein	0.08	2.06	0.17	94.10	0.24	< 0.02	3.79	< 0.02	100.43	Co
Troi	Inc	< 0.02	0.05	0.46	62.26	< 0.02	36.09	0.09	0.08	98.95	Co
Troi	Inc	< 0.02	0.08	0.36	64.86	< 0.02	32.28	1.04	0.03	98.62	Co

a phases: Coh = cohenite, Troi = troilite

b locations: Sph = spherule inclusion, Vein = vein material, Inc = inclusion in silicate

c place of measurements: Co = Cologne, Gö = Göttingen

## 12.1.4 EET87517

### *Silicates (EPMA)*

Mineral	SiO <sub>2</sub> [wt%]	TiO <sub>2</sub> [wt%]	FeO [wt%]	Al <sub>2</sub> O <sub>3</sub> [wt%]	MgO [wt%]	CaO [wt%]	Cr <sub>2</sub> O <sub>3</sub> [wt%]	MnO [wt%]	wt-total	EPMA <sup>a</sup>
Olivine	41.70	< 0.02	3.97	0.06	52.92	0.41	0.38	0.46	100.0	Gö
Olivine	41.30	0.04	5.85	0.07	52.07	0.35	0.69	0.51	100.9	Gö
Olivine	41.14	< 0.02	6.19	0.08	51.76	0.33	0.39	0.44	100.4	Gö
Olivine	41.23	0.03	6.63	0.08	51.61	0.31	0.68	0.54	101.1	Gö
Olivine	40.89	< 0.02	6.64	0.07	50.98	0.38	0.36	0.39	99.8	Gö
Olivine	41.20	0.03	6.86	0.13	51.69	0.31	0.37	0.41	101.0	Co
Olivine	41.00	< 0.02	7.31	0.08	52.12	0.28	0.37	0.40	101.6	Co
Olivine	40.74	0.06	7.33	0.03	52.08	0.33	0.38	0.39	101.3	Co
Olivine	41.72	< 0.02	7.48	< 0.02	50.38	0.31	0.33	0.46	100.8	Co
Olivine	41.27	0.04	7.58	0.05	51.52	0.30	0.36	0.40	101.5	Co
Olivine	41.63	< 0.02	7.62	< 0.02	50.65	0.32	0.36	0.41	101.0	Co
Olivine	40.95	< 0.02	7.71	0.05	50.70	0.30	0.34	0.42	100.5	Gö
Olivine	40.91	< 0.02	7.72	0.04	52.10	0.31	0.34	0.44	101.9	Co
Olivine	41.89	< 0.02	7.80	< 0.02	52.98	0.31	0.35	0.38	103.7	Co
Olivine	39.64	< 0.02	7.83	< 0.02	52.10	0.32	0.33	0.42	100.6	Co
Olivine	41.88	< 0.02	7.85	0.04	53.11	0.27	0.45	0.41	104.0	Co
Olivine	40.89	0.04	7.91	0.06	49.98	0.29	0.37	0.37	100.0	Gö
Olivine	41.78	< 0.02	7.93	< 0.02	52.22	0.28	0.39	0.39	103.0	Co
Olivine	40.96	0.04	7.99	< 0.02	51.83	0.31	0.43	0.36	101.9	Co
Olivine	41.26	< 0.02	8.13	0.04	51.82	0.31	0.46	0.39	102.4	Co
Olivine	41.57	< 0.02	8.17	0.04	51.80	0.31	0.34	0.40	102.6	Co
Olivine	40.88	< 0.02	8.17	0.05	50.14	0.32	0.38	0.40	100.4	Gö
Olivine	40.86	0.05	8.20	0.06	50.30	0.36	0.40	0.40	100.7	Gö
Olivine	38.16	0.03	10.47	0.12	48.74	0.41	0.39	0.40	98.8	Co
Olivine	40.22	< 0.02	12.02	0.17	46.52	0.36	0.70	0.48	100.5	Gö
Olivine	39.83	0.03	13.22	0.05	45.07	0.35	0.72	0.42	99.7	Gö
Olivine	40.01	< 0.02	13.38	< 0.02	48.19	0.30	0.76	0.47	103.1	Co
Opx	58.47	0.16	4.91	0.57	34.90	2.55	0.47	0.41	102.5	Co
Opx	58.20	0.19	4.92	0.62	35.50	2.57	0.50	0.31	102.8	Co
Opx	56.48	0.18	7.30	0.54	34.53	2.46	0.51	0.38	102.4	Co
Opx	58.17	0.16	5.11	0.56	35.40	2.54	0.52	0.40	102.9	Co
Opx	57.92	0.12	4.96	0.49	35.17	2.54	0.52	0.45	102.2	Co
Opx	58.40	0.18	4.97	0.57	35.71	2.51	0.52	0.42	103.3	Co
Opx	58.46	0.18	4.83	0.50	33.69	2.58	0.52	0.44	101.2	Co
Opx	56.11	0.09	4.45	0.55	33.58	2.38	0.53	0.34	98.0	Co
Opx	57.64	0.11	5.10	0.47	35.58	2.50	0.53	0.40	102.3	Co
Opx	57.83	0.09	4.95	0.57	35.03	2.52	0.53	0.40	101.9	Co
Opx	57.45	0.14	6.71	0.51	34.61	2.36	0.53	0.35	102.7	Co
Opx	58.84	0.15	5.04	0.52	35.21	2.58	0.54	0.42	103.4	Co
Opx	56.85	0.16	5.54	0.59	33.33	2.62	0.54	0.36	100.1	Gö
Opx	58.41	0.14	4.99	0.54	35.48	2.43	0.54	0.45	103.0	Co
Opx	55.94	0.13	5.14	0.52	33.11	2.39	0.54	0.36	98.2	Co
Opx	58.70	0.13	4.81	0.51	33.93	2.62	0.54	0.39	101.7	Co
Opx	58.51	0.09	4.80	0.56	34.86	2.50	0.55	0.36	102.2	Co
Opx	56.54	0.13	6.06	0.60	33.50	2.51	0.55	0.42	100.5	Gö
Opx	58.29	0.21	4.62	0.51	35.20	2.49	0.55	0.41	102.4	Co
Opx	58.88	0.05	4.99	0.51	35.67	2.59	0.55	0.36	103.7	Co

Opx	57.70	0.16	4.99	0.53	35.55	2.54	0.55	0.41	102.4	Co
Opx	57.48	0.19	5.17	0.58	33.70	2.60	0.55	0.44	100.8	Gö
Mineral	SiO <sub>2</sub> [wt%]	TiO <sub>2</sub> [wt%]	FeO [wt%]	Al <sub>2</sub> O <sub>3</sub> [wt%]	MgO [wt%]	CaO [wt%]	Cr <sub>2</sub> O <sub>3</sub> [wt%]	MnO [wt%]	wt-total	EPMA <sup>a</sup>
Opx	58.75	0.07	5.22	0.57	35.32	2.54	0.55	0.35	103.5	Co
Opx	57.01	0.16	5.28	0.55	33.36	2.61	0.56	0.37	100.0	Gö
Opx	58.15	0.09	4.92	0.53	35.18	2.50	0.56	0.40	102.3	Co
Opx	57.41	0.19	5.16	0.54	33.59	2.58	0.56	0.43	100.6	Gö
Opx	58.25	0.13	5.07	0.54	35.36	2.57	0.56	0.33	102.8	Co
Opx	55.79	0.15	6.77	0.55	32.93	2.58	0.56	0.35	99.8	Gö
Opx	58.10	0.12	5.62	0.51	35.09	2.52	0.57	0.43	103.0	Co
Opx	57.31	0.11	4.86	0.53	35.04	2.54	0.57	0.27	101.2	Co
Opx	56.63	0.10	7.04	0.51	34.54	2.57	0.58	0.35	102.4	Co
Opx	58.88	0.14	4.93	0.52	35.38	2.61	0.58	0.42	103.5	Co
Opx	57.48	0.14	5.00	0.52	33.55	2.57	0.58	0.36	100.3	Gö
Opx	56.28	0.12	5.61	0.55	32.98	2.53	0.58	0.45	99.3	Gö
Opx	58.67	0.10	4.58	0.56	35.03	2.49	0.58	0.41	102.5	Co
Opx	58.29	0.17	4.81	0.55	34.98	2.55	0.58	0.36	102.3	Co
Opx	58.64	0.11	4.73	0.53	35.62	2.59	0.59	0.38	103.3	Co
Opx	58.63	0.13	4.69	0.54	35.98	2.59	0.59	0.32	103.5	Co
Opx	58.75	0.16	4.86	0.56	35.09	2.53	0.59	0.45	103.0	Co
Opx	58.50	0.09	5.34	0.54	35.19	2.43	0.59	0.43	103.1	Co
Opx	57.58	0.15	5.17	0.57	33.87	2.62	0.59	0.42	101.0	Gö
Opx	57.53	0.14	4.93	0.58	34.49	2.50	0.59	0.43	101.3	Co
Opx	58.12	0.17	5.18	0.58	35.40	2.55	0.59	0.35	103.0	Co
Opx	58.27	0.14	4.90	0.52	35.69	2.49	0.60	0.39	103.1	Co
Opx	58.32	0.12	5.04	0.54	35.29	2.49	0.60	0.38	102.8	Co
Opx	57.42	0.16	6.00	0.63	34.48	2.61	0.60	0.38	102.3	Co
Opx	58.36	0.16	5.30	0.49	36.00	2.54	0.61	0.31	103.8	Co
Opx	58.67	0.21	5.05	0.58	35.62	2.56	0.61	0.40	103.9	Co
Opx	56.24	0.12	6.35	0.50	33.62	2.38	0.61	0.38	100.2	Co
Opx	58.53	0.14	5.88	0.58	34.68	2.50	0.61	0.43	103.4	Co
Opx	59.19	0.15	4.97	0.54	35.55	2.59	0.63	0.40	104.1	Co
Opx	58.40	0.26	4.93	0.53	35.41	2.45	0.63	0.49	103.2	Co
Opx	57.57	0.16	5.11	0.59	34.87	2.47	0.63	0.38	101.8	Co
Opx	58.56	0.14	5.39	0.60	35.36	2.45	0.63	0.33	103.6	Co
Opx	59.03	0.09	5.29	0.54	35.60	2.47	0.64	0.42	104.1	Co
Opx	57.76	0.11	4.89	0.53	34.06	2.60	0.64	0.39	101.0	Co
Opx	58.06	0.11	4.80	0.56	35.52	2.54	0.64	0.40	102.6	Co
Opx	58.44	0.16	5.04	0.50	34.82	2.56	0.64	0.41	102.6	Co
Opx	58.19	0.12	5.29	0.55	35.54	2.47	0.64	0.42	103.3	Co
Opx	59.04	0.18	5.34	0.57	35.39	2.51	0.65	0.40	104.1	Co
Opx	58.94	0.17	5.02	0.55	35.79	2.58	0.65	0.35	104.1	Co
Opx	58.86	0.15	4.64	0.53	35.42	2.57	0.66	0.39	103.3	Co
Opx	58.04	0.15	5.03	0.66	35.04	2.64	0.66	0.44	102.8	Co
Opx	56.41	0.12	8.17	0.60	30.00	3.25	1.09	0.47	100.2	Gö
Opx	56.14	0.07	8.31	0.62	30.42	3.38	1.11	0.42	100.6	Gö
Opx	57.58	0.12	8.40	0.53	31.35	3.45	1.15	0.47	103.1	Co

<sup>a</sup> place of measurements: Co = Cologne, Gö = Göttingen

### ***Silicates (LA-ICP-MS)***

Mineral	NiO [ $\mu\text{g}\cdot\text{g}^{-1}$ ]	$2\sigma$	CoO [ $\mu\text{g}\cdot\text{g}^{-1}$ ]	$2\sigma$
Olivine	45.6	4.1	22.6	2.0
Opx	29.5	3.3	11.3	1.1
Opx	13.8	1.6	10.1	1.0
Opx	23.6	5.4	12.2	0.9
Opx	43.1	6.6	12.6	1.0

### ***Vein material and inclusions (EPMA)***

Phase <sup>a</sup>	Loc <sup>b</sup>	P [wt%]	Si [wt%]	Cr [wt%]	Fe [wt%]	Co [wt%]	S [wt%]	Ni [wt%]	Mn [wt%]	wt-total	EPMA <sup>c</sup>
Coh	Sph	< 0.02	< 0.02	0.26	89.63	0.29	< 0.02	1.78	0.03	92.1	Gö
Coh	Sph	< 0.02	< 0.02	0.17	90.23	0.29	< 0.02	1.71	< 0.02	92.5	Co
Coh	Sph	< 0.02	0.04	0.26	90.35	0.28	< 0.02	1.69	< 0.02	92.7	Gö
Coh	Sph	< 0.02	0.03	0.08	90.20	0.27	< 0.02	1.66	0.03	92.3	Co
Coh	Sph	0.24	< 0.02	0.08	89.60	0.36	0.27	2.00	< 0.02	92.6	Co
Coh	Sph	0.19	0.06	0.06	86.84	0.48	0.24	5.80	< 0.02	93.8	Gö
Metal	Sph	0.16	0.03	0.06	91.73	0.58	< 0.02	8.12	< 0.02	100.7	Co
Metal	Sph	0.29	< 0.02	0.04	90.09	0.59	< 0.02	8.26	< 0.02	99.4	Gö
Metal	Sph	0.28	1.20	0.08	91.59	0.47	< 0.02	5.45	< 0.02	99.2	Gö
Metal	Sph	0.11	1.24	0.07	91.80	0.45	< 0.02	5.49	< 0.02	99.2	Co
Metal	Sph	0.40	0.04	< 0.02	92.61	0.41	< 0.02	5.32	< 0.02	98.9	Gö
Metal	Sph	0.22	< 0.02	< 0.02	95.90	0.43	< 0.02	5.56	< 0.02	102.1	Co
Metal	Sph	0.11	0.03	0.04	94.30	0.48	< 0.02	6.18	< 0.02	101.1	Co
Metal	Sph	0.16	< 0.02	< 0.02	94.19	0.39	< 0.02	6.04	< 0.02	100.8	Co
Metal	Sph	0.11	0.08	0.04	93.25	0.53	0.06	6.08	0.03	100.1	Co
Metal	Vein	0.11	0.03	0.27	95.53	0.19	< 0.02	3.62	< 0.02	99.7	Co
Metal	Vein	0.10	0.03	0.25	93.98	0.34	< 0.02	3.83	< 0.02	98.5	Co
Metal	Vein	0.09	0.04	0.21	96.08	0.23	< 0.02	3.89	< 0.02	100.5	Co
Metal	Vein	0.21	0.07	0.26	93.34	0.29	< 0.02	3.91	< 0.02	98.2	Gö
Metal	Vein	0.20	0.06	0.25	93.07	0.29	< 0.02	3.91	0.03	97.9	Gö
Metal	Vein	0.09	< 0.02	0.25	96.12	0.31	< 0.02	4.09	< 0.02	100.9	Co
Metal	Vein	0.12	4.74	0.05	91.11	0.30	< 0.02	4.93	< 0.02	101.2	Co
Metal	Vein	0.12	1.36	0.10	92.57	0.41	< 0.02	5.26	< 0.02	99.8	Co
Metal	Vein	0.26	1.25	0.07	90.93	0.46	< 0.02	5.32	0.03	98.4	Gö
Metal	Vein	0.09	1.19	0.03	93.16	0.43	< 0.02	5.36	< 0.02	100.3	Co
Metal	Vein	0.12	1.29	0.03	93.71	0.51	< 0.02	5.37	0.05	101.0	Co
Metal	Vein	0.07	1.32	0.06	91.99	0.47	< 0.02	5.43	< 0.02	99.3	Co
Metal	Vein	0.32	1.36	0.06	92.11	0.50	< 0.02	5.43	< 0.02	99.8	Co
Metal	Vein	0.21	1.24	0.05	90.69	0.46	< 0.02	5.46	< 0.02	98.2	Gö
Metal	Vein	0.08	1.26	0.06	94.12	0.46	< 0.02	5.46	< 0.02	101.5	Co
Metal	Vein	0.11	1.33	0.04	92.81	0.43	< 0.02	5.48	< 0.02	100.2	Co
Metal	Vein	0.08	1.30	< 0.02	91.91	0.41	< 0.02	5.56	< 0.02	99.3	Co
Metal	Vein	0.10	1.25	0.04	92.53	0.51	0.04	5.63	< 0.02	100.1	Co
Metal	Vein	0.07	1.27	< 0.02	93.07	0.46	< 0.02	5.64	< 0.02	100.6	Co
Metal	Vein	0.09	1.34	0.07	93.14	0.44	< 0.02	5.69	< 0.02	100.8	Co
Metal	Vein	0.09	1.14	0.06	93.39	0.44	< 0.02	5.72	< 0.02	100.9	Co
Metal	Sph	0.12	< 0.02	0.24	97.12	0.25	< 0.02	2.66	0.04	100.4	Co
Metal	Inc	0.07	0.04	0.07	94.16	0.41	< 0.02	5.28	0.05	100.0	Co
Metal	Inc	0.11	0.04	0.24	95.08	0.27	< 0.02	3.71	< 0.02	99.4	Co
Metal	Inc	0.17	1.14	0.08	93.08	0.43	< 0.02	5.67	< 0.02	100.6	Co
Metal	Inc	0.08	1.25	0.03	92.24	0.41	< 0.02	6.24	< 0.02	100.2	Co

Phase <sup>a</sup>	Loc <sup>b</sup>	P	Si	Cr	Fe	Co	S	Ni	Mn	wt-total	EPMA <sup>c</sup>
		[wt%]	[wt%]	[wt%]	[wt%]	[wt%]	[wt%]	[wt%]	[wt%]		
Metal	Inc	0.09	1.26	0.06	90.94	0.51	0.04	5.73	< 0.02	98.6	Co
Metal	Inc	0.14	1.29	0.08	91.85	0.43	< 0.02	5.47	< 0.02	99.3	Co
Metal	Inc	0.09	1.30	0.09	93.83	0.48	< 0.02	5.36	0.03	101.2	Co
Metal	Inc	0.08	1.32	0.09	92.52	0.42	< 0.02	5.53	< 0.02	100.0	Co
Metal	Inc	0.08	1.48	< 0.02	92.62	0.38	< 0.02	5.69	0.03	100.3	Co
Troi	Sph	< 0.02	< 0.02	2.12	59.55	< 0.02	37.32	0.10	0.49	99.6	Gö
Troi	Sph	< 0.02	0.05	2.01	60.93	< 0.02	36.15	0.14	0.49	99.1	Co
Troi	Sph	< 0.02	0.03	1.59	59.45	< 0.02	37.14	0.16	0.07	98.5	Gö
Troi	Sph	< 0.02	0.03	1.61	60.60	< 0.02	36.50	0.08	0.03	98.8	Co
Troi	Sph	< 0.02	0.03	6.68	52.97	< 0.02	38.19	0.13	0.79	98.8	Gö
Troi	Sph	< 0.02	0.04	6.66	54.52	< 0.02	36.75	0.10	0.75	98.0	Co
Troi	Sph	< 0.02	0.08	1.24	61.10	< 0.02	36.21	0.13	0.05	98.7	Co
Troi	Vein	< 0.02	0.15	8.14	50.16	< 0.02	37.90	0.14	0.92	97.5	Gö
Troi	Vein	< 0.02	0.08	5.25	55.45	< 0.02	36.79	0.12	0.66	97.6	Co
Troi	Vein	< 0.02	0.10	6.64	53.47	< 0.02	37.11	0.11	0.66	97.3	Co
Troi	Vein	< 0.02	0.03	5.57	55.24	< 0.02	37.27	0.05	0.59	98.1	Co

<sup>a</sup> phases: Coh = cohenite, Troi = troilite

<sup>b</sup> locations: Sph = spherule inclusion, Vein = vein material, Inc = inclusion in silicate

<sup>c</sup> place of measurements: Co = Cologne, Gö = Göttingen

## 12.1.5 EET96042

### *Silicates (EPMA)*

Mineral	SiO <sub>2</sub> [wt%]	TiO <sub>2</sub> [wt%]	FeO [wt%]	Al <sub>2</sub> O <sub>3</sub> [wt%]	MgO [wt%]	CaO [wt%]	Cr <sub>2</sub> O <sub>3</sub> [wt%]	MnO [wt%]	wt-total	EPMA <sup>a</sup>
Olivine	41.64	< 0.02	1.77	0.37	55.56	0.32	0.79	0.55	101.0	Gö
Olivine	40.21	0.03	6.93	0.10	50.37	0.35	0.71	0.57	99.3	Gö
Olivine	38.62	< 0.02	12.45	< 0.02	47.84	0.30	0.66	0.48	100.4	Co
Olivine	40.11	< 0.02	12.63	0.05	46.11	0.41	0.83	0.51	100.7	Gö
Olivine	40.37	< 0.02	14.40	< 0.02	45.25	0.35	0.68	0.44	101.6	Co
Olivine	39.40	< 0.02	14.83	< 0.02	43.11	0.37	0.78	0.38	98.9	Co
Olivine	38.09	< 0.02	14.98	0.04	45.38	0.27	0.60	0.54	99.9	Co
Olivine	39.48	< 0.02	15.11	0.12	44.49	0.56	0.54	0.43	100.8	Gö
Olivine	39.52	0.04	15.38	< 0.02	44.09	0.34	0.82	0.40	100.7	Co
Olivine	37.83	< 0.02	15.46	< 0.02	45.03	0.31	0.73	0.47	99.9	Co
Olivine	39.57	< 0.02	15.70	0.05	43.63	0.41	0.89	0.49	100.8	Gö
Olivine	38.69	< 0.02	15.71	0.04	42.14	0.38	0.82	0.47	98.2	Co
Olivine	40.10	< 0.02	15.74	0.03	43.58	0.36	0.79	0.45	101.0	Co
Olivine	38.78	0.03	15.75	0.03	41.57	0.33	0.80	0.42	97.7	Co
Olivine	39.97	< 0.02	15.79	0.05	43.89	0.33	0.88	0.45	101.4	Co
Olivine	39.85	< 0.02	15.85	0.03	44.06	0.31	0.77	0.50	101.4	Co
Olivine	40.01	< 0.02	15.85	< 0.02	44.52	0.35	0.86	0.40	102.0	Co
Olivine	39.79	< 0.02	15.91	< 0.02	43.20	0.36	0.84	0.44	100.6	Co
Olivine	39.45	< 0.02	15.92	0.05	43.03	0.33	0.80	0.39	100.0	Co
Olivine	40.33	< 0.02	16.03	0.04	44.18	0.35	0.92	0.48	102.4	Co
Olivine	39.30	0.03	16.05	0.04	43.45	0.33	0.88	0.40	100.5	Co
Olivine	39.78	0.04	16.07	0.03	43.10	0.32	0.81	0.47	100.6	Co
Olivine	39.27	< 0.02	16.14	< 0.02	44.08	0.31	0.82	0.45	101.1	Co
Olivine	39.28	< 0.02	16.16	< 0.02	42.52	0.33	0.79	0.43	99.6	Co
Olivine	39.96	0.07	16.19	0.03	43.82	0.34	0.81	0.41	101.7	Co
Olivine	38.05	< 0.02	16.21	< 0.02	44.92	0.31	0.90	0.39	100.9	Co
Olivine	37.87	< 0.02	16.24	0.07	44.31	0.31	0.87	0.46	100.1	Co
Olivine	39.97	< 0.02	16.26	0.04	43.33	0.34	0.79	0.43	101.2	Co
Olivine	37.81	< 0.02	16.26	0.03	44.10	0.32	0.75	0.44	99.8	Co
Olivine	37.37	< 0.02	16.29	< 0.02	44.85	0.30	0.71	0.46	100.1	Co
Olivine	38.99	< 0.02	16.38	0.09	42.90	0.34	0.75	0.45	99.9	Gö
Olivine	40.02	< 0.02	16.40	0.04	43.27	0.33	0.81	0.45	101.3	Co
Olivine	39.73	0.04	16.45	0.04	43.23	0.37	0.79	0.51	101.2	Co
Olivine	38.04	0.04	16.45	0.04	44.47	0.28	0.77	0.44	100.5	Co
Olivine	38.00	< 0.02	16.47	< 0.02	43.92	0.31	0.81	0.42	99.9	Co
Olivine	40.07	0.04	16.50	< 0.02	44.38	0.33	0.86	0.47	102.7	Co
Olivine	38.24	< 0.02	16.51	0.03	44.77	0.33	0.76	0.38	101.1	Co
Olivine	39.75	< 0.02	16.56	0.04	43.02	0.32	0.82	0.47	101.0	Co
Olivine	39.85	0.05	16.57	0.06	43.60	0.35	0.82	0.51	101.8	Co
Olivine	39.39	< 0.02	16.63	0.03	42.68	0.33	0.78	0.46	100.3	Co
Olivine	39.19	< 0.02	16.66	0.05	42.56	0.36	0.79	0.44	100.1	Gö
Olivine	39.46	0.06	16.70	0.07	43.26	0.37	0.81	0.47	101.2	Gö
Olivine	37.15	< 0.02	16.70	< 0.02	44.40	0.32	0.80	0.41	99.8	Co
Olivine	39.60	< 0.02	16.72	0.05	44.43	0.28	0.86	0.47	102.5	Co
Olivine	37.87	< 0.02	16.73	< 0.02	44.54	0.31	0.73	0.41	100.6	Co
Olivine	39.77	< 0.02	16.75	0.05	43.82	0.37	0.79	0.45	102.0	Co
Olivine	37.65	< 0.02	16.77	< 0.02	44.41	0.32	0.65	0.54	100.3	Co

Olivine	40.17	< 0.02	16.80	0.04	43.41	0.33	0.78	0.44	102.0	Co
Olivine	39.91	< 0.02	16.84	0.03	43.73	0.34	0.83	0.41	102.1	Co
Mineral	SiO <sub>2</sub> [wt%]	TiO <sub>2</sub> [wt%]	FeO [wt%]	Al <sub>2</sub> O <sub>3</sub> [wt%]	MgO [wt%]	CaO [wt%]	Cr <sub>2</sub> O <sub>3</sub> [wt%]	MnO [wt%]	wt-total	EPMA <sup>a</sup>
Olivine	40.27	< 0.02	16.90	0.04	43.42	0.35	0.80	0.47	102.3	Co
Olivine	37.37	< 0.02	16.92	0.04	44.32	0.31	0.83	0.42	100.3	Co
Olivine	39.11	0.04	16.94	0.06	42.38	0.37	0.80	0.41	100.2	Gö
Olivine	37.82	0.06	16.99	< 0.02	44.23	0.34	0.74	0.45	100.7	Co
Opx	55.87	0.11	7.74	0.86	29.19	4.86	1.35	0.52	100.6	Gö
Opx	55.41	0.11	8.81	1.09	27.98	4.81	1.40	0.47	100.2	Gö
Opx	55.42	0.05	10.03	0.79	27.25	4.83	1.31	0.44	100.2	Gö
Opx	55.56	0.08	10.12	0.76	27.08	4.75	1.33	0.47	100.2	Gö
Opx	53.51	0.06	9.85	0.59	28.60	4.48	1.30	0.48	98.9	Co
Opx	55.40	0.07	9.34	0.73	27.48	4.64	1.39	0.41	99.6	Co
Opx	55.56	0.09	9.50	0.76	27.93	4.66	1.40	0.44	100.4	Co
Opx	55.86	0.14	9.44	0.67	27.34	4.57	1.30	0.51	99.9	Co

<sup>a</sup> place of measurements: Co = Cologne, Gö = Göttingen

### ***Silicates (LA-ICP-MS)***

Mineral	NiO [µg·g <sup>-1</sup> ]	2σ	CoO [µg·g <sup>-1</sup> ]	2σ
Olivine	73.6	5.9	40.0	3.3
Olivine	74.6	6.2	37.7	3.1
Olivine	69.7	5.7	37.8	3.1
Olivine	59.6	7.6	38.0	3.6
Olivine	77.2	3.7	45.6	1.7
Opx	34.2	3.6	18.7	1.8
Opx	24.8	3.0	16.5	1.3
Opx	27.5	3.0	17.7	1.4

### ***Vein material and inclusions (EPMA)***

Phase <sup>a</sup>	Loc <sup>b</sup>	P [wt%]	Si [wt%]	Cr [wt%]	Fe [wt%]	Co [wt%]	S [wt%]	Ni [wt%]	Mn [wt%]	wt-total	EPMA <sup>c</sup>
Metal	Inc	0.11	0.03	0.15	99.64	0.05	< 0.02	0.12	< 0.02	100.1	Co
Metal	Inc	0.09	0.03	0.10	100.97	< 0.02	< 0.02	0.15	< 0.02	101.4	Co
Metal	Inc	< 0.02	0.03	0.17	100.89	0.04	0.03	0.22	< 0.02	101.4	Co
Metal	Inc	0.11	0.04	0.12	99.62	0.05	0.03	0.75	< 0.02	100.7	Co
Metal	Inc	0.13	0.05	0.15	99.11	< 0.02	0.03	0.97	0.04	100.4	Co
Metal	Inc	0.04	0.11	0.14	96.52	0.04	< 0.02	1.14	0.04	98.0	Co
Metal	Inc	0.13	< 0.02	0.26	99.09	0.07	< 0.02	1.38	0.04	101.0	Co
Metal	Inc	0.11	0.04	0.15	97.80	0.12	< 0.02	1.74	< 0.02	100.0	Co
Metal	Inc	0.03	0.06	0.14	97.23	0.07	< 0.02	2.48	< 0.02	100.0	Co
Metal	Inc	0.12	0.03	0.05	98.22	0.15	< 0.02	2.60	< 0.02	101.2	Co
Metal	Inc	0.07	0.03	0.13	98.28	0.11	0.03	3.11	< 0.02	101.8	Co
Metal	Inc	0.05	0.03	0.13	95.43	0.14	< 0.02	3.69	0.04	99.5	Co
Metal	Inc	0.06	1.18	0.22	93.38	0.28	< 0.02	3.93	0.03	99.1	Co
Metal	Inc	0.13	0.03	0.14	95.66	0.28	< 0.02	4.25	< 0.02	100.5	Co
Metal	Inc	0.22	0.03	0.06	92.11	0.41	0.03	5.80	0.03	98.7	Co
Troi	Inc	< 0.02	0.25	0.57	63.83	< 0.02	33.48	0.22	0.11	98.3	Co
Troi	Inc	< 0.02	0.04	0.83	67.05	< 0.02	31.16	0.07	0.16	99.1	Co
Troi	Inc	< 0.02	0.06	1.23	60.85	< 0.02	36.81	0.08	0.18	99.0	Co
Troi	Inc	< 0.02	0.05	1.63	61.74	< 0.02	36.18	0.14	0.25	99.7	Co
Troi	Inc	< 0.02	0.04	2.15	61.21	< 0.02	36.53	0.12	0.23	99.9	Co

Troi	Inc	< 0.02	0.19	3.71	57.55	< 0.02	35.91	0.04	0.62	97.3	Co
Troi	Inc	< 0.02	0.07	3.86	58.00	< 0.02	36.52	0.10	0.44	98.5	Co
Phase <sup>a</sup>	Loc <sup>b</sup>	P [wt%]	Si [wt%]	Cr [wt%]	Fe [wt%]	Co [wt%]	S [wt%]	Ni [wt%]	Mn [wt%]	wt- total	EPMA <sup>c</sup>
Troi	Inc	< 0.02	0.09	6.76	52.32	< 0.02	36.87	1.50	0.46	97.5	Co
Troi	Inc	< 0.02	0.07	8.28	51.69	0.07	37.27	1.49	0.25	98.9	Co
Troi	Inc	< 0.02	< 0.02	9.14	51.00	< 0.02	37.31	0.22	0.32	97.6	Co
Metal	Sph	0.06	0.04	0.13	96.81	0.10	< 0.02	3.66	0.04	100.8	Co
Troi	Sph	< 0.02	0.18	1.35	61.73	< 0.02	35.62	< 0.02	0.16	98.8	Co
Metal	Vein	0.18	< 0.02	0.08	97.07	0.13	< 0.02	3.36	< 0.02	100.8	Co
Metal	Vein	0.13	< 0.02	0.04	97.65	0.35	0.03	4.46	< 0.02	102.7	Co
Metal	Vein	0.10	5.35	0.09	90.47	0.29	< 0.02	4.34	< 0.02	100.6	Co
Metal	Vein	0.09	4.81	0.04	88.68	0.23	0.03	4.50	< 0.02	98.4	Co
Metal	Vein	0.12	4.71	0.05	91.88	0.35	< 0.02	4.64	< 0.02	101.8	Co
Metal	Vein	0.10	4.86	0.10	91.76	0.28	< 0.02	4.72	< 0.02	101.8	Co
Metal	Vein	0.20	4.41	0.16	91.75	0.36	< 0.02	4.81	< 0.02	101.7	Co
Metal	Vein	0.09	5.02	0.08	89.80	0.27	< 0.02	4.89	0.03	100.2	Co
Metal	Vein	0.17	4.99	0.10	90.66	0.31	< 0.02	4.96	< 0.02	101.2	Co
Metal	Vein	0.07	4.97	< 0.02	91.05	0.27	< 0.02	5.01	< 0.02	101.4	Co
Metal	Vein	0.11	5.25	0.15	91.66	0.26	< 0.02	5.02	< 0.02	102.5	Co
Metal	Vein	0.13	4.72	0.04	89.56	0.31	< 0.02	5.07	< 0.02	99.8	Co
Metal	Vein	0.16	4.82	< 0.02	91.09	0.33	0.03	5.18	< 0.02	101.6	Co
Metal	Vein	0.14	4.65	0.10	91.26	0.30	0.04	5.57	< 0.02	102.1	Co
Troi	Vein	< 0.02	< 0.02	0.41	63.03	< 0.02	36.00	0.13	0.05	99.5	Co
Troi	Vein	< 0.02	< 0.02	1.27	61.91	< 0.02	36.97	0.05	0.09	100.2	Co
Troi	Vein	< 0.02	< 0.02	1.34	61.97	< 0.02	36.70	< 0.02	0.23	100.0	Co
Troi	Vein	< 0.02	< 0.02	5.77	55.92	< 0.02	35.94	0.10	0.14	97.7	Co
Troi	Vein	< 0.02	0.30	5.78	55.35	< 0.02	36.05	0.27	0.37	97.7	Co
Troi	Vein	< 0.02	< 0.02	5.82	56.83	< 0.02	37.33	0.04	0.09	100.0	Co
Troi	Vein	< 0.02	< 0.02	7.03	55.06	< 0.02	36.75	0.13	0.28	98.9	Co
Troi	Vein	< 0.02	0.04	8.00	52.54	< 0.02	37.22	0.11	0.43	97.8	Co
Troi	Vein	< 0.02	< 0.02	8.93	51.53	< 0.02	37.79	0.06	0.45	98.3	Co

<sup>a</sup> phases: Troi = troilite

<sup>b</sup> locations: Sph = spherule inclusion, Vein = vein material, Inc = inclusion in silicate

<sup>c</sup> place of measurements: Co = Cologne, Gö = Göttingen

## 12.1.6 EET96331

### *Silicates (EPMA)*

Mineral	SiO <sub>2</sub> [wt%]	TiO <sub>2</sub> [wt%]	FeO [wt%]	Al <sub>2</sub> O <sub>3</sub> [wt%]	MgO [wt%]	CaO [wt%]	Cr <sub>2</sub> O <sub>3</sub> [wt%]	MnO [wt%]	wt-total	EPMA <sup>a</sup>
Olivine	41.06	< 0.02	9.85	0.04	51.27	0.25	0.47	0.59	103.6	Co
Olivine	41.30	< 0.02	9.11	0.05	50.58	0.28	0.52	0.61	102.5	Co
Olivine	40.36	< 0.02	11.56	< 0.02	48.11	0.25	0.45	0.53	101.3	Co
Olivine	40.32	0.03	12.29	0.05	48.37	0.27	0.50	0.55	102.4	Co
Olivine	40.15	0.03	11.24	< 0.02	48.70	0.27	0.50	0.53	101.4	Co
Olivine	40.19	< 0.02	11.59	0.04	48.09	0.28	0.46	0.66	101.3	Co
Olivine	39.91	0.04	11.33	0.03	47.67	0.28	0.45	0.51	100.2	Co
Olivine	40.42	< 0.02	11.99	0.06	48.11	0.26	0.45	0.55	101.8	Co
Olivine	40.36	0.09	12.18	0.04	48.19	0.25	0.47	0.52	102.1	Co
Olivine	40.96	0.06	10.99	0.03	48.71	0.26	0.45	0.55	102.0	Co
Olivine	40.84	< 0.02	10.77	0.04	49.13	0.28	0.47	0.54	102.1	Co
Olivine	40.44	< 0.02	11.70	0.04	48.12	0.27	0.50	0.47	101.6	Co
Olivine	40.92	< 0.02	12.68	0.03	49.66	0.28	0.50	0.57	104.7	Co
Olivine	40.73	0.04	11.42	0.05	50.09	0.28	0.45	0.61	103.8	Co
Olivine	40.71	< 0.02	11.43	0.05	49.88	0.28	0.48	0.54	103.4	Co
Olivine	40.90	0.03	11.94	0.04	49.95	0.28	0.43	0.58	104.1	Co
Olivine	40.86	< 0.02	10.71	< 0.02	50.97	0.26	0.50	0.63	104.0	Co
Olivine	40.30	< 0.02	11.59	0.03	49.05	0.28	0.57	0.57	102.4	Co
Olivine	41.05	< 0.02	11.21	< 0.02	49.61	0.23	0.50	0.60	103.2	Co
Olivine	40.50	0.04	11.97	0.06	49.74	0.27	0.52	0.56	103.7	Co
Olivine	40.62	0.05	12.01	0.06	48.91	0.30	0.56	0.54	103.1	Co
Olivine	41.02	< 0.02	12.40	0.04	49.67	0.26	0.52	0.49	104.5	Co
Olivine	40.46	< 0.02	10.88	< 0.02	49.14	0.27	0.49	0.52	101.8	Co
Olivine	40.76	0.03	12.37	0.03	48.87	0.27	0.46	0.60	103.5	Co
Olivine	40.24	< 0.02	12.05	< 0.02	49.33	0.29	0.51	0.53	103.0	Co
Olivine	40.49	< 0.02	11.84	0.04	49.09	0.26	0.50	0.58	102.9	Co
Olivine	40.92	< 0.02	12.24	0.05	49.50	0.24	0.44	0.53	103.9	Co
Opx	55.17	0.09	7.31	1.25	32.25	2.33	0.91	0.50	99.8	Co
Opx	56.57	0.10	8.17	1.23	32.87	2.35	0.95	0.53	102.8	Co
Opx	55.56	0.21	6.98	1.22	32.05	2.36	1.03	0.46	99.9	Co
Opx	56.81	0.10	7.88	1.19	32.43	2.37	0.96	0.50	102.3	Co
Opx	55.98	0.11	7.53	1.33	32.12	2.38	0.90	0.45	100.8	Co
Opx	56.41	0.11	7.35	1.15	32.25	2.38	0.93	0.53	101.1	Co
Opx	56.64	0.14	7.24	1.21	31.92	2.39	0.97	0.56	101.1	Co
Opx	56.23	0.09	7.38	1.15	31.33	2.40	1.09	0.46	100.1	Co
Opx	56.05	0.15	7.29	1.20	32.58	2.40	0.88	0.55	101.1	Co
Opx	56.22	0.07	7.50	1.12	32.07	2.41	1.05	0.51	101.0	Co
Opx	56.90	0.13	7.76	1.22	32.86	2.42	0.97	0.56	102.8	Co
Opx	56.21	0.12	8.16	1.23	32.95	2.42	0.93	0.45	102.5	Co
Opx	57.03	0.09	6.88	1.09	32.02	2.42	0.91	0.53	101.1	Co
Opx	55.50	0.13	7.17	1.25	32.29	2.42	1.06	0.53	100.4	Co
Opx	55.98	0.16	6.94	1.11	31.59	2.42	0.97	0.57	99.8	Co
Opx	56.44	0.14	7.72	1.31	32.64	2.43	0.99	0.50	102.2	Co
Opx	56.36	0.11	7.15	1.15	32.04	2.44	1.08	0.45	100.8	Co
Opx	56.62	0.18	7.12	1.21	31.81	2.44	1.06	0.60	101.1	Co
Opx	56.72	0.07	7.68	1.18	33.24	2.45	0.97	0.53	102.9	Co
Opx	56.27	0.11	6.86	1.21	32.18	2.45	1.04	0.45	100.7	Co

Opx	57.26	0.18	7.38	1.15	32.84	2.46	1.00	0.62	102.9	Co
Opx	56.25	0.13	7.31	1.08	31.95	2.47	0.98	0.60	100.8	Co
Mineral	SiO <sub>2</sub> [wt%]	TiO <sub>2</sub> [wt%]	FeO [wt%]	Al <sub>2</sub> O <sub>3</sub> [wt%]	MgO [wt%]	CaO [wt%]	Cr <sub>2</sub> O <sub>3</sub> [wt%]	MnO [wt%]	wt-total	EPMA <sup>a</sup>
Opx	56.61	0.10	7.21	1.22	32.61	2.47	1.07	0.61	101.9	Co
Opx	56.66	0.09	7.66	1.25	33.31	2.47	1.01	0.55	103.0	Co
Opx	56.67	0.11	7.15	1.22	31.31	2.48	1.04	0.55	100.6	Co
Opx	56.65	0.15	7.48	1.18	32.54	2.48	1.10	0.51	102.2	Co
Opx	56.58	0.09	7.48	1.22	32.74	2.48	0.97	0.50	102.2	Co
Opx	56.42	0.13	7.48	1.20	32.45	2.49	1.01	0.57	101.8	Co
Opx	56.03	0.06	7.71	1.29	33.02	2.49	0.96	0.54	102.1	Co
Opx	56.98	0.06	7.22	1.28	32.94	2.50	1.01	0.53	102.5	Co
Opx	56.85	0.11	7.08	1.20	33.08	2.51	1.13	0.49	102.5	Co
Opx	56.60	0.12	7.53	1.22	32.75	2.52	1.03	0.57	102.4	Co
Cpx	52.96	0.27	4.14	1.95	19.20	17.85	1.13	0.43	98.1	Co
Cpx	53.65	0.20	4.19	1.91	19.88	18.07	1.31	0.36	99.8	Co
Cpx	54.53	0.30	4.19	1.94	20.58	18.14	1.26	0.36	101.6	Co

<sup>a</sup> place of measurements: Co = Cologne, Gö = Göttingen

### ***Silicates (LA-ICP-MS)***

Mineral	NiO		CoO	
	[ $\mu\text{g}\cdot\text{g}^{-1}$ ]	2 $\sigma$	[ $\mu\text{g}\cdot\text{g}^{-1}$ ]	2 $\sigma$
Olivine	17.8	1.7	7.6	0.7
Olivine	18.5	2.1	7.9	0.8
Olivine	28.4	3.6	8.0	0.7
Olivine	18.9	1.7	6.7	0.4
Olivine	24.2	2.1	8.1	0.6
Opx	13.5	1.7	4.2	0.4
Opx	13.5	1.5	4.0	0.4
Opx	5.4	1.2	3.2	0.4
Opx	7.0	1.8	3.6	0.4
Opx	17.7	2.7	4.1	0.5

***Vein material and inclusions (EPMA)***

Phase <sup>a</sup>	Loc <sup>b</sup>	P [wt%]	Si [wt%]	Cr [wt%]	Fe [wt%]	Co [wt%]	S [wt%]	Ni [wt%]	Mn [wt%]	wt-total	EPMA <sup>c</sup>
Metal	Inc	0.08	0.05	0.13	98.26	0.04	0.16	0.47	0.03	99.3	Gö
Metal	Inc	0.14	0.05	0.11	96.82	0.04	< 0.02	0.85	0.03	98.1	Gö
Metal	Inc	0.09	0.05	0.14	95.23	0.16	< 0.02	3.98	0.04	99.8	Gö
Metal	Vein	0.26	3.30	0.12	90.51	0.34	< 0.02	4.97	0.04	99.6	Gö
Metal	Vein	0.21	3.31	0.15	90.46	0.31	< 0.02	5.11	< 0.02	99.7	Gö
Metal	Vein	0.19	4.91	0.08	89.09	0.31	0.03	4.67	< 0.02	99.4	Gö
Metal	Vein	0.30	4.43	0.12	90.42	0.31	< 0.02	4.85	< 0.02	100.5	Gö
Metal	Vein	0.34	4.65	0.06	89.50	0.34	< 0.02	4.78	< 0.02	99.8	Gö
Metal	Vein	0.22	4.59	0.04	89.09	0.34	< 0.02	5.09	< 0.02	99.5	Gö
Troi	Inc	< 0.02	0.16	0.33	60.96	< 0.02	36.07	0.21	0.16	97.9	Gö
Troi	Inc	< 0.02	< 0.02	0.42	61.22	< 0.02	37.40	0.16	0.08	99.3	Gö
Troi	Inc	< 0.02	0.39	0.68	61.03	< 0.02	36.00	0.05	0.16	98.4	Gö
Troi	Inc	< 0.02	0.10	0.79	62.24	< 0.02	34.87	0.05	0.15	98.2	Gö
Troi	Inc	< 0.02	0.49	4.57	54.94	< 0.02	36.86	0.03	0.78	97.7	Gö
Troi	Inc	< 0.02	0.10	9.75	47.85	< 0.02	38.87	0.08	0.80	97.5	Gö
Troi	Inc	< 0.02	< 0.02	13.38	44.71	< 0.02	39.08	0.04	0.41	97.7	Gö

<sup>a</sup> phases: Troi = troilite

<sup>b</sup> locations: Sph = spherule inclusion, Vein = vein material, Inc = inclusion in silicate

<sup>c</sup> place of measurements: Co = Cologne, Gö = Göttingen

## 12.1.7 GRA95205

### *Silicates (EPMA)*

Mineral	SiO <sub>2</sub> [wt%]	TiO <sub>2</sub> [wt%]	FeO [wt%]	Al <sub>2</sub> O <sub>3</sub> [wt%]	MgO [wt%]	CaO [wt%]	Cr <sub>2</sub> O <sub>3</sub> [wt%]	MnO [wt%]	wt-total	EPMA <sup>a</sup>
Olivine	40.97	< 0.02	4.82	0.05	52.38	0.20	0.56	0.47	99.5	Gö
Olivine	40.98	< 0.02	8.11	0.06	49.75	0.27	0.64	0.41	100.3	Gö
Olivine	40.55	< 0.02	9.38	0.07	48.90	0.29	0.64	0.50	100.4	Gö
Olivine	40.20	< 0.02	10.81	0.10	47.83	0.23	0.63	0.46	100.4	Gö
Olivine	39.61	< 0.02	15.09	0.05	44.19	0.28	0.76	0.52	100.6	Gö
Olivine	40.12	< 0.02	15.20	0.06	43.74	0.29	0.68	0.48	100.6	Gö
Olivine	39.32	0.03	15.28	0.03	43.42	0.24	0.60	0.42	99.4	Gö
Olivine	39.72	< 0.02	15.85	0.05	43.76	0.28	0.58	0.48	100.7	Gö
Olivine	39.60	< 0.02	17.51	< 0.02	45.06	0.25	0.61	0.44	103.5	Co
Olivine	38.85	< 0.02	17.70	0.05	42.25	0.27	0.60	0.45	100.2	Gö
Olivine	38.93	< 0.02	17.73	0.04	44.70	0.27	0.70	0.40	102.8	Co
Olivine	38.75	< 0.02	17.81	0.04	42.45	0.27	0.64	0.50	100.5	Gö
Olivine	39.34	0.03	17.96	0.03	43.23	0.23	0.68	0.39	101.9	Co
Olivine	39.10	< 0.02	18.11	0.03	42.98	0.28	0.64	0.42	101.6	Co
Olivine	39.04	< 0.02	18.31	0.04	42.85	0.25	0.52	0.40	101.4	Co
Olivine	38.60	< 0.02	18.34	0.04	43.24	0.29	0.62	0.46	101.6	Co
Olivine	39.87	0.04	18.42	0.03	43.39	0.34	0.63	0.45	103.2	Co
Olivine	38.66	< 0.02	18.46	0.06	43.22	0.27	0.68	0.40	101.8	Co
Olivine	39.63	< 0.02	18.49	< 0.02	44.93	0.22	0.58	0.39	104.2	Co
Olivine	38.56	< 0.02	18.51	0.07	41.34	0.30	0.64	0.45	99.9	Gö
Olivine	38.75	< 0.02	18.54	0.05	43.72	0.26	0.73	0.43	102.6	Co
Olivine	39.75	0.03	18.55	0.06	44.52	0.35	0.65	0.45	104.4	Co
Olivine	38.98	< 0.02	18.62	0.03	43.82	0.26	0.65	0.42	102.8	Co
Olivine	39.24	0.05	18.64	< 0.02	43.42	0.24	0.61	0.56	102.7	Co
Olivine	39.21	0.04	18.65	< 0.02	43.07	0.27	0.67	0.41	102.4	Co
Olivine	39.16	< 0.02	18.69	0.04	43.78	0.26	0.68	0.45	103.1	Co
Olivine	38.93	0.04	18.71	0.05	42.81	0.27	0.62	0.41	101.9	Co
Olivine	39.28	< 0.02	18.72	0.04	43.35	0.27	0.68	0.43	102.8	Co
Olivine	39.46	< 0.02	18.73	< 0.02	42.92	0.28	0.60	0.41	102.4	Co
Olivine	39.20	< 0.02	18.75	< 0.02	43.36	0.24	0.61	0.38	102.6	Co
Olivine	39.31	< 0.02	18.79	0.08	43.09	0.40	0.73	0.46	102.9	Co
Olivine	39.62	0.04	18.79	0.10	43.28	0.37	0.65	0.46	103.3	Co
Olivine	39.62	< 0.02	18.80	0.03	43.61	0.24	0.64	0.44	103.5	Co
Olivine	40.21	< 0.02	18.82	0.05	42.69	0.50	0.70	0.43	103.4	Co
Olivine	39.67	< 0.02	18.84	0.09	43.00	0.36	0.72	0.42	103.3	Co
Olivine	39.49	< 0.02	18.86	0.05	44.06	0.33	0.56	0.53	103.9	Co
Olivine	39.43	< 0.02	18.89	0.05	43.15	0.17	0.54	0.41	102.6	Co
Olivine	38.81	< 0.02	18.89	0.05	43.08	0.29	0.54	0.43	102.1	Co
Olivine	38.49	< 0.02	18.90	< 0.02	43.65	0.26	0.48	0.43	102.3	Co
Olivine	39.35	< 0.02	18.95	< 0.02	43.38	0.26	0.63	0.43	103.1	Co
Olivine	39.21	< 0.02	18.96	0.05	44.05	0.33	0.66	0.41	103.7	Co
Olivine	39.57	< 0.02	18.97	0.04	43.64	0.25	0.68	0.50	103.8	Co
Olivine	38.16	< 0.02	18.97	0.06	43.00	0.29	0.71	0.40	101.6	Co
Olivine	39.26	0.04	19.01	0.03	44.26	0.26	0.66	0.37	104.0	Co
Olivine	39.13	< 0.02	19.01	0.03	43.56	0.29	0.72	0.37	103.2	Co
Olivine	39.08	< 0.02	19.06	0.03	43.32	0.30	0.72	0.39	102.9	Co
Olivine	39.42	0.05	19.06	0.04	44.36	0.25	0.68	0.45	104.3	Co

Olivine	40.20	0.03	19.07	0.06	43.74	0.31	0.80	0.46	104.7	Co
Olivine	38.79	< 0.02	19.09	< 0.02	43.95	0.27	0.63	0.41	103.2	Co
Mineral	SiO <sub>2</sub> [wt%]	TiO <sub>2</sub> [wt%]	FeO [wt%]	Al <sub>2</sub> O <sub>3</sub> [wt%]	MgO [wt%]	CaO [wt%]	Cr <sub>2</sub> O <sub>3</sub> [wt%]	MnO [wt%]	wt-total	EPMA <sup>a</sup>
Olivine	39.36	< 0.02	19.13	< 0.02	43.29	0.19	0.57	0.40	103.0	Co
Olivine	38.08	0.04	19.13	0.03	44.15	0.26	0.62	0.38	102.7	Co
Olivine	38.81	< 0.02	19.14	0.07	40.46	0.32	0.63	0.41	99.9	Gö
Olivine	39.39	0.03	19.19	< 0.02	43.12	0.26	0.68	0.37	103.1	Co
Olivine	39.95	< 0.02	19.20	< 0.02	43.97	0.29	0.62	0.36	104.4	Co
Olivine	39.90	0.05	19.20	0.05	43.98	0.28	0.73	0.43	104.6	Co
Olivine	39.02	< 0.02	19.23	0.03	43.42	0.24	0.63	0.44	103.1	Co
Olivine	38.56	0.03	19.25	0.05	42.82	0.35	0.66	0.38	102.1	Co
Olivine	39.87	< 0.02	19.27	0.03	44.35	0.20	0.61	0.45	104.8	Co
Olivine	39.43	< 0.02	19.28	0.03	44.52	0.27	0.59	0.33	104.5	Co
Olivine	39.51	< 0.02	19.29	0.04	43.82	0.26	0.61	0.41	104.0	Co
Olivine	39.44	< 0.02	19.33	0.05	43.60	0.27	0.61	0.42	103.7	Co
Olivine	38.73	0.06	19.34	0.09	42.21	0.28	0.75	0.38	101.9	Co
Olivine	38.80	< 0.02	19.42	< 0.02	43.39	0.24	0.64	0.38	102.9	Co
Olivine	38.65	< 0.02	19.46	0.07	43.06	0.25	0.71	0.46	102.7	Co
Olivine	38.49	< 0.02	19.53	0.03	43.18	0.24	0.64	0.37	102.5	Co
Olivine	38.34	< 0.02	19.66	0.04	42.77	0.25	0.66	0.46	102.2	Co
Olivine	39.11	< 0.02	19.66	0.07	43.43	0.30	0.53	0.41	103.5	Co
Olivine	39.14	< 0.02	19.71	< 0.02	43.83	0.29	0.66	0.39	104.1	Co
Olivine	38.47	0.03	20.20	0.04	43.72	0.25	0.62	0.42	103.8	Co
Olivine	38.57	< 0.02	20.98	< 0.02	41.81	0.22	0.60	0.37	102.6	Co
Opx I	57.58	0.05	6.33	0.36	30.80	4.34	1.10	0.55	101.2	Gö
Opx I	55.82	0.07	9.65	0.66	28.54	4.57	1.29	0.43	101.1	Co
Opx I	55.90	0.10	10.06	0.67	28.72	4.59	1.36	0.44	101.9	Co
Opx I	54.01	0.08	9.86	0.71	28.44	4.59	1.40	0.48	99.8	Co
Opx I	55.39	0.09	9.65	0.74	29.29	4.90	1.36	0.45	102.0	Co
Opx II	57.31	0.10	10.72	0.39	32.09	1.20	1.10	0.37	103.3	Co
Opx II	56.19	0.05	10.58	0.43	30.90	1.39	1.10	0.40	101.0	Co
Opx II	55.91	0.03	10.77	0.89	30.48	1.83	1.15	0.36	101.5	Co
Opx II	56.20	0.09	11.12	1.10	30.51	1.84	1.22	0.40	102.6	Co
Opx II	54.22	0.08	11.16	0.90	30.55	1.91	1.06	0.36	100.4	Co
Opx II	54.89	0.10	9.91	1.05	31.06	1.92	1.08	0.35	100.5	Co
Opx II	56.07	0.09	10.18	0.40	31.05	2.11	1.03	0.44	101.4	Co

<sup>a</sup> place of measurements: Co = Cologne, Gö = Göttingen

### ***Silicates (LA-ICP-MS)***

Mineral	NiO		CoO	
	[ $\mu\text{g}\cdot\text{g}^{-1}$ ]	$2\sigma$	[ $\mu\text{g}\cdot\text{g}^{-1}$ ]	$2\sigma$
Olivine	76.2	8.5	45.8	3.9
Olivine	104.7	8.9	51.9	4.5
Olivine	91.1	7.1	49.6	4.0
Olivine	82.1	6.3	49.1	3.9
Olivine	95.3	11.6	49.5	4.6
Olivine	88.1	6.8	51.2	4.3
Olivine	87.2	7.9	50.6	4.5
Olivine	106.5	11.1	48.2	4.0
Olivine	74.1	6.3	44.6	3.7
Olivine	111.2	9.7	50.7	4.3
Opx	50.0	8.9	24.5	2.3
Opx	25.8	1.8	19.7	0.9
Opx	34.5	3.7	24.4	1.7
Opx	24.7	3.5	22.2	1.7
Opx	26.6	2.7	21.1	1.0

### ***Vein material and inclusions (EPMA)***

Phase <sup>a</sup>	Loc <sup>b</sup>	P	Si	Cr	Fe	Co	S	Ni	Mn	wt-total	EPMA <sup>c</sup>
		[wt%]	[wt%]	[wt%]	[wt%]	[wt%]	[wt%]	[wt%]	[wt%]		
Metal	Inc	0.26	0.13	0.09	95.43	0.12	< 0.02	1.51	0.03	97.7	Gö
Metal	Inc	0.25	0.04	0.08	95.47	0.13	< 0.02	1.52	0.03	97.6	Gö
Metal	Inc	0.14	0.96	0.30	94.74	0.35	< 0.02	4.05	< 0.02	100.5	Co
Metal	Inc	0.19	< 0.02	0.10	97.64	0.30	< 0.02	4.03	< 0.02	102.3	Co
Metal	Inc	0.08	< 0.02	0.03	98.30	0.05	< 0.02	1.03	< 0.02	99.5	Co
Metal	Inc	0.11	1.20	0.41	95.13	0.24	< 0.02	2.68	< 0.02	99.8	Co
Metal	Inc	0.18	0.03	0.11	98.51	0.19	< 0.02	2.26	0.03	101.3	Co
Metal	Inc	0.04	0.04	0.16	98.43	0.03	< 0.02	0.69	0.05	99.4	Co
Metal	Inc	0.21	0.03	0.05	98.33	0.21	< 0.02	2.37	< 0.02	101.2	Co
Metal	Inc	0.11	0.05	0.14	98.75	0.13	0.03	1.45	0.04	100.7	Co
Metal	Inc	0.46	0.04	0.06	97.60	0.16	< 0.02	2.50	0.04	100.8	Co
Metal	Inc	0.11	< 0.02	0.08	99.09	0.14	< 0.02	1.91	0.04	101.4	Co
Metal	Inc	0.13	0.35	0.10	98.91	0.10	< 0.02	1.28	< 0.02	100.9	Co
Metal	Inc	0.04	0.84	0.18	95.00	0.20	< 0.02	2.75	< 0.02	99.0	Co
Metal	Inc	0.07	0.03	0.10	97.59	0.04	< 0.02	0.96	< 0.02	98.8	Co
Metal	Inc	0.10	1.19	0.38	96.36	0.21	0.03	3.09	0.03	101.4	Co
Metal	Inc	0.12	1.65	0.40	96.88	0.23	< 0.02	2.83	< 0.02	102.1	Co
Metal	Inc	0.16	0.94	0.16	95.62	0.21	< 0.02	2.99	< 0.02	100.1	Co
Metal	Inc	0.14	0.04	0.08	99.16	0.09	< 0.02	1.15	< 0.02	100.7	Co
Metal	Inc	0.08	0.05	0.10	99.38	0.12	< 0.02	1.09	< 0.02	100.8	Co
Metal	Vein	0.19	< 0.02	0.03	97.13	0.20	< 0.02	3.15	< 0.02	100.7	Co
Metal	Vein	0.22	< 0.02	0.05	96.94	0.26	< 0.02	3.64	< 0.02	101.1	Co
Metal	Vein	0.19	< 0.02	0.16	98.30	0.28	< 0.02	3.57	0.03	102.5	Co
Metal	Vein	0.16	< 0.02	0.03	98.47	0.30	< 0.02	3.20	< 0.02	102.2	Co
Metal	Vein	0.16	< 0.02	0.08	95.69	0.33	< 0.02	4.00	< 0.02	100.3	Co
Metal	Vein	0.17	< 0.02	0.03	98.58	0.26	< 0.02	3.05	< 0.02	102.1	Co
Metal	Vein	0.27	< 0.02	0.05	98.48	0.18	< 0.02	2.66	< 0.02	101.6	Co
Metal	Vein	0.23	< 0.02	0.05	98.24	0.30	< 0.02	3.08	< 0.02	101.9	Co
Metal	Vein	0.25	0.03	0.08	95.68	0.25	< 0.02	3.65	< 0.02	99.9	Co

Phase <sup>a</sup>	Loc <sup>b</sup>	P [wt%]	Si [wt%]	Cr [wt%]	Fe [wt%]	Co [wt%]	S [wt%]	Ni [wt%]	Mn [wt%]	wt-total	EPMA <sup>c</sup>
Metal	Vein	0.23	0.06	0.06	96.35	0.27	< 0.02	3.82	< 0.02	100.8	Co
Metal	Vein	0.25	0.06	0.06	97.84	0.22	< 0.02	3.31	< 0.02	101.7	Co
Metal	Vein	0.24	0.09	0.21	97.73	0.32	< 0.02	4.64	< 0.02	103.2	Co
Metal	Vein	0.24	0.09	0.12	96.17	0.28	< 0.02	3.94	< 0.02	100.9	Co
Metal	Vein	0.51	0.09	0.17	95.00	0.33	< 0.02	4.45	< 0.02	100.6	Gö
Metal	Vein	0.15	0.18	0.12	97.45	0.18	< 0.02	3.18	< 0.02	101.3	Co
Metal	Vein	0.40	0.19	0.20	93.18	0.29	< 0.02	3.82	< 0.02	98.2	Gö
Metal	Vein	0.16	0.23	0.13	97.14	0.21	< 0.02	3.08	< 0.02	101.0	Co
Metal	Vein	0.21	0.26	0.18	95.65	0.32	< 0.02	4.37	< 0.02	101.0	Co
Metal	Vein	0.43	0.29	0.21	94.48	0.29	< 0.02	3.98	< 0.02	99.8	Gö
Metal	Vein	0.13	0.33	0.21	94.58	0.27	< 0.02	3.91	< 0.02	99.4	Co
Metal	Vein	0.20	0.47	0.17	97.58	0.27	< 0.02	3.38	< 0.02	102.1	Co
Metal	Vein	0.15	0.47	0.17	95.64	0.19	< 0.02	2.80	< 0.02	99.4	Co
Metal	Vein	0.17	0.50	0.13	96.09	0.23	< 0.02	3.44	< 0.02	100.6	Co
Metal	Vein	0.17	0.61	0.18	95.25	0.25	< 0.02	3.62	< 0.02	100.1	Co
Metal	Vein	0.25	0.65	0.27	93.80	0.31	< 0.02	4.62	< 0.02	99.9	Co
Metal	Vein	0.44	0.69	0.26	94.39	0.33	< 0.02	4.39	< 0.02	100.6	Gö
Metal	Vein	0.19	0.70	0.26	96.44	0.30	< 0.02	4.09	< 0.02	102.0	Co
Metal	Vein	0.19	0.72	0.23	94.52	0.25	< 0.02	3.55	< 0.02	99.5	Co
Metal	Vein	0.19	0.86	0.22	95.98	0.27	< 0.02	4.02	< 0.02	101.5	Co
Metal	Vein	0.17	0.90	0.28	96.78	0.21	< 0.02	3.56	< 0.02	101.9	Co
Metal	Vein	0.18	0.99	0.28	94.71	0.28	< 0.02	4.11	< 0.02	100.6	Co
Metal	Vein	0.16	1.00	0.28	95.17	0.34	< 0.02	4.50	< 0.02	101.5	Co
Metal	Vein	0.16	1.03	0.31	97.94	0.22	< 0.02	3.25	< 0.02	102.9	Co
Metal	Vein	0.19	1.07	0.33	96.17	0.26	< 0.02	4.52	< 0.02	102.5	Co
Metal	Vein	0.38	1.12	0.26	92.91	0.31	< 0.02	4.09	< 0.02	99.2	Gö
Metal	Vein	0.14	1.13	0.27	96.18	0.20	< 0.02	3.01	< 0.02	100.9	Co
Metal	Vein	0.26	1.14	0.31	95.45	0.22	< 0.02	2.99	< 0.02	100.5	Gö
Metal	Vein	0.41	1.15	0.27	93.93	0.28	< 0.02	4.11	< 0.02	100.3	Gö
Metal	Vein	0.13	1.22	0.26	96.62	0.23	0.03	3.14	< 0.02	101.6	Co
Metal	Vein	0.12	1.35	0.28	93.57	0.20	< 0.02	3.19	< 0.02	98.7	Co
Metal	Vein	0.10	1.36	0.41	97.72	0.15	< 0.02	2.56	< 0.02	102.3	Co
Metal	Vein	0.14	1.36	0.32	96.62	0.19	< 0.02	3.27	< 0.02	101.9	Co
Metal	Vein	0.11	1.52	0.32	95.45	0.19	< 0.02	3.09	< 0.02	100.7	Co
Metal	Vein	0.12	1.55	0.32	96.48	0.29	< 0.02	3.88	< 0.02	102.6	Co

<sup>a</sup> phases: Coh = cohenite, Troi = troilite

<sup>b</sup> locations: Sph = spherule inclusion, Vein = vein material, Inc = inclusion in silicate

<sup>c</sup> place of measurements: Co = Cologne, Gö = Göttingen

## 12.1.8 Kenna

### *Silicates (EPMA)*

Mineral	SiO <sub>2</sub> [wt%]	TiO <sub>2</sub> [wt%]	FeO [wt%]	Al <sub>2</sub> O <sub>3</sub> [wt%]	MgO [wt%]	CaO [wt%]	Cr <sub>2</sub> O <sub>3</sub> [wt%]	MnO [wt%]	wt-total	EPMA <sup>a</sup>
Olivine	40.04	< 0.02	10.80	0.04	47.30	0.44	0.83	0.60	100.1	Gö
Olivine	39.51	< 0.02	13.96	0.05	45.68	0.41	0.73	0.49	100.9	Gö
Olivine	39.84	0.04	14.39	0.04	44.41	0.45	0.88	0.52	100.6	Gö
Olivine	38.83	< 0.02	14.62	0.08	43.83	0.44	0.73	0.49	99.0	Gö
Olivine	38.36	< 0.02	15.21	0.02	43.26	0.42	0.76	0.58	98.6	Gö
Olivine	38.83	0.05	17.30	0.02	42.54	0.38	0.75	0.38	100.3	Gö
Olivine	39.23	< 0.02	17.44	0.04	42.10	0.42	0.75	0.46	100.5	Gö
Olivine	38.88	0.03	18.37	0.06	40.60	0.44	0.76	0.42	99.6	Gö
Olivine	39.11	< 0.02	18.44	0.03	41.26	0.39	0.72	0.49	100.5	Gö
Olivine	39.28	< 0.02	18.46	0.04	40.76	0.44	0.70	0.44	100.1	Gö
Olivine	38.92	0.03	18.50	0.07	41.03	0.40	0.75	0.44	100.2	Gö
Olivine	38.64	< 0.02	18.74	0.06	40.35	0.43	0.71	0.46	99.5	Gö
Olivine	38.62	0.04	19.21	0.03	39.57	0.42	0.72	0.43	99.1	Gö
Olivine	38.66	< 0.02	19.35	0.05	39.94	0.43	0.73	0.37	99.6	Gö
Olivine	38.49	< 0.02	19.48	0.08	40.78	0.44	0.76	0.38	100.4	Gö
Olivine	39.50	< 0.02	19.18	0.02	42.14	0.36	0.70	0.44	102.3	Co
Olivine	39.44	< 0.02	19.28	0.00	42.17	0.37	0.58	0.47	102.3	Co
Olivine	38.16	< 0.02	19.80	0.05	42.25	0.37	0.75	0.38	101.8	Co
Opx	54.95	0.04	11.28	0.67	26.31	4.89	1.15	0.39	99.8	Gö
Opx	55.16	0.08	11.47	0.69	26.31	4.97	1.12	0.42	100.3	Gö
Opx	55.07	0.10	11.66	0.69	26.51	4.90	1.18	0.41	100.6	Gö
Opx	54.48	0.12	11.67	0.68	26.86	4.94	1.16	0.45	100.4	Gö
Opx	55.44	0.08	11.36	0.62	27.80	4.75	1.17	0.36	101.6	Co
Opx	56.17	0.10	11.60	0.65	27.10	4.76	1.11	0.41	102.0	Co
Opx	56.11	0.10	11.25	0.65	27.64	4.78	1.22	0.45	102.3	Co
Opx	55.44	0.04	11.43	0.59	27.38	4.81	1.10	0.44	101.3	Co
Opx	56.80	0.07	11.16	0.67	26.84	4.89	1.10	0.38	102.0	Co

<sup>a</sup> place of measurements: Co = Cologne, Gö = Göttingen

**Silicates (LA-ICP-MS)**

Mineral	NiO		CoO	
	[ $\mu\text{g}\cdot\text{g}^{-1}$ ]	$2\sigma$	[ $\mu\text{g}\cdot\text{g}^{-1}$ ]	$2\sigma$
Olivine	88.8	8.4	53.6	4.6
Olivine	88.2	7.8	52.9	4.6
Olivine	101.0	9.4	55.2	5.0
Olivine	103.8	18.7	62.0	5.6
Olivine	113.9	10.3	58.5	5.1
Olivine	84.2	8.8	53.0	4.6
Olivine	98.4	12.6	51.8	5.1
Olivine	103.9	9.9	49.3	4.3
Olivine	88.0	7.4	54.9	4.6
Olivine	83.2	7.8	52.3	4.6
Olivine	109.3	10.6	56.6	5.6
Olivine	87.8	3.6	55.1	1.7
Opx	23.8	2.8	23.3	2.2
Opx	25.8	2.4	23.5	2.1
Opx	29.9	1.9	24.4	1.1

**Vein material and inclusions**

Phase	Loc <sup>b</sup>	P [wt%]	Si [wt%]	Cr [wt%]	Fe [wt%]	Co [wt%]	S [wt%]	Ni [wt%]	Mn [wt%]	wt-total	EPMA <sup>c</sup>
Metal	Inc	0.26	0.08	0.12	95.72	0.21	< 0.02	2.94	< 0.02	99.4	Gö
Metal	Inc	0.08	0.07	0.12	97.55	0.25	< 0.02	2.94	< 0.02	101.0	Co
Metal	Inc	0.07	0.08	0.07	99.57	0.10	< 0.02	0.676	< 0.02	100.6	Co
Metal	Inc	0.13	0.75	0.35	92.69	0.32	< 0.02	4.42	< 0.02	98.7	Co
Metal	Vein	0.16	0.95	0.50	94.08	0.38	0.03	4.75	< 0.02	100.8	Co

<sup>b</sup> locations: Sph = spherule inclusion, Vein = vein material, Inc = inclusion in silicate

<sup>c</sup> place of measurements: Co = Cologne, Gö = Göttingen

## 12.1.9 LEW85440

### *Silicates (EPMA)*

Mineral	SiO <sub>2</sub> [wt%]	TiO <sub>2</sub> [wt%]	FeO [wt%]	Al <sub>2</sub> O <sub>3</sub> [wt%]	MgO [wt%]	CaO [wt%]	Cr <sub>2</sub> O <sub>3</sub> [wt%]	MnO [wt%]	wt-total	EPMA <sup>a</sup>
Olivine	42.22	< 0.02	0.74	0.11	56.64	0.31	0.21	0.40	100.6	Gö
Olivine	41.76	< 0.02	1.14	0.09	56.16	0.23	0.17	0.22	99.8	Gö
Olivine	41.26	< 0.02	1.58	0.11	55.48	0.25	0.38	0.43	99.5	Gö
Olivine	41.22	< 0.02	3.96	0.07	53.77	0.35	0.50	0.47	100.4	Gö
Olivine	41.29	< 0.02	4.56	0.06	53.46	0.27	0.45	0.44	100.6	Gö
Olivine	41.27	< 0.02	4.81	0.06	52.71	0.31	0.52	0.45	100.2	Gö
Olivine	40.95	< 0.02	5.27	0.07	52.42	0.32	0.48	0.48	100.0	Gö
Olivine	41.26	< 0.02	5.83	0.10	51.98	0.31	0.55	0.49	100.6	Gö
Olivine	39.82	< 0.02	7.78	0.06	50.28	0.32	0.50	0.50	99.3	Gö
Olivine	40.68	< 0.02	8.23	0.08	49.51	0.29	0.53	0.50	99.9	Gö
Olivine	39.50	< 0.02	8.47	0.10	49.38	0.33	0.50	0.48	98.8	Gö
Olivine	40.97	0.04	8.58	0.09	49.59	0.32	0.50	0.46	100.6	Gö
Olivine	40.33	< 0.02	8.68	0.06	49.67	0.31	0.53	0.43	100.0	Gö
Olivine	40.71	< 0.02	8.68	0.09	49.49	0.30	0.46	0.55	100.3	Gö
Olivine	40.69	0.03	8.69	0.08	49.97	0.32	0.46	0.47	100.7	Gö
Olivine	40.71	0.03	8.79	0.04	49.43	0.29	0.54	0.46	100.3	Gö
Olivine	40.45	< 0.02	8.52	< 0.02	51.35	0.29	0.47	0.49	101.6	Co
Olivine	40.91	0.04	8.25	0.05	51.11	0.28	0.46	0.40	101.5	Co
Olivine	40.40	0.06	8.47	0.04	51.17	0.29	0.54	0.47	101.5	Co
Olivine	40.40	0.05	8.79	< 0.02	51.40	0.31	0.58	0.41	101.9	Co
Olivine	40.49	0.04	8.29	< 0.02	50.80	0.33	0.39	0.44	100.8	Co
Olivine	40.29	< 0.02	8.17	0.06	48.91	0.27	0.46	0.43	98.6	Co
Olivine	41.76	0.08	8.32	< 0.02	50.25	0.30	0.42	0.40	101.5	Co
Olivine	41.28	0.06	8.18	0.03	50.22	0.28	0.46	0.46	101.0	Co
Olivine	41.34	0.03	8.70	< 0.02	49.98	0.31	0.51	0.53	101.4	Co
Olivine	40.34	0.05	8.03	0.05	49.37	0.31	0.52	0.43	99.1	Co
Olivine	40.42	< 0.02	8.06	0.05	48.52	0.31	0.46	0.40	98.3	Co
Opx	57.26	0.11	5.44	0.86	33.02	2.67	0.83	0.45	100.7	Gö
Opx	56.37	0.17	5.10	0.77	33.76	2.52	0.83	0.45	100.0	Co
Opx	57.11	0.15	5.11	0.75	33.78	2.56	0.88	0.43	100.8	Co
Opx	56.61	0.10	4.92	0.71	33.87	2.58	1.00	0.41	100.3	Co
Opx	55.52	0.14	4.78	0.70	33.71	2.52	0.92	0.39	98.7	Co
Opx	56.41	0.13	5.24	0.69	33.75	2.55	0.82	0.47	100.1	Co
Opx	56.65	0.14	5.13	0.75	33.82	2.60	0.89	0.48	100.5	Co
Opx	56.45	0.12	4.85	0.74	33.57	2.51	0.85	0.40	99.5	Co
Opx	56.19	0.14	5.02	0.72	33.72	2.55	0.74	0.44	99.5	Co
Opx	56.09	0.11	5.24	0.73	33.72	2.51	0.73	0.42	99.6	Co
Opx	56.94	0.14	4.84	0.74	33.73	2.55	0.81	0.48	100.3	Co
Opx	57.37	0.15	5.15	1.24	33.26	2.82	0.76	0.48	101.3	Co
Opx	56.81	0.12	4.98	0.76	34.18	2.55	0.78	0.39	100.6	Co
Opx	56.80	0.14	5.24	0.71	33.88	2.58	0.74	0.44	100.6	Co
Opx	56.84	0.09	5.14	0.75	33.31	2.52	0.79	0.43	99.9	Co
Opx	56.20	0.15	5.15	0.70	33.49	2.56	0.89	0.47	99.6	Co
Opx	57.41	0.15	5.01	0.71	33.96	2.60	0.76	0.48	101.1	Co
Opx	57.27	0.21	5.20	0.72	33.74	2.58	0.80	0.38	100.9	Co
Opx	56.74	0.13	4.82	0.74	33.56	2.65	0.76	0.51	99.9	Co
Opx	57.45	0.14	4.86	0.81	33.30	2.62	0.76	0.47	100.4	Co

Opx	57.87	0.09	4.86	0.80	33.49	2.61	0.72	0.44	100.9	Co
Opx	57.46	0.11	5.07	0.73	32.83	2.64	0.80	0.44	100.1	Co
Mineral	SiO <sub>2</sub> [wt%]	TiO <sub>2</sub> [wt%]	FeO [wt%]	Al <sub>2</sub> O <sub>3</sub> [wt%]	MgO [wt%]	CaO [wt%]	Cr <sub>2</sub> O <sub>3</sub> [wt%]	MnO [wt%]	wt-total	EPMA <sup>a</sup>
Opx	57.12	0.10	5.02	0.83	32.86	2.57	0.79	0.36	99.7	Co
Opx	55.88	0.19	4.84	0.76	32.49	2.56	0.73	0.42	97.9	Co
Opx	58.23	0.11	5.29	0.83	33.88	2.58	0.84	0.43	102.2	Co
Opx	58.03	0.18	5.15	0.80	33.63	2.64	0.82	0.47	101.7	Co
Opx	56.43	0.16	5.40	0.71	33.83	2.66	0.75	0.43	100.4	Co
Opx	57.69	0.13	5.18	0.77	33.39	2.63	0.89	0.48	101.2	Co
Opx	57.27	0.15	4.88	0.77	33.47	2.66	0.79	0.40	100.5	Co
Opx	57.64	0.21	5.03	0.79	33.24	2.66	0.83	0.46	100.9	Co
Opx	57.69	0.09	5.21	0.78	33.41	2.53	0.86	0.49	101.1	Co
Opx	56.71	0.11	5.25	0.76	31.77	2.51	0.75	0.46	98.4	Co
Opx	57.46	0.10	5.06	0.82	32.78	2.60	0.88	0.41	100.1	Co
Opx	57.79	0.12	4.72	0.77	33.17	2.62	0.85	0.51	100.5	Co
Opx	57.59	0.11	4.81	0.80	32.74	2.62	0.81	0.40	99.9	Co
Opx	57.35	0.12	4.92	0.83	32.89	2.58	0.86	0.36	100.0	Co
Opx	58.03	0.12	5.07	0.78	33.35	2.62	0.80	0.33	101.2	Co
Opx	56.57	0.10	5.24	0.78	32.26	2.52	0.76	0.46	98.8	Co
Opx	58.11	0.11	5.13	0.81	33.76	2.57	0.84	0.45	101.9	Co
Opx	56.86	0.14	4.57	0.97	32.80	3.08	0.76	0.40	99.7	Co
Aug	54.62	0.28	3.28	1.23	22.00	17.42	0.87	0.36	100.2	Co

<sup>a</sup> place of measurements: Co = Cologne, Gö = Göttingen

### ***Silicates (LA-ICP-MS)***

Mineral	NiO		CoO	
	[µg·g <sup>-1</sup> ]	2σ	[µg·g <sup>-1</sup> ]	2σ
Olivine	50.6	5.7	16.3	1.5
Olivine	42.0	4.3	17.3	1.8
Olivine	38.2	3.1	16.1	1.2
Olivine	50.6	6.2	16.5	1.0
Olivine	28.1	2.4	12.2	1.4
Olivine	42.9	3.9	15.3	1.4
Olivine	33.4	2.5	14.5	0.7
Opx	12.1	1.7	6.9	0.7
Opx	9.5	1.1	6.8	0.7
Opx	11.0	1.0	6.9	0.4
Opx	10.1	1.5	7.0	0.5

### ***Vein material and inclusions***

Phase <sup>a</sup>	Loc <sup>b</sup>	P	Si	Cr	Fe	Co	S	Ni	Mn	wt-total	EPMA <sup>c</sup>
		[wt%]	[wt%]	[wt%]	[wt%]	[wt%]	[wt%]	[wt%]	[wt%]		
Metal	Vein	0.13	< 0.02	0.08	95.6	0.31	< 0.02	3.65	< 0.02	99.8	Co
Metal	Vein	0.11	< 0.02	0.22	94.5	0.30	< 0.02	3.83	< 0.02	99.0	Co
Metal	Vein	0.11	< 0.02	0.39	96.3	0.27	< 0.02	3.82	< 0.02	100.9	Co
Metal	Vein	0.10	< 0.02	0.30	95.2	0.29	< 0.02	4.37	< 0.02	100.3	Co
Metal	Vein	0.28	< 0.02	0.25	94.1	0.31	< 0.02	3.91	< 0.02	99.0	Gö
Metal	Vein	0.08	< 0.02	0.41	95.7	0.24	< 0.02	3.83	< 0.02	100.3	Co
Metal	Vein	0.10	< 0.02	0.37	95.4	0.37	< 0.02	4.71	< 0.02	100.9	Co
Metal	Vein	0.10	< 0.02	0.06	96.0	0.26	< 0.02	3.58	< 0.02	100.0	Co
Metal	Vein	0.14	0.03	0.19	95.9	0.26	< 0.02	3.57	< 0.02	100.1	Co

Phase <sup>a</sup>	loc <sup>b</sup>	P [wt%]	Si [wt%]	Cr [wt%]	Fe [wt%]	Co [wt%]	S [wt%]	Ni [wt%]	Mn [wt%]	wt- total	EPMA <sup>c</sup>
Metal	Vein	0.25	0.03	0.34	93.3	0.28	< 0.02	4.04	< 0.02	98.3	Gö
Metal	Vein	0.14	0.03	0.27	94.5	0.27	< 0.02	4.03	< 0.02	99.2	Co
Metal	Vein	0.14	0.03	0.15	94.5	0.36	< 0.02	4.07	< 0.02	99.3	Co
Metal	Vein	0.15	0.04	0.32	95.6	0.35	< 0.02	4.62	< 0.02	101.0	Co
Metal	Vein	0.12	0.04	0.25	95.8	0.27	< 0.02	3.35	< 0.02	99.8	Co
Metal	Vein	0.28	0.13	0.25	92.6	0.26	< 0.02	3.82	0.03	97.5	Gö
Metal	Vein	0.22	0.84	0.05	93.7	0.26	< 0.02	3.74	< 0.02	98.9	Gö
Metal	Vein	0.10	0.92	0.09	94.2	0.26	< 0.02	4.08	< 0.02	99.6	Co
Metal	Vein	0.07	1.11	0.07	93.8	0.26	< 0.02	3.73	0.03	99.1	Co
Metal	Vein	0.13	4.97	0.17	89.5	0.31	< 0.02	4.94	< 0.02	100.1	Co
Troi	Vein	< 0.02	0.04	1.08	61.2	< 0.02	36.52	0.03	< 0.02	98.7	Co
Troi	Vein	< 0.02	0.44	1.96	58.5	< 0.02	36.19	0.08	0.08	97.1	Co
Troi	Vein	< 0.02	0.03	5.16	55.6	< 0.02	37.44	< 0.02	0.20	98.1	Co
Troi	Vein	< 0.02	< 0.02	5.66	55.6	< 0.02	36.93	< 0.02	0.29	98.1	Co
Metal	Sph	0.14	0.03	0.07	90.1	0.41	0.03	8.41	< 0.02	99.1	Co
Troi	Sph	< 0.02	0.05	0.34	63.5	< 0.02	36.60	< 0.02	0.04	100.4	Co
Troi	Inc	< 0.02	0.76	2.89	57.7	< 0.02	36.47	0.09	0.16	98.1	Gö
Troi	Inc	< 0.02	0.26	2.12	58.7	< 0.02	36.66	0.15	0.05	97.8	Co
Troi	Inc	< 0.02	0.14	2.00	60.4	< 0.02	36.87	0.04	0.14	99.4	Co
Troi	Inc	< 0.02	0.12	1.53	60.0	< 0.02	36.35	< 0.02	0.03	97.9	Co
Troi	Inc	< 0.02	0.18	2.69	58.5	< 0.02	36.19	0.04	0.10	97.5	Co
Troi	Inc	< 0.02	0.09	2.72	58.7	< 0.02	37.11	< 0.02	0.05	98.5	Co
Troi	Inc	< 0.02	0.21	2.47	58.4	< 0.02	36.37	< 0.02	0.36	97.4	Co
Metal	Inc	0.11	< 0.02	0.29	97.2	< 0.02	< 0.02	0.65	0.05	98.4	Gö
Metal	Inc	0.07	0.06	0.08	99.3	0.04	< 0.02	0.80	0.04	100.3	Co
Metal	Inc	0.05	< 0.02	0.28	100.3	< 0.02	< 0.02	0.80	< 0.02	101.5	Co
Metal	Inc	0.11	0.12	0.11	97.1	0.09	< 0.02	1.28	< 0.02	98.8	Co
Metal	Inc	0.07	0.03	0.14	97.7	0.09	0.03	1.33	< 0.02	99.4	Co
Metal	Inc	0.20	0.04	0.11	97.0	0.05	< 0.02	1.33	< 0.02	98.7	Co
Metal	Inc	0.20	0.80	0.12	94.7	0.09	< 0.02	1.55	0.04	97.6	Gö
Metal	Inc	0.09	0.06	0.08	96.4	0.14	< 0.02	1.60	< 0.02	98.3	Co
Metal	Inc	0.08	0.38	0.08	97.8	0.12	0.03	1.60	< 0.02	100.1	Co
Metal	Inc	0.22	0.29	0.13	96.0	0.12	< 0.02	1.61	0.06	98.5	Gö
Metal	Inc	0.20	0.14	0.15	96.5	0.09	< 0.02	1.69	0.03	98.9	Gö
Metal	Inc	0.08	0.03	0.06	97.3	0.11	< 0.02	2.46	< 0.02	100.1	Co
Metal	Inc	0.13	0.09	0.08	96.8	0.19	< 0.02	3.23	< 0.02	100.5	Co
Metal	Inc	0.09	0.84	0.06	94.8	0.28	< 0.02	3.60	< 0.02	99.7	Co
Metal	Inc	0.10	0.07	0.09	95.8	0.20	< 0.02	3.68	0.04	99.9	Co
Metal	Inc	0.05	0.04	0.09	93.7	0.15	0.06	4.25	0.04	98.4	Co

<sup>a</sup> phases: Troi = troilite

<sup>b</sup> locations: Sph = spherule inclusion, Vein = vein material, Inc = inclusion in silicate

<sup>c</sup> place of measurements: Co = Cologne, Gö = Göttingen

## 12.2 Bulk chondrite compositions

Table 36 Chondritic bulk compositions used in this work. Data taken from LODDERS and FEGLEY (1998).

	SiO <sub>2</sub> [wt%]	CaO [wt%]	Na <sub>2</sub> O [wt%]	MgO [wt%]	Al <sub>2</sub> O <sub>3</sub> [wt%]	TiO <sub>2</sub> [wt%]	FeO [wt%]	Cr <sub>2</sub> O <sub>3</sub> [wt%]	MnO [wt%]	CoO [wt%]	NiO [wt%]	SO <sub>2</sub> [wt%]	C [wt%]
CI	22.76	1.30	0.67	22.47	1.63	0.07	23.09	0.39	0.25	0.06	1.40	10.81	3.45
CV	33.59	2.57	0.46	33.13	3.17	0.15	29.81	0.51	0.20	0.08	1.68	4.39	0.53
H	36.58	1.71	0.82	32.66	2.00	0.11	34.51	0.51	0.30	0.11	2.18	4.00	0.21
L	39.79	1.86	0.93	34.52	2.19	0.11	27.59	0.54	0.33	0.07	1.58	4.39	0.25
LL	40.43	1.85	0.92	35.44	2.23	0.11	25.12	0.54	0.34	0.06	1.35	4.19	0.31

## **13 Danksagung**

Zunächst möchte ich mich bei Herrn Prof. Dr. Andreas Pack für die Betreuung, ständige Unterstützung und Motivation bei meiner Promotion bedanken. Mein Dank gilt auch dem Koreferenten Prof. Dr. Addi Bischoff.

Ein besonderes Dankeschön geht an meine liebe Ehefrau Dana Gabriel, die nicht nur meine Launen klaglos ertragen hat, sondern mit ihren Englischkenntnissen und einem scharfen Blick für Ungereimtheiten maßgeblich zur Fertigstellung dieser Arbeit beigetragen hat.

Mein Dank geht weiterhin an all diejenigen, die mich bei meinen Messungen und Analysen unterstützt haben: an Dr. Jan Schuessler und Prof. Dr. Ronny Schönberg von der Universität Hannover, an Dr. Günther Suhr für seine Betreuung an der Mikrosonde an der Universität Köln, an Dr. Klaus Simon für seine Betreuung an der LA-ICP-MS, an Dr. Andreas Kronz, der mich in großartiger Weise bei meiner Arbeit an der Mikrosonde unterstützte, sowie an Erwin Schiffczyk und Ingrid Reuber, die mir bei der Probenvorbereitung halfen.

Ein großes Dankeschön auch an Dr. Ghylaine Quitté, die für uns die Ni-Isotopenanalysen an der ENS Lyon durchgeführt hat.

Weiterhin möchte ich all meinen Leidensgenossen danken, die mir mit Rat und Tat und Witz und manchem mehr oder weniger aufmunternden Wort zur Seite standen: Dr. Christoph Toulouse, Dr. Andreas Kropf, Magdalena Hofman, Wenke Wegner, Nadine Schäfer, Christina Heller, Kristina Rathsack und meinem erklärten Lieblings-IT-Spezialisten Stefan Möller-McNett.

Großer Dank gilt auch meinen Großeltern, Dr. Siegfried Lächelt und Dr. Anja Lächelt, die mich überhaupt erst in Richtung Mineralogie geschubst haben, auch wenn ich bis heute das Gefühl habe, es wäre ihnen lieber gewesen, ich hätte Geologie studiert.

## 14 Lebenslauf

Name: Aron D. Gabriel

Adresse: Alter Teichweg 29  
22081 Hamburg  
Email: [aron.gabriel@gmx.de](mailto:aron.gabriel@gmx.de)

Geburtsdatum/-ort: 03. Oktober 1977 in Berlin  
Familienstand: verheiratet

### 14.1 Beruflicher Werdegang

2/2006 – 4/2009      Wissenschaftlicher Mitarbeiter zum Zwecke der Promotion an der Universität Hannover und der Universität Göttingen  
*(Arbeitsplatzwechsel aufgrund der Berufung des Doktorvaters Prof. Dr. Andreas Pack an die Universität Göttingen)*

### 14.2 Studium

10/1998 – 3/2005      Studium der Mineralogie an der TU Bergakademie Freiberg,  
Abschluss: Diplom (Note 1.7)  
Kernfach: Lagerstättenlehre/Petrologie  
Nebenfächer: Geochemie, Strukturgeologie

10/2005 – 1/2006      Titel der Diplomarbeit: *„Zonierungen innerhalb eines polymetallischen schwarzen Rauchers aus dem Satanic Mills Gebiet, PACMANUS, Papua Neu Guinea unter der besonderen Berücksichtigung des Auftretens und der Verteilung von Gold“*  
Studium der Geophysik an der Universität Hamburg  
*Aufgabe des Studiums zur Aufnahme einer Doktorandenstelle an der Universität Hannover*

Nebentätigkeiten

5/2003 – 10/2003      Wissenschaftliche Hilfskraft (Nasschemische Analytik volatiler Elemente)

6/2004 – 8/2004      Wissenschaftliche Hilfskraft (Mechanische Probenaufbereitung für Spurenelementanalytik)

### 14.3 Schulische Ausbildung

9/1984 – 2/1991      4. Polytechnische Oberschule „Gustav Schiefelbein“

2/1991 – 2/1992      3. Gymnasium – Wedding

2/1992 – 7/1997      3. Oberschule Gymnasium Prenzlauer Berg „Käthe Kollwitz“  
Abschluss: Abitur (Note 2.5)

## 14.4 Publikationen

- Gabriel, A. and Pack, A. (2008). Fe, Co and Ni in Ureilite Metal and Silicates - Constraints for the Origin of Ureilite Metal, *39th Lunar and Planetary Science Conference*, League City, Texas, #1391.
- Gabriel, A., Quitté, G., and Pack, A. (2008). Chemistry and Ni-isotope composition of ureilites and their components, *86th Annual Meeting of the German Mineralogical Society - DMG*, Berlin, Germany, #428
- Gabriel, A., Quitté, G., and Pack, A. (2008). Chemistry and Ni-isotope composition of ureilites and their components, *3rd European Planetary Science Congress*, Münster, Germany, PSC2008-A-00570.
- Gabriel, A. and Pack, A. (2007). Fe, Co and Ni in Ureilites: Metal-silicate equilibration in the UPB, *Goldschmidt 2007*, Cologne, Germany, A301
- Gabriel, A., Pack, A., Quitté, G., Schönberg, R., and Schüssler, J. (2006). Iron and nickel concentrations and isotopes in Kenna ureilite silicates - implications for the evolution of the ureilite parent body, *84th Annual Meeting of the German Mineralogical Society - DMG*, Hannover, #1247
- Gabriel, A., Quitté, G., Schönberg, R., Schüssler, J., and Pack, A. (2006). Iron and nickel in ureilite silicates-chemistry and isotopes. *Meteoritics & Planetary Science* **41**, A60.